Development and Function of the *Drosophila* Giant Fiber Neural Circuit

By

Tyler Joseph Kennedy

Dissertation

Submitted to the Faculty of the

Graduate School of Vanderbilt University

In partial fulfillment of the requirements

for the degree of

DOCTOR OF PHILOSOPHY

in

Biological Sciences

May 10, 2019

Nashville, Tennessee

Approved:

Douglas McMahon, Ph.D.

Kendal Broadie, Ph.D.

David Miller, Ph.D.

Manuel Ascano, Jr., Ph.D.

Todd Graham, Ph.D.

Dedication

This dissertation is dedicated to Amanda, Finnegan, Janning, Scott and Jorie,

all of whom are quite simply the best.

Acknowledgements

I first want to express my appreciation for the educational environment and wide range of resources Vanderbilt University provides. It has been a pleasure to spend time on this beautiful campus, interacting with the wonderful educators, students and staff that comprise this institution. The Biological Sciences Department is a very special part of Vanderbilt and I am grateful for the broad scientific exposure I received while here, especially the diversity of classes and seminars. Both department chairs during my degree, Dr. Charles Singleton and Dr. Douglas McMahon have been incredibly kind and helpful with all matters, especially in their support for the Graduate School Association activities. I would also like to thank Dr. Kathy Friedman and Dr. Donna Webb for all of their work as Director of Graduate Studies. They were always available to help with any issue relating to graduate work and unhesitating in offering guidance, support and kind words. I also cannot express enough appreciation for the help I received from the department's front office. Alicia Goostree has been eternally patient and helped me with every problem that came up, big and small. Carol Wiley knows everything there is to know about grant submission and I cannot imagine having successfully completed mine without her. Leslie Maxwell was here when I began the program and helped me get settled into Nashville and navigate my way through beginning a PhD. LaDonna Smith has my enduring thanks for helping me with my endless questions about funding, traveling for conferences, and finishing the PhD.

I want to give a special thanks to the Program in Developmental Biology. I credit this amazing organization with a great deal of my scientific maturation. Their weekly journal club has broadened my scientific knowledge, helped me understand how to critique a paper and shown me how to give high-quality presentations. PDB would not be possible without a number of dedicated individuals, but I want to especially thank Chris Wright for his impassioned dedication to this project and warm welcome to the program.

My personal scientific research has benefitted from a huge number of people. I first would like to thank the innumerable individuals I called, emailed and spoke with over the years for sharing their advice and reagents. It is always humbling and amazing to realize how large the scientific community around the world is and to see how far people are willing to go to help a student with a strange science question. Next, I would like to thank the incredible members of my committee. Dr. Douglas McMahon has been a wonderful chair and helped me keep my proposals organized and concise. Dr. David Miller, Dr. Manual Ascano Jr., and Dr. Todd Graham have been very supportive throughout the research process while also keeping a sharp eye on my work and helping me identify potential weaknesses in my arguments. I would like to thank Dr. Nick Reiter who has changed universities but was a highly valued member of my committee before he left. I also wish to express my sincere gratitude to Dr. Donna Webb, who is no longer with us. I was fortunate enough to take classes with Donna, rotate through her lab, and have her as a member of my committee. She was passionate about science and her students and was always available to help anyone who needed it. She gave extensive input on my dissertation proposal and was immensely helpful in the organization of my experiments. I still think about her often and miss having her delightful personality around the department.

Of key importance to all of the work that follows is the Broadie lab. I am grateful to Dr. Kendal Broadie for accepting me into his lab and providing me guidance for all of these years. He is a tireless, talented editor and his input on my work has made it immeasurably better. Our bi-monthly meetings have been filled with extensive discussions about research, ideas, techniques and his inside view of the academic and scientific worlds. I've learned a great deal from him and vastly improved my scientific abilities by working in his lab. The members of the Broadie laboratory have been an unending well of scientific knowledge and an incredible community. Meeting this group of people has changed me fundamentally and helped shape the scientist I am today. I will always be grateful for the conversations with, and input I received from Emma Rushton, Cheryl Gatto, Caleb Doll, James Sears, Neil Dani, Will

Parkinson, Mary Lynn Dear, Danielle Kopke, Dominic Vita, Randy Golovin and Qing Xia Chen. I would especially like to thank Emma for being my rotation advisor when I first joined the lab and introducing me to the world of *Drosophila* research. I also gained valuable lessons mentoring Moon Ryu, Ryan Moore and Demi Ajao. I had no idea how to train someone to become a scientist when I arrived at Vanderbilt, and I made a lot of mistakes along the way. I appreciate the patience my mentees had for me throughout the process. It has been an absolute joy to work in the lab with this wonderful collection of scientists and I will miss the spirited discussions during lab meeting and around the bench.

I also wish to acknowledge and thank my many mentors prior to arriving at Vanderbilt whose dedication to teaching helped me make it into and through a PhD program. Pam Durkee, my high school biology teacher was a powerful influence on my interest in the life sciences. She is a passionate and dedicated teacher and her devotion to her craft stimulated my interest in learning and sent me down a path towards biological research. I followed that path to the University of Redlands where I was given an excellent education by teachers who truly care about their students and the pursuit of knowledge. I especially want to thank Susan Blauth, Teresa Longin and David Soulsby, not only for leading fascinating classroom discussions, but also for mentoring me during my first true research projects and helping me learn how to read the scientific literature. After college, I took a job with Applied Speciation and Consulting, where I met two of my greatest mentors to date: Russ Gerads and Hakan Gürleyük. Working with Russ and Hakan changed the way I looked at science. They were willing to talk through anything, dissect the methods and findings of any paper and attempt any research project that came their way. They instilled a healthy sense of skepticism and critical thinking in me, which I think are among the most important attributes a scientist can have.

Lastly, I could not have made it to this point without the unending support of my family. My parents, Janning and Scott, have always made my education their highest priority and encouraged me in everything I've done. My Mom was my first science teacher and is the source of my scientific curiosity.

She always has a new science topic to discuss and I love hearing her insights on various findings. I couldn't ask for a better role model in work or life. My Dad has always pushed me to be the best I can be and given endless encouragement to my pursuits. He has taken an interest in my work and asked detailed questions about my projects. His passion for life is infectious and he has helped keep a proper perspective throughout this program. My sister Jorie is one of my true inspirations and I am forever jealous of her talents. She is devoted to helping others, creating a better world and seeing beauty in everything. Having her in my life has reoriented my priorities and beliefs and I couldn't ask for a better sister. The bulk of the work in supporting me through this PhD has fallen on my partner in life, Amanda Clayton. She is the most incredible and brilliant person I can imagine spending the beginning and end of every day with. Every time I have run up against obstacles, she has been unendingly positive and uplifting. I can always discuss my work with her and my writing has benefitted greatly from her sharp proofreading. She is always ready to celebrate successes and talk through disappointments. She has worked hard to make sure we enjoy everything life has to offer and ensures I do not spend all of my time working in. She has brought more joy to me than I thought possible and I cannot thank her enough for choosing to share her life with me. And, finally, the newest member of my support team is Finnegan Kennedy. He has perhaps been the most disruptive person to my research program and has done everything he can to stop me from working on it so that I can play with him. Regardless, he brings pure unbridled happiness to my life and just seeing his little smile and hearing his little laugh is enough to prepare me for any trials the day may bring. Thank you, everyone, from the bottom of my heart.

Acknowledgement of Funding

This work was supported by National Institutes of Health Grants MH084989 (to K.B.), and NS092250 and HD007502 (to T.K.).

Publications

Fragile X Mental Retardation Protein Restricts Small Dye Iontophoresis Entry into Central Neurons. Kennedy T. and Broadie K. JNeuro. 2017 Sep 8; 0723—17.

Newly Identified Electrically Coupled Neurons Support Development of the Drosophila Giant Fiber Model Circuit. Kennedy T. and Broadie K. eNeuro. 2018 Nov 26; 0346-18.

Table of Contents

List of Figures

List of Tables

List of Abbreviations

4-AP	4-Aminopyridine
9-AC	9-Anthracenecarboxylic Acid
ACh	Acetylcholine
AG	Abdominal Ganglia
Ag	Silver
AIS	Axon Initial Segment
AMPA	α-amino-3-hydroxy-5-methyl-4-isoxazolepropionic Acid
APF	After Puparium Formation
ASD	Autism Spectrum Disorder
ATR	All-Trans Retinal
Bap	Bagpipe
BC1	Bran Cytoplasmic RNA 1
BCA	Bicinchoninic Acid
Ben	Bendless
BK	Big Potassium
BrdU	Bromodeoxyuridine
Brp	Bruchpilot
BSA	Bulk Segregant Analysis
BSA	Bovine Serum Albumin
Bsn	Bassoon
CAM	Cell Adhesion Molecule
CaMKII	Calcium/Calmodulin-Dependent Protein Kinase Type II

CC	Cervical Connective
Ced-6	Cell Death Protein 6
Chmp4	Charged Multivesicular Body Protein 4A
ChR	Channelrhodopsin
Cl	Chloride
CNS	Central Nervous System
CNV	Copy Number Variant
CRISPR	Clustered Regularly Interspersed Palindromic Repeats
Csw	Corkscrew
DAG	Diacylglycerol
DenMark	Dendritic Marker
dfmr1	*Drosophila* Fragile X Mental Retardation 1
DgkK	Diacylglycerol Kinase, Kappa
DLM	Dorsal Longitudinal Muscle
DLMn	Dorsal Longitudinal Motor Neuron
eIF4F	Eukaryotic Initiation Factor Complex 4F
EM	Electron Microscopy
ERK	Extracellular-Signal Regulated Kinases
FIB/SEM	Focused Ion Beam/Scanning Electron Microscopy
Flp	Flippase
FMR1	Fragile X Mental Retardation 1
FMRP	Fragile X Mental Retardation Protein
FRAP	Fluorescence Recovery After Photobleaching
FRT	Flp Recombination Target

FXPOI	Fragile X-Associated Primary Ovarian Insufficiency
FXR1	Fragile X Mental Retardation Syndrome-Related Protein 1
FXR2	Fragile X Mental Retardation Syndrome-Related Protein 2
FXS	Fragile X Syndrome
FXTAS	Fragile X-Associated Tremor/Ataxia Syndrome
Fz	Frizzled
GCI	Giant Commissural Interneuron
GF	Giant Fiber
GFC	Giant Fiber Coupled
GFI	Giant Fiber Interneuron
GFP	Green Fluorescent Protein
Gig	Gigas
GLEAM	Gal4 Limited Enchainment Activated Marker
GOF	Gain of Function
GRASP	GFP Reconstruction Across Synaptic Partners
Hid	Head Involution Defective
HITS-CLIP	High-Throughput Sequencing of RNA Isolated by Crosslinking Immunprecipitation
hnRNP	Heterogeneous Nuclear Ribonucleoprotein
IB	Inframedial Bridge
iBLINC	*in vivo* Biotin Labeling of Intercellular Contacts
IHC	Immunohistochemistry
Irk2	Inwardly Rectifying Potassium Channel 2
KAc	Potassium Acetate

KCl	Potassium Chloride
KH	K Homology
LTD	Long Term Depression
LTP	Long Term Potentiation
LY	Lucifer Yellow
MAP1B	Microtubule Associated Protein 1B
MAPseq	Multiplexed Analysis of Projections by Sequencing
MB	Mushroom Body
MCFO	Multicolor FlpOut
mGluR	Metabotropic Glutamate Receptor
MiMIC	Minos Mediated Integration Cassette
MIP	Maximum Intensity Projection
MMP	Matrix Metalloprotease
mTOR	Mammalian Target of Rapamycin
Na	Sodium
NATF	Native and Tissue Specific Fluorescence
NB	Neurobiotin
Nrg	Neuroglian
Nrx	Neurexin
NS	Not Significant
PA	Phosphatidic Acid
PBS	Phosphate Buffered Saline
POI	Protein of Interest
PSD-95	Postsynaptic Density 95

PSI	Peripherally Synapsing Interneuron
PTEN	Phosphatase and Tensin Homolog
Pum	Pumilio
Rac	Ras-Related C3 Botulinum Toxin Substrate
RBP	RNA Binding Protein
RGG	Arginine-Glycine-Glycine
Rho	Ras Homolog
RNAi	RNA Interference
ROI	Region of Interest
RSD	Relative Standard Deviation
SEM	Standard Error of the Mean
Sema-1a	Semaphorin-1a
ShakB	Shaking B
Shaw	Shaker Cognate W
Shh	Sonic Hedgehog
SNP	Single-Nucleotide Polymorphism
spGal4	Split-Gal4
STaR	Synaptic Tagging with Recombination
Stau	Staufen
Syb	Synaptobrevin
SynCAM	Synaptic Cell Adhesion Molecule
Syt	Synaptotagmin
TDE	2, 2’ Thiodiethanol
TEA	Tetraethylammonium

TG	Thoracic Ganglia
TRITC	Tetramethylrhodamine Isothiocyanate
Trp	Transient Receptor Potential
TTM	Tergotrochanteral Muscle
TTMn	Tergotrochanteral Motor Neuron
UAS	Upstream Activating Sequence
UPR	Unfolded Protein Response
UTR	Untranslated Region
VNC	Ventral Nerve Cord
WB	Western Blot
WGA	Wheat Germ Agglutinin
WGS	Whole Genome Sequencing
Wnt	Wingless/Integrated

Chapter I

Overview of Dissertation

The goal of this dissertation was to study Fragile X Mental Retardation Protein's (FMRP) roles in neural circuit development and to advance our understanding of Fragile X syndrome (FXS), the human disorder caused by loss of this protein. FXS causes intellectual disability, autism spectrum disorder (ASD) and other neurological impairments, and is therefore a useful model for uncovering treatments for a wide variety of neuropathies (Harris et al., 2008). I performed my work in the *Drosophila* Giant Fiber (GF) neural circuit, which coordinates the escape reflex in response to threatening stimuli (Allen et al., 2006; Boerner and Godenschwege, 2011). More specifically, I used the central Giant Fiber Interneuron (GFI) as a model for neuron development and function due to its large size and amenability to manipulation. My initial experiments were intended to expand on research showing loss of FMRP causes overgrown synaptic connectivity with reduced maturity (Comery et al., 1997; Irwin et al., 2001; Zhang et al., 2001). FMRP is canonically known as an RNA-binding protein and my aim was to identify new target RNAs related to FXS connectivity defects, as well as to study other RNA-binding proteins which may partner with FMRP, such as Pumilio (Pum) and Staufen (Stau; Brown et al., 2001; Darnell et al., 2001, 2011; Dubnau et al., 2003; Vessey et al., 2006; Olesnicky et al., 2012; Pai et al., 2013).

The GFI proved an amenable model neuron and I was able to identify a synaptic overgrowth phenotype in mutants null for the FMRP gene, *Drosophila fragile x mental retardation 1* (*dfmr1*; Wan et al., 2000; Zhang et al., 2001). Pursuing this finding, I asked whether the overgrowth results from increased connections to normal partners or new connections to inappropriate partners. In the process of investigating this using dye injection to determine the GFI synaptic partners, I found that *dfmr1* null neurons take up far more dye than paired controls, a puzzling phenotype that has never been reported

before. This finding was the focus of my first paper, included in this dissertation as Chapter 2 (Kennedy and Broadie, 2017). Another outcome of these dye filling experiments was the identification of several dye-coupled members of the GF circuit which had been previously unreported. A recently published library of Gal4 transgenic drivers, many of which provide near single-neuron resolution, allowed a fine-scale mapping of this expanded GF circuit (Brand and Perrimon, 1993; Jenett et al., 2012; Tirian and Dickson, 2017). The identification of these neurons was the subject of my second paper, included in this dissertation as Chapter 3 (Kennedy and Broadie, 2018).

While publishing these two papers, I continued to study the connectivity overgrowth in the GFI, looking for FMRP targets or RNA-binding proteins that might modulate the phenotype. However, a series of control experiments eventually uncovered a surprising result: the phenotype was not caused by loss of FMRP, but instead by a background mutation in the *dfmr1* null line (*dfmr1*^{50M}*;* Zhang et al., 2001). As this phenotype is central to an important aspect of developmental neurobiology, namely how a neuron regulates synaptic connectivity, I pursued the mutation's identity using whole genome sequencing (WGS). This work is ongoing but is expected to identify a gene that controls synaptogenesis. This work is described in Chapter 4 of this dissertation and is currently being finalized for publication.

While this dissertation work has deviated significantly from the original aims, it has remained true to the broader intent of better understanding neurodevelopment and neuropathies. I discovered a new phenotype caused by loss of FMRP, which may underlie some of the symptoms of the FXS disease state. The expanded GF neural circuit described here characterizes numerous interconnected neurons, which may prove useful for more complex neurodevelopmental studies than have been possible before. And finally, the work on the synaptogenic gene mutation found in the background of the *dfmr1*^{50M} allele not only may open up a new set of targets with which to study synaptic growth and regulation, but also provides a cautionary tale on the background mutations that can accumulate in commonly used genetic lines. The remainder of this introduction provides background on the extensive literature on FXS, the GF

neural circuit, and synapse localization mechanisms. I then conclude with an outline of the remaining chapters.

Fragile X Syndrome

FXS is caused by the loss or inactivation of the *fragile X mental retardation 1* (*FMR1)* gene and occurs in approximately 1:7,000 males and 1:11,000 females (Hunter et al., 2014). FXS is the leading known genetic cause of ASD and intellectual disability, and subsets of patients also present with attention deficits, anxiety, hyperactivity, childhood seizures, depression, elongated facial features, large ears and macroorchidism (Bailey et al., 2008). The *FMR1* gene was first cloned in 1991 and has since been the subject of enormous study (Dietrich et al., 1991; Willemsen and Kooy, 2017). The majority of FXS cases are caused by a CGG triplicate expansion in the 3' untranslated region (UTR) of the gene (Fu et al., 1991). Unaffected members of the population have 50 or fewer of these repeats, while those with 200 or more manifest the disorder, due to hypermethylation of the CGG repeats leading to gene silencing (Oberlé et al., 1991). Intermediate numbers of repeats are considered a "pre-mutation condition," and are associated with disabilities, such as Fragile X-Associated Primary Ovarian Insufficiency (FXPOI) and Fragile X-Associated Tremor/Ataxia Syndrome (FXTAS, Jacquemont et al., 2007; Hunter et al., 2008). Several point mutations and deletions have also been uncovered that cause FXS by disrupting functional domains in the protein (Feng et al., 1997a; Myrick et al., 2015).

Within neurons, FMRP localizes primarily to the cell body where it resides in the cytosol and traffics to and from the nucleus (Feng et al., 1997b; Doll and Broadie, 2015; He and Ge, 2017). FMRP is also observed in large protein/RNA granules trafficking along dendrites and into synaptic terminals (Fig. **1**, Kanai et al., 2004; Antar et al., 2005). Axonal growth cones contain FMRP and some research suggests FMRP is present in mature axons as well, though this remains contentious (Antar et al., 2006; Price et al., 2006; Akins et al., 2017). FMRP expression in Glia has been observed to also play a role in neural

development, but this work is still in the early stages of research (Higashimori et al., 2013, 2016; Connor et al., 2017). The primary model organisms used for FXS research are mice and *Drosophila.* Zebrafish and *Xenopus* FXS models exist, but they are less well studied, with fewer than 10 total publications for each at the close of 2018. *C. elegans* interestingly does not appear to contain an *FMR1* homolog, suggesting FMRP arose after brain evolution and specialization were well underway (Shtang et al., 1999).

The enormous amount of research into FMRP function can be categorized in different ways. For this dissertation, I have summarized the research in four categories; 1) FMRP as an RNA-binding protein, 2) FMRP as a channel-binding protein, 3) activity-dependent FMRP roles, and 4) clinical FXS treatment.

FMRP: RNA-Binding Functions

FMRP was originally characterized as an mRNA-binding protein and is currently recognized to have at least three RNA-binding domains: two heterogeneous nuclear ribonucleoprotein (hnRNP) K Homology (KH) domains and an Arginine-Glycine-Glycine (RGG) box (Ashley et al., 1993; Siomi et al., 1993, 1994; Darnell et al., 2005a). There is also reported to be a less well understood RNA-binding domain at the FMRP N-terminus (Adinolfi et al., 2003; Zalfa et al., 2005). The initial discovery that FMRP binds mRNA set off a search to determine target transcript(s), with the hope that misregulated expression could be corrected in clinical treatments. Unfortunately, multiple studies using a range of techniques have shown FMRP binds a long list of RNAs, with one early study showing up to 4% of brain RNAs are bound (Ashley et al., 1993). More recent studies have identified upwards of 900 putative mRNA targets (Brown et al., 2001; Darnell et al., 2011; Ascano et al., 2013). While overwhelming, these target lists provided candidates that could be studied in model organisms missing the *FMR1* gene. The initial model established was the mouse *FMR1* knockout, generated in 1994 by a Dutch-Belgian consortium (The Dutch-Belgian Fragile X Consorthium et al., 1994). A *Drosophila* FXS model was later developed in 2000 and has been instrumental in studying the disease (Wan et al., 2000; Zhang et al., 2001). Humans and mice both have two FMRP paralogs, Fragile X

Mental Retardation Syndrome-Related Protein 1 and 2 (FXR1 and 2), which interact with FMRP and can also bind RNA (Tamanini et al., 1997; Spencer et al., 2006; Darnell et al., 2009). *Drosophila* has only the single *dfmr1* gene and no known paralogs (Siomi et al., 1995; Zhang et al., 1995; Wan et al., 2000). The genetics of FMRP are further complicated by splicing: humans have at least five coding isoforms of the FMR1 gene, while flies have six, not including a large number of UTR isoforms (Flybase.org, 12/3/18; NCBI.NLM.NIH.gov 12/3/18). The roles of these many isoform are largely unknown.

Over the course of nearly three decades of research on FMRP RNA-binding capabilities, three major results have emerged. First, the vast majority of target genes studied show increased expression when FMRP is lost, indicating FMRP acts primarily as a translational repressor (Brown et al., 2001; Darnell et al., 2001, 2005a; Phan et al., 2011; Niere et al., 2012; Gkogkas et al., 2014). However, exceptions exist including a list of very long RNAs, the postsynaptic scaffold Postsynaptic Density Protein 95 (PSD-95) and Diacylglycerol Kinase, Kappa (DgkK), all of which are cases of FMRP promoting expression as a translational activator (Zalfa et al., 2007; Bechara et al., 2009; Tabet et al., 2016; Greenblatt and Spradling, 2018). Reduced DgkK expression in *FMR1* nulls has been proposed as the actual culprit in the loss of translational repression, as it acts in the Diacylglycerol (DAG) to Phosphatidic Acid (PA) conversion pathway thought to control general protein translation (McMahon and Rosbash, 2016; Tabet et al., 2016). Importantly, this argument suggests *DgkK* RNA is the primary FMRP target, and all others are false positives. However, this contradicts observations that FMRP binds the ribosome and can impede its procession along RNA, which has been suggested to be one mechanism of FMRP translational repression (Fig. **1**, Darnell et al., 2011). Moreover, a wide range of independent studies have shown FMRP binding transcript targets (Kim et al., 2009; Yan and Denman, 2011; Braat et al., 2015).

The second result that has emerged is that FMRP uses a complex method to discriminate mRNA targets, which has thus far eluded researchers (Veneri et al., 2004; Darnell et al., 2005b). No agreed consensus binding sequence exists, although several motifs have been found, including UGGA, ACUK and

GAC (K = G or U). However, these motifs are not well agreed upon, nor complex enough to specifically delineate FMRP targets. Some work suggests high numbers of these motifs recruit sufficient FMRP to mediate its role in repression (Ascano et al., 2013; Ray et al., 2013; Suhl et al., 2014; Anderson et al., 2016). G-quartets and uridine tracts have also been suggested as guiding sequences, but again these structures are not specific to FMRP targets or present in all targets (Chen et al., 2003; Dolzhanskaya et al., 2003; Ramos et al., 2003). One difficulty in these experiments is that the list of FMRP targets is still indeterminate, thus preventing robust study. A consensus has also not been reached on the RNA region bound by FMRP, with groups separately finding either the UTR or the coding sequence is the primary target (Brown et al., 1998; Sung et al., 2003; Darnell et al., 2011; Ascano et al., 2013; Zhang et al., 2014b; Anderson et al., 2016). The lack of a target sequence has created speculation that FMRP uses other mechanisms to regulate transcripts. There is work showing FMRP acts via RNA interference (RNAi) machinery, and other forms of untranslated RNA, such as Brain Cytoplasmic RNA 1 (BC1), to block translation (Zalfa et al., 2003; Jin et al., 2004). Partner RNA-binding proteins (RBPs) such as Pum and Stau have been suggested as well, and have been shown to interact with FMRP at genetic, cellular and behavioral levels, but not yet in molecular terms (Barbee et al., 2006; Elvira et al., 2006; Wells, 2006; Bolduc et al., 2008; Sialana et al., 2016; Zhang et al., 2017). It is known that FMRP coexists with several RBPs in RNA granules, mobile conglomerations of RBPs, RNA, ribosomes and scaffolds which bind motor proteins and are trafficked along the neuronal cytoskeleton (Fig. **1**; Anderson and Kedersha, 2006; Thomas et al., 2011).

The third result that has emerged is that restoring many presumptive FMRP targets corrects FXS phenotypes. For example, corrected expression of Microtubule Associated Protein 1B (MAP1B, *Drosophila* Futsch), Charged multivesicular body protein 4A (Chmp4, *Drosophila* Shrub), matrix metalloproteases (MMPs), adenylyl cyclase, DAG kinase and others have ameliorated a range of phenotypes in mouse and *Drosophila* FXS disease models (Zhang et al., 2001; Lu et al., 2004; Siller and Broadie, 2011; Tabet et al.,

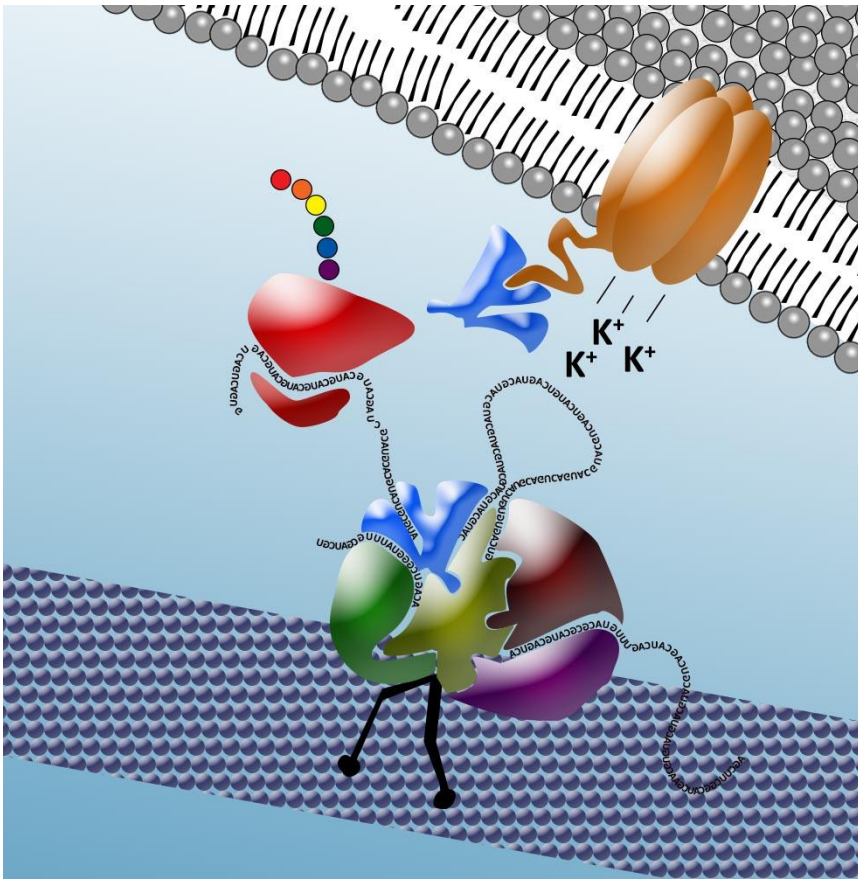

Figure 1. FMRP's Roles in the Neuron
FMRP (blue) travels in RNA granules with other RNA binding proteins (green, yellow, purple, dark red). These complexes are carried along the microtubule cytoskeleton attached to motor proteins such as kinesin (black). By stalling ribosomes (red) along mRNA, FMRP can repress translation. FMRP also regulates ion channels, such as Slack (orange), increasing their ion conductivity.

2016; Sethna et al., 2017; Vita and Broadie, 2017). Frequently studied phenotypes include brain morphology, synaptic architecture, calcium signaling, long term potentiation and depression (LTP and LTD), learning and memory, anxiety, repetitive behavior, hyperactivity and seizures (Irwin et al., 2001; Nimchinsky et al., 2001; Bear et al., 2004; Bolduc et al., 2008; Gatto and Broadie, 2008; Spencer et al., 2011; Gholizadeh et al., 2014; Koga et al., 2015; Ruby et al., 2015; Doll and Broadie, 2016; Tian et al., 2017). Published studies often correct one FMRP target and find restoration of a subset of the known phenotypes. It is difficult to reconcile how so many different proteins can seemingly treat FXS in model organisms, but two possibilities might explain these results. First, targets may operate within overlapping pathways, and correcting one target may modify or stabilize multiple targets leading to the finding that multiple proteins can rescue the same phenotype (Bear et al., 2004; Sharma et al., 2010; Tabet et al., 2016). Second, the wide variety of disruptions seen in FXS means researchers could be rescuing some phenotypes with their experiment, but not others (Strumbos et al., 2010; Portera-Cailliau, 2011). In

this case, the many FXS rescues in the literature are only partial, correcting a subset of the disrupted pathways.

It is tempting to link all of the FXS symptoms together, suggesting, for example, that altered neuronal activity is due to overelaborated synaptic connectivity and is the root of weakened memory, seizures and hyperactivity; but it is worth remembering that FXS patients do not have homogenous symptom profiles (Bailey et al., 2008). Correcting one misregulated pathway may partially or completely fix one FXS phenotype, while leaving others uncorrected, and the total correction of the disorder may require repair of many separate pathways. The range of FXS severity suggests a third possibility to explain the disparate findings noted above: FXS is caused by the interaction of FMRP loss and other background mutations. This idea is supported by findings that different mouse strains display different *FMR1* null phenotypes (Dobkin et al., 2000; Spencer et al., 2011). This could complicate the analysis of some of the rescue experiments mentioned above: clean genetic backgrounds in the mice and flies carrying the rescue construct could unintentionally mask background mutations, reducing phenotypes and emulating rescue (Burgess, 2011; Chandler et al., 2013). Overall, the disparate findings across FXS research may be reconcilable by attempting to place the many "verified" FMRP targets in common pathways and identifying core proteins responsible for specific phenotypes. Furthermore, background effects must be carefully accounted and controlled for to either remove modifiers or identify and bring them into the FXS disease model as potential therapeutic targets themselves.

FMRP: Channel-Binding Functions

Compared to well established RNA-binding roles the FMRP channel-binding function is a relatively new discovery, and the full implications have not yet been determined. FMRP has been shown to regulate expression levels of ion channels by RNA-binding mechanisms, but in 2010 it was found that FMRP also has a direct protein-protein interaction with the sodium-activated potassium channel Slack (Fig. **1**, Brown

et al., 2010; Strumbos et al., 2010; Lee et al., 2011; Zhang et al., 2012). Later research showed that Big Potassium (BK) calcium-activated potassium channels also directly interact with FMRP (Deng et al., 2013; Zhang et al., 2014a). FMRP interaction with Slack causes an increase in the open state of the channel, helping to hyperpolarize neurons through increased net conductance. Therefore, FMRP loss may leave neurons more sensitive to stimulation, which is a phenotype often reported in FXS disease models (Zhang et al., 2012; Contractor et al., 2015). FMRP is also known to increase BK channel conductance, though researchers believe this is accomplished by increasing the sensitivity to calcium (Deng et al., 2013; Zhang et al., 2014a). BK channels shape action potentials by releasing potassium in response to high calcium levels (Contet et al., 2016). At presynaptic terminals they help end neurotransmitter release by terminating action potentials and repolarizing the neuron. The loss of FMRP causes action potential broadening as the BK channels are slower to respond to calcium influx, and thus delay repolarization (Deng et al., 2013). Interestingly, there is little to no strong evidence showing FMRP exists in mature axon terminals, indicating the interactions may be with somatic or dendritic BK channels, though several experiments have suggested this is not the case (Deng et al., 2013). Future studies may require enhanced imaging techniques to reveal FMRP at presynaptic sites or further examination of the FMRP-BK channel interaction in other neuronal compartments (Bock and Stuart, 2016). Lastly, FMRP has been shown to interact with the neuronal N-type voltage gated calcium channel, $Ca_v2.2$ (Ferron et al., 2014). Again, this interaction is shown to be direct, rather than RNA mediated; however, in contrast to the potassium channels, it appears FMRP does not regulate the biophysical properties of $Ca_v2.2$. Instead, FMRP participates in escorting the channel to the proteasome for degradation. When FMRP is lost $Ca_v2.2$ degradation is diminished and levels increase. As $Ca_v2.2$ regulates synaptic vesicle release, one consequence of FMRP loss is increased vesicle exocytosis, which could be one source of the hyperexcitability seen in FXS models and patients (Turner et al., 1993; Bailey et al., 2008).

The FMRP-channel interaction raises the question of what role this function plays in the FXS disease state. A recent paper suggests loss of the channel interaction is responsible for intellectual disability and seizures in FXS patients. The authors identified a novel mutation in the FMRP coding sequence in an FXS patient that disrupts the segment of the protein responsible for binding to BK channels. Importantly, this FMRP single nucleotide polymorphism (SNP), R138Q, retains RNA binding capabilities thus suggesting channel binding is a critical part of FMRP function (Myrick et al., 2015). Separately, another human FMRP SNP, I367N, has been identified that blocks FMRP-ribosome interaction but does not impair channel binding. The patient with this mutation also displayed severe intellectual disability, seizures and other typical FXS symptoms. This suggests FMRP's regulation of both RNA and channels is required to avoid neurological disorders (De Boulle et al., 1993; Feng et al., 1997a). It remains to be seen whether there is a functional association between the FMRP RNA-binding and channel-binding roles. One possibility is that these roles exist in separate compartments (pre- vs. postsynaptic), and separately impact cognitive development and function. Alternatively, these two functions may be linked, and FMRP presence on channels positions it to sense activity and alter RNA translation in response (Ferron, 2016). Such an interaction would be well in line with research on FMRP responses to neuronal activity.

FMRP Response to Activity

Over time a consensus has emerged that the primary function of FMRP is to regulate protein translation in response to neuronal activity, acting as an on-demand dispenser of new synaptic proteins (Zalfa et al., 2003; Weiler et al., 2004; Price et al., 2006). As noted above, this seems at odds with the vast bulk of FMRP concentration being in the soma rather than in neuronal processes or at synapses (Tang et al., 2001; Doll and Broadie, 2015). In addition, FMRP binds a wide array of disparate transcripts, and the majority of these target mRNAs are not localized to synapses or known to be involved in activity-

dependent processes. Moreover, several studies have identified roles for FMRP in the neuronal soma and nucleus, albeit these studies are in the distinct minority (Shamay-Ramot et al., 2015; Filippini et al., 2017; Guo et al., 2017; Zhou et al., 2017). It remains to be seen whether FMRP's critical neurodevelopmental functions take place at the soma or if this is simply a loading station for FMRP to pick up mRNAs and carry them into processes for activity-dependent translation.

The metabotropic glutamate receptor (mGluR) theory posed in 2004 is the most studied mechanism of FMRP activity-dependent translation (Bear et al., 2004). mGluRs respond to specific activity patterns by enacting a protein synthesis dependent form of LTD which leads to the removal of excitatory α-amino-3-hydroxy-5-methyl-4-isoxazolepropionic acid (AMPA) glutamate receptors from the postsynaptic membrane (Snyder et al., 2001; Xiao et al., 2001). Removal of AMPA receptors weakens, and can lead to removal of, synapses (Schikorski and Stevens, 1997; Nusser et al., 1998). According to the mGluR theory, the translation of the proteins necessary for AMPA removal is regulated by FMRP. The theory suggests activity triggers liberation of RNAs from FMRP control, permitting their translation and beginning the process of synaptic degradation. Importantly, FMRP represses its own mRNA, which is included in the liberated targets (Brown et al., 1998). The newly synthesized FMRP begins to repress the mRNAs again and terminates AMPA receptor removal, which is termed end-product inhibition. When FMRP is absent, the process becomes uncontrolled and excessive synaptic removal results, presumably leading to the immature synapses seen in human patients (Hinton et al., 1991). It seems likely other proteins are capable of at least partially regulating this process, otherwise no synapses would form in FMRP's absence. Studies have also suggested FMRP is an intermediary between mGluR signaling and mammalian Target of Rapamycin (mTOR) and Extracellular-Signal Regulated Kinases (ERK). These proteins control complex signaling pathways, including regulating RNA translation via members of the translation machinery such as eukaryotic initiation factor complex 4F (eIF4F; Sharma et al., 2010; Sawicka et al., 2016; Ehyai et al., 2018). Both pathways have been shown to be hyperactivated when FMRP is lost, and their

inhibition can correct FXS model phenotypes (Wang et al., 2012; Richter et al., 2015; Sawicka et al., 2016). The overarching mGluR theory was supported by several studies in mouse and fly models, which show genetic and pharmacological approaches to reduce mGluR activity can correct FXS phenotypes (McBride et al., 2005; Yan et al., 2005; Pan and Broadie, 2007; Pan et al., 2008). However, clinical trials designed to transition this theory into a human treatment have thus far been unsuccessful. The mGluR antagonist Mavoglurant (AFQ056) failed to provide significant improvement in FXS patients (Jeste and Geschwind, 2016). This result is not necessarily a repudiation of the mGluR theory (see below), but does mirror a string of failed clinical trials, suggesting the many roles of FMRP will not be so easily corrected (Erickson et al., 2017).

How does FMRP respond to activity? The protein is regulated by several phosphorylation sites, including the well-studied S500 site (S499 in mice, S406 in *Drosophila*; Ceman et al., 2003; Bartley et al., 2016). Dephosphorylation of S500 permits translational activation and is accomplished through protein phosphatase 2A, which can be activated by stimulated membrane receptors (Narayanan et al., 2007). Phosphorylation of S500 is believed to trigger translational repression by FMRP (Coffee et al., 2012). This function is controlled by the kinases Casein Kinase II and p70 S6 kinase 1, and possibly others (Narayanan et al., 2008; Bhattacharya et al., 2012; Bartley et al., 2016). Recent research suggests sumoylation also contributes to FMRP activation (Khayachi et al., 2018). Each of these identified interactions, while complicating the picture of what FMRP does and how it functions, have provided potential therapeutic targets for future FXS treatment drug development.

Clinical Studies on FXS

The complex interactions of FMRP identified thus far have suggested numerous targets that might be susceptible to pharmacological treatment, resulting in many FXS clinical trials (Darnell and Klann, 2013). Targets have included mGluR antagonists (e.g. Mavoglurant, Basimglurant), GABA receptor

agonists (e.g. Arbaclofen, Riluzole), MMP inhibitors (e.g. Minocycline), and ERK/mTOR pathway modulators (e.g. Lovastatin, Metformin; Bilousova et al., 2009; Erickson et al., 2011; Siller and Broadie, 2011; Osterweil et al., 2013; Ligsay and Hagerman, 2016; Gantois et al., 2017). While some FXS patients have responded positively to treatments, often based on caregiver assessments, overall these trials have been largely unsuccessful in providing statistical improvements in various parameters (Table **1**, Davenport et al., 2016; Erickson et al., 2017). It is unclear why successful treatments in model organisms have not yet been replicated in human patients, though several proposals exist. Model organisms are limited in their ability to replicate human-specific disease traits. Seizures, some forms of memory, and hyperactivity can be assessed fairly well in FXS models, but social and mental disorders such as ASD and intellectual disability are much harder to score. Thus some of the most crucial parts of the disorders scientists are attempting to correct are relatively inaccessible to their research (Watson and Platt, 2012; Sestan and State, 2018).

It can also be difficult to evaluate whether a drug has been effective in treating FXS. As noted above, FMRP loss impinges on many pathways and causes a wide range of symptoms in FXS patients. If these are mediated by separate pathways, distinct measurements may be needed for each symptom. Further, some of these symptoms are part of broad categories. Within intellectual disability should spatial learning or associative learning be monitored? For autistic children, which social or repetitive behavior tests should be applied? As one cannot tell which outcomes the drugs might improve, it is difficult to know what to assay when designing trials (Berry-Kravis et al., 2013). Another difficulty is determining when to treat. For ethical reasons, very few clinical trials have been conducted on children under the age of 5, but it could be that those are the only treatable timepoints for FXS (Caldwell et al., 2004; Jacquemont et al., 2014). FMRP levels peak very early in development suggesting a specific role in brain formation (Lu et al., 2004; Tessier and Broadie, 2008; Pacey et al., 2013). Much of the current FXS model research is conducted using rescue treatments that are present from conception. Because of this, it is unclear whether FMRP

roles are developmental, during adult function or both, leaving drug developers with the question of when treatment needs to be applied to maximally correct the disorder. Can pharmaceuticals applied to adults correct FXS, or must the treatment be given *in utero*? Some studies have addressed this timing issue; however, they are split on the answer with some suggesting correction is possible in adults (e.g. Michalon et al., 2012; Dolan et al., 2013; Sun et al., 2016), and others showing intervention must come during development (Doll and Broadie, 2016).

Perhaps a more promising approach than drug treatment is the emerging possibility of genomic editing, which has the potential to clip away the excess *FMR1* CGG repeats or correct SNPs to treat the disorder. Such treatment would have to overcome numerous technical and ethical challenges, but is making rapid progress (Park et al., 2015; Yrigollen and Davidson, 2019). Despite a single protein being the root cause of FXS, research into treating the disorder has been stymied by the extraordinary degree of complexity surrounding this protein. FMRP not only interacts with potentially hundreds of RNAs, but also directly regulates channels, and perhaps sits within the inner circle of extremely complex signal transduction pathways. Still, the field has made extraordinary gains in identifying FMRP roles in the brain and has come to understand much about autism and intellectual disability along the way. Many new drugs are in the pipeline which target newly identified FMRP pathways and researchers are optimistic that we are nearing a viable treatment despite past disappointments.

Drug	Mechanism of Action	Test Subject Age	Clinical Trial Status
Donepezil	Acetylcholine esterase inhibitor	12+	Complete
Ampalex	AMPA receptor positive allosteric modulator	18-50	Complete
Arbaclofen	GABA receptor agonist	5-50	Complete
Ganaxolone	GABA receptor positive allosteric modulator	13-22	Complete
Trofinetide	Insulin like growth factor analog	12-45	Complete
Basimglurant	mGluR5 negative allosteric modulator	5-50	Complete
Oxytocin	Oxytocin receptor agonist	13-29	Complete
Aripiprazole	Serotonin receptor agonist, Dopamine receptor agonist/antagonist	5-35	Complete
Metadoxine	Serotonin receptor antagonist, GABA transaminase inhibitor	6-40	Complete
Zoloft	Serotonin transporter inhibitor (SSRI)	2-6	Complete
Riluzole	Sodium channel inhibitor	18+	Complete
ZYN002	Cannabinoid receptor agonist	3-18	Ongoing
Gaboxadol	GABA receptor agonist	13-22	Ongoing
AZD7325	GABA receptor positive allosteric modulator	18-50	Ongoing
Acamprosate	GABA receptor positive allosteric modulator, NMDA receptor antagonist	5-55	Ongoing
Mavoglurant	mGluR5 antagonist	3-45	Ongoing
Minocycline	MMP9 inhibitor	3.5-55	Ongoing
Metformin	MMP9 inhibitor, ERK signaling inhibitor	10-17	Ongoing
Lovastatin	ERK signaling inhibitor	6-55	Ongoing
BPN14770	Phosphodiesterase allosteric modulator	18-45	Ongoing
Epigallocatechin Gallate (ECGC)	Undetermined	6-60	Ongoing
Vitamin C, E	Undetermined	1-18	Ongoing

Table 1. A Summary of Clinical Trials Performed for FXS.
Clinical trials have been run for numerous drugs that target pathways associated with FMRP. Most studies have not resulted in beneficial outcomes for patients and have been abandoned. Some of the ongoing trials have shown promising results but are still in early stages. Pharmaceutical treatment has been attempted as early as 2 years of age to correct developmental disruptions. Data compiled from www.clinicaltrials.gov (accessed 2/1/19).

The *Drosophila* Genetic Model System

This dissertation research was performed using the *Drosophila* genetic model, which is simple enough to assay single genes in single neurons, yet complex enough to have intricate brain organization and sophisticated behavioral outputs. The ~10-day lifecycle and large populations of *Drosophila* permit a wide range of genetic manipulations. The embryo develops for one day in the egg before hatching and entering the larval stage. The larvae go through three developmental stages, termed instars, with the first two instars lasting one day each and the third instar lasting two days. The larval stage is followed by a four-day pupal stage after which the adult ecloses and becomes sexually mature within eight hours. *Drosophila* genetics are relatively simple, with ~14,000 protein-coding genes on 4 chromosomes. Despite having fewer proteins than humans, *Drosophila* has homologs for ~75% of human disease causing genes (Reiter et al., 2001). One result of this slim genome is far fewer paralogs for each gene. For targets of FMRP, the reduced paralogs make for easier manipulations. MMPs for example are represented by 2 genes in the fly, 24 in mice and 23 in humans (Page-McCaw et al., 2007; Dear et al., 2017). Similarly, *Drosophila* have 8 gap junction genes, part of the innexin family, while humans have gap junctions from two families: 3 genes for the closely related pannexins and 21 genes in the connexin family (Stebbings et al., 2002; Söhl and Willecke, 2003; Baranova et al., 2004). These simplifications help in manipulations of the nervous system such as, for example, determining and removing gap junctions expressed in a neuron of interest.

The *Drosophila* genome is amenable to a myriad of manipulations. Mutagenesis was originally carried out by chemical or physical assault on DNA but was later simplified by the discovery of P-element transposons that can be inserted randomly into the genome (Spradling and Rubin, 1982; Price, 2005). These transposons can be imprecisely excised to create small mutations, such as the $dfmr1^{50M}$ mutation used in this work (Rorth et al., 1998; Zhang et al., 2001; Kennedy and Broadie, 2017). P-elements have a preference for 5' insertion in genes and typically avoid introns (Bellen et al., 2004; Aleksic et al., 2009).

Other transposons, such as Minos elements, are helping to probe more of the genome (Venken et al., 2011). Of course, the Clustered Regularly Interspersed Palindromic Repeats (CRISPR) technique has obviated these strategies, making targeted *Drosophila* genome editing precise and routine (Jinek et al., 2012; Gratz et al., 2013). Naturally, many mutations block viability or fertility, and balancer chromosomes are used to circumvent this problem (Casso et al., 1999). A lethal or infertile mutation of interest is maintained in a heterozygous state over a balancer which has its own lethal mutation. As neither chromosome can propagate as a homozygote, the mutation of interest in maintained over generations. Dominant markers make it easy to select for or against the balancer in genetic crosses. Balancer inversions block genetic recombination by interfering with chromosome alignment, thus preventing the shedding of deleterious mutations.

Another powerful *Drosophila* resource is the binary Gal4/Upstream Activating Sequence (UAS) system, a yeast transcription factor/enhancer element pair that allows all manner of transgenic manipulations (Brand and Perrimon, 1993). The Gal4 sequence downstream of an enhancer region of interest drives expression in target cells (Mlodzik and Hiromi, 1992; Jenett et al., 2012). The UAS responder is linked to a protein coding or RNAi sequence, both of which are available for a wide range of genes (Dietzl et al., 2007; Ni et al., 2009). Endogenous genes, with or without tagged fluorophores, enable studies of rescue, localization and function (Zhang et al., 2002; Christiansen et al., 2011; Chen et al., 2014). Exogenous genes allow structural studies (membrane green fluorescent proteins (GFPs)), functional manipulations (channelrhodopsins (ChRs)), and calcium recordings (GCaMP), permitting exquisite cellular experiments (Nagel et al., 2003; Pfeiffer et al., 2010; Akerboom et al., 2012). Recently, two groups have made an enormous effort to randomly insert small Gal4 enhancer elements into individual fly lines and screen UAS-*gfp* expression patterns across the brain (Jenett et al., 2012; Tirian and Dickson, 2017). This has resulted in a collection of Gal4 drivers that can express in small subsets of neurons, even single cells, opening new avenues for circuit mapping, developmental studies and neuron-neuron interactions. This

technology was further expanded by creating split-Gal4 (spGal4) versions of many of these lines. spGal4s operate by expressing the DNA binding half and RNA polymerase recruiting half of Gal4 under separate enhancers, requiring an overlapping expression pattern to form a complete Gal4, thus greatly reducing the neurons targeted (Luan et al., 2006; Pfeiffer et al., 2010).

In terms of neurodevelopment, the *Drosophila* brain provides an excellent model for research. *Drosophila* have ~100,000 neurons, which is much more tractable than the ~70 million found in mice (Herculano-Houzel et al., 2006; Chiang et al., 2011). Even with relatively few neurons, flies demonstrate a diverse behavioral repertoire controlled by fairly complex, but accessible, neural circuits (O'Kane, 2011; Kennedy and Broadie, 2018; Namiki et al., 2018). The high density of the central nervous system (CNS) means flies still must solve complex developmental problems such as axon pathfinding and target selection in a crowded arena, providing an accessible way to study such processes at high resolution. Moreover, rapid development makes the *Drosophila* brain amenable to live imaging of neuron formation and maturation. *Drosophila* is even beginning to challenge *C. elegans*, with a full mapping of all of the brain neurons and their synapses in the works (Zheng et al., 2017). Hence *Drosophila* provides a particularly attractive model for neurodevelopmental research and neurological disease modeling. Within the *Drosophila* nervous system, one of the best models for studying individual neuron formation and function is the Giant Fiber Circuit.

***Drosophila* Giant Fiber Circuit**

The *Drosophila* GF neural circuit, first described by Maxwell Power in 1948, is an escape reflex arc like those found in a range of invertebrates, from squid to cockroach (Hodgkin and Huxley, 1939; Power, 1948; Keegan and Comer, 1993). The circuit rapidly carries information about threatening stimuli from sensory modalities to muscles, enabling a quick escape behavior (Pézier et al., 2014). GF neurons have been used extensively to study neurodevelopment and model human neuropathies including FXS,

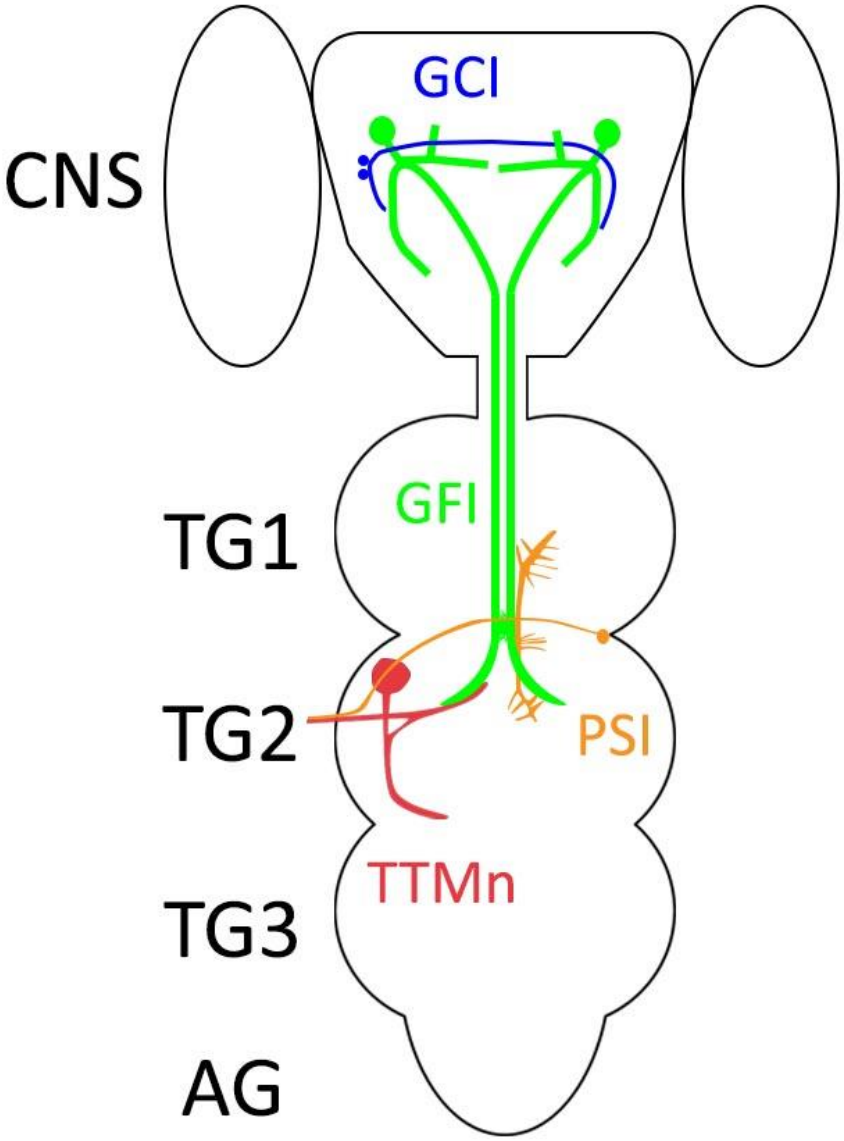

Figure 2. Map of the Known Giant Fiber Circuit

This cartoon represents the known neurons of the GF circuit prior to the work described in this dissertation. The Giant Commissural Interneuron (GCI, blue) interconnects the paired Giant Fiber Interneurons (GFI, green) in the Central Nervous System (CNS). The GFI axons descend into the Ventral Nerve Cord (VNC), which is composed of three Thoracic Ganglia (TG1-3) and an Abdominal Ganglion (AG). The GFI axons synapse on the Peripherally Synapsing Interneuron (PSI, orange) at the Inframedial Bride (IB), and the Tergotrochanteral Motor neuron (TTMn, red) along large axonal bends. All of these neurons are bilaterally symmetric, but only the GFIs are shown as such here for clarity. Not pictured are sensory neurons upstream of the GFI/GCI which activate the circuit in response to threatening stimuli, and the DLMns which control the wings.

tauopathies and L1 syndrome (Tanouye et al., 1981; Martinez et al., 2007; Kudumala et al., 2013; Lee and Godenschwege, 2014; Orr et al., 2014; Kadas et al., 2019). These studies take advantage of the known synaptic connectivity, established electrophysiology recording paradigms, and large neuron size. The GF circuit also contains numerous genetically tractable interneurons which permit the study of neuron-neuron interactions at single cell resolution.

The GF circuit architecture begins with visual, auditory and mechanical sensory organs collecting information on threatening stimuli, which is then passed to the central brain GFIs, the paired central interneurons which conduct responses downstream (Fig. **2**, Allen et al., 2006; Pézier et al., 2014). The GFIs are interconnected by the Giant Commissural Interneurons (GCI) through mixed chemical/electrical synapses, which are believed to create a balanced response on both sides of the body. Each GFI projects an axon into the ventral nerve cord (VNC) where they come together at the posterior end of thoracic ganglion segment 1 (TG1) to form the Inframedial Bridge (IB). The axons then move latterly apart to terminate in large bends. These bends are the sites of synaptic output to the Tergotrochanteral motor neuron (TTMn), which controls the jump reflex of the central legs. The IB is a site of multiple small extensions from the GFI, and the location of mixed chemical and electrical synapses on the Peripherally Synapsing Interneuron (PSI). The PSI connects through a cholinergic synapse to the Dorsal Longitudinal Motor neurons (DLMns), which control the wing depressing muscles (Mejia et al., 2013).

Several characteristics of the GF circuit make it appealing for studying neurodevelopment, including the large diameter neurons (Allen et al., 1998). As flies lack the myelin sheathing found in vertebrates, they use large neuron calibers to increase transmission speed. The GFI neurons are so large relative to the other *Drosophila* neurons that they can be individually recognized under a 10x microscope objective. This size offers two benefits. First, the GF neurons are easily targeted and manipulable, allowing access via glass electrodes which can deliver dye or other molecules. Dye injections rapidly label the entire neuron, with no requirement of transgenic labels such as GFP. As the GFI contains electrical synapses,

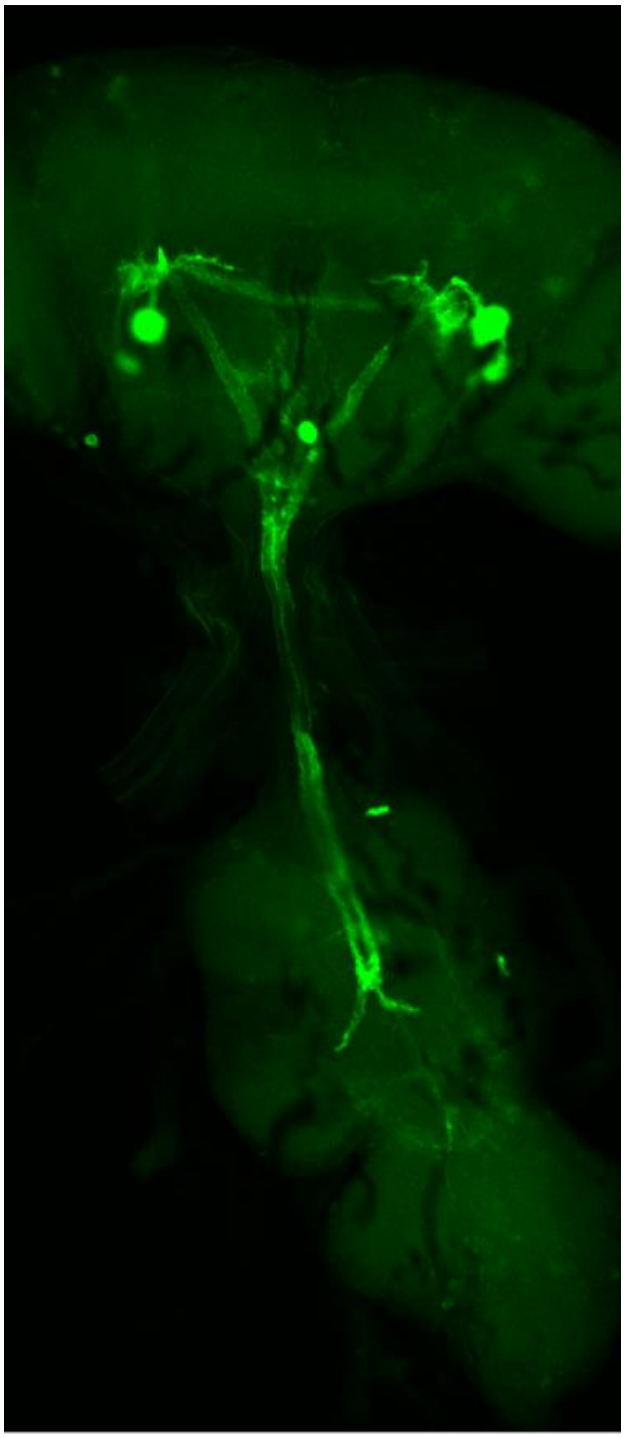

Figure 3. Gal4 Driven Expression of mCD8::GFP in the GFI
The 91H05-Gal4 driver expresses strongly and specifically in the GCI and GFI. The GCI runs horizontally across the CNS to interconnect the GFI. The large GFI cell bodies form dendrites in the CNS and send axons into the VNC, where they briefly contact at the IB and then diverge to form the characteristic bends.

small tracers can also be injected to map connected neurons (Boerner and Godenschwege, 2011). Second, the size of the GF neurons makes characterization and quantification much easier, allowing for rapid and confident assessment of diameters, synaptic sites, and structural abnormalities (Mejia et al., 2010; Kudumala et al., 2013; Borgen et al., 2017). These neurons are also genetically tractable, and highly specific Gal4 drivers are available to manipulate each neuron in the GF circuit. Early drivers (such as A307 and C17) were less specific, but still enabled excellent studies on GF circuit development (Phelan et al., 1996; Allen et al., 1999). The Janelia Farms and Vienna *Drosophila* Resource Center collectives have since generated new drivers, which provide near single neuron resolution for most members of this circuit (Fig. **3;** Jenett et al., 2012; Tirian and Dickson, 2017). The motor outputs of the GF circuit also allow electrophysiology characterization. A simple recording can be taken from the two muscle targets of the circuit, providing information on how the circuit develops and functions (Tanouye and Wyman, 1980; Augustin et al., 2011).

The GFI is the best studied GF circuit neuron and has been the central focus of the studies here (Fig. **3**). Bromodeoxyuridine (BrdU) labeling indicates the GFI is born during embryogenesis, although it waits until pupation to begin forming its connections (Allen et al., 1998). Once outgrowth begins, GFI axons reach their TTMn targets within about one day and then spend another day initiating synapse formation. On the last day of pupation the GFI neurons stabilize and mature their synaptic connections. The *bendless* (*ben*) mutation in an E2 ubiquitin-conjugating enzyme causes the GFI axon to terminate at the IB during development, losing its characteristic bend along the TTMn (Thomas and Wyman, 1984; Muralidhar and Thomas, 1993). This transition from axonal outgrowth to synaptogenesis is additionally controlled by the transmembrane cell-adhesion molecule Semaphorin-1a (Sema-1a), which helps guide the axon to postsynaptic partners (Murphey, 2003; Uthaman et al., 2008). Once the axon has arrived it removes Sema-1a from the surface, allowing synaptogenesis to proceed (Godenschwege et al., 2002). Further work indicated that the transmembrane cell adhesion molecule (CAM) Neuroglian (Nrg), located presynaptically on the GFI and postsynaptically on the TTMn, interacts homophilically to signal for Sema-1a removal from the membrane, thus ending pathfinding/target recognition and initiating synaptogenesis (Godenschwege and Murphey, 2008). Interestingly, manipulating these targets only prevents TTMn synapses from forming; PSI synapses at the IB develop normally. This indicates separate membrane proteins dictate synapse formation, even within the same neuron.

The GF circuit also provides an important model for electrical synapse connectivity. As noted above, the GFI connects to most of its targets through mixed chemical and electrical synapses. Electrical synapses transmit an action potential across a synapse almost instantaneously, as compared to ~0.5 milliseconds for chemical synapses (Katz and Miledi, 1965, 1967; Wheatley, 1998). As noted above, the invertebrate gap junction family is referred to as innexins, which are homologous to pannexins in vertebrates (Baranova et al., 2004). Vertebrates also have a larger family of gap junctions known as connexins, which share no sequence homology with the innexins/pannexins, though they are structurally

similar, with four transmembrane domains (Phelan, 2005; Beyer and Berthoud, 2018). Invertebrate gap junctions are typically composed of six innexin subunits which create an innexon hemichannel, although some examples of eight member hemichannels have been reported (Ambrosi et al., 2010). Innexins can form homomeric or heteromeric hemichannels, and gap junctions can be homotypic or heterotypic, depending on whether the pre- and postsynaptic neurons use the same or different innexons. The GF circuit uses the Shaking-B (ShakB) innexin, which is spliced into three isoforms: ShakB(Neural (N)), ShakB(N+16) and ShakB(Lethal (L)). The GFI exclusively expresses ShakB(N+16) to form heterotypic gap junctions with the TTMn and PSI, which both use ShakB(L) (Phelan et al., 2008). These different combinations allow gap junctions to have variable properties, such as restricting flow of certain sized or charged molecules, and determining the direction of ionic flow (Nielsen et al., 2012). The pore size of gap junctions is typically capable of passing up to 1kDa molecules, thus allowing secondary messengers such as calcium and cyclic AMP through (Weber et al., 2004). Gap junctions can also pass dyes through their pores, which has aided efforts to map the GF circuit and study the processes of synapse formation and degradation (Bacon and Strausfeld, 1986; Jacobs et al., 2000; Pézier et al., 2014).

Neural Circuit Mapping

The innate behavior of animals is a result of the wiring pattern in their nervous system. Evolution has long honed these systems to respond optimally to the local environment, creating a diverse repertoire of hard-wired behaviors necessary for acquisition of nutrients, reproduction, and offspring rearing. These innate behaviors contrast with learned behaviors, which are more evolutionarily recent and can be modified throughout life (Tierney, 1986). Researchers have long pursued maps of the neural circuitry responsible for a wide range of behaviors and taken many approaches to do so. An immense effort was made to map of the entire *C. elegans* hermaphrodite brain, which was published in an extensive electron microscopy (EM) study (White et al., 1986). More recently subsets of the *Drosophila* and mouse brain

have similarly been completely mapped (Chiang et al., 2011; Kasthuri et al., 2015; Eichler et al., 2017; Zheng et al., 2017). These mapping projects have several goals, including enabling studies on how different regions of the brain interconnect, how such connectivity has evolved, which circuits deteriorate in neurological disorders, and how neural circuits are assembled and change over time.

Numerous lower resolution circuit maps have contributed greatly to neuroscience research in model organisms. In mice, these circuits range from the hippocampal trisynaptic circuit, composed of the dentate gyrus, CA1, and CA3 and thought to process and store memories, to the optic circuit in the retina, which is responsible for pre-processing incoming visual information (Sanes and Masland, 2015; Stepan et al., 2015). There are also circuits studied for their roles in disease, such as the dopamine neurons of the Basal Ganglia, whose degeneration leads to Parkinson's disease (Rizzi and Tan, 2017). In *Drosophila*, alongside the work performed in the GF circuit, circuit maps connecting the olfactory system to the learning and memory centers of the mushroom body (MB) have helped drive enormous amounts of research on the mechanisms of synaptogenesis and activity-dependent synapse modification (Doll and Broadie, 2015; Golovin and Broadie, 2016; Hige, 2018). Similar to work in the mouse, the circuits of the fly visual system have allowed researchers to examine parallel neural pathways in neurons, and helped to predict and understand the organization found in the more complex vertebrate brains (Lee et al., 2003b; Sanes and Zipursky, 2010). As these circuits are increasingly mapped, more in depth experiments can be performed, such as simultaneously imaging activity in all of the neurons in a circuit to understand information flow (Chen et al., 2012; Prevedel et al., 2014; Streit et al., 2016). The *C. elegans* field is taking advantage of its complete nervous system map in an ambitious project to sequence the RNA in every neuron (Hammarlund et al., 2018). This project should enable comparative studies on individual neurons, providing answers on the transcriptional programs that underlie identities and the specificity of synaptic connectivity. Such experiments foreshadow what will be possible for higher order brains once their neural circuit maps are complete.

Method	Mapping ability	Advantages	Disadvantages
EM Reconstruction	Neurons and their synapses	Complete circuit and synapse map	Expensive, slow
Rabies Virus	Chemically connected partners	Precise; genetically controlled	Mammalian only, slow
Wheat Germ Agglutinin	Chemically connected partners	Simple to use, genetically controlled	Imprecise, may not work
***trans*-tango**	Chemically connected partners	Genetically encoded, reveals first degree partners	Does not work in all neurons
Dye injection	Electrically connected partners	Rapid, cheap	Requires gap junctions and large neurons
MAPSeq	Neuron projection pattern	Rapid, large scale	Expensive, target neurons not identified
GRASP	Confirms synaptic partnerships	Genetically encoded, shows synapse location	Requires knowledge of potential partners
iBLINC	Confirms synaptic partnerships	Genetically encoded, shows synapse location	Requires knowledge of potential partners

Table 2. Summary of Circuit Mapping Methods
Many methods are available for mapping neurons and their synapses, with several of the most commons approaches listed here. More thorough methods are often slower and more expensive, while partners and synapse locations can often be quickly determined by genetic manipulations.

Circuit mapping is accomplished through a number of means, with some of the most common examples summarized in Table **2** (Lichtman et al., 2008). The most thorough but labor intensive and time-consuming is EM reconstruction which reveals neuron architecture and chemical and electrical synapses. As noted above, this was completed for the *C. elegans* hermaphrodite in 1986, while the male was completed much later, in 2012, due to its more complex connectome (White et al., 1986; Jarrell et al., 2012). This approach is accelerating thanks to new serial EM techniques, such as Focused Ion Beam/Scanning Electron Microscopy (FIB/SEM), and automated reconstruction algorithms (Xu et al., 2017; Zhao et al., 2018). While EM techniques can reconstruct the entire nervous system in an unbiased fashion, other approaches typically start with one neuron and identify its synaptic partners, slowly spiraling outwards through the circuit. Rabies virus can be expressed in a neuron of interest and then be tracked as it travels retrogradely across mammalian synapses (Wickersham et al., 2007). Wheat germ

agglutinin (WGA) is another trans-synaptic tracer that can reveal neuronal partners, though its effectiveness is questionable (Braz et al., 2002). More recent techniques have utilized the Gal4/UAS binary expression system to express pre- and postsynaptic transmembrane proteins that only interact in very close proximity. One recent example is *trans*-tango, which is constructed such that interaction of two contacting proteins across a synaptic cleft causes release of the QF transcription factor (which is similar to Gal4) in downstream neurons. QF acts on the QUAS enhancer to turn on a fluorescent protein, thus labeling partners of the neuron of interest (Talay et al., 2017). New partners can be identified by expressing the presynaptic half of the tool in the neuron of interest and the postsynaptic half pan-neuronally. Once the partner neurons' structures are identified, they can be pursued by screening through databases of known neurons (Akram et al., 2018; Otsuna et al., 2018).

Other recent mapping approaches include GFP Reconstruction Across Synaptic Partners (GRASP) and *in vivo* Biotin Labeling of INtercellular Contacts (iBLINC). These techniques can test whether neurons are in close enough proximity to form synapses, identifying neuronal partners. GRASP uses a split GFP system with the two pieces of the protein expressed extracellularly on the membrane of the two potential partners. Contact between the neurons allows the GFP to recombine and fluoresce, signifying closely opposed membranes (Feinberg et al., 2008). iBLINC operates in a similar fashion, but uses a biotin-conjugating enzyme to affix biotin to a proximal acceptor protein, priming it for avidin labeling (Desbois et al., 2015). Both of these techniques have been modified to enhance synapse labeling by fusing them to synaptic vesicle proteins, such as the v-SNARE Synaptobrevin (Syb; Macpherson et al., 2015). Another new technique, Multiplexed Analysis of Projections by Sequencing (MAPseq), harnesses high-throughput sequencing by creating randomly barcoded RNA expressing viral vectors, which are injected into a region of interest (Kebschull et al., 2016). The individual RNA barcodes expressed in each individual cell are trafficked out to axonal processes. The brain can then be dissected into regions of interest, each of which is used to generate an RNA library. Sequencing the libraries from each brain region reveals where the

barcodes localized, thus mapping where each injected neuron projects (Kebschull et al., 2016). Circuit mapping can also be accomplished through dye injection, albeit only in cases where the neurons share gap junctions. Gap junctions are not common in most mature circuits, so this technique is not frequently used; however, it is unparalleled in rapidly revealing connectivity. The original dyes consisted of colorful heavy metals (e.g. cobalt), but much better tools have become available, including lucifer yellow (LY), which is fluorescent, and neurobiotin (NB), which can be stained post-injection by fluorescently conjugated avidin (Levine and Tracey, 1973; Huang et al., 1992; Hanani, 2012).

Mechanisms of Synapse Localization

Neural circuits are formed when neurons project to specific locations, find their targets and create synapses. Integral to this process is the determination of how many synapses to make and how strongly to establish the overall synaptic connection between partners. Each synaptic connection will be modified throughout the life of the animal based on experiences, but the initial connection sets the stage for communication between the neurons (Cline, 2001). Neurons are particular in their synapse placement, restricting synapses to specific zones even if two partners contact multiple times or are in close proximity over long distances (Lin et al., 2001; Ango et al., 2004; Kummer et al., 2006; Kurshan et al., 2018). The reasons for this selectiveness are not entirely clear, but it may be for functional reasons, such as co-localizing inputs from multiple neurons, placing synapses in range of modulatory neurotransmitters, such as serotonin, or positioning postsynapses a certain distance from the soma to manage their signaling strength (Koch et al., 1983; Arnth-Jensen et al., 2002; Williams and Stuart, 2003; Nadim and Bucher, 2014; Boivin and Nedivi, 2018). Synaptic zones may also be determined by temporal coincidence, occurring only at times when neurons are in contact and synaptogenesis occurs (Allen et al., 2006). There are likely many mechanisms controlling synapse localization, and we are just beginning to understand a few basic processes (Fig. **4)**.

Pruning is perhaps the best studied mechanism of determining synaptic localization. Neurons typically build excessive synapses with appropriate and inappropriate partners during development and later trim the excess away, often via activity-dependent synapse elimination (Tessier, 2009; Riccomagno and Kolodkin, 2015; Borgen et al., 2017). This pruning is achieved internally by co-opting proteins from the apoptosis pathway, including caspases (Unsain and Barker, 2015). Extracellularly, glia are recruited to remove unwanted synapses by phagocytosis (Schafer and Stevens, 2013). This process is not easily observable, making it difficult to parse out how much of the synaptic sculpting is due to pruning rather than general retraction of failed axonal outgrowths (Corty and Freeman, 2013). Further, it is unclear how synapses in appropriate partnerships are properly trimmed. It has been difficult to find markers that identify which synapses are to be removed and which should be maintained. Glia can also function as positive reinforcement for synapses. In vertebrate NMJs, glial Schwann cells are necessary for the formation of synapses between the motor neuron and the muscle, thus dictating synaptic zones (Sugiura and Lin, 2011; Darabid et al., 2014). Experiments with central interneurons have shown similar synaptogenic roles for glia (Singh et al., 2016; Farhy-Tselnicker et al., 2017). in *C. elegans*, epithelial cells can perform such roles by using trans-synaptic signaling to encourage synapse formation between neuronal and muscle targets (Shen and Bargmann, 2003).

Synaptic sites can also be sculpted by extracellular morphogens. The extensive Wingless/Integrated (Wnt) family plays important roles in transsynaptic signaling, helping pre- and postsynaptic partners localize and grow their synapses (Budnik and Salinas, 2011; Park and Shen, 2012). Signaling occurs through many receptors, including the canonical target Frizzled (Fz), and leads to clustered synaptic components (e.g. PSD-95 and Bassoon (Bsn)), organized cytoskeletal architecture via microtubule binding proteins (e.g. MAP1B), and activation of synaptogenic modulatory kinases (e.g. Calcium /calmodulin-dependent protein kinase type II (CaMKII), Ciani et al., 2004; Ahmad-Annuar et al., 2006; Farías et al., 2009). Wnts have also been shown to inhibit synapses in specific locations. In *C. elegans*

a high posterior Wnt gradient partially blocks synapse formation along the DA9 motor neuron which controls a muscle used for tail movement. High levels of Wnt cause Fz receptors on the DA9 axon to be endocytosed, which inactivates nearby neurexin (Nrx), a synaptic stabilization protein. Nearby synapses in low Wnt concentrations are unaffected (Klassen and Shen, 2007; Kurshan et al., 2018). An extensive array of other diffusible extracellular proteins are also at play in synapse patterning including Neurotrophins, Cholesterol, TGF-beta and Sonic Hedgehog (Shh), which can act at the local and tissue level (Vicario-Abejón et al., 2002; Salinas, 2003; Goritz et al., 2005; Harwell et al., 2012).

The simplest mechanism for synaptic site selection might be neuronal positioning of transmembrane synaptogenic proteins on the extracellular membrane. However, it still remains unclear how often neurons decide cell-autonomously where to localize their synapses on their own (Ribeiro et al.,

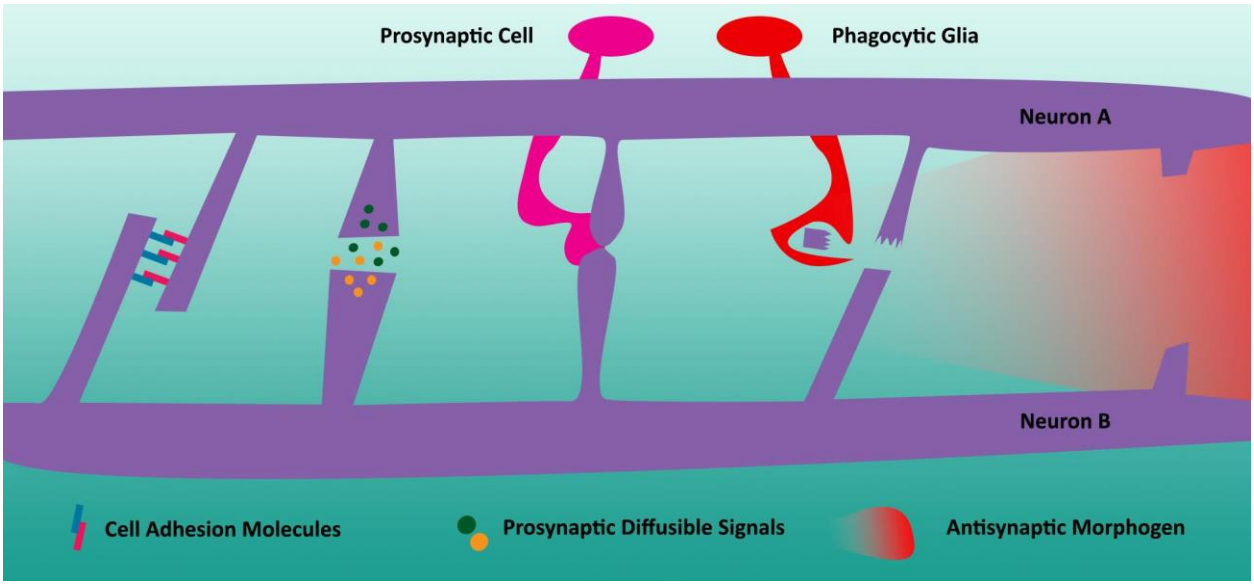

Figure 4. Modulators of Synaptic Formation During Development
Neurons use a combination of mechanisms to localize their synapses and several examples are shown here. Morphogens can provide pro- or antisynaptic guidance, determining synaptic location by the concentration of the gradient. Phagocytic glia can prune away synapses by engulfing the neuronal contact sites. Prosynaptic cells, including glia and epithelial cells can promote synaptogenic contact between neurons. Neurons can also direct their own synapse formation by secreting diffusible signals or by directly contacting each other via cell adhesion molecules.

2018). One known mechanism is to have well-defined sub-regions within the membrane which contain site-restricted synaptogenic proteins. This is the case at the axon initial segment (AIS) of Purkinje neurons, where Spectrin is specifically localized to initiate synapses with GABAeric neurons (Ango et al., 2004). Other proteins involved in synapse initiation, such as Liprin-alpha, Nrx and Synaptic Cell Adhesion Molecule (SynCAM) are known to be a first step in synapse initiation, but there is not yet evidence for them localizing to highly specific sites in neuronal membranes prior to synapse formation the way Spectrin does at the AIS (Scheiffele et al., 2000; Biederer et al., 2002; Patel et al., 2006). In *C. elegans,* Nrx is required for a motor neuron to form synapses with a muscle target, but not a neighboring GABA neuron target. This suggests unique localization may occur to specify this synapse, but Nrx is widely expressed and has not been demonstrated to transit to specific sites prior to synapse formation (Philbrook et al., 2018). Evidence for such prepatterning does exist at muscles, where postsynaptic regions are prepared in anticipation of the incoming neuron (Broadie and Bate, 1993; Jing et al., 2009). It remains to be seen whether neural synaptogenic proteins can accumulate before the partner neuron has arrived, or whether the arrival of the partner or support cells cause such proteins to aggregate.

In summary, neurons have a variety of mechanisms to coordinate where and how strongly to synapse with their targets. The process can be controlled by extracellular morphogens, other cells (such as glia and epithelial cells), and intrinsically by cell-autonomous mechanisms. In this dissertation work, I have pursued new molecular mechanisms that control this process, which are detailed in Chapter 4. Synaptic localization is a key part in neural circuit development, and one of the many steps in the synaptogenic process that requires more intensive research.

Summary

In this dissertation, I studied neural development at single cell resolution using *Drosophila* genetic approaches and the GF circuit. I particularly focused on probing the *Drosophila* FXS disease model and

testing how FMRP loss affects the properties of a single GF neuron. These results, which are presented in Chapter 2, show a new phenotype wherein FMRP restricts dye entry into a neuron. While performing this work, I identified several previously unreported dye-coupled neurons that connect with the GF circuit, and characterized their structure, polarization and interactions with the central GFI. These findings are reported in Chapter 3. Finally, during further studies of the implications of FMRP loss in the GF circuit, I discovered a synaptic overgrowth phenotype caused by a background mutation in a commonly used FMRP null allele, *dfmr1*^{50M}. Using bulk segregant analysis (BSA) paired with WGS, I have begun the process of identifying the causative mutation and confirming its role in the overgrowth phenotype. These findings are currently being prepared for publication and are presented in Chapter 4. A summary of all of these results, and future directions for each project is contained in the concluding Chapter 5. Also included in Chapter 5 is a summary of two projects that were not published due to time constraints and negative data.

Chapter II

Fragile X Mental Retardation Protein Restricts Small Dye Iontophoresis Entry into Central Neurons

This paper has been published under the same title in Journal of Neuroscience, 2017

Tyler Kennedy[1] and Kendal Broadie[1,2,3]

[1]Department of Biological Sciences, [2]Department of Cell and Developmental Biology, [3]Vanderbilt Brain Institute, Vanderbilt University and Medical Center,

Nashville, TN 37235 USA

Abstract

Fragile X Mental Retardation Protein (FMRP) loss causes Fragile X syndrome (FXS), a major disorder characterized by autism, intellectual disability, hyperactivity and seizures. FMRP is both an RNA- and channel-binding regulator, with critical roles in neural circuit formation and function. However, it remains unclear how these FMRP activities relate to each other and how dysfunction in their absence underlies FXS neurological symptoms. In testing circuit level defects in the *Drosophila* FXS model, we discovered a completely unexpected and highly robust neuronal dye iontophoresis phenotype in the well-mapped Giant Fiber (GF) circuit. Controlled dye injection into the GF Interneuron (GFI) results in a dramatic increase in dye uptake in neurons lacking FMRP. Transgenic wildtype FMRP reintroduction rescues the mutant defect, demonstrating a specific FMRP requirement. This phenotype affects only small dyes, but is independent of dye charge polarity. Surprisingly, the elevated dye iontophoresis persists in *shaking B* mutants that eliminate gap junctions and dye coupling among GF circuit neurons. We therefore used a wide range of manipulations to investigate the dye uptake defect, including timed

injection series, pharmacology and ion replacement, and optogenetic activity studies. The results show FMRP strongly limits the rate of dye entry via a cytosolic mechanism. This study reveals an unexpected new phenotype in a physical property of central neurons lacking FMRP that could underlie aspects of FXS disruption of neural function.

Significance Statement

FXS is a leading heritable cause of intellectual disability and autism spectrum disorders. Although researchers established the causal link with FMRP loss over 25 years ago, studies continue to reveal diverse FMRP functions. The *Drosophila* FXS model is key to discovering new FMRP roles, owing to its genetic malleability and individually-identified neuron maps. Taking advantage of a well-characterized *Drosophila* neural circuit, we discovered that neurons lacking FMRP take up dramatically more current-injected small dye. After examining many neuronal properties, we determined that this dye defect is cytoplasmic and occurs due to a highly elevated dye iontophoresis rate. We also report several new factors affecting neuron dye uptake. Understanding how FMRP regulates iontophoresis should reveal new molecular factors underpinning FXS dysfunction.

Introduction

Fragile X syndrome (FXS), resulting from Fragile X Mental Retardation Protein (FMRP) loss, is the leading heritable cause of autism and intellectual disability, and displays comorbidity with numerous other neurological symptoms including attention deficit, hyperactivity and childhood seizures (Cowley et al., 2016). FMRP is a complex protein with multiple neuronal functions. The canonical FMRP role is direct RNA-binding translation control, regulating activity-dependent expression of a large but indeterminate number of neuronal proteins (Darnell et al., 2011). Without FMRP, numerous proteins become overexpressed, significantly altering the neuronal proteome (Zhang et al., 2001; Cvetkovska et al., 2013;

Ifrim et al., 2015). The major non-canonical FMRP role is direct channel-binding, which regulates functional channel gating properties (Brown et al., 2010; Strumbos et al., 2010). Without FMRP, K^+ and Ca^{2+} channels are dysregulated, altering both action potentials and synaptic transmission (Deng et al., 2013; Contractor et al., 2015). A number of other diverse functions have also been ascribed to FMRP, such as miRNA regulation and chromatin stability control (Jin et al., 2004; Alpatov et al., 2014), expanding the already complex involvement of FMRP in neuronal development and function. Targeted and effective therapies for patients will require an understanding of how these diverse FMRP roles relate to FXS symptoms.

Drosophila disease models provide a potent toolkit to discover novel neuronal mechanisms underlying neurological symptoms. The well-established *Drosophila* FXS disease model exhibits phenotypes analogous to human symptoms, including synaptic overgrowth, hyperactivity and learning/memory deficits (Zhang et al., 2001; Dockendorff et al., 2002; Bolduc et al., 2008), and continues to provide key new insights into FXS (Doll and Broadie, 2014, 2015, 2016; Golovin and Broadie, 2016). Elegant *Drosophila* brain neural circuit maps reveal individual neurons with single-cell resolution, enabling links between neuronal molecular changes and FXS circuitry defects. An excellent set of neurons for such work is the Giant Fiber (GF) circuit, a well-characterized escape circuit comprised of five readily identifiable neurons (King and Wyman, 1980; Allen et al., 1998), which require FMRP for proper circuit function (Martinez et al., 2007). This circuit collects sensory information and relays it to motor neurons via the large GF Interneuron (GFI), enabling rapid escape from aversive stimuli (Tanouye and Wyman, 1980). The toolkit for this circuit includes highly specific genetic reporters (Sun and Wyman, 1996) and an array of transgenic drivers that provide exquisite labeling and manipulation of individual GF neurons (Godenschwege et al., 2002; Lee and Godenschwege, 2014). The large size and easy accessibility of the GFI allows iontophoretic dye injection via sharp electrodes, a critical tool for circuit study (Boerner and Godenschwege, 2011).

Dye iontophoresis represents a classic strategy for neural circuit mapping and uncovering genes required for electrical synapse formation, with many studies in the extensively dye-coupled GF circuit (Phelan et al., 1996; Kudumala et al., 2013; Lee and Godenschwege, 2014). Small ionic dyes, such as neurobiotin and lucifer yellow, pass through gap junctions, labeling the electrically-coupled circuit (Lapper and Bolam, 1991; Hanani, 2012). Most experiments assay simple dye transfer between coupled neurons; however, a recent study tested quantitative relative dye transfer levels via gap junctions (Orr et al., 2014). Expanding on this quantitative dye iontophoresis approach, we began exploring GF circuit dye coupling in the FXS model to test hypothesized changes in circuit connectivity. Instead, we stumbled upon an unexpected and robust dye injection phenotype: *Drosophila fmr1* (*dfmr1*) null mutant neurons take up dramatically more small, charged dyes injected via iontophoretic current. This defect is not related to a multitude of neuronal properties, including size, porosity and circuit connectivity. Indeed, we found a trend toward fewer gap junction electrical synapses in *dfmr1* null neurons, and a persistent dye iontophoresis defect in neurons completely lacking all gap junction connections. We conclude FMRP regulates a cytosolic mechanism determining ionic uptake rates. This study provides new insights into quantitative iontophoresis, broadens understanding of multiple factors modulating neuronal dye injection, and identifies a new neurological disruption in this FXS disease model.

Materials and Methods

Drosophila Genetics

All animals were maintained on standard cornmeal/agar/molasses *Drosophila* food in a 12-hour light:dark cycling incubator at 25^{o}C. For channelrhodopsin experiments, food was made with 100µM all-trans retinal (ATR) or EtOH vehicle as a control (Ataman et al., 2008), and animals were reared in constant darkness. The following *Drosophila* lines were used for genetic crosses, with female offspring used for all

experiments: w^{1118} (RRID:BDSC_3605) | w^{1118}; $dfmr1^{50M}$/TM6B, GFP, Hu (Zhang et al., 2001, RRID:BDSC_6930) | w^{1118}; $dfmr1^{2}$/TM6, Hu (Dockendorff et al., 2002) | w^{1118}; UAS-*dfmr1*, $dfmr1^{50M}$/TM6B, GFP, Hu (9557.3) (Zhang et al., 2001) | w^{1118}; *elav*-Gal4/CyO (RRID:BDSC_8765) | w^{1118}; *elav*-Gal4/CyO; $dfmr1^{50M}$/TM6, Hu | $shakB^{2}$ (Blagburn et al., 1999) | $shakB^{2}$; $dfmr1^{50M}$/TM6, GFP | w^{1118}; P{GMR91H05-Gal4}attP2 (Jenett et al., 2012, RRID:BDSC_40594) | w^{1118}; UAS-*chr2-xxl* (Dawydow et al., 2014) |w^{1118}; 10XUAS-*ivs-mcd8::rfp* (RRID:BDSC_32219) | w^{1118}; P{UAS-*shaw*.RA.FLAG}12B (Hodge et al., 2005, RRID:BDSC_55719) | w^{1118}; UAS-*irk2*A/CyO, GFP (Dahal et al., 2012). All genotypes were verified with visible genotype markers when possible, and PCR when necessary. All crosses were allowed to lay eggs for 2-3 days, with offspring rearing densities carefully matched between compared genotypes.

Dye Iontophoresis

Experimental animals were selected from age-matched rearing tubes 10-13 days after egg laying, yielding staged adults 0-4 days in age. Genotyped animals were pinned submerged in physiological saline (Jan and Jan, 1976), and then cut along the dorsal midline to access the cervical connective (CC), as previously reported (Boerner and Godenschwege, 2011). Sharp glass electrodes (Kwik-Fil Borosilicate glass 1B100F-4, World Precision Instruments) were pulled on a laser electrode puller (Model P-2000, Sutter Instrument Company) to 10MΩ resistance (3M KCl). Electrodes were filled by capillary action with one of the following dye solutions: 0.25% TRITC-Dextran (10kDa, Life Technologies) and 7% Neurobiotin (Vector Laboratories, RRID:AB_2313575), or 1% Lucifer Yellow (LY) potassium salt (Thermo Fisher Scientific). Dyes were dissolved in ddH_2O or 2M potassium acetate (KAc), as indicated. Filled electrodes were placed on a silver-chloride wire mounted on a PCS-5000 micromanipulator (Burleigh). The electrode tip was inserted into the Giant Fiber Interneuron (GFI) at the CC, while a ground electrode was placed in the bath saline. Voltage was manually controlled with a Grass square-pulse stimulator (S48, Astro-Med Inc), providing 7.5 100ms pulses/second for 2 minutes, unless otherwise noted. Delivery of 20nA current was monitored by tracking

the voltage drop across a 1MΩ resistor in the electrode circuit with an AxoClamp2B amplifier, connected to a Digidata 1320A data acquisition system (Axon Instruments), controlled by Clampex software (version 9.2). Reversed polarity was used for LY experiments.

Dye Injection Manipulations

For channelrhodopsin experiments, preparations were illuminated with filtered blue light (440-470nm) from an EBQ100 isolated mercury lamp (Leistungselektronik Jena GmbH) for the duration of dye injection. Channelrhodopsin function was tested by behavioral response to blue light. For K^+ channel blocking, 4-aminopyridine (4-AP, Sigma-Aldrich; 10mM) was added in physiological saline prior to imaging (Singh and Singh, 1999). For cocktail experiments, tetraethylammonium chloride (TEA, Sigma-Aldrich; 10mM) was combined with 10mM 4-AP in the bath, with cesium chloride (140mM) dissolved in KAc-free NB dye injection solution. Drug was added at the beginning of the dissection, with exposure for $\geq$5 minutes prior to dye injection. All drug trial preparations were rinsed 3X in physiological saline with a 3-minute rest before fixation to prevent interaction between drug and fixative. Forced leak experiments were performed following the standard dye injection, followed by a second electrode containing 0.25% TRITC in 2M KAc that was placed into the dye-injected neuron. The order of genotypes assayed in all trials was changed for experiments each day to avoid any possible ordering experimental artifacts.

Confocal Imaging

After dye injections, the entire CNS (brain and thoracic ganglion) was dissected out and fixed for 30 mins in 4% paraformaldehyde (Electron Microscopy Services)/4% sucrose (Thermo Fisher Scientific) in phosphate-buffered saline (PBS, pH 7.2, Life Technology). Fixed preparations were rinsed 3X with PBS, and blocked for 1 hour with 1% bovine serum albumin (BSA, Sigma-Aldrich) in PBST (1X PBS, 0.2% Triton X-100; Thermo Fisher Scientific). Labels were diluted in PBST with 0.2% BSA. The following labels were used:

Streptavidin::Cy5 (1:20, Life Technology), rabbit anti-ShakB (1:250, Phelan et al., 1996) and 633-conjugated goat anti-rabbit (1:250; Life Technology, RRID:AB_141419). Neurobiotin was labeled with streptavidin::Cy5. Incubations were conducted either overnight at 4°C or 2 hours at room temperature (RT). Following antibody incubations, preparations were rinsed 3X for 30 minutes in PBST before a final 30-minute rinse in PBS. Preparations were mounted on glass slides (Probe On Plus 25 x 75 x 1.0mm, Thermo Fisher Scientific) in 2, 2'-Thiodiethanol (TDE, Staudt et al., 2007). To prevent crushing, double-sided poster tape (Scotch) was placed on each side of the brains. Coverslips (No. 1.5H, Zeiss) were sealed with nail polish (Hard as Nails, Sally Hansen). Fluorescent images were collected using a ZEISS LSM 510 META laser-scanning confocal microscope with a 40X oil-immersion objective, focusing on the prothoracic and mesothoracic ganglia regions (Mu et al., 2014). Imaging settings were maintained across all samples, with the exception of GFI dendrites, which required increased brightness for the TRITC injection of w^{1118} and $dfmr1^{50M}$, and the NB injection of $shakB^{2}$ and $shakB^{2}$; $dfmr1^{50M}$. Images show maximum Z-stack projections.

Protein Quantification

Brains were dissected in PBS from adult females (0-4 days at 25°C). 4 brains were collected on ice in lysis buffer (50mM Tris, 100mM NaCl, 1mM EDTA, 1mM PMSF, Protease Inhibitor Cocktail; Sigma-Aldrich), sonicated (Branson Model 102C, Sonifier 250 microtip) for 20 seconds, returned to ice for 20 minutes, then centrifuged at 14,000 RPM for 10 minutes. Protein samples were prepared using a BCA kit (ThermoFisher) and analyzed with a Nanodrop 2000c spectrophotometer (ThermoFisher).

Data Analyses

FIJI software was used for data quantification and processing (Schindelin et al., 2012, RRID:SCR_002285). For dye injection intensity quantification, the number of pixels at each intensity (0-255) was calculated for

each 8-bit image stack. A pixel cutoff of 59 was empirically determined to remove background with minimal signal loss. The total number of pixels above 59 in the full stack is reported as "dye injected." GFI dendrites were quantified in the same manner after masking cell bodies, axons and dye-coupled neurons. A threshold of 90 was used for the TRITC dendrite quantification to offset changes in imaging brightness. Intensity quantification was automated using an ImageJ Macro script to remove any experimenter analytical bias. The dendritic structure was calculated by measuring the GFI primary branches using the FIJI Simple Neurite Trace plugin (Longair et al., 2011). For w^{1118} and $dfmr1^{50M}$, the TRITC signal was used, while for $shakB^{2}$ and $shakB^{2}$; $dfmr1^{50M}$ NB signal was used for the structural comparisons. For anti-ShakB fluorescence quantification, the TRITC dye injection signal was used to create the region of interest (ROI) encompassing the GFI bend. This ROI was then overlaid onto the ShakB channel, and intensities of each pixel above the background threshold (40) were summed for all optical slices containing the GFI bend. All statistical analyses were performed using the Prism software (version 7, GraphPad, RRID:SCR_002798). All single pairwise comparisons were performed by two-tailed student's *t* test for Gaussian distributions, and Mann-Whitney for non-Gaussian distributions. All multiple comparisons were performed using unpaired one-way ANOVA, with Tukey-Kramer pairwise post-hoc tests. Slope comparisons were performed using the ANCOVA test. In all figures, graphs show mean ± standard error of the mean (SEM) with the statistical comparisons displayed as $p>0.05$ (not significant; NS), $p<0.05$ (*), $p<0.01$ (**) and $p<0.001$ (***).

Results

FMRP Selectivity Limits Small Dye Iontophoresis into Neurons

While studying *Drosophila* neural connectivity changes in *dfmr1* null mutants, we discovered a surprising dye iontophoresis phenomenon (Fig. **5**): neurons lacking FMRP accept far more neurobiotin

(NB, 287Da), but no more dextran-tetramethylrhodamine (TRITC, 10kDa), compared to matched genetic background controls. We pursued this intriguing finding in the Giant Fiber (GF) circuit by delivering controlled iontophoretic current to co-inject both NB and TRITC dyes into the GF Interneuron (GFI; Boerner and Godenschwege, 2011). TRITC provides a real-time confirmation of neuron identity, but cannot leave the neuron via gap junctions due to its large size (Phelan et al., 1996). In contrast, the much smaller NB readily crosses gap junctions and labels all of the electrically-coupled neurons within the circuit (Boerner and Godenschwege, 2010). Each brain hemisphere contains one GFI cell body and dendritic arbor (not pictured), with a large descending axon into the thoracic ganglion (TG) terminating in the mesothoracic ganglion with a characteristic bend visible by TRITC labeling (Fig. **5***A*, top, arrow). The GFI axon forms electrical synapses with Peripherally Synapsing Interneurons (PSI), visible by NB dye-coupled labeling (Fig. **5***A*, bottom, arrows), and the Tergotrochanteral Motor Neuron (TTMn), which projects to leg muscles (King and Wyman, 1980; Allen et al., 1998). We compared dye labeling in *dfmr1* null mutants (w^{1118}; $dfmr1^{50M}$) with genetic background controls (w^{1118}). Representative images and data summaries are shown in Figure **5**.

Upon injection, TRITC distributes uniformly along the GFI axon to the distal terminating bend in both controls (Fig. **5***A*, top left) and *dfmr1* nulls (Fig. **5***A*, top right). Dimmer signal towards the bend results from the axon moving progressively deeper into the semi-opaque tissue, which restricts light transmission. There was no quantifiable difference in TRITC dye loading between the two genotypes (Fig.

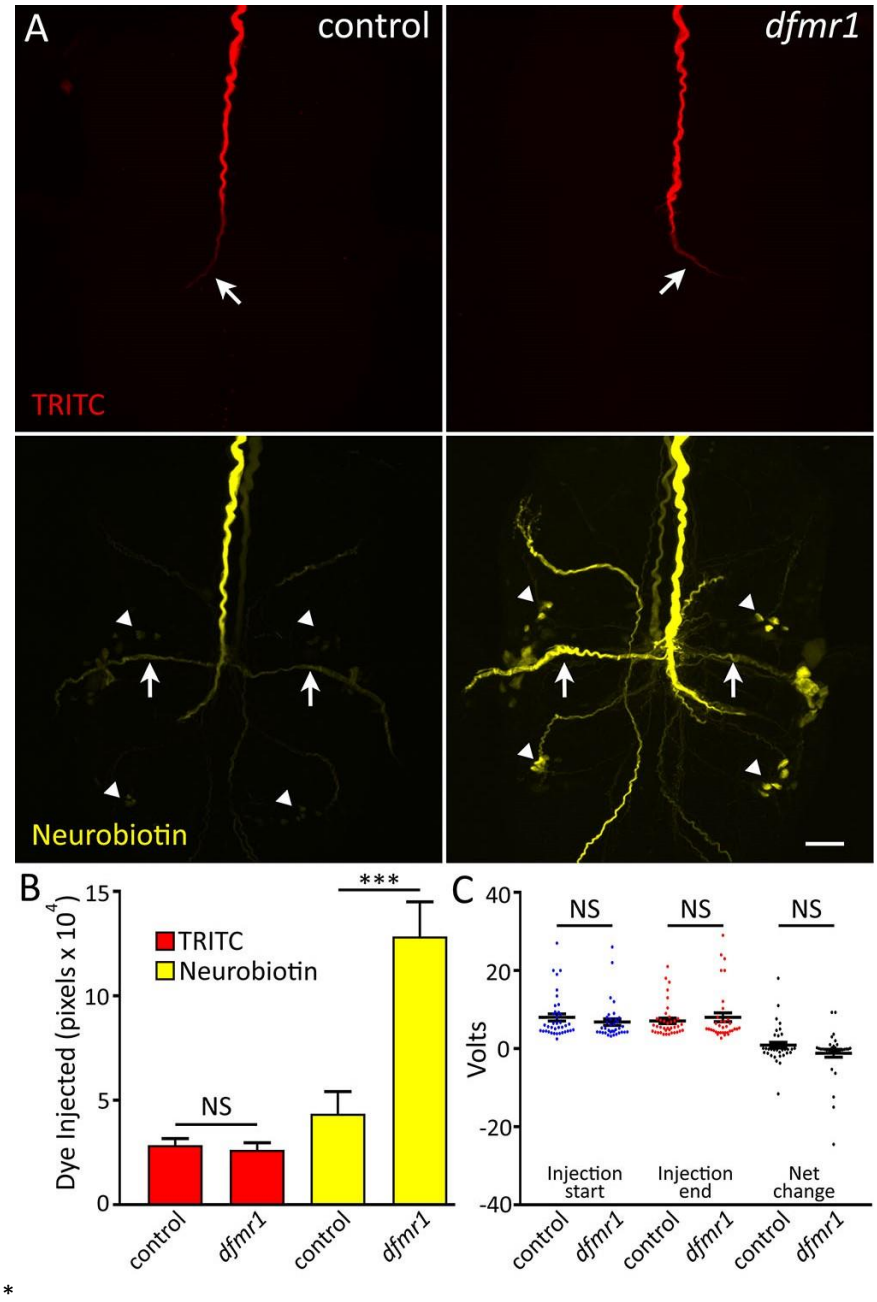

*

Figure 5. Selective Small Dye Iontophoresis is Increased in *dfmr1* Null Neurons

A, Representative images of the Giant Fiber Interneuron (GFI) co-injected with 10kDa dextran conjugated tetramethylrhodamine isothiocyanate (TRITC, red; top) and 287Da neurobiotin (NB, yellow; bottom) dissolved in 2M KAc. Images show the thoracic ganglion for w^{1118} genetic background (control, left) and $dfmr1^{50M}$ null mutant (right). TRITC-dextran is too large to escape the injected GFI neuron, while NB passes through gap junctions to dye-coupled neurons in the GF neural circuit. Arrows indicates GFI bend (top) and Peripherally Synapsing Interneuron (PSI, bottom). Arrowheads indicate coupled cell bodies. Scale bar: 20µm. ***B,*** Quantification of TRITC (red) and NB (yellow) dye injection displayed as mean ± SEM. TRITC: control n=36, *dfmr1* n=33. NB: control n=37, *dfmr1* n=36. ***C,*** Voltage required to deliver 20nA of current to the GFI neuron in control and *dfmr1* null mutants. Voltage is shown at the start (left) and end (middle) of each two-minute injection, and also as the net voltage change after a two-minute injection (right). Control n=38, *dfmr1* n=35. Significance determined from two-tailed unpaired *t* tests (*B)* or two-tailed Mann-Whitney tests (*C*): p***<0.001 and not significant (NS).

dfmr1 nulls (n=33), an indistinguishable difference in loading (p=0.64, two-tailed unpaired *t* test). In sharp contrast, control GFIs contain visibly less NB dye in the axon, especially at the terminal bend (Fig. **5***A*, bottom left), compared to *dfmr1* null mutants (Fig. **5***A*, bottom right). Moreover, the mutants display much more NB signal in the coupled PSI (arrows) and other labeled neurons, including their cell bodies (arrowheads). Null *dfmr1* GFIs are not visibly coupled to any neurons not labeled in controls and maintain a normal circuit pattern. Upon quantification, we found *dfmr1* null neurons take up nearly 3-fold more NB dye than controls (Fig. **5***B*). Mean NB dye intensity in controls was $4.4x10^4 \pm 1.1x10^4$ (n=37) compared to $12.8x10^4 \pm 1.7x10^4$ in $dfmr1^{50M}$ mutants (n=36), a very highly significant increase ($p=6.2x10^{-5}$, two-tailed unpaired *t* test). This selective dye iontophoresis defect is highly replicable and extremely robust, providing an excellent new measure for the effects of FMRP loss. Furthermore, such a genotypic difference in iontophoretic dye loading has never been reported for any mutant condition, to our knowledge.

To test if current delivery differences might cause the differential dye loading between genotypes, we next recorded the voltage required to deliver a constant current (Fig. **5***C*). Any voltage change must be coupled with a resistance change to maintain a constant current. Differing voltage requirements between genotypes would reveal altered conductivity throughout the dye delivery circuit, such as altered plasma membrane permeability. Comparing genetic background controls to *dfmr1* null mutants, we recorded the voltage required to deliver 20nA currents over a 2-minute interval, but found no significant differences between the two genotypes (Fig. **5***C*). The voltage did not differ at the onset of current injection (control: 8.0±0.9 volts, n=38; $dfmr1^{50M}$: 6.8±0.8 volts, n=35, p=0.21, two-tailed Mann-Whitney test; Fig. **5***C*) or at the end of current injection (control: 7.1±0.7 volts; $dfmr1^{50M}$: 8.0±1.1 volts, p=0.66, two-tailed Mann-Whitney test; Fig. **5***C*). The net voltage change also did not differ between the genotypes (control: 0.9±0.7 volts; $dfmr1^{50M}$: -1.2±1.0 volts, p=0.44, two-tailed Mann-Whitney test; Fig. **5***C*). Detailed analyses of instant current readings (1kHz) throughout the injection period also revealed no differential fluctuations between

genotypes that could account for loading differences (not shown). These findings show the electrical circuit resistance does not differ between *dfmr1* nulls and background controls, and indicate that the elevated NB loading in mutants must result from altered fundamental neuron properties in the absence of FMRP.

FMRP-Dependent and Charge-Independent Dye Iontophoresis Defect

We next tested whether the altered neuronal properties were specifically due to loss of FMRP. We first compared the w^{1118} genetic background control (Fig. **6***A*, top left) with a second, independent *dfmr1* null allele, $dfmr1^{2}$ (Fig. **6***A*, top right). To rule out recessive background effects, we tested the heteroallelic combination with $dfmr1^{50M}$. This mutant replicated the specific NB dye loading defect (control: $3.9x10^4 \pm 1.3x10^4$, n=6; $dfmr1^{2/50M}$: $12.1\ x10^4 \pm 1.1x10^4$, n=6, p=0.0008, two-tailed unpaired *t* test; Fig. **6***B*), supporting a causative FMRP role. We next tested if transgenic expression of wildtype dFMRP in *dfmr1* null neurons rescues the phenotype using neuron-specific *elav*-Gal4 as the driver (Brand and Perrimon, 1993). Dye loading in the rescue condition was comparable to the paired control, and greatly reduced compared to the *dfmr1* null (Fig. **6***A*,*B*). Quantification supports the conclusion that wildtype dFMRP reintroduction rescues the dye loading phenotype (*elav*-Gal4/+: $6.1x10^4 \pm 1.3x10^4$, n=17; *elav*-Gal4/+; $dfmr1^{50M}$, *UAS-dfmr1*/$dfmr1^{50M}$: $7.8x10^4 \pm 1.5x10^4$, n=18; *elav*-Gal4/+; $dfmr1^{50M}$/$dfmr1^{50M}$: $13.4x10^4 \pm 1.9x10^4$, n=13), with no significant difference between control and rescue conditions (p=0.68), but a significant difference existing between the rescue and mutant (p=0.03) and persisting between the control and mutant (p=0.005, unpaired ANOVA, Tukey-Kramer pairwise post-hoc test; Fig. **6***B*). Taken together, these findings confirm that FMRP specifically regulates NB dye iontophoresis, ruling out genetic background and non-specific effects.

We next tested whether the dye loading phenotype is NB-specific or occurs with other small dyes. We repeated the dye injection studies with the commonly-used negatively charged small dye lucifer

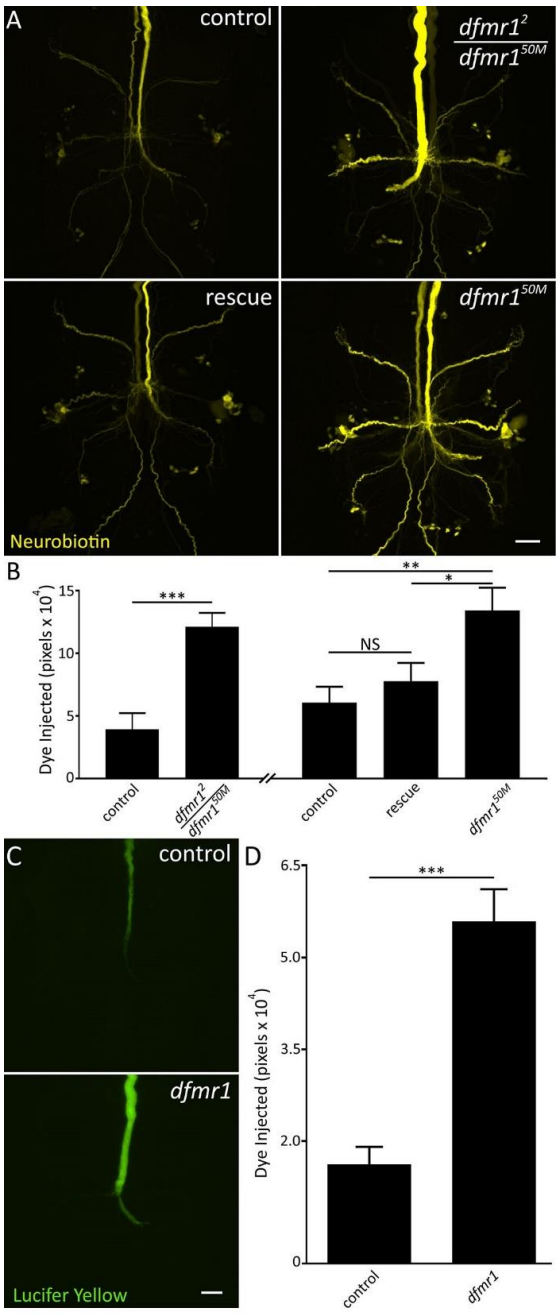

Figure 6. Dye Iontophoresis Defect is FMRP Dependent and Charge Independent

A, Representative NB images of GFI injections (2M KAc) for w^{1118} genetic background (control, top left), heteroallelic *dfmr1* null ($dfmr1^{2}/dfmr1^{50M}$, top right), wildtype UAS-*dfmr1* driven with neural *elav*-Gal4 (rescue, bottom left) in $dfmr1^{50M}$ null background and the $dfmr1^{50M}$ null alone (bottom right). Scale bar: 20µm. ***B,*** Quantification of dye injection in the above four genotypes. The heteroallelic combination and transgenic rescue experiment occurred independently and are displayed with their separate genetic controls. All graphs show data as mean ± SEM. Heteroallelic: control n=6, $dfmr1^{2/50M}$ n=6. Rescue: control n=17, rescue n=18, $dfmr1^{50M}$ n=13. ***C,*** Representative images of lucifer yellow dye injections (in ddH_2O) into the GFI neuron in the w^{1118} genetic background (control, top) and $dfmr1^{50M}$ null mutant (bottom). Scale bar: 20µm. ***D,*** Quantification of lucifer yellow injection in both genotypes. Control n=13, *dfmr1* n=12. Significance determined from two-tailed unpaired *t* test (*B*, left; *D*) and unpaired ANOVA (*B*, right): p*<0.05, p**<0.01, p***<0.001 and not significant (NS).

yellow (LY, 430Da), which had the added benefit of testing for a role of charge polarity (Hanani, 2012). LY is fluorescent and visible during injection, requiring no amplification prior to imaging. Utilizing the same iontophoresis paradigm, but with reversed polarity, we again found a dramatic increase in dye uptake in the *dfmr1* mutants (Fig. **6***C*). Compared to w^{1118} genetic controls (top), *dfmr1* nulls load far more LY dye (bottom), with increased signal continuously along the descending axon and terminating bend (Fig. **6***C*). Y passage to electrically coupled neurons is much slower than NB, thereby largely limiting analysis to the injected GFI (Boerner and Godenschwege, 2011). Similar to NB dye, quantification shows controls ($1.6x10^4 \pm 0.3x10^4$, n=13) loaded 3-fold less LY dye than *dfmr1* null mutants ($5.6x10^4 \pm 0.5x10^4$, n=12), a very highly significant difference ($p=3.1x10^{-6}$, two-tailed unpaired *t* test; Fig. **6***D*). These results show the *dfmr1* mutant defect is generalizable for small dyes, regardless of dye charge polarity. The selective elevation in small dye iontophoresis, with large TRITC dye loading unchanged, strongly suggested the phenotype arises from a gap junction mechanism.

Increased Dye Iontophoresis Persists in the Absence of Gap Junctions

The obvious factor that could determine dye loading based on dye size is gap junction electrical synapses. FXS patients and models exhibit synaptic overgrowth (Comery et al., 1997; Irwin et al., 2000; Zhang et al., 2001; Doll and Broadie, 2015), but these analyses have focused on chemical, not electrical, synapses. We hypothesized that increased electrical connectivity mirrors increased chemical synapse connectivity in the FXS disease state, promoting dye movement into electrically-coupled neurons and thereby bringing more total dye into the GF circuit. All GFI electrical synapses require the Shaking B (ShakB) N+16 isoform (Phelan et al., 2008), allowing tests of gap junction abundance between controls and *dfmr1* nulls. Using a ShakB N+16 antibody, TRITC injected neurons were assayed for fluorescence intensity at TTMn synapses along the GFI bend (Fig. **7***A*). Contrary to our hypothesis, we found ShakB levels in controls (top) trend higher than in *dfmr1* nulls (bottom). ShakB punctae along the GFI bend (arrows)

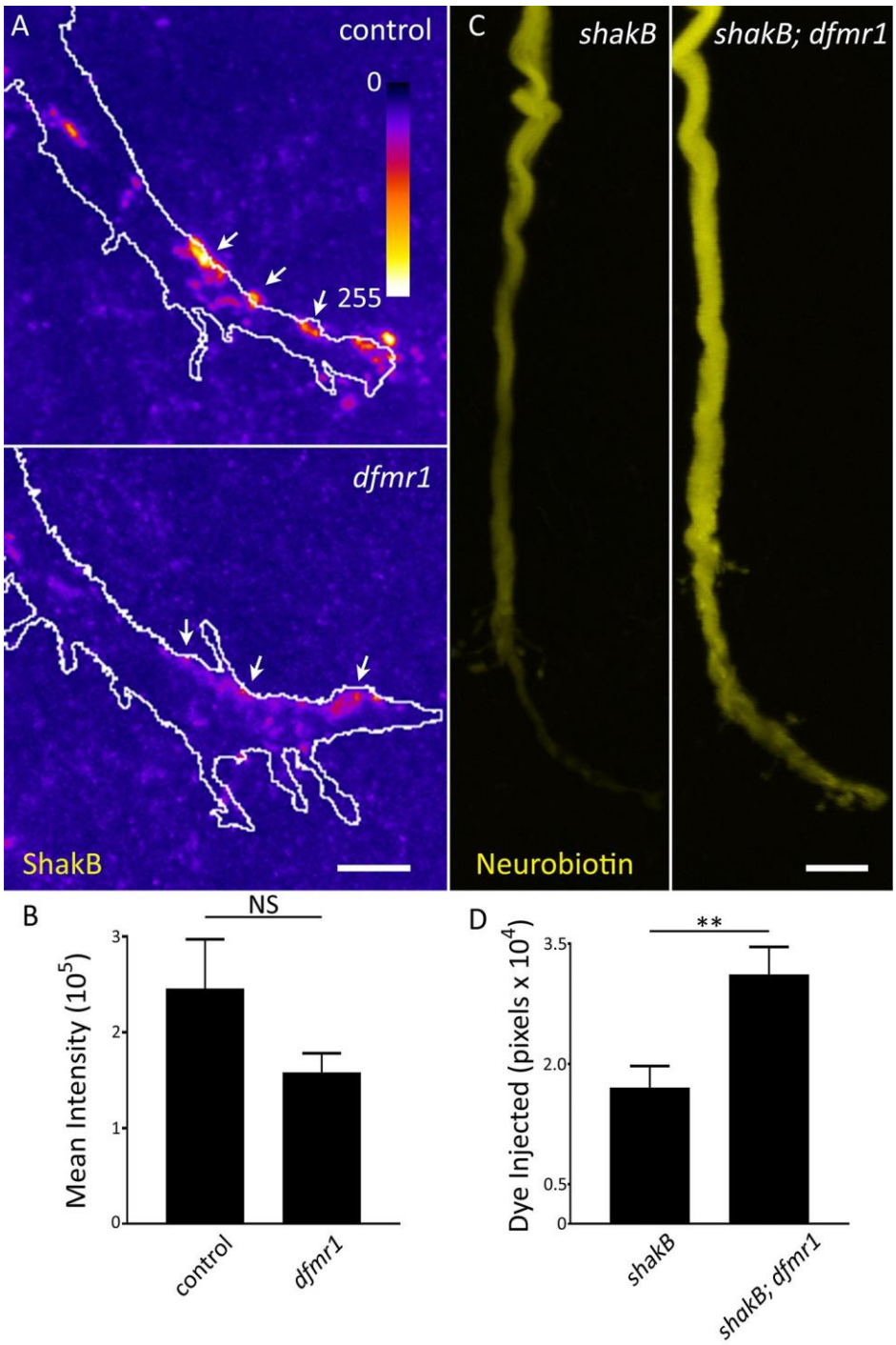

Figure 7. Null *dfmr1* Neurons Manifest Dye Injection Defect Without Gap Junctions

A, Representative images of anti-ShakB labeling in the GFI for the w^{1118} genetic background (control, top) and $dfmr1^{50M}$ null mutant (bottom). White outline indicates GFI bend as labeled by injected TRITC signal. ShakB signal intensity is represented as a heat map. Arrows indicate ShakB punctae. Scale bar: 5µm. ***B,*** Quantification of ShakB signal intensity in both genotypes, displayed as mean ± SEM. Control n=27, *dfmr1* n=26. ***C,*** Representative NB injections into the GFI (2M KAc) for the $shakB^{2}$ single mutant (left) and $shakB^{2}$; $dfmr1^{50M}$ double mutant (right). Scale bar: 10µm. ***D,*** Quantification of the injected dye levels in both genotypes, displayed as mean ± SEM. Control n=30, *dfmr1* n=31. Significance was determined from two-tailed unpaired *t* tests: p**<0.01 and not significant (NS).

connect to the TTMn (Phelan et al., 2008). Punctae were reduced in *dfmr1* mutants, potentially indicating weaker connections (Fig. **7***A*). Quantification of ShakB intensity shows weak mutant signal (control: $2.5x10^5 \pm 0.5x10^5$, n=27; $dfmr1^{50M}$: $1.6x10^5 \pm 0.2x10^5$, n=26), although the decrease is not significant with a large sample size (p=0.13, two-tailed unpaired *t* test; Fig. **7***B*). This surprising finding runs counter to our hypothesis that the dye iontophoresis defect results from increased gap junction connectivity. However, it remained possible that gap junctions in *dfmr1* mutants are more conductive or spend more time in an open conformation than controls (Niculescu and Lohmann, 2014), thus promoting a loading increase.

To determine if gap junction changes cause increased dye loading in *dfmr1* nulls, we examined GFI dye injection patterns in the $shakB^2$ null mutant, an allele that does not produce the ShakB N+16 isoform, thus completely uncoupling GFI connectivity (Blagburn et al., 1999). We performed NB dye injections on both $shakB^2$ null mutants and $shakB^2$; $dfmr1^{50M}$ double null mutants. The $shakB^2$ allele completely abolished all dye coupling in both cases, preventing injected NB dye from leaving the GFI (Fig. **7***C*). Again, against our expectations, the excessive NB dye loading defect persisted in *dfmr1* nulls in the absence of gap junctions. In $shakB^2$ single mutants (left), the NB signal is much reduced all along the descending GFI axon as well as terminal bend, compared to the relatively highly elevated signal in $shakB^2$; $dfmr1^{50M}$ double mutants (Fig. **7***C*, right). Quantification of dye loading shows nearly twice the signal in *dfmr1* nulls compared to the matched single mutant controls ($shakB^2$: $1.7x10^4 \pm 0.3x10^4$, n=30; $shakB^2$; $dfmr1^{50M}$: $3.1x10^4 \pm 0.4x10^4$, n=31), a very significant increase (p=0.0025, two-tailed unpaired *t* test; Fig. **7***D*). Note that we used only 10-second injections in these $shakB^2$ studies, as the above 2-minute injection paradigm caused complete loss of NB/TRITC signals, presumably due to GFI lysis from overloading a constrained volume via electroosmotic effects (see Discussion). Taken together, these findings indicate the dye iontophoresis defect in *dfmr1* null neurons does not depend on gap junction electrical synapses.

Having ruled out connectivity changes, we next turned to intrinsic neuron properties to trace the impacted mechanism.

GFI Dendrites are Structurally Unaltered and Display Dye Loading Defect

The polarized structure of neurons provides one hypothesis for the mechanism underlying increased dye loading: dye compartmentalization varies between genotypes. We therefore tested whether increased *dfmr1* null axonal dye levels result from reduced dendritic dye accumulation, due either to inhibited retrograde dye movement or decreased dendrite architecture. We measured dendritic dye loading, volume and coverage in both the w^{1118} and $shakB^{2}$ genetic backgrounds to address dye-coupled and -uncoupled circuits. Representative images in Figure **8***A* show the complete GFI dendritic field, with a dorsal projection connecting the cell body (arrowhead), and the GFI axon projecting towards the bottom right in each image (arrow). Control dendrites (e.g. $shakB^{2}$, top left) load significantly less NB dye than *dfmr1* mutants ($shakB^{2}$; $dfmr1^{50M}$, top right), in the absence of discernable structural differences. Quantification of NB signal in w^{1118} controls versus *dfmr1* nulls (Fig. **8***B*, left), and $shakB^{2}$ versus $shakB^{2}$; $dfmr1^{50M}$ (Fig. **8***B*, right), shows elevated dye loading in dendrites replicating axonal phenotypes. Both conditions show significant increases in *dfmr1* nulls (control: $0.1x10^{4}\pm0.03x10^{4}$, n=20; $dfmr1^{50M}$: $1.6x10^{4}\pm0.2x10^{4}$, n=20, $p=2.7x10^{-7}$, two-tailed unpaired *t* test. $shakB^{2}$: $2.1x10^{4}\pm0.4x10^{4}$, n=27; $shakB^{2}$; $dfmr1^{50M}$: $3.4x10^{4}\pm0.3x10^{4}$, n=30, p=0.009, two-tailed unpaired *t* test; Fig. **8***B*). This finding indicates there is not a reduction in dye in *dfmr1* null dendrites relative to controls that could offset the increase seen in axons.

To determine whether the *dfmr1* null GFI dendritic architecture is reduced, thereby forcing more injected NB dye into axons, we measured dendritic length, volume and coverage. TRITC labeling in the GFI dendrites shows no detectable changes in the GFI dendritic field comparing w^{1118} controls (left) and *dfmr1* nulls (right; Fig. **8***A*, bottom). Quantification of the injected TRITC dye shows dendrite volume in the controls ($3.2x10^{4}\pm0.5x10^{4}$, n=17) trends smaller than *dfmr1* nulls ($3.8x10^{4}\pm0.8x10^{4}$, n=17), but the difference is not significant (p=0.54, two-tailed unpaired *t* test; Fig. **8***C*). Measurement of the primary dendritic branches also shows similar dendritic branch length between w^{1118} controls (148.2±7.1μm, n=17)

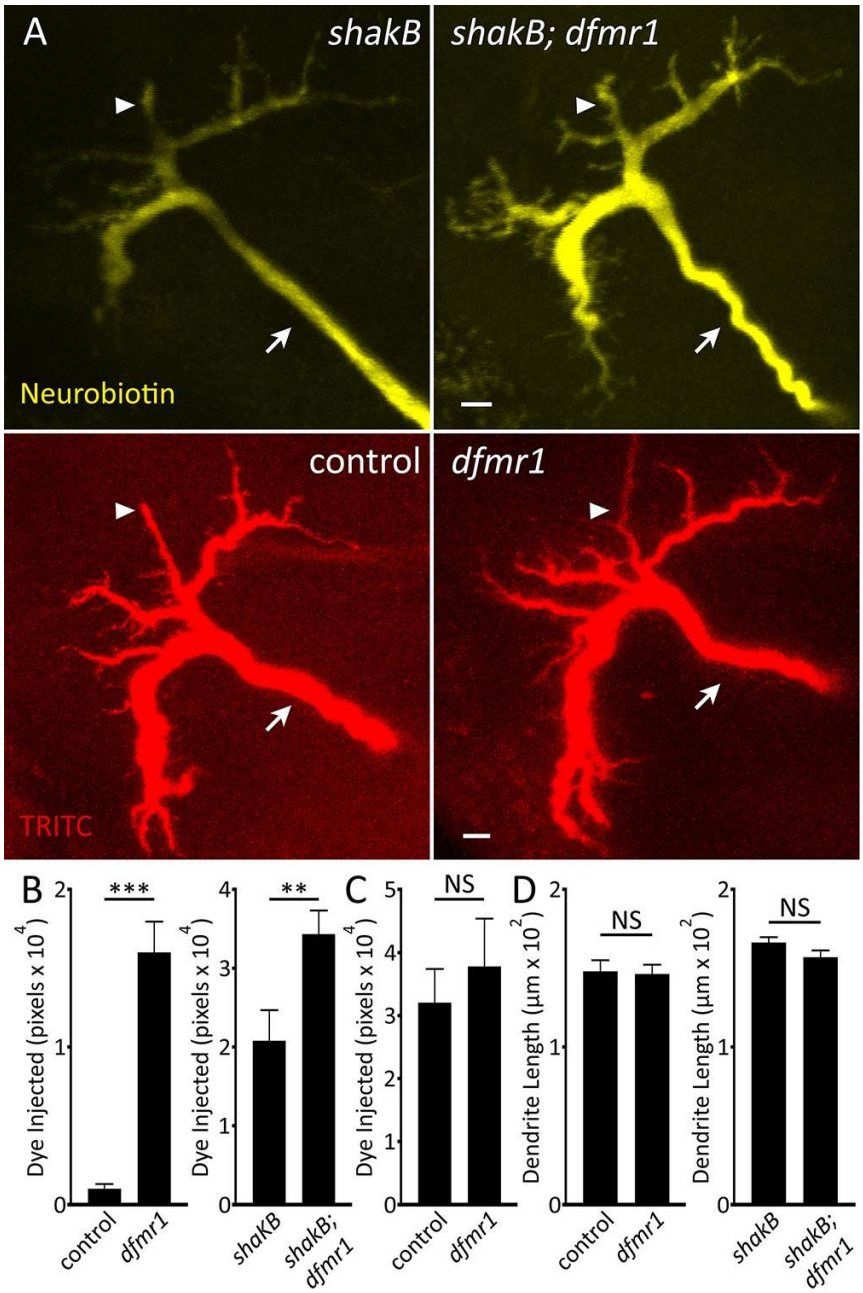

Figure 8. Specific Small Dye Iontophoresis is Increased in *dfmr1* GFI Dendritic Arbors

A, Representative images of the GFI dendritic arbors in *shakB*^{2} single mutant (top left) and *shakB*^{2}*; dfmr1*^{50M} double mutants (top right) labeled with NB injection (yellow, ddH_2O), and *w*^{1118} genetic control (bottom left) and *dfmr1*^{50M} null (bottom right) labeled with TRITC injection (red, ddH_2O). Arrowheads indicate dendritic projections connected to the cell body (out of focus). Arrows indicate the descending axons. Scale bars: 5µm. ***B,*** NB injection quantification of GFI dendritic arbor for *w*^{1118} control versus *dfmr1*^{50M} null (left), and *shakB*^{2} versus *shakB*^{2}*; dfmr1*^{50M} (right), displayed as the mean ± SEM. *w*^{1118} n=20, *dfmr1*^{50M} n=20, *shakB*^{2} n=27, *shakB*^{2}*; dfmr1*^{50M} n=30. ***C,*** TRITC injection quantification of GFI dendritic arbor for *w*^{1118} control versus *dfmr1*^{50M} null, displayed as the mean ± SEM. *w*^{1118} n=17, *dfmr1*^{50M} n=17. ***D,*** Dendritic branch length quantification for *w*^{1118} control versus *dfmr1*^{50M} null (left), and *shakB*^{2} versus *shakB*^{2}*; dfmr1*^{50M} (right), displayed as the mean ± SEM. *w*^{1118} n=17, *dfmr1*^{50M} n=18, *shakB*^{2} n=26, *shakB*^{2}*; dfmr1*^{50M} n=28. Significance was determined from two-tailed unpaired *t* tests: p**<0.01, p***<0.001 and not significant (NS).

and *dfmr1* null mutants (*dfmr1*^{50M}: 146.4±6.0µm, n=18, p=0.85, two-tailed unpaired *t* test; Fig. **8***D*, left). Likewise, dendritic branching was similar in the dye-uncoupled circuit comparing *shakB*^{2} versus *shakB*^{2}*; dfmr1*^{50M} double mutants (*shakB*^{2}: 166.6±3.3µm, n=26; *shakB*^{2}*; dfmr1*^{50M}: 157.3±4.2µm, n=28, p=0.09, two-tailed unpaired *t* test; Fig. **8***D*, right). Overall, dye loading is increased in *dfmr1* null dendrites, similar to our findings in axons, indicating the dye loading increase occurs throughout the neuron. Moreover, gross dendritic arbor volume and branching is unchanged in *dfmr1* mutants, ruling out the possibility that smaller *dfmr1* dendrites drive more dye entry into axons. It is worth noting that there is similarly elevated dye loading in the *dfmr1* null cell bodies relative to controls (not pictured). Given this global increase in dye iontophoresis, we next tested multiple other neuronal properties that could impact dye uptake.

Intrinsic Neuronal Properties Unrelated to Dye Injection Defect

We first tested whether an increase in axon size could elevate NB dye loading in *dfmr1* nulls, despite unaltered TRITC uptake (Fig. **5**). We hypothesized larger volume, could accommodate more injected dye, causing the noticeable increase in signal along the GFI axon. We used the TRITC signal, an internal control unchanged between genotypes, to measure GFI axon diameter in control (left) versus *dfmr1* null (right) neurons (Fig. **9***A*). We found no difference in diameter between genotypes over a GFI axonal length of 40µm (Fig. **9***B*), with controls averaging 4.9±0.2µm (n=15) and *dfmr1* nulls 5.0±0.2µm (n=16) in diameter, a non-significant difference (p=0.79, two-tailed unpaired *t* test; Fig. **9***B*). We confirmed this finding by labeling the GFI with membrane RFP (UAS-*mcd8::rfp*) driven with a GFI-specific Gal4 driver (91H05-Gal4; Jenett et al., 2012). With this independent transgenic label (not shown), we again found similar axonal diameters comparing *dfmr1* nulls (5.9±0.4µm, n=12) versus controls (5.2±0.3µm, n=12; p=0.16, two-tailed unpaired *t* test), showing FMRP loss does not impact size. We also tested *dfmr1* mutants for elevated protein levels as a consequence of increased translation by extracting protein from control versus *dfmr1* null brains and comparing protein levels using the BCA assay. Quantified

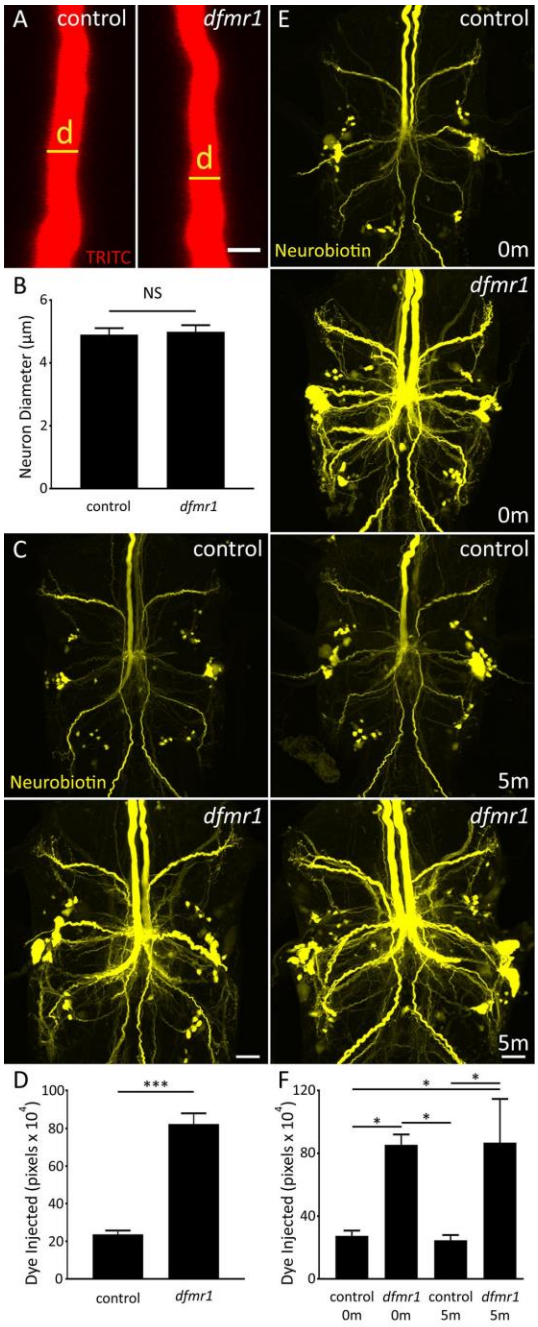

Figure 9. Dye Injection Defect is not Related to Multiple GFI Neuron Properties

A, Representative TRITC injections (ddH_2O) showing the GFI descending axon for w^{1118} genetic background (control, left) and $dfmr1^{50M}$ null mutant (right). Scale bar: 5µm. ***B,*** Quantification of the axon diameter in both genotypes, displayed as the mean ± SEM. Control n=15, *dfmr1* n=16. ***C,*** Representative NB dye injections into GFI for the w^{1118} genetic background (control, top) and the $dfmr1^{50M}$ null mutant (bottom) using only KAc-free dye solution (ddH_2O). Scale bar: 20µm. ***D,*** Quantification of the injected dye levels, displayed as mean ± SEM. Control n=25, *dfmr1* n=26. ***E,*** Representative NB injections (ddH_2O) into GFI for w^{1118} genetic background (control, panel 1, 3) and $dfmr1^{50M}$ null mutant (panel 2, 4). After dye injection, samples were either immediately dissected (0 min) or injected with TRITC for 5 minutes (5m) with positive current prior to dissection. Scale bar: 20µm. ***F,*** Quantification of injected dye levels, displayed as the mean ± SEM. 0m: control n=6, *dfmr1* n=6. 5m: control n=6, *dfmr1* n=5. Significance determined from two-tailed unpaired *t* test (*D*) and unpaired ANOVA (*F*): p*<0.05, p***<0.001 and not significant (NS).

comparisons of total brain protein levels confirm a highly significant increase in *dfmr1* nulls relative to controls by 14.5% (w^{1118} control: 1.40±0.04µg/brain, n=11; $dfmr1^{50M}$: 1.61±0.03µg/brain, n=11, p=0.0003, two-tailed unpaired *t* test). Thus, neuron size is unchanged in *dfmr1* mutants but protein concentration is elevated, consistent with expectations. We next explored the possibility that the standard 2M potassium acetate (KAc) in the dye injection electrode (Phelan et al., 1996; Kudumala et al., 2013; Lee and Godenschwege, 2014) is related to the iontophoretic differences between genotypes. We hypothesized that *dfmr1* mutants preferentially accept NB^+ ions over K^+ ions from the electrode due to intrinsic differences in membrane K^+ conductivity, characteristic of FXS disease models (Strumbos et al., 2010; Lee et al., 2011). We repeated dye injections with NB/TRITC dissolved in ddH_2O and found far more NB loaded in both controls and mutants (Fig. **9***C*). Incredibly, KAc-free injection controls contained as much dye signal as 2M KAc injected *dfmr1* null mutants typically display (compare Figs. **9***C* and **5***A*). KAc-free injection in *dfmr1* nulls revealed far more dye-coupled neurons, showing the extraordinary degree of GF circuit connectivity. In both genotypes, signal increased in GFIs and coupled neurons; however, the relative difference between *dfmr1* null and control remained unchanged (Fig. **9***C*,*D*). Mutants show a 3.5-fold increase in NB signal over controls (control: $23.6x10^4$±$2.1x10^4$, n=25; $dfmr1^{50M}$: $82.3x10^4$±$5.7x10^4$, n=26), a very significant elevation ($p=6.2x10^{-11}$, two-tailed unpaired *t* test; Fig. **9***D*). While this does not rule out a role for neuronal [K^+] or K^+ channel function in the dye loading phenotype, we found K^+ in the dye solution has no demonstrable impact on relative dye loading between controls and *dfmr1* nulls. We further explore the role for K^+ currents later (see below), but first we tested a simpler explanation: does loss of FMRP reduce NB dye leakage from neurons?

Besides gap junctions, many neuronal membrane pores permit escape of small ionic molecules (like NB) to the extracellular space, including innexin hemi-channels, transient receptor potential (TRP) channels and purinergic receptors (Bennett et al., 2003; Meyers et al., 2003). The broad FMRP role in mRNA translational regulation makes disruption of these protein levels a possibility in the FXS disease

state, although only tenuous links are currently known (Darnell et al., 2011; Naviaux et al., 2013; Kong et al., 2014). We used multiple experiments to test the hypothesis that membrane pores cause controls to leak more dye than *dfmr1* null neurons. First, we modified our protocol to rapidly fix brains after 2M KAc dye injection, dramatically shortening the potential NB dye leak period. When comparing the new rapid-fix w^{1118} control and *dfmr1* null neurons, we found no correction of the NB dye loading defect (control: $5.3x10^4 \pm 1.7x10^4$, n=9; $dfmr1^{50M}$: $16.4x10^4 \pm 2.1x10^4$, n=10), with a highly significant increase in mutants (p=0.0007, two-tailed unpaired *t* test; not shown). Second, we performed above KAc-free injections and then allowed preparations to sit for 5 minutes (5m) after injection, to intensify the effects of putative dye leakage. Quantification of dye loading shows no difference in signal with increased time for leakage (no delay (0m) w^{1118}: $30.1x10^4 \pm 4.8x10^4$, n=7; delay (5m) w^{1118}: $38.8x10^4 \pm 6.6x10^4$, n=8; p=0.32, two-tailed unpaired *t* test; not shown). Together, these two studies do not support a passive dye leakage effect causing the differential dye loading.

In a final trial, we tested the hypothesis that NB dye leakage occurs only during the actual current injection. The hypothesis was that controls produce more membrane pores than *dfmr1* nulls, but only current can drive NB through these pores, permitting leakage solely during iontophoresis. We tested this idea by performing KAc-free NB/TRITC injections for 2 minutes, and then injecting TRITC dissolved in 2M KAc for another 5 minutes. We found no difference between standard injections (Fig. **9***E,* 0 min) and additional current injections (Fig. **9***E*, 5 min) for either controls or *dfmr1* mutants, clearly ruling out the possibility of an electrically induced dye leak from the GFI. Moreover, the dye iontophoresis defect was not modulated, with far more NB signal in *dfmr1* mutants compared to controls (Fig. **9***E*). Quantification shows that injected dye remains following prolonged post-injection current for 5 minutes (0m control (c0): $27.6x10^4 \pm 3.2x10^4$, n=6; 0m $dfmr1^{50M}$ (*d*0): $85.5x10^4 \pm 6.7x10^4$, n=6; 5m control (c5): $24.7x10^4 \pm 3.4x10^4$, n=6; 5m $dfmr1^{50M}$ (*d*5): $86.8x10^4 \pm 27.9x10^4$, n=5), with significant differences persisting in all comparisons between controls and mutants (c0 v. *d*0: p=0.018, c0 v. c5: p=0.998, c0 v. *d*5: p=0.022, c5 v. *d*0: p=0.013,

c5 v. *d*5: p=0.015, *d*0 v. *d*5: p=1.00, unpaired ANOVA, Tukey-Kramer pairwise post-hoc test; Fig. **9***F*). After ruling out the possibility that dye leaks from the circuit, we turned our attention to cation movement to test whether changes in endogenous K^+ conductance alters NB injection.

Ionic Manipulations Alter Dye Loading but do not Resolve *dfmr1* Defect

A recent large body of work links FMRP to K^+ channel expression and function (Brown et al., 2010; Strumbos et al., 2010; Gross et al., 2011; Lee et al., 2011; Deng et al., 2013). We therefore hypothesized that *dfmr1* neurons more efficiently expel K^+ ions, reducing charge buildup to permit accumulation of more NB^+ ions. The above work supports this hypothesis by showing that removing KAc from the injection solution increases dye signal (Fig. **9***C,D*). We first used the K^+ channel blocker 4-aminopyridine (4-AP, 10mM; Singh and Singh, 1999) to test whether reduced K^+ conductance impairs NB dye loading (Fig. **10***A*). Comparing control (top) and *dfmr1* nulls (bottom) without (left) or with 4-AP (right), we found blocking K^+ channels greatly reduced dye loading in both genotypes. Importantly, however, a significant difference between drug-treated controls and *dfmr1* null mutants remains despite the major reduction in dye uptake (Fig. **10***A*). Quantification shows that 4-AP treatment strongly reduces NB loading, but also that the *dfmr1* defect persists (control 0mM 4-AP (c-): $8.4x10^4 \pm 1.2x10^4$, n=15; $dfmr1^{50M}$ 0mM 4-AP (*d*-): $18.2x10^4 \pm 1.7x10^4$, n=15; control 10mM 4-AP (c+): $2.2x10^4 \pm 0.7x10^4$, n=15; $dfmr1^{50M}$ 10mM 4-AP (*d*+): $10.1x10^4 \pm 1.2x10^4$, n=15), with highly significant differences remaining (c- v. *d*-: p<0.0001, c- v. c+: p=0.004, c- v. *d*+: p=0.79, c+ v. *d*-: p=0.0001, c+ v. *d*+: p=0.0002, *d*- v. *d*+: p=0.0001, unpaired ANOVA, Tukey-Kramer pairwise post-hoc test; Fig. **10***B*). Thus, K^+ channel function appears not to explain the *dfmr1* defect.

To rule out the possibility that 4-AP was not fully blocking all K^+ channels involved in the phenotype, we assayed a cocktail consisting of both 4-AP (10mM) and tetraethylammonium (TEA, 10mM) in the bath, and cesium chloride (140mM) in the injection pipette. We again found reduced NB dye loading, but the expanded cocktail still does not correct the relative *dfmr1* mutant phenotype (control

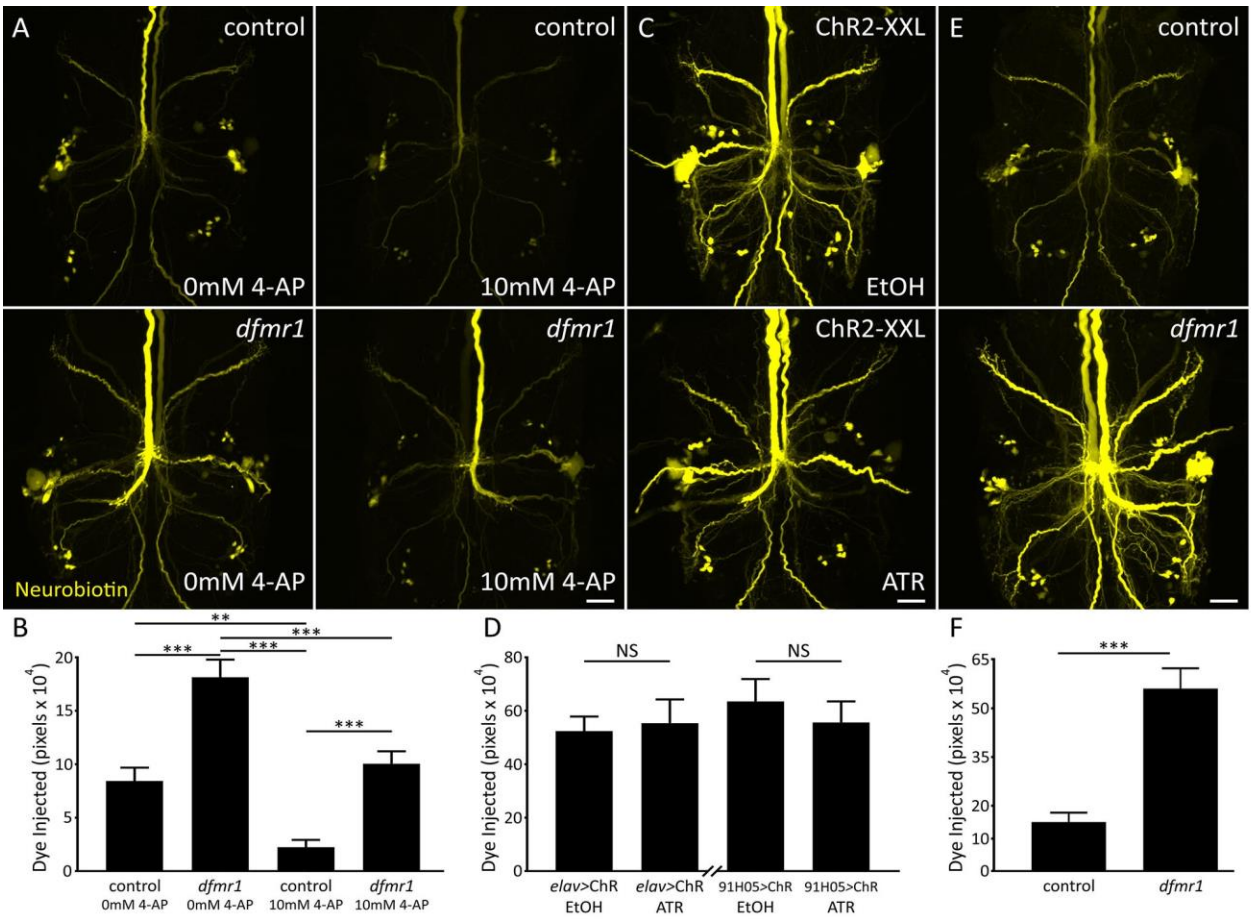

Figure 10. K⁺ Channel Block Reduces Dye Loading Without Correcting *dfmr1* Defect

A, Representative NB dye injections (2M KAc) into GFI in w^{1118} genetic background (control, top) and $dfmr1^{50M}$ null mutant (bottom). Samples were bathed in standard saline (left) or standard saline + 10mM 4-AP (right). Scale bar: 20µm. ***B,*** Quantification of injected dye levels, displayed as mean ± SEM. 0mM 4-AP: control n=15, *dfmr1* n=15. 10mM 4-AP: control n=15, *dfmr1* n=15. ***C,*** Representative NB injections into GFI (ddH_2O) for *elav*-Gal4 driven UAS-*chr2-xxl* animals raised on EtOH vehicle (top) or ATR co-factor (bottom). Scale bar: 20µm. ***D,*** Quantification of injected NB dye levels for both *elav*-Gal4 and 91H05-Gal4 (images not shown) driven UAS-*chr2-xxl*, displayed as mean ± SEM. *elav:* EtOH n=14, ATR n=14. 91H05: EtOH n=10, ATR n=12. ***E,*** Representative NB dye injections into GFI (ddH_2O) using an internal ground also within the GFI for the w^{1118} genetic background (top) and $dfmr1^{50M}$ null mutant (bottom). Scale bar: 20µm. ***F,*** Quantification of injected dye levels for both genotypes, displayed as mean ± SEM. Control n=9, *dfmr1* n=10. Significance determined with two-tailed unpaired *t* test (*F*) and unpaired ANOVA (*B*, *D*): p**<0.01, p***<0.001 and not significant (NS).

untreated (c-): $24.3x10^4±3.4x10^4$, n=16; $dfmr1^{50M}$ untreated (*d*-): $49.4x10^4±5.4x10^4$, n=14; control K^+ cocktail (c+): $6.3x10^4±1.2x10^4$, n=17; $dfmr1^{50M}$ K^+ cocktail (*d*+): $19.4x10^4±2.7x10^4$, n=16, c- v. *d*-: p<0.0001, c- v. c+: p=0.0007, c- v. *d*+: p=0.29, c+ v. *d*-: p= p<0.0001, c+ v. *d*+: p=0.0124, *d*- v. *d*+: p<0.0001, unpaired

ANOVA, Tukey-Kramer pairwise post-hoc test). We also repeated assays with the LY^- dye to test whether the reduced dye loading caused by K^+ channel blockade is specific to cationic dyes. We found that 10mM 4-AP during LY injection also reduces dye uptake in both control and *dfmr1* null neurons and maintains the pattern of increased loading in the absence of FMRP (LY control 0mM 4-AP (c-): $1.0x10^4 \pm 0.3x10^4$, n=35; LY *dfmr1*^{50M} 0mM 4-AP (*d*-): $2.3x10^4 \pm 0.4x10^4$, n=34; LY control 10mM 4-AP (c+): $0.5x10^4 \pm 0.2x10^4$, n=36; LY *dfmr1*^{50M} 10mM 4-AP (*d*+): $0.7x10^4 \pm 0.2x10^4$, n=36, c- v. *d*-: p=0.017, c- v. c+: p=0.57, c- v. *d*+: p=0.85, c+ v. *d*-: p=0.0002, c+ v. *d*+: p=0.96, *d*- v. *d*+: p=0.0012, unpaired ANOVA, Tukey-Kramer pairwise post-hoc test). Note that the lowered dye injection levels following 4-AP application makes fluorescence readings more variable and complicates determination of the significance of the LY effects. We conclude that 4-AP reduces NB/LY dye loading in both genotypes, but blocking K^+ channels does not alleviate differential dye loading between *dfmr1* and controls. To further test the role of ionic conductance, we next assayed increased conductivity.

We increased K^+ conductance via K^+ channel overexpression, including Irk2 (Inwardly rectifying K^+ channel 2; mammalian Kir2.1) and Shaw (Shaker cognate w; mammalian Kv3.2). Neural *elav*-Gal4 driven Irk2A causes a trending but non-significant increase in NB dye loading (*elav*/+ control: $22.2x10^4 \pm 2.5x10^4$, n=25; *elav*/UAS-*irk2*: $30.9x10^4 \pm 4.1x10^4$, n=22, p=0.08, two-tailed unpaired *t* test). Neural *elav*-Gal4 Shaw overexpression proved to be lethal and therefore could not be examined, but targeted GFI-specific 91H05-Gal4 driven Shaw expression has no discernable effect on dye loading (91H05/+: $57.5x10^4 \pm 4.7x10^4$, n=14; 91H05/UAS-*shaw*: $58.4x10^4 \pm 7.0x10^4$, n=14, p=0.91, two-tailed unpaired *t* test). We also used blue light-gated channelrhodopsin with the all-trans retinal (ATR) co-factor (Nagel et al., 2003) to provide temporal and pharmacological control over elevated cation conductivity. To maximize current, we used high-conductance ChR2-XXL channels (Dawydow et al., 2014) both pan-neuronally (*elav*-Gal4) and targeted to the GFI (91H05-Gal4). Both drivers show no difference in dye loading between controls fed the EtOH vehicle (Fig. **10***C*, top) and experimentals fed the essential ATR co-factor (bottom). Quantification shows

ChR2-XXL activation causes no increase in dye loading for either driver (*elav*-Gal4 EtOH: $52.4x10^4 \pm 5.5x10^4$, n=14; *elav* ATR: $55.4x10^4 \pm 8.9x10^4$, n=14, p=0.78, two-tailed unpaired *t* test; 91H05-Gal4 EtOH: $63.5x10^4 \pm 8.4x10^4$, n=10; 91H05 ATR: $55.7x10^4 \pm 7.9x10^4$, n=12, p=0.5, two-tailed unpaired *t* test; Fig. **10***D*). These results show increased K^+ permeability is unlikely to be the cause of increased *dfmr1* dye loading.

To more broadly test if conductance across the membrane alters dye loading we inserted both dye iontophoresis and ground electrodes into the GFI neuron, short-circuiting current flow across the membrane. We hypothesized that this "closed circuit" should prevent the dye loading phenotype if the *dfmr1* dye defect arises from membrane conductivity differences. With this dye injection paradigm (KAc-free), the *dfmr1* dye defect persisted (Fig. **10***E*). Controls showed the normal basal labeling of the injected GFI and dye-coupled neurons (top), whereas *dfmr1* null mutants showed an elevated, intense dye signal (bottom). Quantification of injected dye shows an internal ground maintains the iontophoresis defect (control: $15.0x10^4 \pm 3.0x10^4$, n=9; $dfmr1^{50M}$: $56.0x10^4 \pm 6.3x10^4$, n=10), with a highly significant effect ($p=5.5x10^{-5}$, two-tailed unpaired *t* test; Fig. **10***F*). Thus, results from removing the plasma membrane from the injection circuit suggest the defect does not arise from membrane ionic flux differences between the genotypes. Taken together, blocking K^+ channels with 4-AP reduces total dye loading dramatically, but does not equalize signal in controls and *dfmr1* mutants, dye loading is not impacted by introducing *Drosophila* K^+ or exogenous cation channels and removing membrane roles does not correct differential dye loading. This suggests that cytoplasmic changes in the absence of FMRP must contribute to the rate at which small charged dyes accumulate in neurons during iontophoresis.

Elevated Intracellular Dye Iontophoresis Rate in *dfmr1* Null Neurons

To test how more NB dye enters the GF circuit over time in *dfmr1* null mutants, we performed KAc-free dye injections for a series of durations: 10 seconds, 30 seconds, 1 minute and 2 minutes (Fig. **11**). We hypothesized dye signal would increase linearly as a function of time in both genotypes, with a

reduced slope in controls compared to mutants. To our surprise, timed injection results showed a much more striking difference in dye loading (Fig. **11***A*): control neurons display relatively limited dye uptake increases after the first 10 seconds of injection (left) compared with *dfmr1* null's steady, strong increase at each time point (right). In controls, the GFI axon and PSI cell bodies did not load significantly more dye over time, and the coupled neurons remained relatively weakly labeled after they reached an apparent equilibrium point (Fig. **11***A*). In sharp contrast, the *dfmr1* mutants began with similar NB dye levels compared to controls in the first 10 seconds, but then continuously accumulated more dye in the injected GFI as well as dye-coupled neurons, as evidenced by the dramatically broadening circuit dye incorporation over time. In *dfmr1* nulls, dye-coupled neurons that were not visible after 10 seconds of iontophoresis began to reach the quantification threshold after 30 seconds, and greatly contributed to the overall signal by 2 minutes (Fig. **11***A*). Note that dye was present in the same circuit neurons for both genotypes, and the broader pattern in *dfmr1* nulls results from more neurons crossing the quantification threshold, rather than new circuit partners.

Quantified comparisons show a significantly elevated rate of dye loading in *dfmr1* mutants (Fig. **11***B*). After 10 seconds of injection, there was no significant difference (control: $18.0x10^4 \pm 3.4x10^4$, n=10; $dfmr1^{50M}$: $20.9x10^4 \pm 2.3x10^4$, n=10; p=0.48), but by 30 seconds a small but significant elevation was apparent in the mutants (control: $29.1x10^4 \pm 5.0x10^4$, n=10; $dfmr1^{50M}$: $44.0x10^4 \pm 3.9x10^4$, n=10; p=0.03). After a full minute, a 2.5-fold increase was present in *dfmr1* nulls (control: $27.0x10^4 \pm 5.4x10^4$, n=10; $dfmr1^{50M}$: $68.3x10^4 \pm 7.5x10^4$, n=9; $p=4.7x10^{-4}$), which grew to more than a 4-fold increase by 2 minutes of injection (control: $24.6x10^4 \pm 3.5x10^4$, n=10; $dfmr1^{50M}$: $101.4x10^4 \pm 10.1x10^4$, n=10; $p=1.6x10^{-5}$, two-tailed unpaired *t* test; Fig. **11***B*). The result is a significant difference in the dye loading slope (p=0.003 unpaired ANCOVA), with a nearly 25-fold increase in the *dfmr1* nulls compared to the matched controls (Fig. **11***B*). In contrast to NB dye, TRITC levels increased linearly at a comparable rate between the two genotypes (Fig. **11***A*, insets), with no significant difference between the slopes (p=0.61, unpaired ANCOVA),

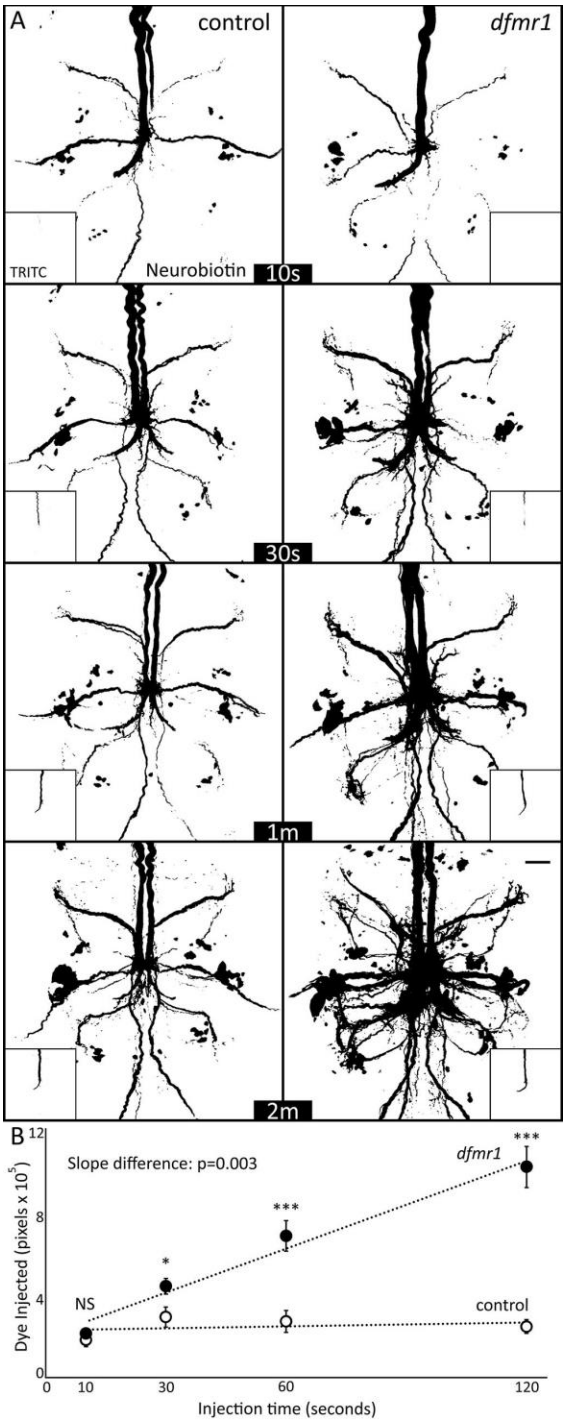

Figure 11. Dye Iontophoresis Rate is Highly Elevated in *dfmr1* Null Mutant Neurons

A, Representative NB dye injection (ddH_2O) images of GFI for the w^{1118} genetic background (control, left) and $dfmr1^{50M}$ null mutant (right) with progressively increasing periods of iontophoresis (10, 30, 60 and 120 seconds). The main images show NB dye loading, and insets show co-injected TRITC dye loading within the same neurons. All images display pixels above the threshold of 59. Scale bar: 20µm. ***B,*** Quantification of injected dye levels at each of the 4 time points for both genotypes, displayed as mean ± SEM. Control 10s n=10, control 30s n=10, control 1m n=10, control 2m n=10, *dfmr1* 10s n=10, *dfmr1* 30s n=10, *dfmr1* 1m n=9, *dfmr1* 2m n=10. Significance determined from two-tailed unpaired *t* test (points) and unpaired ANCOVA (slope): p*<0.05, p**<0.01, p***<0.001 and not significant (NS).

supporting our findings that FMRP loss does not affect TRITC dye loading (Fig. **5**) Together, these results show a highly selective FMRP-dependent dye iontophoresis rate defect, with *dfmr1*-null mutants losing a temporal restriction on iontophoresis. We conclude the FXS model lacks a barrier to small charged dye uptake, increasing dye loading in injected neurons and, consequently, signal throughout the electrically-coupled circuit.

Discussion

We have discovered an unexpected new effect of FMRP loss in the *Drosophila* FXS model: dye iontophoresis rates dramatically increase in neurons lacking FMRP, with the effect dependent on dye size but not charge. The defect is gap junction independent, but also increases dye transfer to downstream electrically-coupled neurons within the circuit. Evidence that genotype differences can affect neural dye iontophoresis is totally unprecedented, to our knowledge, despite extensive dye injection studies over many decades (Schofield, 2008; Lanciego and Wouterlood, 2011; Hanani, 2012). Both NB and LY dye loading defects are striking, but the absence of loading differences for the larger TRITC dye complicates the findings. Trans-dermal studies show electromigration primarily drives rapid electrophoretic ion movement for small molecules, while the slower movement of larger molecules depends more on electroosmosis (Marro et al., 2001; Kalia et al., 2004). Electroosmosis is an electric field dependent solvent flow caused by bulk movement of ions that accumulate along solid-liquid interfaces (Pikal, 2001). Here, this would result in ionic flux along the electrode sides, carrying a slow flow of solvent and larger dye molecules into the neuron. This effect may explain why larger TRITC responds differently than smaller NB and LY dyes: the slow electroosmotic solvent flow remains unchanged in *dfmr1* mutants, while the rapid electromigration rate becomes significantly disrupted.

Several tests show FMRP loss specifically causes dye iontophoresis elevation. First, we replicated the defect with a second *dfmr1* null allele, ruling out non-specific recessive effects. Second, we rescued

the phenotype with wildtype FMRP targeted to neurons, showing neuronal FMRP restricts dye uptake. Third, we showed the defect in *shakB*^{2} mutants in the Oregon-R background, not only ruling out gap junction connectivity defects (discussed below), but also showing persistence across genetic backgrounds. We found the defect is not NB-specific by repeating with negatively charged LY, eliminating NB-specific explanations, such as biotinidase degradation (Mishra et al., 2010), and positive charge specific theories, such as anionic precipitation. Gap junction coupling only allows passage of small molecules (<1kDa), regardless of charge, and seemed the obvious explanation here (Weber et al., 2004). Increased electrical synapses appeared a predicted consequence of well-reported FXS synaptic overgrowth and hyper-connectivity (Comery et al., 1997; Irwin et al., 2001; Zhang et al., 2001; Doll and Broadie, 2015). Indeed, recent work hints that FXS models have elevated gap junctions (Kong et al., 2014). However, we found *dfmr1* nulls show a trending gap junction reduction (ShakB levels), and complete gap junction loss (*shakB*^{2} null) does not correct the *dfmr1* dye loading phenotype. Likewise, LY loading was primarily limited to the GFI under our injection conditions, similar to *shakB*^{2} results, further confirming that dye movement to coupled neurons is not required for differential dye loading. Note the dye loading differences between *dfmr1* and control were reduced in the *shakB*^{2} background, suggesting partial rescue. The assay's shorter injection times may explain the difference, but it is possible that elevated interneuron connectivity is a separable neuronal property causing *dfmr1* nulls to increase dye uptake.

In our experiments, the only manipulation that increased dye loading was removing K^+ from the injection electrode, although the *dfmr1* phenotype persisted. The likely explanation is that dye no longer competes with smaller, more mobile, K^+ ions and thus constitutes more of the injection current; a shift well-known in trans-dermal iontophoresis (Pikal, 2001). K^+-free injection allows lower currents to deliver more dye over shorter periods, an advantage employed in subsequent experiments. The *dfmr1* dye loading defect holds for dyes of both polarities, so it remained possible, although not parsimonious, that FMRP loss disrupts multiple ion channel classes, altering anionic and cationic flow. We first tested K^+

channel function, known to be disrupted in FXS models (Brager and Johnston, 2014; Contractor et al., 2015). Importantly, application of K^+ channel blocker 4-AP (Singh and Singh, 1999) reduces dye loading, although the relative *dfmr1* phenotype persisted. A relationship between K^+ currents and iontophoretic loading has not been previously reported, to our knowledge, but suggests that increased *dfmr1* dye loading could result from elevated K^+ currents (Contractor et al., 2015). However, we could not significantly increase dye loading by elevating conductance with Irk2 or Shaw K^+ channels, or transgenic channelrhodopsin. Of course, changes to endogenous K^+ conductance in *dfmr1* nulls may not be sufficiently replicated with channel manipulations. However, persistence of the phenotype after removal of the plasma membrane from the injection circuit supports the conclusion that ion channels are not the primary cause of altered *dfmr1* null dye loading.

Another possibility is that *dfmr1* null neurons have a shifted iontophoretic current composition that does not affect net current flow. The current composition is the percent of charge carried by each ion group in the system. Each ionic contribution is determined by its charge, concentration, size and surrounding environment, represented by the transference number (Sackin and Boulpaep, 1981). FMRP loss could shift current composition, making it more difficult for neuronal ions to enter the electrode, favoring instead dye ions entering the neuron. This could be accomplished either by changing the ratio of ion groups in the cytoplasm or the cytoplasmic viscosity ions experience. The importance of ion ratios was demonstrated when we removed the small K^+ ion from the dye injection electrode and caused more dye to enter neurons without changing the iontophoretic current. A related change could occur in *dfmr1* null neurons, with the mutant cytoplasm containing a higher ratio of large ions than controls, thus reducing average cytoplasmic ion speed and favoring dye transfer into the neuron. An increase in large ion concentration may be a consequence of the known disruptions to multiple ion channel classes in the FXS model, altering neuronal resting ionic concentrations (Contractor et al., 2015). Testing such a hypothesis may require more sophisticated channel manipulations. Alternatively, the increased protein

concentrations in *dfmr1* nulls, confirmed in this work, could shift current composition to favor dye uptake if their charged residues alter the ionic composition of the cytosol (Qin et al., 2005; Tessier and Broadie, 2008). A similar shift could come from byproducts of disrupted enzymatic metabolism in the FXS condition (Lima-Cabello et al., 2016). Importantly, correcting protein levels via slowing the elevated translation rate ameliorates many FXS symptoms (Bolduc et al., 2008; Osterweil et al., 2013), and could prove equally efficacious for the increased *dfmr1* null dye loading.

In timed iontophoresis experiments, control neurons approach dye equilibrium after just 10 seconds of injection, whereas *dfmr1* null neurons exhibit constant dye accumulation over minutes. The limitation on dye loading is not caused by leakage, as fluorescence intensity remains constant regardless of time between dye injection and fixation. Dye loading was increased in all regions of *dfmr1* null neurons, including dendrites and axons, showing that differential dye compartmentalization or preferential subcellular filling does not explain the defect. We also rule out neuronal dye capacity, as both dendrite and axon sizes are unaltered. Moreover, any internal capacity differences would similarly affect the larger TRITC dye, which loaded equally in both genotypes. Further, iontophoretic differences based on neuronal capacity would not permit the increased dye loading caused by removing K^+ from the injection electrode. It is possible that increased cytoplasmic viscosity in *dfmr1* nulls shifts the ratio of incoming to outgoing ions by altering ionic flux (Kühn et al., 2011). This defect could arise from increased cytosolic concentration of proteins resulting from the loss of FMRP translational repression (Qin et al., 2005; Tessier and Broadie, 2008), Such a disruption would have wide-ranging developmental and functional effects on neural circuits in the FXS disease state.

In conclusion, we have uncovered a robust new consequence of FMRP loss in *Drosophila* FXS model neurons. Quantitative dye iontophoresis reveals *dfmr1* null neurons selectively lack an impediment to small charged dye entry. The FMRP mechanism limits iontophoretic rate, strictly capping the maximum dye transfer. The *dfmr1* mutant defect is limited to small NB^{+1} and LY^{-1} dyes, with no effect on the larger

TRITC^{+1} dye. Increased gap junction coupling seemed the obvious explanation for our findings, but persistence of the NB loading defect in *shakB*^{2} nulls lacking gap junctions, as well as the GFI-restricted LY loading defect in *dfmr1* nulls, rules out neuronal coupling as causative. Neuron size, membrane porosity and ion channel function all appear to play negligible roles in the phenotype. This study has also shed new light on the classic iontophoretic dye-injection technique, showing that: 1) genotype can dictate dye iontophoresis rate, 2) ionic composition can limit dye loading, and 3) K^+ channel currents can enhance dye transfer. All of these findings are unprecedented, despite extensive dye studies for decades, and force us to expand our understanding of this classic technique. FMRP regulates numerous transcript targets (Darnell et al., 2011), primarily repressing translation (Cvetkovska et al., 2013; Ifrim et al., 2015), and also regulates numerous ion channel classes (Contractor et al., 2015), providing several avenues for future investigation of the FMRP intersection with dye loading. Determining the causative mechanism(s) underlying disrupted dye iontophoresis will be a difficult, albeit important goal, as it may help identify neuronal causes of FXS symptoms.

Chapter III

Newly Identified Electrically Coupled Neurons Support Development of the *Drosophila* Giant Fiber Model Circuit

This paper has been published under the same title in eNeuro, 2018.

Nine movies were included as part of this work which can be found at

http://www.eneuro.org/content/early/2018/11/22/ENEURO.0346-18.2018

Tyler Kennedy[1] and Kendal Broadie[1,2,3]

[1]Department of Biological Sciences, [2]Department of Cell and Developmental Biology, [3]Vanderbilt Brain Institute, Vanderbilt University and Medical Center,

Nashville, TN 37235 USA

Abstract

The *Drosophila* Giant Fiber (GF) escape circuit is an extensively studied model for neuron connectivity and function. Researchers have long taken advantage of the simple linear neuronal pathway, which begins at peripheral sensory modalities, travels through the central GF Interneuron (GFI) to motor neurons, and terminates on wing/leg muscles. This circuit is more complex than it seems however, as there exists a complex web of coupled neurons connected to the GFI, which widely innervate the thoracic ganglion. Here, we define four new neuron clusters dye-coupled to the central GFI, which we name GF Coupled (GFC) 1-4. We identify new transgenic Gal4 drivers that express specifically in these neurons, and map both neuronal architecture and synaptic polarity. GFC1-4 share a central site of GFI connectivity, the Inframedial Bridge (IB), where the neurons each form electrical synapses. Targeted apoptotic ablation of

GFC1 reveals a key role for proper development of the GF circuit, including the maintenance of GFI connectivity with upstream and downstream synaptic partners. GFC1 ablation frequently results in loss of one GFI, which is always compensated for by contralateral innervation from a branch of the persisting GFI axon. Overall, this work reveals extensively coupled interconnectivity within the GF circuit, and the requirement of coupled neurons for circuit development. Identification of this large population of electrically-coupled neurons in this classic model, and the ability to genetically manipulate these electrically synapsed neurons, expands the GF system capabilities for the nuanced, sophisticated circuit dissection necessary for deeper investigations into brain formation.

Significance Statement

Genetic model neural circuits with individually identifiable neurons help us understand how nervous systems wire together during development, and then operate through coordinated chemical and electrical signaling. The *Drosophila* Giant Fiber circuit has long served as such a model, due to large neuron size, genetic malleability and easily visualized behavioral output: a jump in response to a threat. This study unveils new members of this circuit, all of which synapse with the circuit at one site on the central Giant Fiber Interneuron. We use new tools to identify and transgenically manipulate these neurons and show that these neurons are required for proper circuit development. This study provides a detailed circuit map for further dissection of neuronal connectivity and electrically-coupled communication.

Introduction

The *Drosophila* Giant Fiber (GF) circuit is particularly suitable for single-neuron resolution neurodevelopmental studies for a number of reasons, all related to its role as an escape response circuit (Allen et al., 2006; Boerner and Godenschwege, 2011). The need for rapid signal conduction from the senses through brain to muscles promoted evolution of very large neurons throughout this circuit,

facilitating their visualization and manipulation (Power, 1948; Borgen et al., 2017). This enlargement is most prominent in the long-distance Giant Fiber Interneuron (GFI), which consolidates sensory information in the brain and projects through the neck into the thoracic ganglion (TG) via giant axons (Allen et al., 1998; Pézier et al., 2014). To increase communication speed and fidelity between neurons, the GF circuitry uses mixed chemical and electrical synapses (Thomas and Wyman, 1984; Blagburn et al., 1999; Fayyazuddin et al., 2006). These electrical synapses, composed of the Shaking-B innexin, can pass small tracer dyes to identify coupled partner neurons (Phelan et al., 1996).

The GF circuit targets two large muscle sets used for rapid escape behavior, the Tergotrochanteral Muscle (TTM), which controls the legs for jumping, and the Dorsal Longitudinal Muscle (DLM), which controls the wings (Tanouye and Wyman, 1980). The escape behavior is easily scored and muscles are accessible to electrophysiological recordings, providing two outlets to study whole circuit function (Martinez et al., 2007; Augustin et al., 2011; von Reyn et al., 2014). The GFI connects to the TTM via the Tergotrochanteral Motor neuron (TTMn) and to the DLM via the Peripherally Synapsing Interneuron (PSI), which in turn synapses onto the Dorsal Longitudinal Motor neuron (DLMn; Tanouye and Wyman, 1980; Allen et al., 2006). While the GF circuit is reported to be quite simple, electrophoretic injections with small dyes make it clear that the GFI is actually part of a much larger circuit network of undescribed neurons (Boerner and Godenschwege, 2011; Enneking et al., 2013; Kennedy and Broadie, 2017).

This larger GF circuit should come as no surprise, as most classically studied circuits are continuously being updated to include new neurons, increasing appreciation of the complexity and interconnectivity within the brain (Lin et al., 2016; Talay et al., 2017; Zheng et al., 2017; Cande et al., 2018). Describing the wiring diagrams of classic circuits within model brains is important for understanding how local circuits accomplish processing tasks, while also overriding or promoting behaviors controlled by separated but interconnected circuits (Gaudry and Kristan, 2009; Stensmyr et al., 2012; von Reyn et al., 2014). More complex model circuits can better help answer questions about how circuits develop and

evolve over time (Ward et al., 2015; Tosches, 2017). Combining GF circuit manipulability with the full complement of GFI-coupled neurons should enable robust new avenues for experimentation on how neurons select partners, determine synaptic strength and regulate neighboring circuits.

In this study, we use neurobiotin dye injection to map previously uncharacterized GF Coupled (GFC) neurons. We take advantage of the Flylight Gal4 library collection to identify transgenic drivers for the GFCs (Brand and Perrimon, 1993; Jenett et al., 2012). This approach defined four new GFI-coupled neuron clusters (GFC1-4) within the GF circuit, which we characterize for their architecture, neuronal polarity and synaptic connectivity. We show that the Inframedial Bridge (IB; Allen et al., 1998) is the GFI site where all the GFC neurons come together to synapse with the circuit. We ablate GF neurons by transgenic expression of the apoptotic Head Involution Defective (Hid) protein (Zhou et al., 1997) to find that GFC1 and PSI are required for proper GFI development. We also find GFI axons always compensate for loss of their bilaterally symmetric partner through new contralateral innervation. Together, this work broadens the known GF circuit and opens new avenues for studying electrically-coupled circuit development, function and plasticity.

Materials and Methods

Drosophila Genetics

All animals were maintained on a standard cornmeal/agar/molasses *Drosophila* food in a 12-hour light:dark cycling incubator at 25°C. Timed-lay eggs were collected for 2-3 days, and experimental animals were selected from rearing tubes 10-14 days later. The following *Drosophila* lines were used for genetic crosses: w^{1118} (RRID:BDSC_3605) | w^{1118}; P{GMR78A06-Gal4}attP2 (Jenett et al., 2012) | w^{1118}; P{GMR73C07-Gal4}attP2 (RRID:BDSC_46689) | w^{1118}; P{GMR24H07-Gal4}attP2 (RRID:BDSC_49317) | w^{1118}; P{GMR42A06-Gal4}attP2 (RRID:BDSC_41245) | w^{1118}; R10B11-p65.AD}attP40 (Dionne et al., 2018;

RRID:BDSC_68807) | *w*^{1118}*;* P{GMR14A06-Gal4.DBD}attP2 (RRID:BDSC_68738) | *w*^{1118}, *y*^{1}; 10X UAS-*ivs-mcd8*::*gfp* attP40 (Pfeiffer et al., 2010) | UAS-*hid*.Z/CyO (Zhou et al., 1997; RRID:BDSC_65403) | *w*^{1118}*;* UAS-*denmark*, UAS-*syt::gfp* (Zhang et al., 2002; Nicolai et al., 2010; RRID:BDSC_33064). Both females and males were used in this study, with sex-specific selection stated in figure legends. All genotypes were verified with visible markers.

Dye Iontophoresis

GFI dye injections were performed similar to the previously published methods (Boerner and Godenschwege, 2011; Kennedy and Broadie, 2017). Briefly; glass electrodes (Kwik-Fil Borosilicate glass 1B100F-4, World Precision Instruments) were pulled on a laser electrode puller (Model P-2000, Sutter Instrument Company) to 10MΩ resistance (3M KCl). Electrodes were filled with 0.25% TRITC-Dextran (10kDa, Life Technologies) and 7% neurobiotin (Vector Laboratories, RRID:AB_2313575) in ddH_2O. Filled electrodes were placed on a silver-chloride wire mounted on a PCS-5000 micromanipulator (Burleigh). Animals in physiological saline were cut along the dorsal midline to access the cervical connective (CC), at which electrodes were inserted into the GFI. A square-pulse stimulator (Grass S48, Astro-Med) provided 7.5 100ms pulses/second for 2 mins with the 20nA injected current monitored by an AxoClamp2B amplifier. A Digidata data acquisition system (1320A, Axon Instruments) was controlled with Clampex 9.2 software.

Confocal Imaging

Brains were fixed for 30 mins in 4% paraformaldehyde/sucrose (Electron Microscopy Services) in phosphate-buffered saline (PBS, pH 7.2, Life Technology) and then rinsed 3X with PBS, and blocked for 1 hr with 1% bovine serum albumin (BSA, Sigma-Aldrich) in PBST (PBS + 0.2% Triton X-100; Thermo Fisher Scientific). Labels were diluted in PBST with 0.2% BSA. The following labels were used: Streptavidin::Cy5

(1:20, Life Technology), rabbit anti-ShakB (1:250, Phelan et al., 1996), rabbit anti-GFP (1:2000; Abcam, RRID:AB_303395), FITC Goat anti-GFP (1:500; Abcam, RRID:AB_305635), Rabbit anti-RFP (1:500; Rockland, RRID:AB_2209751), Alexa 488-conjugated donkey anti-goat (1:250; Thermo Fisher, RRID:AB_2534102), Alexa 488-conjugated donkey anti-rabbit (1:250; Thermo Fisher, RRID:AB_2556546), Alexa-568 conjugated donkey anti-rabbit (1:250; Thermo Fisher, RRID:AB_2534017), Alexa-647 conjugated donkey anti-rabbit (1:250; Thermo Fisher, RRID:AB_2536183), and Alexa-633 conjugated goat anti-rabbit (1:250; Thermo Fisher, RRID:AB_141419). Next, preparations were rinsed 3X for 30 mins in PBST, 1X in PBS, and then mounted on glass microscope slides (Probe On Plus 25 x 75 x 1.0mm, Thermo Fisher Scientific) in 2, 2'-Thiodiethanol (TDE, Sigma-Aldrich; Staudt et al., 2007). To prevent crushing, double-sided poster tape (Scotch) was placed on each side of the brains. Coverslips (No. 1.5H, Zeiss) were sealed with nail polish (Hard as Nails, Sally Hansen). Fluorescent images were collected using a ZEISS LSM 880 confocal microscope with an AiryScan module, which has increased lateral resolution (161nm) and signal-to-noise ratio (Sivaguru et al., 2016). Images show maximum Z-stack projections under standard confocal mode, unless otherwise noted in the figure legends.

Data Analyses

Data processing and image creation was done with FIJI software (version 2, RRID:SCR_002285; Schindelin et al., 2012; Schneider et al., 2012). Neuronal models and movies were created using Imaris (version 9.2, RRID:SCR_007370).

Results

The Giant Fiber Circuit Exhibits Extensive Dye-Coupled Connectivity

Small, gap junction permeable dyes used to study the Giant Fiber (GF) circuit have consistently revealed an extensive, but uncharacterized, network of dye-coupled neurons (Boerner and Godenschwege, 2011; Enneking et al., 2013; Kennedy and Broadie, 2017). In order to thoroughly study the architecture and properties of these neurons, we iontophoretically injected the Giant Fiber Interneuron (GFI) with the highly gap-junction permeable neurobiotin (NB) dye, and then labeled the brains post-hoc with a streptavidin-conjugated fluorophore (Huang et al., 1992). Consistent with previously published work, this intracellular dye injection reveals an extensive network of neurons dye-coupled to the GFI (Fig. **12**). This dye-coupling is the direct result of gap junction connectivity, as eliminating gap junctions using *shaking-B* mutants (*shakB*^{2}) prevents all NB dye transfer (data not shown; Blagburn et al., 1999; Kennedy and Broadie, 2017). A summary of this newly identified GF circuitry is shown in Figure **12**.

Although there are a large number of dye-labeled processes widely distributed throughout the thoracic ganglion (TG; Fig. **12***A*), all published GF circuit maps name only two GFI-coupled cells: 1) Tergotrochanteral Motor neuron (TTMn) and 2) Peripherally Synapsing Interneuron (PSI; Fig. **12***B*, 'old circuit map'). Here, we map and characterize all of the dye-coupled neurons whose projections we can trace back to an identifiable cell soma. We have named these neurons "Giant Fiber Coupled" (GFC) followed by an identifying number (Fig. **12***A*, *B*). In this study, we report the characterization of 4 neuron clusters (GFC1-4), each of which represents a bilaterally-symmetric set of 2-7 neurons (Fig. **12***B*, 'new circuit map'). The processes of these neurons contact the descending GFI axons and reach into all three TG segments (TG1-3), but do not cross into the brain or abdominal ganglion (AG). To understand how the GFCs integrate into the GF circuit, we began by obtaining selective genetic access to these neurons.

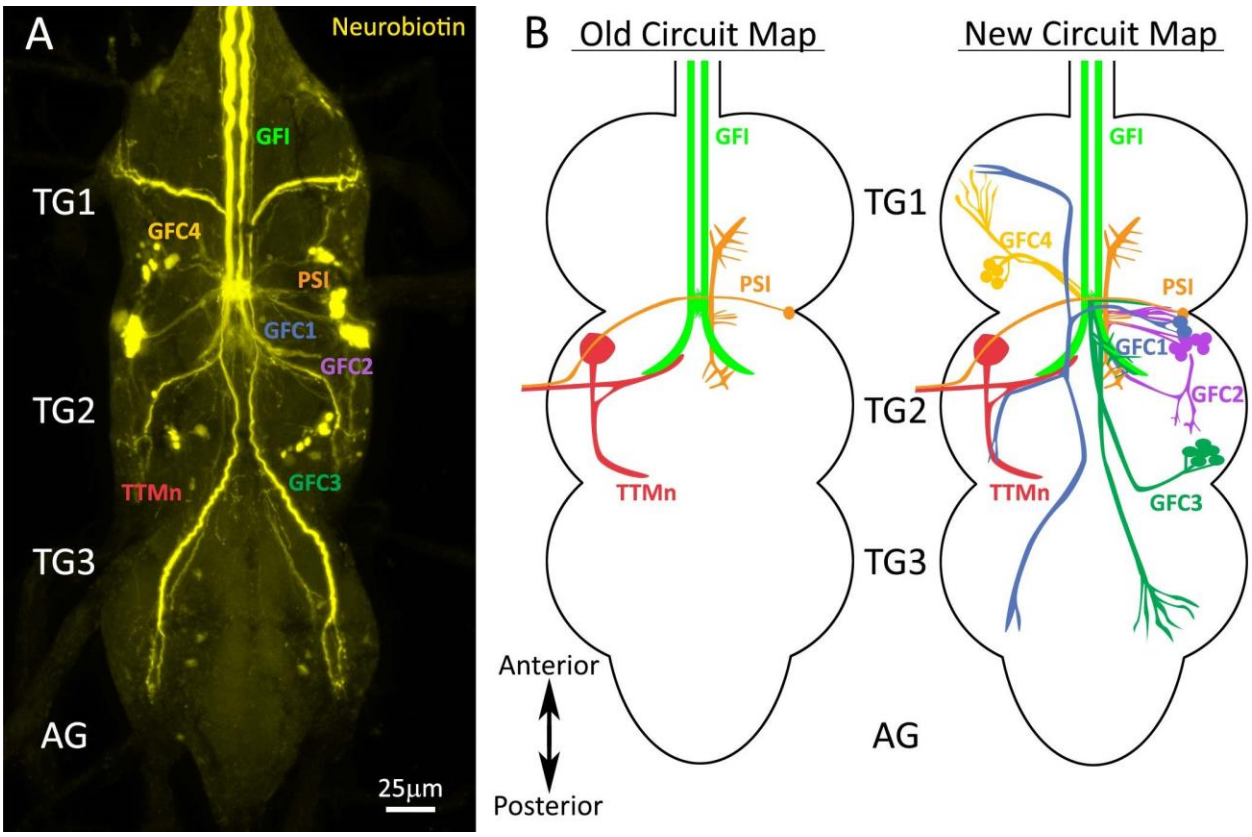

Figure 12. Giant Fiber Interneuron Dye Injection Reveals Coupled Neurons
A, The Giant Fiber Interneuron (GFI) iontophoretically injected with neurobiotin (yellow) shows extensive dye-coupling to neurons in the thoracic ganglion (TG). The established GFI-coupled neurons are 1) the Peripherally Synapsing Interneuron (PSI; orange) and 2) the Tergotrochanteral Motor neuron (TTMn; red). The newly identified GFCs project into all three TG segments (TG1-3), but do not extend into the abdominal ganglia (AG). ***B,*** Left: The old GF circuit map showing both of the previously characterized GFI (green) dye-coupled neurons: PSI (orange) and TTMn (red). Right: The new GF circuit map with the addition of all the newly identified GFC neurons from this study: GFC1 (blue), GFC2 (purple), GFC3 (dark green) and GFC4 (yellow).

Transgenic Gal4 Drivers for Newly Identified Giant Fiber Coupled Neurons

To accurately map and manipulate the separate GFC neuron populations, we set forth to identify Gal4 drivers with highly specific expression for each GFC using two approaches. First, we conducted an *in silico* screen through the entire Janelia FlyLight library, which includes lines generated from the Vienna Tiles project (9,436 lines; Jenett et al., 2012; Tirian and Dickson, 2017). Using images of the GFI dye-labeled

circuit (Fig. **12***A*), we screened for matching GFP expression patterns (Fig. **13**). We identified highly specific Gal4 drivers for GFC1 (78A06; Fig. **13***A*) and GFC2 (73C07; Fig. **13***B*), as well as less specific drivers for GFC3 and GFC4. Second, for cleaner GFC3 and GFC4 drivers, we used the recent automated Color-depth Maximum Intensity Projection (MIP) tool for the *Drosophila* transgenic database (Otsuna et al., 2018). Using the less specific driver lines as templates to search this library, we screened for specific Gal4 drivers for GFC3 and GFC4. This complementary approach uncovered a highly specific driver for GFC3 (24H07; Fig. **13***C*), and a combined driver for GFC3/4 (42A06; Fig. **13***D*). During our search with the MIP tool, we identified many additional GF circuit drivers, aside from the ones used in this study. We selected the cleanest drivers and report them in Table **3** for use in future experiments.

GFI	GCI	TTMn	PSI	GFC1	GFC2	GFC3
R14A01	R32C04	R25D08	R26E04	R93E07	R13C08	R44D02
VT004455	R74E09	R88F07	R75E05	R87D02	R77C12	R58E04
VT042336	VT002209	VT038335	VT030598	VT059438	VT043662	R75D03

Table 3. Transgenic Gal4 Driver Lines for the Giant Fiber Circuit
New Gal4 drivers (distinct from those used in this study) that express selectively within the GF circuit, as compiled from the Janelia Flylight and Vienna Tiles library collections. Selective lines for GFC4 have not been uncovered and thus are not reported here. Abbreviations: GFI: Giant Fiber Interneuron, GCI: Giant Commissural Interneuron, TTMn: Tergotrochanteral Motor neuron, PSI: Peripherally Synapsing Interneuron, GFC: Giant Fiber Coupled neurons.

To confirm that the new Gal4 transgenic driver lines label the *bona fide* GFC components of the GF circuit, we crossed each Gal4 line with the UAS-*mcd8::gfp* membrane reporter (Fig. **13**, column 1) and injected the GFI with NB (Fig. **13**, column 2). The merged images show perfect overlap between each transgenic driver line and the specified subset of the dye labeled neurons (Fig. **13**, column 3). Cell bodies are strongly labeled in all cases (arrowheads), and individual neuronal processes of GFC1-4 can be traced for both the GFP and NB signals (arrows). However, in some cases, such as GFC2 (73C07-Gal4), the dye injection signal is much dimmer than for other neurons, such as GFC1 (78A06-Gal4). Each GFC cluster is schematically represented within the TG, with full color on one side (Fig. **12** color scheme) and dashed

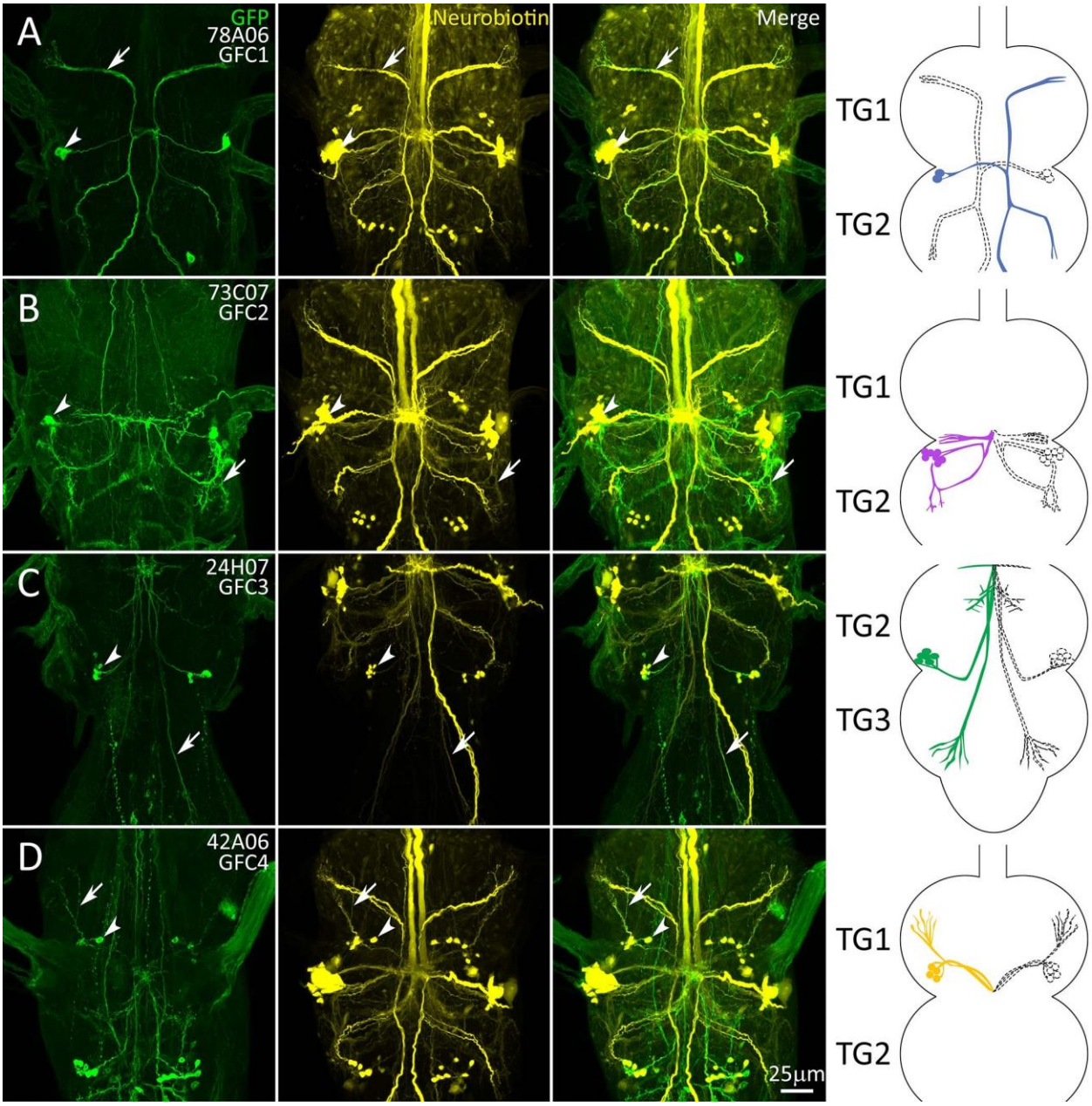

Figure 13. Transgenic Gal4 Drivers for the Newly Identified GFC Neurons

Gal4-driven expression of UAS-*mcd8::gfp* (green, column 1) overlapping with the GFI injection of neurobiotin dye (yellow, column 2) showing the identification of GFC drivers (merge, column 3). Arrows indicate processes with overlapping GFP and NB labeling, and arrowheads show the GFC cell bodies. The GFC neurons are drawn both in color (Fig. **12** color scheme) and perforated outlines to show their bilateral pattern (column 4). Thoracic ganglia (TG) segments are selected to best show GFC projection architecture. All injections were performed on females. ***A,*** 78A06-Gal4 labels GFC1. The driver strength is relatively weak, with a somewhat stochastic labeling of the GFC1 neurons. ***B,*** 73C07-Gal4 labels GFC2. This driver is moderately strong, but also labels other neurons. ***C,*** 24H07-Gal4 labels GFC3. This driver strength is moderate, with labeling of other neurons. ***D,*** 42A06-Gal4 labels both GFC3 and GFC4 neurons. The driver is relatively weak, with stochastic labeling of GFC4 neurons.

outlines on the other side, to show each individual GFC neuron as well as their bilaterally symmetrical pattern (Fig. **13**, column 4). Using these Gal4-driven GFP expression patterns, we are able to map each GFC cluster within the TG.

Projection Architecture of GFC Neurons Within the Thoracic Ganglion

GFC1 is comprised of 2 bilaterally symmetrical neurons on each side of TG2 (Fig. **13***A*). Each soma projects a process medially, which crosses the midline at the Inframedial Bridge (IB; Allen et al., 1998) and then splits, sending one branch anteriorly and one posteriorly. The anterior process travels halfway up TG1, then bends laterally and ventrally to terminate in the anterior corner of TG1, almost at the ventral-most point of the TG (Fig. **13***A*). This process extends several thin terminals, beginning in the same plane as the GFI bend. The posterior process splits halfway down TG2, just below the GFI bend. One branch proceeds laterally, then turns posteriorly towards the TG2 edge, with a ventral dive and several thin terminals, before terminating in the TG2 posterior lateral corner (Fig. **13***A*). The other process descends into TG3, bends inward towards the midline, then laterally to the anterior edge. From here, the process projects posteriorly and ventrally to end in a similar fashion to the other two terminals (Fig. **13***A*). All three GFC1 projections appear to innervate the leg neuropils (Namiki et al., 2018).

The 7 bilaterally symmetric GFC2 neurons are largely restricted to TG2 (Fig. **13***B*). These cell bodies neighbor GFC1 and similarly project fasciculating processes medially. However, two-thirds of the way to the midline, the processes bend posteriorly and then laterally, to curve ventrally towards the lower edge of TG2 in the region of the GFI axon bend (Fig. **13***B*). The processes then curve anteriorly back towards the cell bodies, with a slight dorsal trajectory before termination, projecting several short, heavily-branched termini in anterior and posterior directions. Another process doubles back towards the posterior deflection, travels medially to the midline and then sends out two branches posteriorly (Fig. **13***B*). One curves ventrolaterally to terminate along the first ventral spiral, and the other travels dorsolaterally along

the path of the original anterior process, terminating as it turns up towards the soma. There are two other processes that depart from the midline: one travels dorsally and slightly posteriorly before terminating, and one projects anteriorly and dorsolaterally to terminate in the lower central TG1 (Fig. **13***B*). These processes both appear to innervate the wing neuropils (Namiki et al., 2018).

GFC3 is comprised of 5 bilaterally symmetrical neurons with the cell bodies positioned dorsally in the posteriolateral corner of TG2 (Fig. **13***C*). These cells send out fasciculating processes that first proceed ventrally in a medial-anterior direction up to the central IB connection with the GFI. At the IB, extensive GFC3 branches are visible, extending laterally and dorsally, but no further in either anterior or ventral directions (Fig. **13***C*). These processes also track along the large terminal bend of the GFI axon. Dorsal to the IB, the main GFC3 processes reverse course to travel posteriolaterally, while remaining ipsilateral to their cell bodies. The projection direction is ventral until TG3 is reached, at which point the processes move dorsally once again (Fig. **13***C*). These processes terminate near the anterior portion of TG3 within the leg neuropil, in a series of thin processes at approximately the same axial plane as the IB and GFI axonal bends (Fig. **13***C*). Of note, both GFC1 and GFC3 were unintentionally captured in a recent screen for descending neurons (Namiki et al., 2018).

The 4 bilaterally symmetric GFC4 neurons are largely restricted to TG1 (Fig. **13***D*). The GFC4 cell bodies lie in the TG1 dorsal lateroposterior corner. The GFC4 processes first fasciculate to project ventrally, then posterior-medially, running to the central IB (Fig. **13***D*). From the IB, the GFC4 processes then reverse course, remaining ipsilateral to their cell bodies as they project dorsally, back the way they came towards their cell bodies (Fig. **13***D*). When the GFC4 processes are directly below their cell bodies, they turn ventrally, and then travel towards the TG1 anteriolateral corner to terminate in long finger-like projects (Fig. **13***D*). Like the other GFCs, the GFC4 processes appear to innervate the leg neuropils (Namiki et al., 2018). Overall, these transgenic driver lines allow detailed analysis of GFC architecture, and provide

highly specific genetic control over the GFC neurons. To determine how these neurons interact with the GF circuit, we next examined their contact points with the GFI.

The Inframedial Bridge Connectivity Site of GFI-GFC Intersection

GFC1-4 are all dye-coupled to GFI via direct or indirect gap junction connections (Fig. **12**), and all of these neurons project to the central Inframedial Bridge (IB) to overlap with the GFI (Fig. **13**). The IB has been defined as a region proximal to the GFI lateral axonal bend, where the GFI axon puts forth tufted projections and connects to the PSI (Allen et al., 1998). We therefore hypothesized the IB is the primary site of GFI-GFC connectivity. To determine the location of potential synaptic sites between the GFI and GFCs, we injected the GFI with the large, non-permeant dye tetramethylrhodamine (TRITC-dextran, 10 kDa; Boerner and Godenschwege, 2011; Enneking et al., 2013; Kennedy and Broadie, 2017) for all the UAS-*mcd8::gfp* labeled GFC1-4 lines (Fig. **14**). We then assayed for overlap regions where GFC membrane signal (Fig. **14**, column 1) contacts the GFI TRITC signal (Fig. **14**, column 2). Merging the two channels to create static (Fig. **14**, column 3) and dynamic (Movies 1-4) 3D reconstructions of the spatial overlap provides clear identification of GFI-GFC contact points.

GFP and TRITC signals are color coded by depth to visualize the Z dimension (FIJI plugin: Temporal-Color Code), with neurons proximal in Z space displaying the same color (Fig. **14**, columns 1, 2). Overlap between neurons is shown for GFCs (green) and GFI (magenta; Fig. **14**, column 3). The results show that GFC1 contacts the GFI only at the IB with a simple crossing branch (Fig. **14***A*, arrows; Movie 1). GFC2-4 also contact the GFI directly at the IB, but with a much higher level of complexity (Fig. **14***B-D*, arrows; Movie 2-4). Further, GFC2 and 3 have processes that branch from the IB and overlap the large terminal bend of the GFI axon (Fig. **14***B,C*; arrowheads; Movies 2 and 3). This is the first example, to our knowledge, of any contact along the GFI axonal bend other than TTMn. We also observe a third contact point between GFI and GFC3. The GFI axon bend occasionally extends small processes, which can contact GFC3 on posteriorly

descending processes (Fig. **14***C*, arrowhead; magnified in inset). As these overlaps are likely sites for gap junction connectivity within the circuit, we investigated these membrane contacts for electrical synapses.

Shaking-B Gap Junction Synapses Between GFI and GFC Neurons

The GF circuit is characterized by mixed chemical and electrical synapses (Blagburn et al., 1999; Allen et al., 2006). To map GFI-GFC electrical synapses, we labeled for the Shaking-B (ShakB) innexin, using an antibody recognizing the "N+16" isoform present at GFI synapses (Phelan et al., 2008). Flies in which GFC1-4 neurons are labeled with UAS-*mcd8::gfp* (Fig. **15**, column 1, green) were GFI-injected with TRITC (column 2, magenta) and co-labeled with ShakB antibody (column 3, cyan). All three channels were modeled with 3D rendering software to visualize ShakB-positive GFI-GFC contacts (Fig. **15**, column 4; Movies 5-9). GFC1 (78A06-Gal4) exhibits a simple arborization, with a process coming across the IB, and making a characteristic anterior-posterior split (Fig. **15***A*; Movie 5). ShakB is clearly visible in the 3D models, localized between the GFI and GFC1 as the process exits the IB (arrows and inset). GFC1 projects axons to all three TG segments, indicating that there is a set of outputs triggered by the GFI escape response in parallel to TTM and DLM activation.

GFC2 neurons have a larger process field, forming a hemi-circle in front of the GFI (Fig. **15***B;* Movie 6). Multiple ShakB electrical synapses clearly occur between the GFI and GFC2, although due to the complexity of these connections, it is not possible to determine if the GFI is contacting the GFC2 processes that come from the contra- or ipsilateral sides of the TG, or both (Fig. **15***B*). GFC2 also contacts the GFI along the distal axonal bend (Fig. **14***B*), so we also investigated these sites for ShakB co-localization. The results show contact between the GFI and GFC2 near the tip of the bend, however ShakB punctae are rarely seen co-localizing at these contacts (Fig. **15***C*; Movie 7), suggesting these are primarily chemical synapse connections. GFC3 has the most extensive IB contacts among all the GFCs, as well as broad interactions with surrounding neurons (Fig. **15***D*; Movie 8). GFC3 contacts the GFI with ShakB electrical

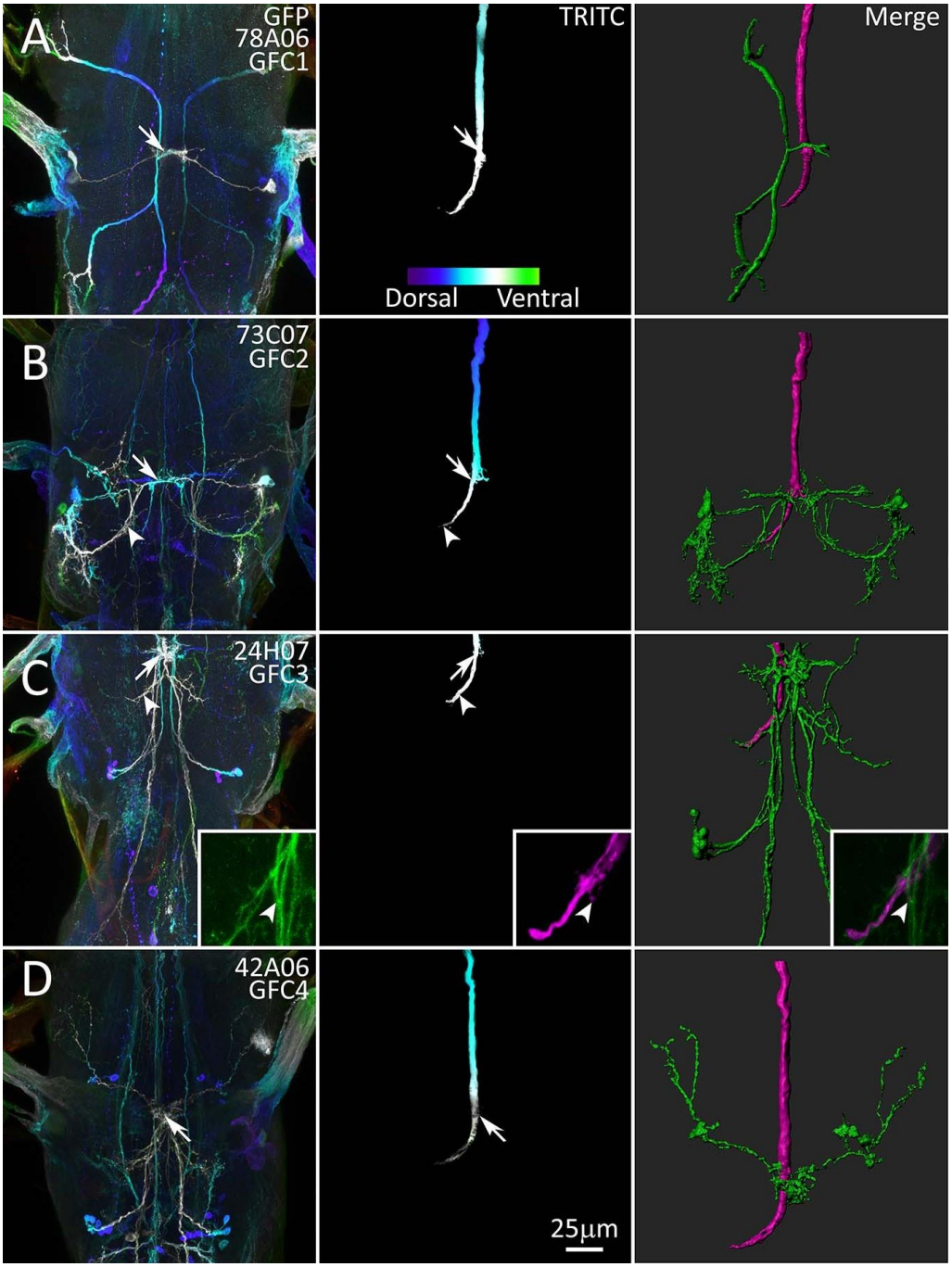

Figure 14. The GFI Interacts with the GFC Neurons at the Inframedial Bridge

Gal4 lines driving UAS-*mcd8::gfp* (column 1) intersect with the GFI axon revealed by injection of tetramethylrhodamine (TRITC, column 2), at the GFI Inframedial Bridge (IB) and the GFI axonal bend (merge, column 3). The first 2 columns use depth color coding to represent Z-position within the TG, with more dorsal regions displaying cool colors and ventral regions displaying warm colors (see color scale bar in ***A***, column 2). Arrows indicate overlapping membrane contact between GFCs and GFI at the IB. Arrowheads indicate GFC contact at the GFI axon bend. All injected flies are female. ***A,*** GFC1 (78A06-Gal4) interacts with the GFI exclusively at the IB. ***B,*** GFC2 (73C07-Gal4) interacts with the GFI at the IB, and the GFI axonal bend. ***C,*** GFC3 (24H07-Gal4) interacts with the GFI extensively at the IB and the GFI axonal bend. The GFI also produces small side projections that contact GFC3 (inset, arrowheads). ***D,*** GFC4 (42A06-Gal4) interacts with the GFI at the IB.

synapses (arrows), but GFC3 branches extending beyond the IB are mostly ShakB negative (Fig. **15***D*), indicating few electrical synapses. GFC3 contacts the GFI axon bend even more extensively than GFC2, but similarly has a small number of ShakB electrical synapse contacts (Fig. **15***E*; Movie 9). All images of GFI-GFC3 IB contact sites exhibit ShakB-positive electrical synapses, but only one image of the GFI-GFC3 axonal bend shows a synaptic connection (Fig. **15***E*, arrow). GFI axon bends are presynaptic to the TTMn, with extensive ShakB electrical synapses (Phelan et al., 2008), but it appears only a small portion of this gap junction connectivity is used for GFC2 and 3, with the primary GFI-GFC electrical connections in the IB (Fig. **15***B*,*D*). Without a GFC4-specific driver, we are unable to specifically test GFI-GFC4 ShakB synaptic connections. To determine the direction of information flow across GFI-GFC synapses, as well as connectivity in other regions of the TG, we next mapped the pre- and postsynaptic neuronal polarity of GFC1-4 synapses.

Pre- and Postsynaptic Polarity of Thoracic Ganglion GFC Neurons

To investigate GFC postsynaptic domains, we used the UAS-*denmark* dendrite reporter, composed of the exogenous mouse ICAM5 dendritic protein fused to RFP (Nicolai et al., 2010). For presynaptic labeling, we used the UAS-*synaptotagmin::gfp* (Syt::GFP) reporter, composed of the Synaptotagmin1 (Syt1) integral synaptic vesicle protein fused to GFP (Zhang et al., 2002). In GFC1, the DenMark signal is absent from the finger-like projections at the process termini (Fig. **16***A*, column 1), and Syt::GFP is strongly present in a punctate array, indicating these processes are presynaptic sites (Fig. **16***A*, column 2). In contrast, DenMark strongly labels GFC1 within the IB (arrow), indicating this site is postsynaptic to the GFI (Fig. **16***A*, image column 3, top). The Syt::GFP signal is absent (Fig. **16***A*, image column 3, bottom), suggesting the IB site is solely for input. Together, these data indicate GFC1 neurons receive presynaptic input onto their dendrites at the IB and then project their contralateral axons for synaptic output into the leg neuropil (Namiki et al., 2018).

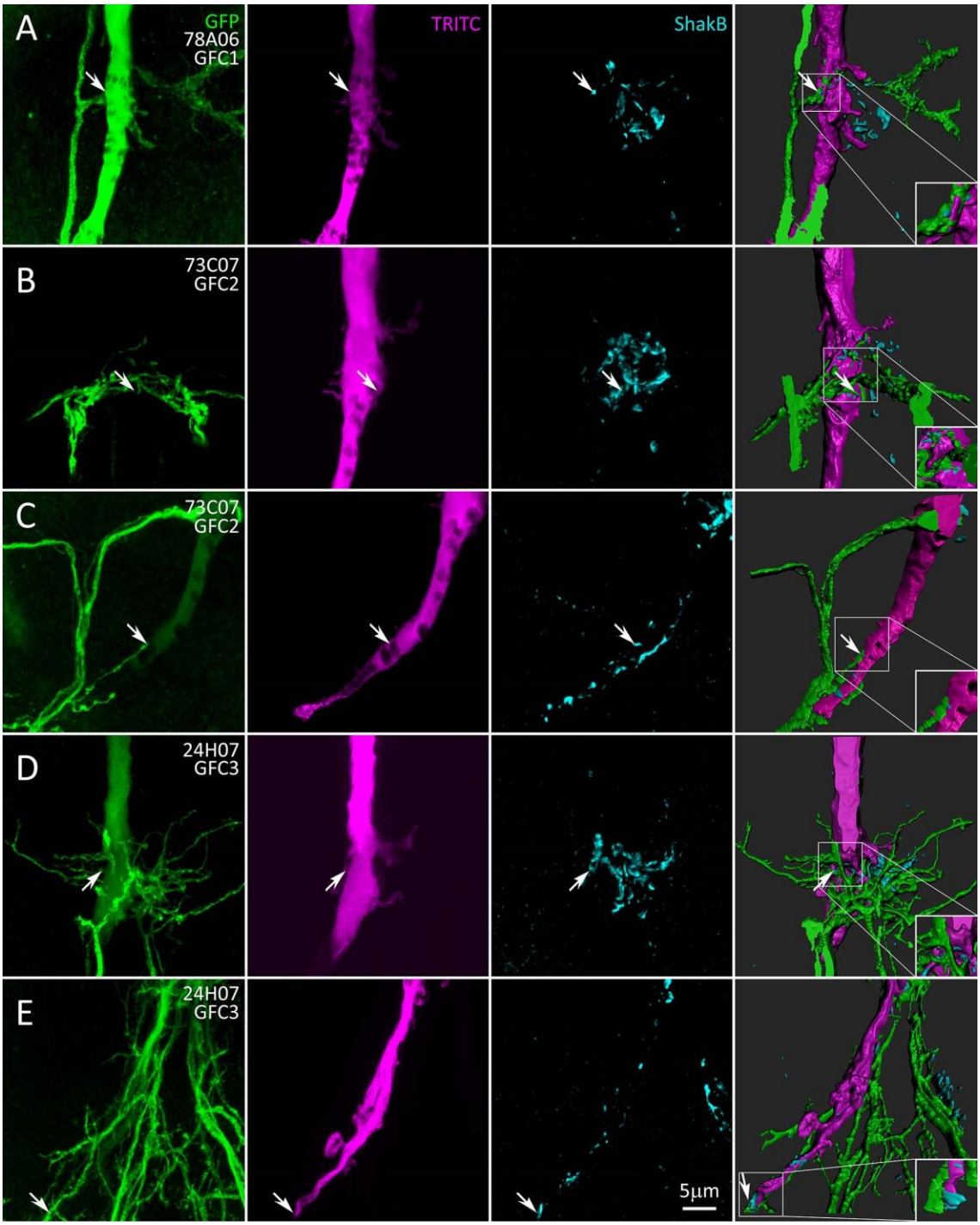

Figure 15. GFCs Form Electrical Synapses with the GFI at the Inframedial Bridge
Electrical synapses between GFI and GFC neurons are shown in Gal4-driven UAS-*mcd8::gfp* animals (green, column 1) with TRITC dye injection into the GFI (magenta, column 2), while co-labeling with the Shaking-B antibody (cyan, column 3). Images were taken using the microscope's AiryScan mode. The three merged channels (column 4) show the regions of shared ShakB contact between GFI-GFCs. Arrows indicate sites of the GFI-GFC ShakB synaptic contacts (magnified in insets). All injected flies are female. ***A,*** GFC1 (78A06-Gal4) makes ShakB electrical synapse contacts with the GFI at the IB. ***B,*** GFC2 (73C07-Gal4) forms several ShakB electrical synapse contacts with the GFI. ***C,*** GFC2 (73C07-Gal4) contacts the GFI along the axonal bend. ***D,*** GFC3 (24H07-Gal4) contacts the GFI with multiple ShakB electrical synapses. ***E,*** GFC3 (24H07-Gal4) minimally contacts the GFI along the axonal bend (arrow).

In contrast, GFC2 looped processes are strongly labeled by DenMark, including contacts at the GFI axon bend (Fig. **16***B*, column 1), with strongly co-localizing Syt::GFP (column 2). Only the dorsolaterally projecting processes in the wing neuropil display Syt::GFP without DenMark present. Similarly within the IB, DenMark and Syt::GFP again co-localize, although DenMark is at a low level (Fig. **16***B*, image column 3). Thus, GFC2 neurons appear to have many co-localized pre- and postsynaptic domains. Note that it is not possible to tell where in the loop GFC2 processes double back, and the pre- and postsynaptic compartments may be in separate, adjacent processes (Fig. **16***B*). Based on our ShakB findings (Fig. **15*B***), it is likely GFI and GFC2 directly synapse, but both appear presynaptic at the IB and they may also share postsynaptic targets that mediate GFI-GFC2 coupling. Another possibility is that GFI-GFC2 dye transfer does not occur at the IB, but instead they couple indirectly via an intermediary neuron. This could explain why the GFC2 is relatively poorly labeled by NB dye injection into the GFI, compared to other GFCs.

GFC3 has pre- and postsynaptic domains similar to GFC1 (Fig. **16***C*). The GFC3 long finger-like process projections in TG3 have very weak DenMark signal (column 1) and very clear Syt::GFP punctae (column 2). Therefore, these sites are presumably presynaptic in leg neuropil (Namiki et al., 2018). At the IB, GFC3 strongly expresses DenMark (Fig. **16***C*, image column 3), which is thus postsynaptic. However, Denmark expression expands beyond the IB to include GFC3 branches that parallel the GFI axon bend and descending processes (Fig. **16***C*, arrowheads). Syt:GFP is undetectable at all of these GFC3 sites, indicating they are solely postsynaptic (Fig. **16***C*, image column 3). Surprisingly, DenMark/Syt::GFP expression is lethal with the 42A06-Gal4 driver, and we were therefore unable to evaluate GFC4 pre- and postsynaptic domains. Based on similarities to GFC3, we predict GFC4 has postsynaptic sites at the IB and presynaptic sites in the TG1 leg neuropil. Overall, DenMark and Syt::GFP clearly distinguish pre- and postsynaptic regions of all GFC neurons, except GFC2. As the GFCs are so intimately interconnected with the GFI, we next tested if these coupled neurons play a role in GF circuit development or maintenance.

GFC Requirements for the Development of GF Circuit Architecture

We used Gal4-targeted expression of the Head Involution Defective (Hid) protein to drive apoptosis in GFC neurons, in an attempt to eliminate each GFC and study the effects on the GF circuit architecture (Zhou et al., 1997; Muthukumar et al., 2014). Unfortunately, all of the GFC drivers used above (Fig. **13**) are lethal in combination with UAS-*hid*. We repeated the study using split-Gal4 (spGal4) lines 10B11-AD ∩ 14A06-DBD (Luan et al., 2006; Pfeiffer et al., 2010; Dionne et al., 2018) to eliminate the apoptosis of off-target cells. These spGal4 lines were identified using the MIP search tool, and were selected for their strong expression in GFC1 with minimal overlap in non-specific neurons. This spGal4 combination expresses strongly in GFC1, but also in PSI, as seen when crossed with UAS-*mcd8::gfp* (Fig. **17***A*, green) with injected TRITC (magenta) to label the GFI. In the brain (Fig. **17***A*, top), only TRITC dye is present in the GFI, where the GFI cell bodies (arrow) and their dendrites (arrowheads) reside. Importantly, no mCD8::GFP is present in the GFI (Fig. **17***A*, green). Similarly, the Giant Commissural Interneuron (GCI), which interconnects the GFIs, displays no mCD8::GFP. In the TG, GFC1 (arrow) and PSI (arrowhead) express mCD8::GFP (Fig. **17***A*, bottom).

NB dye injection into GFI in a UAS-*hid*/+ control animal shows both GFIs labeled in the brain (Fig. **17***B*, arrows). The GCI (arrowheads) interconnecting the GFI cell bodies (Allen et al., 1998) is also dye labeled. In the TG, the intact dye-coupled GF circuit is present in all UAS-*hid* /+ control animals (Fig. **17***B*, bottom). When the spGal4 driver is crossed to UAS-*hid* and the GFI injected with NB, GFC1 is ablated in 18/20 animals (90%); fully in 14/20, partially in 4/20 (Fig. **17***C*). Partial ablations are defined as several, but not all, neurons within GFC1 clusters being killed. PSI is eliminated in 16/20 animals (80%). Two animals had no visible cervical connective (CC) axons and could not be injected for analysis. The ablation of coupled cells causes stronger dye labeling in the persisting neurons, as expected due to the reduced volume of the GF circuit. As a consequence, the standard 2-minute NB dye injection can cause lysis of the GF circuit, and therefore injection times were reduced to $\leq$30 seconds for these ablation experiments. This finding is

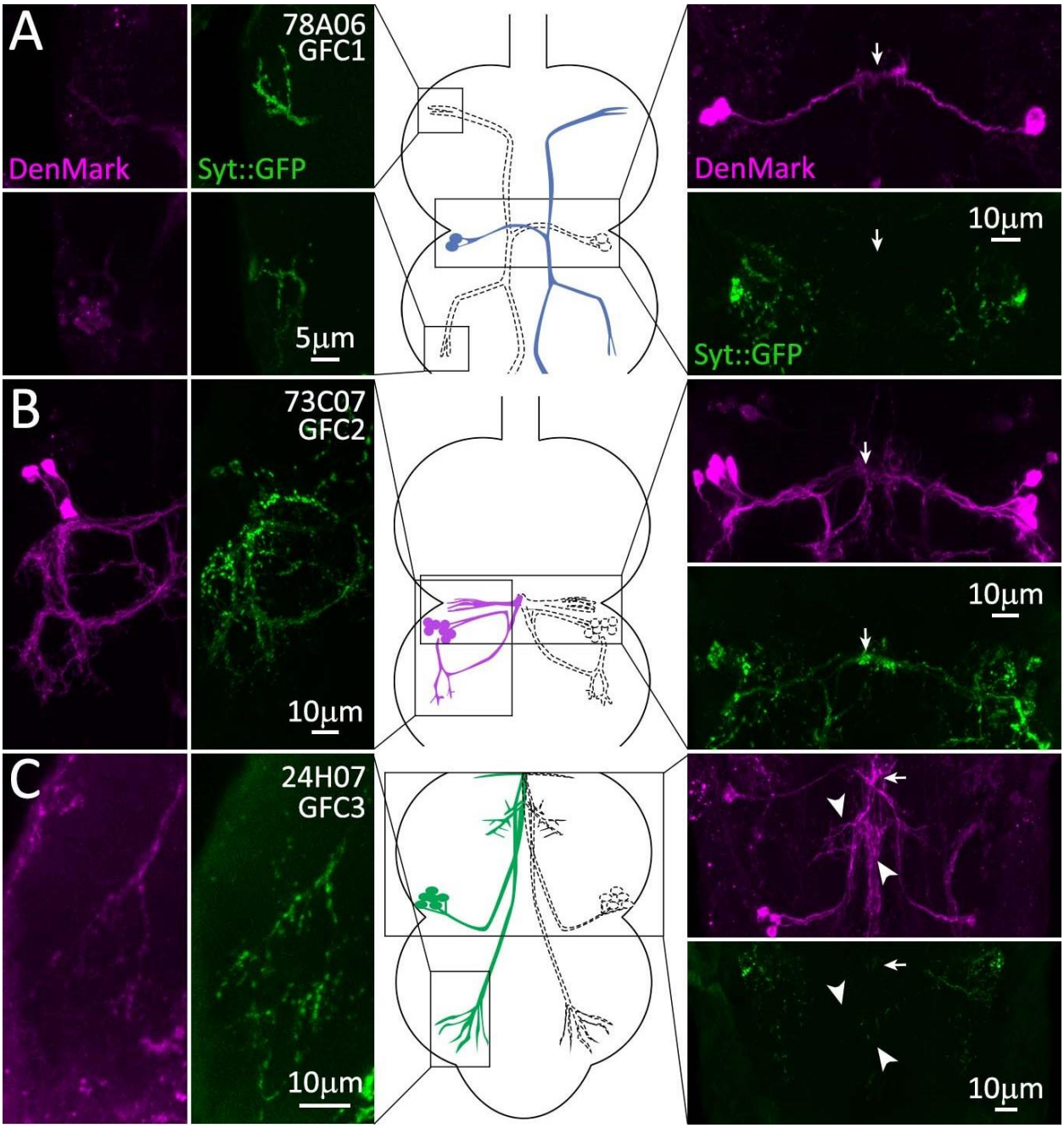

Figure 16. **Pre- and Postsynaptic Polarity of the Newly Identified GFC Neurons**
GFC neuronal polarity is shown using the dendrite/soma label DenMark (magenta) and the presynaptic label Synaptotagmin::GFP (Syt::GFP, green). Substacks of the regions of interest for each GFC are shown for DenMark (column 1) and Syt::GFP (column 2), with above and below paired comparisons (image column 3). Arrows indicate the position of the Inframedial Bridge (IB). GFC schematic representations are shown (center column), with regions of interest outlined in black boxes. ***A,*** GFC1 (78A06-Gal4) processes are labeled by presynaptic Syt::GFP in both TG1 (top) and TG2 (bottom) segments, while the IB is labeled by postsynaptic DenMark. ***B,*** GFC2 (73C07-Gal4) processes in TG2 (column 1) are co-labeled by both DenMark (column 1) and the Syt::GFP marker (column 2). The IB is labeled by presynaptic Syt::GFP, but also has the DenMark signal (column 4). ***C,*** GFC3 (24H07-Gal4) has punctate Syt::GFP within the finger-like processes in TG3 (column 2). The IB is labeled by DenMark, with no Syt::GFP marker (column 4). GFC3 processes along the GFI axonal bend also express the DenMark label (arrowheads).

similar to previous reports when GFI dye coupling is eliminated through lack of interconnecting gap junctions (Kennedy and Broadie, 2017).

When testing the GF circuit for connectivity changes, we find GFC1/PSI ablation causes a striking impact on GFI development (Fig. **17***C*). All control animals (UAS-*hid*/+, n=21) display a completely normal dye-coupled GF circuit without detectable defects (Fig. **17***B*). With targeted UAS-*hid* ablation (spGal4 10B11-AD ⋂ 14A06-DBD>UAS-*hid*, n=20 animals), in 9/14 animals (~65%) with complete GFC1 ablation (including 1 case with the PSI present; Fig. **17***C*, arrowhead), one of the GFI neurons is completely absent (Fig. **17***D,E*). In partial GFC1 ablation cases, only 1/4 animals (25%) lost a GFI. When a GFI is lost, there is no visible dye within the neuron, including the soma and the axon (Fig. **17***C*), and we only detect one axon traveling through the CC by light microscopy. The remaining GFI always extends a compensating axon to the contralateral side (10/10 animals; 100%) and forms a normal terminal axon bend (Fig. **17***C*, arrow).

Targeted UAS-*hid* expression is restricted to GFC1 and PS1, with no evidence of either GFI or GCI expression. A full summary of the experimental results is compared between UAS-*hid*/+ controls (n=21) and the spGal4 10B11-AD ⋂ 14A06-DBD>UAS-*hid* targeted ablation (n=20; Fig. **17***D,E*). Interestingly, in an animal with a fully intact GFC1 and only PSI ablation, both GFIs are present. In an animal with neither PSI nor GFC1 ablated, both GFIs are present (Fig. **17***D,E*). PSI ablation alone does not appear to be responsible for GFI loss, as GFI loss occurs when GFC1 alone is missing, but not when PSI alone is missing. We therefore conclude that GFC1 helps maintain GFI during GF circuit development. Another interesting ablation result is the loss of GFI dye-coupling to GCI in 5/10 animals (50%) where a GFI is lost (Fig. **17***C*). Surprisingly, this loss of GCI also occurs in 2 animals where both GFIs are present; one with only GFC1 ablated, and the other with only PSI ablated. These results suggest the GFC neurons, alongside the classic GF circuit neurons, play an important role in neural circuit development.

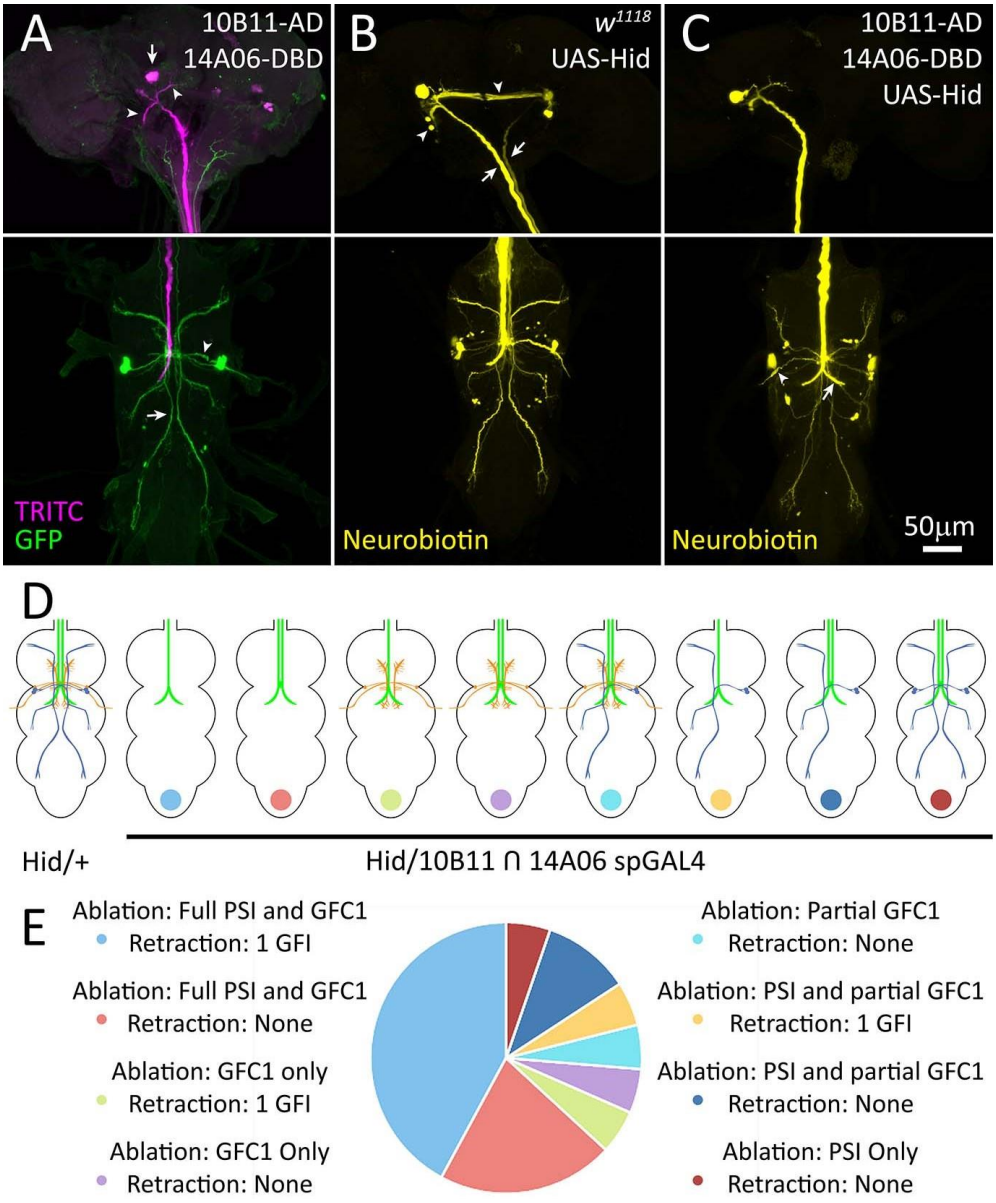

Figure 17. GFC Neurons Support GF Circuit Architectural Development

A, The GFI labeled by iontophoretically injected TRITC (magenta) reveals the soma (arrow) and dendritic branches (arrowheads) in the brain (top panel), and descending axon in thoracic ganglion (bottom panel). Split-Gal4 (spGal4) 10B11-AD ∩ 14A06-DBD drives UAS-*mcd8::gfp* (green) in GFC1 (bottom, arrow) and PSI (bottom, arrowhead). ***B,*** Iontophoretic NB injection into the GFI (yellow) in the UAS-*hid*/+ control reveals the GFI (arrows) interconnected by the Giant Commissural Interneurons (GCI, arrowheads) in the brain (top panel), and normal dye-coupling in the thoracic ganglion (bottom panel). ***C,*** Driving UAS-*hid* with spGal4 10B11-AD ∩ 14A06-DBD results in the loss of GFC1 with occasional PSI survival (arrowhead). When GFC1 is ablated, the GCI labeling is often lost (top), one of the GFI axons is typically absent, and the remaining GFI axon always extends a compensatory contralateral axon projection (arrow). All NB injections were performed on males. ***D,*** Schematic representations of GF circuit outcomes with UAS-*hid*/+ controls and spGal4 10B11-AD ∩ 14A06-DBD driven UAS-*hid* cell ablation. Not pictured are instances where neither GFC1 or PSI are ablated, and instances where both GFIs are absent. ***E,*** Frequency of each GF circuit outcome with the targeted spGal4 10B11-AD ∩ 14A06-DBD driven UAS-*hid* cell ablation. The pie chart color is coded to dots at the bottom of schematics in panel D. The sample size for UAS-*hid*/+ genetic controls is 21 animals, and for the spGal4 cell ablation is 20 animals.

Discussion

We describe here newly discovered neurons in the classic *Drosophila* Giant Fiber (GF) neural circuit (Power, 1948; Sun and Wyman, 1997; Jacobs et al., 2000; Allen et al., 2006) by characterizing four Giant Fiber Coupled (GFC) neuron clusters. We identify specific transgenic drivers to both label and manipulate GFC1-4, and map neuronal architecture and polarity. We show these neurons couple to the Giant Fiber Interneuron (GFI) via ShakB N+16 innexin (Phelan et al., 2008) primarily at the central Inframedial Bridge (IB; Allen et al., 1998), but also at the downstream axonal bend. Alongside the already well-established benefits of this circuit, including the large cell size, genetic malleability and accessible functional/behavioral readouts (Power, 1948; Tanouye and Wyman, 1980; Phelan et al., 1996; Trimarchi et al., 1999), this expanded set of coupled neurons can aid future experiments in neurodevelopment, such as the study of axonal selection between multiple dendritic partners. This circuit map could be further refined using advanced tools, such as MultiColor FlpOut (Nern et al., 2015), as was recently accomplished for *Drosophila* brain descending neurons (Namiki et al., 2018).

This detailed circuit map is most useful for genetic analyses of electrical synapse partner connectivity between individually defined neurons. The GFCs identified in this study are comprised of 2-7 bilaterally symmetrical neurons clustered on each side of the thoracic ganglion (TG) segments. Similar clusters of repeated neurons with apparent connectivity redundancy have been recently identified in *Drosophila* brain descending neurons, where it is also unclear why neurons have such tightly overlapping projection patterns (Namiki et al., 2018). We have insufficient resolution to determine whether the GFC neurons truly are duplicates, or if they have distinct, proximally adjacent synaptic targets, like the closely overlapping Kenyon cells of the adult brain Mushroom Body (Crittenden et al., 1998). It has been proposed that neuron duplication may allow for a sliding scale of response within a circuit, whereby more neurons are activated to increase the strength of the response. Alternatively, if the neurons contact similar

proximal synaptic targets, their role may be to provide ultra-fine control of muscle movement in the GF circuit escape response (Namiki et al., 2018).

Complex leg and wing movements are thought to be controlled by extensive TG neural circuits, which are activated by a small number of descending neurons, including the GFI dedicated to rapid escape behavior (Cardona et al., 2009; Hsu and Bhandawat, 2016; Cande et al., 2018; Namiki et al., 2018). The roles of GFC neurons uncovered here have yet to be elucidated, although their electrical coupling to the GFI strongly suggests a close relationship to behaviors promoting or otherwise facilitating the rapid escape jump-and-flight response. Our preliminary attempts to optogenetically activate the GFC neurons through blue-light stimulation of Gal4-targeted ChR2-H134R (Nagel et al., 2005) or ChOP-XXL (Dawydow et al., 2014) channels did not produce behaviors. We suspect the stimulation paradigm was not strong enough, that appropriate sensory co-stimulation conditions may not have been provided (von Reyn et al., 2014), that behavioral scoring methods were not sensitive enough to detect subtle motor output changes (Cande et al., 2018), or that these neurons modulate internal processes not directly manifest in rapid escape behavior (Joseph et al., 2017).

Based on the very recently proposed ventral nerve cord (VNC) regional map (Namiki et al., 2018), the most likely targets of the 4 GFCs identified here are the TG1-3 leg neuropils. GFC2 also appears to target the TG2 wing neuropil. Both leg and wing outputs are integral to the GF circuit escape response (von Reyn et al., 2014). GFC1 targets all three TG leg neuropil segments; GFC2 targets TG2; and GFC3 and GFC4 target TG3 and TG1, respectively. This extensive leg neuropil connectivity may regulate tension in the front and hind legs, allowing the central legs to execute a more effective escape jump (Trimarchi and Schneiderman, 1993; von Reyn et al., 2014; Namiki et al., 2018). In support of this hypothesis, our work indicates GFCs 1-3 are all directly gap junction coupled to the descending GFI, receiving input primarily at the IB, and thus share in the rapid conduction speed of the GF circuit (Phelan et al., 2008). Further, GFC3

neurons extend postsynaptic processes that parallel the PSI processes, indicating GFC3 may collect input from multiple neurons in the GF circuit.

Like the PSI, all 4 GFCs appear to synapse on their downstream targets via only chemical synapses, based on Syt::GFP synaptic vesicle marker and lack of ShakB electrical synapse labeling at GFC termini (Allen et al., 2006). It might appear possible that another innexin could mediate these GFC connections (Stebbings et al., 2002; Phelan, 2005); however, the complete absence of dye-coupling to neurons downstream of GFCs indicates electrical synapses are absent. In contrast to the other GFCs, GFC2 appears both pre- and postsynaptic at the IB connectivity hub, suggesting it may share postsynaptic partners with GFI, potentially including GFC1, 3, 4 and/or PSI. Given this circuit connectivity, GFC2 may trigger the rapid escape jump reflex independently of the GFI, in a parallel circuit output long speculated to exist, but not previously identified (Trimarchi and Schneiderman, 1995; Fotowat et al., 2009). Indeed, GFC2 extends presynaptic processes into the Tergotrochanteral Motor neuron dendritic field, thus mimicking GFI connectivity (King and Wyman, 1980).

DenMark and Syt::GFP reporters are extremely useful in defining neuron polarity (Zhang et al., 2002; Nicolai et al., 2010; Bidaye et al., 2014; Frank et al., 2015), but they have limitations that can make interpretation difficult. Both reporters preferentially mark appropriate synaptic regions, but can mis-localize due to transgenic overexpression (Chen et al., 2014; Kanca et al., 2017). A likely example here is dim DenMark signal near bright Syt::GFP punctae (Fig. **16***C*). DenMark signal-to-noise is much worse than the IB labeling, while Syt::GFP signal-to-noise is much stronger; hence our conclusion this region is presynaptic. A more problematic example may be the DenMark/Syt::GFP overlap in GFC2 (Fig. **16***B*). This labeling likely shows adjacent pre- and postsynaptic processes, which we cannot distinguish; although shared compartments have been reported in Mushroom Body Kenyon cells (Christiansen et al., 2011; Zheng et al., 2018). It is also worth noting the 73C07-Gal4 line for GFC2 is the strongest driver employed and may cause DenMark or Syt::GFP mis-localization via transgenic overexpression (Chen et al., 2014;

Kanca et al., 2017). The 42A06-Gal4 driver for GFC3/4 is lethal with UAS-*denmark*, *syt::gfp*, showing these markers can also have detrimental effects.

Our targeted ablation studies indicate a role for GFCs in GF circuit development, and demonstrate the ability of the circuit to compensate for the loss of a GFI, much like ocular dominance columns in Hubel and Wiesel's classic work (Hubel and Wiesel, 1970; Hubel et al., 1977). PSI ablation does not appear to be responsible for the GFI loss, based on the fact that GFIs are present when PSI alone is ablated, and GFIs are lost only when GFC1 is ablated. Another impact of ablation is lost GCI coupling when a GFI, GFC1 or PSI is removed. As GCI coupling loss occurs both when GFC1 alone is lost and when PSI alone is lost, it appears that complete GF circuit formation depends upon feedback from multiple circuit members (Kandler and Katz, 1995; Hanganu et al., 2009; Maher et al., 2009; Belousov and Fontes, 2013). This finding suggests neurons not directly coupled can feedback through an intermediary circuit neuron; an intriguing but poorly studied hypothesis (Kandler and Katz, 1995; Belousov and Fontes, 2013). We note that the TTMn only occasionally dye-couples with GFI, suggesting gap junction transitions between open and closed states could also contribute.

Previous studies have shown ablation of the GFI using neurotoxins, such as ricin (Smith et al., 1996), and have even found that single GFIs are lost at very low frequency in wildtype animals (Allen et al., 1998). In the latter case, the authors also found midline crossing of a compensatory contralateral process from the enduring GFI, as in our work. We hypothesize the GFI loss reported here results from lost GFI stabilization by GFC1 due to loss of trophic/synaptic signaling or physical contact (Gorin and Johnson, 1979; Pearson and Stoffler, 1992; Antonini and Stryker, 1993; Crowley et al., 1994; Uesaka, 2005; Gibson and Ma, 2011). Other GFI postsynaptic targets (PSI, TTMn, GFC2-4) presumably also participate in GFI stabilization, although Gal4 drivers tested thus far for these neurons have proved lethal in combination with UAS-*hid* (Zhou et al., 1997; Muthukumar et al., 2014). These animals die early in development, showing the need for spGal4 lines capable of avoiding off-target cells. Pursuing this

phenotype with more specific drivers and screening approaches could elucidate molecular mechanisms these neurons use to stabilize synaptic partners (Cohen-Cory, 2002).

Other methods shown to cause GFI axonal retraction and neuronal loss include blocking membrane endocytosis (e.g. using dominant negative *shibire*/Dynamin) and the overexpression of select transmembrane receptors, such as Semaphorin-1A (Godenschwege et al., 2002; Murphey, 2003; Godenschwege and Murphey, 2008). However, in these cases, GFI axon retraction is typically only to the IB, rather than beyond the CC, or causing complete cell loss. The molecular pathways responsible for these phenotypes may be shared with the axon retraction caused by loss of synaptic partners, with Highwire/MYCBP2, Wallenda/DLK and Basket/JNK as prime candidates (Ghosh et al., 2011; Borgen et al., 2017). While gap junctions play extensive roles in neuronal development (Elias and Kriegstein, 2008; Belousov and Fontes, 2013; Baker and Macagno, 2017), it is unlikely that GFI loss results from loss of electrical coupling only, as the total removal of gap junctions from the GFI does not cause axon retraction or neuronal cell death (Blagburn et al., 1999).

The GFI axon split across the midline in response to the absence of its partner is reminiscent of sensory neuron plasticity following input deprivation (Poirier et al., 2006; Collignon et al., 2009; Rabinowitch et al., 2016) and motor circuit development changes in response to lost motor neurons (Modney and Muller, 1994; Büschges et al., 2000). This corrective rewiring could stem from either normal pathfinding and synaptogenesis, or new repair pathways activated in response to unpartnered neurons. The axon split duplication with a GFI loss is different from the recent report on failed GFI pruning (Borgen et al., 2017), as the new GFI axon path is always a perfect mirror-image of the normal axon bend, rather than an untrimmed posteriorly branched axon outgrowth. This new circuit rewiring model could be used in *Drosophila* genetic screens of GF circuit development (Mohr, 2014; Bassett et al., 2015; Heigwer et al., 2018) to help answer a number of important questions. Such work will be greatly aided by single-cell transgenic manipulation of pre- and postsynaptic neurons in the GF circuit.

In conclusion, we hope that the increase in manipulatable GFI coupled neurons reported here will further enhance this genetic model circuit. The GF circuit is ideally suited to query a wide range of important neurodevelopmental questions, including mechanisms of pathfinding, target recognition, synaptogenesis and stabilization during neural circuit assembly and maintenance. Although the GF circuit is rightly considered one of the most straightforward and accessible *Drosophila* circuits, the higher degree of connectivity revealed in this study indicates a greater complexity, which is amenable to answering more in-depth questions. The large number of inputs onto, and outputs from, this model circuit provides further evidence that even the most basic circuits are deeply interconnected with the rest of the brain circuitry. As the benefits of single-cell resolution studies cannot be overstated, we hope this enlarged GF circuit model, and the transgenic tools characterized here, will help form part of the underpinning for future work on neural circuit dynamics.

Chapter IV

dfmr1^{50M} Background Mutation Causes Hyper-Connectivity Within the GF Circuit

This manuscript is currently being prepared for publication

Abstract

Neural circuits are assembled during development when neurons synapse with selected partners, though these initial contacts are often imprecise and need to be optimized by maturity. Connections with appropriate partners are stabilized as mature synapses while others are retracted or pruned away. Disruptions to synaptic formation and refinement impair circuit connectivity and are associated with a range of neurological disorders. One of the best studied is Fragile X syndrome (FXS), a heritable cause of intellectual disability and autism spectrum disorder (ASD) often characterized by excessive neuronal overgrowth. Fragile X Mental Retardation Protein (FMRP) loss causes FXS, likely due to its many roles in synapse development. In the well-characterized *Drosophila* FXS disease model, we identified overelaborated synaptic connections in the central Giant Fiber (GF) circuit, with excessive filopodial processes during synaptogenesis and overabundant synaptic projections at maturity in the GF Interneuron (GFI) axon. The excess contacts contain both chemical and electrical synapse markers and target known GF circuit neurons, causing circuit hyper-connectivity. Despite striking similarities to well-characterized FXS synaptic defects, we discovered that a background mutation(s) in our disease model is responsible for this phenotype. We are pursuing the mutation via bulk segregant analysis and whole-genome sequencing, using dye injection to track the phenotype. This ongoing work is expected to reveal new proteins and molecular mechanisms that regulate synaptic connectivity during neural circuit development, potentially in concert with FMRP.

Introduction

During the early stages in neural circuit formation, axons and dendrites extend transitory synaptic processes that contact local partners (Jontes et al., 2000; Tashiro et al., 2003; Waites et al., 2005). Nascent synapses are formed in excess, overgrowing appropriate and inappropriate targets, only to be refined over time through retraction or glial pruning, sculpting mature connectivity patterns (Riccomagno and Kolodkin, 2015). With the onset of environmental input, this refinement process continues and is mediated by sensory-driven synaptic activity (Penn, 2001). The overall synaptic pattern is coordinated by an array of secreted morphogens, transmembrane receptors and cytoskeletal regulators (Salinas, 2003; Favuzzi and Rico, 2018; Südhof, 2018). Disrupted synapse formation and maturation cause severe neurological disorders, including ASD and intellectual disability (Melom and Littleton, 2011). Fragile X syndrome (FXS) patients display both symptoms, making this monogenic disorder a key model to study the link between impaired synaptic development and disease (Pfeiffer and Huber, 2009).

The FXS disease state is caused by loss of the mRNA- and channel-binding Fragile X Mental Retardation Protein (FMRP; Darnell et al., 2011; Ferron, 2016). Overelaborated and immature synapses are hallmark phenotypes in FXS patients and model systems. Most commonly the synaptic overgrowth has been documented in dendritic branches and postsynaptic spines, although studies have also identified overgrown axonal branches and supernumerary presynapses as well (Hinton et al., 1991; Comery et al., 1997; Greenough et al., 2001; Lee et al., 2003a; Pan et al., 2004; Tessier and Broadie, 2008; Vita and Broadie, 2017). While many mechanisms have been proposed for this synaptic overelaboration, including enhanced metabotropic glutamate receptor (mGluR) signaling, elevated microtubule and actin cytoskeleton stabilization and disrupted synapse pruning (Zhang et al., 2001; Bear et al., 2004; Tessier and Broadie, 2008), core consensus pathways have been slow to emerge.

In the current study, we used the well-characterized *Drosophila* FXS model to pursue mechanisms of synaptic connectivity defects. Specifically, we focused on the Giant Fiber (GF) neural circuit due to its large size, well-mapped neurons and the availability of transgenic tools (Power, 1948; Allen et al., 2006). We were seeking to model FXS synaptic connectivity defects in a simple, tractable neural circuit with single cell resolution to test the numerous proposed disease mechanisms. We focused particularly on the central GF Interneurons (GFI); a pair of bilaterally symmetric neurons, with cell bodies and dendrites in the central brain and large axons that project into the thoracic ganglia (Koto et al., 1981). GFI axons synapse first onto the Peripherally Synapsing Interneuron (PSI) and Giant Fiber Coupled 1-4 (GFC1-4) neurons at the Inframedial Bridge (IB), and then diverge to form two large bends that synapse onto the Tergotrochanteral Motor neuron (TTMn) and GFC2-3 (Tanouye and Wyman, 1980; Allen et al., 1998, 2006; Kennedy and Broadie, 2018).

We initially set out to test whether the GFI displays an overgrowth phenotype using the common FXS disease model null allele, *dfmr1*^{50M} (Zhang et al., 2001). Consistent with numerous published reports, *dfmr1*^{50M} mutants displayed excess filopodia during GFI synaptogenesis and increased mature synaptic projections at several timepoints relative to controls, suggesting GFI synaptic connectivity is sensitive to FMRP loss as expected (Zhang et al., 2001; Michel, 2004; Kim et al., 2013; Doll and Broadie, 2015; Vita and Broadie, 2017). The projections synapse on GFC2 and 3, indicating the overgrowth is redundant within the GF circuit and inappropriate connections are not formed. However, subsequent experiments revealed that FMRP loss alone does not cause the GFI synaptic defects and that a background mutation(s) in the *dfmr1*^{50M} stock is the source. We are currently using bulk segregant analysis (BSA) with whole genome sequencing to identify the nature of the genetic change (Pool, 2016). Once identified, we expect this discovery will shed new light on the mechanisms of synaptogenesis.

Materials and Methods

Drosophila Genetics

All animals were maintained on a standard cornmeal/agar/molasses *Drosophila* food in a 12-hour light:dark cycling incubator at 25°C. Timed-lay eggs were collected for 2-3 days, and experimental animals were selected from rearing tubes 10-14 days later, unless otherwise noted. The following *Drosophila* lines were used for genetic crosses: w^{1118} (RRID:BDSC_3605) | w^{1118}*; dfmr1*^{50M}/TM6B, *tb*, *hu, gfp* (Zhang et al., 2001, RRID:BDSC_6930) | w^{1118}*; dfmr1*^{2}/TM6, *hu* (Dockendorff et al., 2002) | w^{1118}*; dfmr1*^{B55} (Inoue et al., 2002) | w^{1118}; Df(3R)BSC621/TM6C, *cu*^{1} *sb*^{1} (*dfmr1* deficiency, RRID:BDSC_25696, Cook et al., 2012) | *shakB*^{2} (Blagburn et al., 1999) | *shakB*^{2}*; dfmr1*^{50M}/TM6B, *tb*, *hu, gfp* | w^{1118}*;* P{GMR91H05-Gal4}attP2 (RRID:BDSC_40594) | w^{1118}*;* P{GMR91H05-Gal4}attP2*; dfmr1*^{50M}/TM6B, *tb*, *hu, gfp* | *dfmr1.14*/CyO, *gfp*; *dfmr1*^{50M}/ TM6, *tb, sb* (Dockendorff et al., 2002) | w^{1118}*;* P{GMR73C07-Gal4}attP2 (RRID:BDSC_46689) | w^{1118}*;* P{GMR24H07-Gal4}attP2 (RRID:BDSC_49317) | w^{1118}; elav-Gal4 (RRID:BDSC_8765, Luo et al., 1994) | *w**; P{da.G32-Gal4}UH1 (Wodarz et al., 1995) | w^{1118}, y^{1}; 10X UAS-*ivs-mcd8*::*gfp* attP40 (Pfeiffer et al., 2010) | *w**; P{UAS-*ivs-mcd8::rfp*}attP40 (RRID:BDSC_32219) | w^{1118}, y^{1}; 10X UAS-*ivs-mcd8*::*gfp* attP40; *dfmr1*^{50M}/TM6B, *tb*, *hu, gfp* | y^{1}, *sc**, v^{1}; TRiP.HMS00248 (RNAi1, Perkins et al., 2015, RRID:BDSC_34944) | y^{1}*, sc***,* v^{1}; P{y[+t7.7] v[+t1.8] TRiP.GL00075 (RNAi2, Perkins et al., 2015, RRID:BDSC_35200) | *w**; PBac{*brp*(*FRT.Stop*)*gfp*} (Brp-FSF-GFP; Chen et al., 2014; RRID:BDSC_55753) | y^{1} *w**; P{ UAS-*flp*1.D} (Duffy et al., 1998; RRID:BDSC_4539) | UAS-*flp1*.D/CyO, *gfp*; 91H05-Gal4 | UAS-*rfp*/CyO, *gfp*; Brp-FSF-GFP | UAS-*flp*1.D; 91H05-Gal4, *dfmr1*^{50M}/TM6B, *tb*, *hu, gfp* | UAS-*rfp*; Brp-FSF, *dfmr1*^{50M}/TM6, *tb*, *sb*.

Dye Iontophoresis

GFI dye injection was performed similarly to previously published methods (Boerner and Godenschwege, 2011; Kennedy and Broadie, 2017). Briefly, glass electrodes (Kwik-Fil Borosilicate glass

1B100F-4, World Precision Instruments) were pulled on a laser electrode puller (Model P-2000, Sutter Instrument Company) to 10MΩ resistance (3M KCl). Electrodes were filled with 0.25% TRITC-dextran (10kDa, Life Technologies) and 7% neurobiotin (Vector Laboratories, RRID:AB_2313575) in ddH_2O. Filled electrodes were placed on a silver-chloride wire mounted on a PCS-5000 micromanipulator (Burleigh). Animals in Jans' saline were cut along the dorsal midline to access the cervical connective, where electrodes were inserted into the GFI axon (Jan and Jan, 1976). A square-pulse stimulator (Grass S48, Astro-Med) provided 7.5 100ms pulses/second for 2 mins with 20nA injected current, monitored by an AxoClamp2B amplifier. A Digidata data acquisition system (1320A, Axon Instruments) was controlled with Clampex 9.2 software.

Confocal Imaging

Brains were fixed in 4% paraformaldehyde/sucrose (Electron Microscopy Services) in phosphate-buffered saline (PBS, pH 7.2, Life Technology) for 30 mins, washed 3X with PBS, and then blocked for 1 hr with 1% bovine serum albumin (BSA, Sigma-Aldrich) in PBST (PBS + 0.2% Triton X-100; Thermo Fisher Scientific). Primary and secondary labeling was performed for either 2 hrs at room temperature or overnight at 4°C. All probes were diluted in PBST with 0.2% BSA. The following probes were used: Streptavidin::Cy5 (1:20, Life Technology), rabbit anti-ShakB (1:200, Phelan et al., 1996), rabbit anti-GFP (1:2000; Abcam, RRID:AB_303395), FITC Goat anti-GFP (1:500; Abcam, RRID:AB_305635), Rabbit anti-RFP (1:500; Rockland, RRID:AB_2209751), Alexa 488-conjugated donkey anti-goat (1:250; Thermo Fisher, RRID:AB_2534102), Alexa 488-conjugated donkey anti-rabbit (1:250; Thermo Fisher, RRID:AB_2556546), Alexa 568-conjugated donkey anti-rabbit (1:250; Thermo Fisher, RRID:AB_2534017), Alexa 647-conjugated donkey anti-rabbit (1:250; Thermo Fisher, RRID:AB_2536183), and Alexa 633-conjugated goat anti-rabbit (1:250; Thermo Fisher, RRID:AB_141419). Preparations were then washed 3X for 30 mins in PBST, 1X in PBS, and mounted on glass microscope slides (Probe On Plus 25 x 75 x 1.0mm, Thermo Fisher

Scientific) in 2, 2'-Thiodiethanol (TDE, Sigma-Aldrich; Staudt et al., 2007). To prevent crushing, double-sided poster tape (Scotch) was placed on each side of the brains. Coverslips (No. 1.5H, Zeiss) were sealed with nail polish (Hard as Nails, Sally Hansen). Fluorescent images were collected using either a Zeiss LSM 510 META confocal microscope or a ZEISS LSM 880 confocal microscope with an Airyscan module. Images show maximum Z-stack projections, unless otherwise noted in the figure legends. Occasionally bidirectional scans were misaligned. Such instances were corrected using the FIJI plugin "Correct X Shift."

Western Blotting

Brains were dissected from adult females in PBS with a protease inhibitor (cOmplete mini EDTA-free protease inhibitor cocktail; Roche). Four brains were collected in RIPA buffer (150mM NaCl, 1% Triton X-100, 50mM Tris, 0.5% Sodium deoxycholate, 0.1% SDS, 1mM EDTA, 50mM TRIS, 1mM PMSF, Protease Inhibitor Cocktail; Sigma-Aldrich) on ice and sonicated for 20 secs (Branson Model 102C, Sonifier 250 microtip). Samples were mixed with 4X LDS buffer (ThermoFisher), brought to 5% beta-mercaptoethanol (Sigma-Aldrich), allowed to incubate at room temperature for 20 mins, boiled at 100^{o}C for 10 mins and centrifuged at 14,000 RPM for 10 mins. The equivalent of two brains worth of protein was loaded on a 4%-16% Bis Tris SDS gel (ThermoFisher) in 1x MES buffer (ThermoFisher). After running, the protein was transferred overnight in 1X transfer buffer/20% methanol (ThermoFisher). Following transfer, the membrane was dried for 1 hr, blocked with 2% milk (Kroger) in TBS-T (150mM NaCl, 0.1% Tween, 5mM KCl, 25mM Tris, pH7.6) for 1 hr at room temperature and then stained with primary antibody in 2% milk/TBS-T for 2 hrs at room temperature (mouse anti-FMRP (1:3,000, Sigma-Aldrich F4554) Rabbit anti-α-tubulin (1:40,000, AbCam Ab52866)). The primary was removed with six 5-min TBS-T washes and the membrane was incubated with secondary (800 Goat anti-mouse (1:20,000, Rockland), Alexa 680 goat anti-rabbit (1:20,000, ThermoFisher)) in 2% milk/TBS-T for 2 hrs at room temperature. The secondary was washed 6 times in TBS-T for 5 mins and then imaged (LI-COR Odyssey).

Bulk Segregant Analysis and Whole Genome Sequencing

The bulk segregant lines were created with multiple generations of inbreeding. To begin, w^{1118} males were crossed with w^{1118}; $dfmr1^{50M}$/ TM6B, *tb*, *hu, gfp* females, and the transheterozygous offspring (w^{1118}; $dfmr1^{50M}$/+) were interbred. The offspring of this cross were then interbred. This process was repeated for a total of 12 generations. Flies from the 9th, 10th 11th, and 12th generations were GFI injected according to the above dye iontophoresis protocol, with the body cryopreserved at -80^{o}C. Upon completion of GFI dye injection and projection quantification, bodies were combined into 3 pools based on quantified GFI projection number; 0-3 projections were placed in the control pool, 5-6 projections in the heterozygous pool and 7+ projections in the homozygous mutant pool. DNA was extracted from each pool using the Qiagen DNeasy Blood and Tissue extraction kit (Qiagen, Cat # 69504). 150bp paired-end read whole genome sequencing was performed on the samples (Hudson Alpha, Illumina NovaSeq).

Data Analyses

Data processing was done with FIJI software (version 2, RRID:SCR_002285; Schindelin et al., 2012; Schneider et al., 2012). GFI projection number represents the projections from one GFI bend, below the IB. If both GFI arms were visible, projection number was averaged. GFI projection lengths were quantified using the FIJI Simple Neurite Trace plugin and were only included if their total length was greater than or equal to 2µm (Longair et al., 2011). For branched projections, the longest continuous branch was followed and the whole structure was counted as one projection. All statistical analyses were performed using Prism software v7 (GraphPad, RRID:SCR_002798). All single pairwise comparisons were performed by two-tailed student's *t* test. All multiple comparisons were performed using an unpaired one-way ANOVA, with Tukey–Kramer pairwise *post hoc* tests. In all figures, graphs show the mean ± SEM with the statistical comparisons displayed as: NS (not significant) $p>0.05$), (*) $p<0.05$, (**) $p<0.01$ and (***) $p<0.001$.

Results

The *dfmr1*^{50M} Allele Causes Excess GFI Axonal Projections

The large central Giant Fiber Interneuron (GFI) can be labeled at single-neuron resolution by injecting TRITC-dextran into the axon in the cervical connective (Fig. **18***A*; Boerner and Godenschwege, 2011). Co-injecting with the small gap junction-permeant Neurobiotin (NB) tracer labels electrically coupled partners (Fig. **18***A*; Huang et al., 1992; Kennedy and Broadie, 2018). The primary presynaptic sites of the GFI are at the Inframedial Bridge (IB; Fig. **18***A*, arrowhead), which synapses with the Peripherally Synapsing Interneuron (PSI) and Giant Fiber Coupled (GFC) neurons 1-4, and the axonal bends (Fig. **18***A,* arrows), which synapse with the Tergotrochanteral Motor neuron (TTMn) and GFC2-3 (King and Wyman, 1980; Allen et al., 1998; Kennedy and Broadie, 2018). The GFI can be genetically targeted at near single-cell resolution using the 91H05-Gal4 driver, permitting a myriad of transgenic manipulations (Borgen et al., 2017). Using GFI-targeted expression of membrane-tethered GFP (mCD8::GFP) or the iontophoretic injection of TRITC-dextran and NB tracer dyes, we identified occasional projections along the GFI axonal bend (Fig. **18***B,* arrows). These putative synaptic contacts were assayed in our Fragile X syndrome (FXS) model, which is characterized by disrupted synapse formation and refinement (Hinton et al., 1991; Comery et al., 1997; Tessier and Broadie, 2008).

We first compared control (w^{1118}) and *dfmr1* null (*dfmr1*^{50M}) GFIs expressing mCD8::GFP and found a very strong axonal projection phenotype when FMRP is removed (Fig. **19***A*). GFI axonal bends in controls display only a few projections, whereas *dfmr1* mutants have many projections growing from the bends, several of which were of substantive size and complexity (Fig. **19***A*, arrows). Quantification of projections $\geq$2µm in length shows controls have an average of 1.4±0.5 projections/bend, while *dfmr1* nulls have 6.0±0.7, a significant increase (p=1.6×10^{-4}, two-tailed unpaired *t* test; Fig. **19***C*). To ensure these projections were not caused by the Gal4 driver or UAS construct, we next dye-injected the GFI axon in the

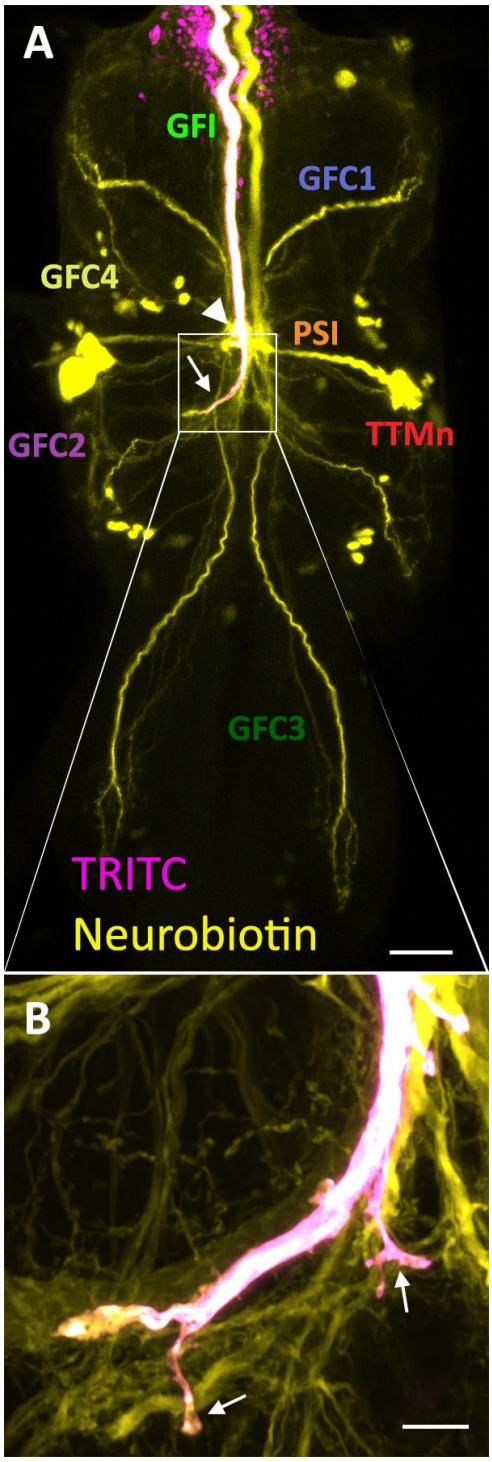

Figure 18. Presynaptic Projections From the Giant Fiber Interneuron Terminal Bend
A, Co-injection of TRITC-dextran (magenta) and Neurobiotin (yellow) into the Giant Fiber Interneuron (GFI) labels the neuron and all the gap-junction connected GF circuit neurons. Visible are the Peripherally Synapsing Interneuron (PSI), the Tergotrochanteral Motor neuron (TTMn) cell body and Giant Fiber Coupled (GFC) 1-4. The GFI Inframedial Bridge (IB, arrowhead) and axonal bends (arrow) located in the second thoracic ganglion segment are the two presynaptic sites. ***B,*** Enlarged image of the GFI axonal bend (see box in ***A***) showing outgrown projections of unknown connectivity (arrows). Scale bar represents 25µm in full image and 5µm in inset.

stock w^{1118} and $dfmr1^{50M}$ lines with TRITC-dextran (Fig. **19***B*). When axonal projections are compared with this labeling strategy, we again find supernumerary processes in $dfmr1^{50M}$ relative to the w^{1118} background control (Fig. **19***B*). Quantification shows control GFIs have an average of 3.3±0.2 projections/bend while *dfmr1* nulls have 7.8±0.4, again a significant elevation (p=4.7×10^{-20}, two-tailed unpaired *t* test; Fig. **19***D*). Taken together, the findings suggest the GFI axonal projections would be ideal to study how FMRP loss affects synaptic connectivity in the *Drosophila* FXS model. The projection phenotype is robust and relatively easy to measure, so we sought to characterize the defect more fully before dissecting the molecular mechanism responsible for the overgrowth.

Increased Axonal Projections Present During Early GFI Synaptogenesis

We first investigated when the overgrown axonal projections develop during GF circuit formation. The GFI reaches its TTMn target approximately 24 hours after puparium formation (APF), at which point synaptogenesis begins. Synapse formation lasts for approximately one day (24-48 hours APF; Allen et al., 1998). In order to examine this synaptogenesis period, we collected animals at approximately 34-50 hours APF by selecting for the "yellow body" localized between the Malpighian tubules on the dorsal side of the pupae (Paul and Bownes, 1981). The GFI 91H05-Gal4 driver was used to express UAS-*mcd8*::*gfp* and examine axonal bend projections over the developmental time course (Fig. **20***A*). Both control (w^{1118}) and *dfmr1* null ($dfmr1^{50M}$) GFIs exhibit far more extensive projection outgrowth than what was seen in adults, but the mutants show a much greater elevation (Fig. **20***A*, arrows). These early GFI projections are usually far more slender than the ones found in adults suggesting they are immature filopodial processes searching for synaptic partners (Tashiro et al., 2003; Armijo-Weingart and Gallo, 2017). Quantification shows that controls have 7.8±1.0 projections/bend and *dfmr1* nulls have 17.8±1.2 (p =1.3×10^{-6}, two-tailed unpaired *t* test; Fig. **20***B*, left). Thus, the FXS model defect is apparent at the early stages of synaptogenesis.

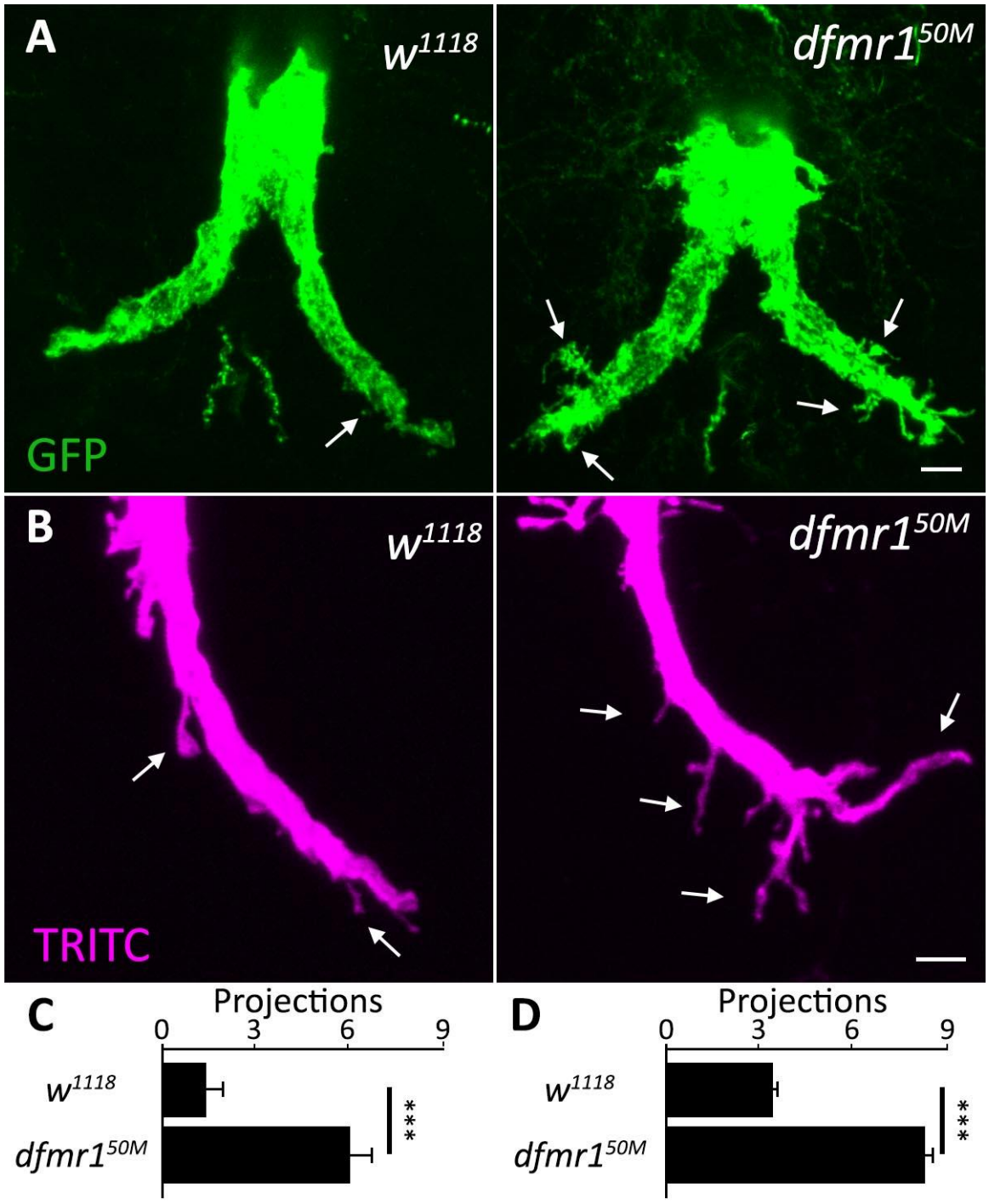

Figure 19. Supernumerary GFI Axonal Projections in *dfmr1*^{50M} Null Mutants

A, The Giant Fiber Interneuron (GFI) visualized with 91H05-Gal4 driving the membrane marker UAS-*mcd8*::*gfp* (green) in *w*^{1118} genetic control (left) and *dfmr1*^{50M} null (right). In controls the axonal bends have few detectable projections compared to an excess number of overgrown projections in the mutants. Arrows indicate the projections. ***B,*** Iontophoretic dye injection of TRITC-dextran (magenta) in *w*^{1118} (left) and *dfmr1*^{50M} (right) stocks show the same phenotype. Scale bars in both images: 5µm. ***C,*** Quantification of the GFP-labeled axonal projections. *w*^{1118}, *n*=8; *dfmr1*^{50M}, *n*=8. ***D,*** Quantification of the TRITC labeled projections. *w*^{1118}, *n*=62; *dfmr1*^{50M}, *n*=48.

We next assayed later stages in GF circuit development, testing two timepoints during synaptic maturation (Fig. **20***A*): 73-78 hours APF and 75-90 hours APF, identified by gray and black colored pupal wings, respectively. At each time point, *dfmr1* nulls still display more GFI axonal projections compared to matched controls, albeit with a progressive decrease in projection number over time (Fig. **20***A,B*). Note the w^{1118} controls decreased their projection number by 73-78 hours APF but showed little decline at 75-90 hours APF (Fig. **20***A*). Quantification supported these observations, showing 73-78 hour controls have 3.7±0.5 projections/bend, while *dfmr1* nulls have 14.1±0.8 (p=2.7×10^{-9}, two-tailed unpaired *t* test; Fig. **20***B*, middle). By 75-90 hours, controls exhibit 3.5±0.3 projections and *dfmr1* mutants 9.2±0.9 (p=2.6×10^{-6}, two-tailed unpaired *t* test; Fig. **20***B*, right). Synaptic overgrowth in FXS models may occur during initial synaptic formation or due to a failure to properly prune synapses (Antar et al., 2006; Gatto and Broadie, 2008; Patel et al., 2014; Connor et al., 2017). Our results indicate GFI overgrowth begins at early synaptogenesis stages but does not rule out a role for faulty pruning later. Some FXS reports show that early synaptic overgrowth is rectified in adults (Antar et al., 2006; Bilousova et al., 2009; He and Portera-Cailliau, 2013), so we next assayed whether the excess GFI projections form mature, persistent synapses.

Overgrown Axonal Projections Contain Chemical Synaptic Machinery

Synaptic markers are notoriously difficult to image in dense neural regions such as the GFI thoracic ganglia neuropil (Chen et al., 2014; Koles et al., 2016). Antibody labeling for presynaptic markers paired with standard confocal microscopy does not provide sufficient resolution to distinguish whether the synaptic marker is in a neuron of interest or neighboring neurons (Hiesinger et al., 2001; Urwyler et al., 2015). Another commonly used approach, the Gal4/UAS transgenic expression of labeled presynaptic markers in neurons of interest, often leads to overexpression which can cause mis-localization and protein aggregation (Christiansen et al., 2011; Chen et al., 2014; Koles et al., 2016). To avoid these difficulties, we employ here the Synaptic Tagging with Recombination (STaR) technique to label Bruchpilot (Brp), a well-

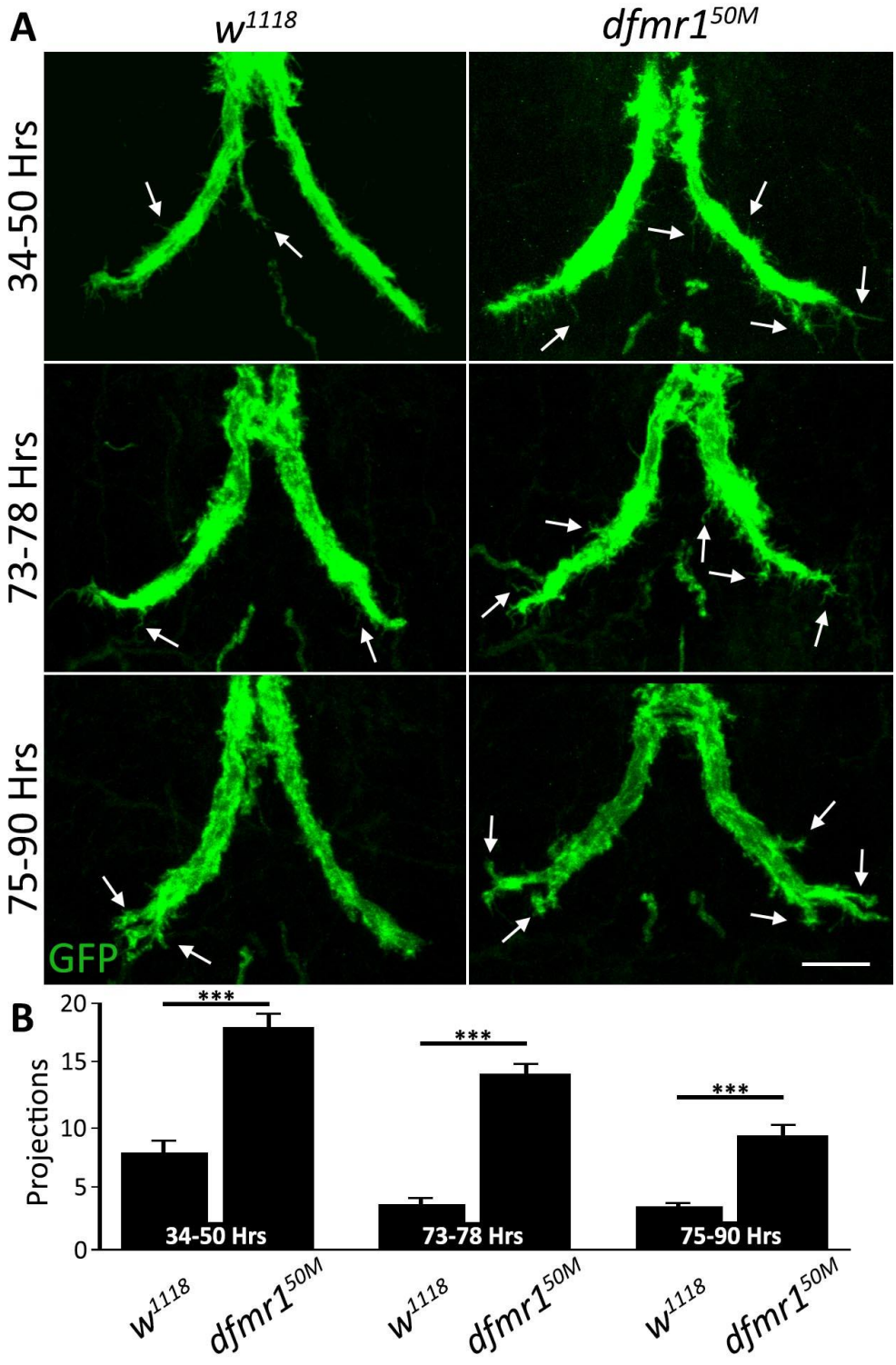

Figure 20. GFI Axonal Projection Overgrowth Begins Early in Synaptogenesis

A, The Giant Fiber Interneuron (GFI) axonal bends visualized with 91H05-Gal4 driven UAS-*mcd8*::*gfp* (green) during development in genetic control (w^{1118}, left) and *dfmr1* null mutant ($dfmr1^{50M}$, right) at 34-50 hours after puparium formation (APF, top), 73-78 hours APF (center) and 75-90 hours APF (bottom). Arrows indicate projections. Scale bar: 10µm. ***B.*** Quantification of the axonal projections at all 3 timepoints for both genotypes. Sample sizes: 34-50h: w^{1118}, *n*=12; $dfmr1^{50M}$, *n*=13. 73-78h: w^{1118}, *n*=10; $dfmr1^{50M}$, *n*=10. 75-90h: w^{1118}, *n*=12; $dfmr1^{50M}$, *n*=12.

studied presynaptic active zone scaffold organizer (Wagh et al., 2006; Chen et al., 2014). STaR labeling requires a stop codon flanked by Flp Recombination Target (FRT) sites followed by a GFP sequence that is inserted downstream of a protein of interest (Brp-FSF-GFP; Fig. **21**). Separately, the flippase (UAS-*flp*) is expressed in the neuron of interest to remove the FRT sites and enclosed stop codon, thus permitting readthrough from Brp to GFP (Brp::GFP; Fig. **21**).

We took advantage of this STaR labeling method to determine if the presynaptic Brp scaffold is present in the GFI axonal bend projections and to assay the maintenance of these synaptic projections from eclosion through adult maturity (Fig. **21**). For these analyses, 91H05-Gal4 was used to drive expression of both membrane mCD8::RFP and Flp to create GFP-labeled Brp in the marked GFI (Fig. **21***A*). w^{1118} and $dfmr1^{50M}$ animals were assayed immediately post-eclosion (1 hour), during a common activity-dependent refinement period (1 day), and at adult maturity (1 week) to assay for the persistence of GFI synaptic projections throughout life (Fig. **21***A*; Doll and Broadie, 2015). Results show that the majority of control and *dfmr1* mutant projections contained the Brp presynaptic scaffold, indicating they contain chemical synapses and are presynaptic processes (Fig. **21***A*). The small Brp::GFP puncta (green) are clearly visible in GFI projections (magenta), both along the projection shafts and at the tips (Fig. **21***A*, inset). The total synaptic projection number appears to remain steady from 1 hour post-eclosion to maturity at 1 week after eclosion (Fig. **21***A*), suggesting either that these projections are being created and removed at the same rate, or, more likely, that they are stable mature synapses that persist into adulthood (Holtmaat et al., 2009).

Quantification of the synaptic projections shows that 1 hour animals have both Brp-negative and Brp-positive processes, albeit with the majority containing chemical synapses (Fig. **21***B*). In both categories, w^{1118} controls have far fewer projections compared to *dfmr1* nulls (w^{1118}: total projections/bend 2.7±0.3, Brp+ projections/bend 1.7±0.2; $dfmr1^{50M}$: total projections/bend 6.3±0.5, $p=1.4\times10^{-5}$, two-tailed unpaired *t* test; Brp+ projections/bend 5.8±0.3, $p=2.7\times10^{-9}$, two-tailed unpaired *t*

test, Fig. **21***B*). By 1 day, nearly all projections were Brp positive in both genotypes, with far more in the mutants (w^{1118}: total projections/bend 2.1±0.4, Brp+ projections/bend 2.0±0.4; $dfmr1^{50M}$: total projections/bend 5.1±0.6, p=2.0×10^{-4}, two-tailed unpaired *t* test, Brp+ projections/bend: 5.0±0.5, p=2.8×10^{-6}, two-tailed unpaired *t* test, Fig. **21***B*). At 1 week, projection numbers were similar to 1 day, and every projection had chemical synapses, with more in the mutants (w^{1118}: Brp+ projections/bend 2.3±0.4; $dfmr1^{50M}$: Brp+ projections/bend 5.5±0.5, p=1.1×10^{-4}, two-tailed unpaired *t* test; Fig. **21***B*). Together, these findings show axonal projections that extend from the GFI bend likely make synaptic connections with postsynaptic partners. As the GFI uses mixed chemical and electrical synapses, we next tested whether these axonal projections also contain electrical synapse markers.

Overgrown Axonal Projections Contain Electrical Synapses

Unlike most synaptic protein antibodies, the Shaking-B (ShakB) antibody specifically labels GF electrical synapses, permitting simple imaging analyses (Phelan et al., 1996). To test whether GFI axon projections electrically couple to partner neurons the GFI axon was injected with TRITC-dextran and labeled with the ShakB antibody (Fig. **22***A*). Unlike Brp, we find ShakB present in a limited subset of projections (Fig. **22***A*, insets), with many projections either negative or below detection limits (Fig. **22***A*, arrowheads). Quantification shows that both w^{1118} controls and *dfmr1* nulls have ShakB in less than half the synaptic projections (Fig. **22***B*). The $dfmr1^{50M}$ animals exhibit projection overgrowth, both for total and ShakB+ projections (w^{1118}: total projections/bend 3.0±0.4, ShakB+ projections/bend 1.2±0.2; $dfmr1^{50M}$: total/bend 8.3±0.5, p=2.1×10^{-11}, two-tailed unpaired *t* test, ShakB+ projections/bend 3.0±0.3, p=6.1×10^{-6}, two-tailed unpaired *t* test; Fig. **22***B*). These results suggest that while axonal projections clearly form electrical synapses, this is not a universal mode of connectivity. We also wanted to test whether the projections depend on electrical synapses for formation or maintenance. Many vertebrate synapses have

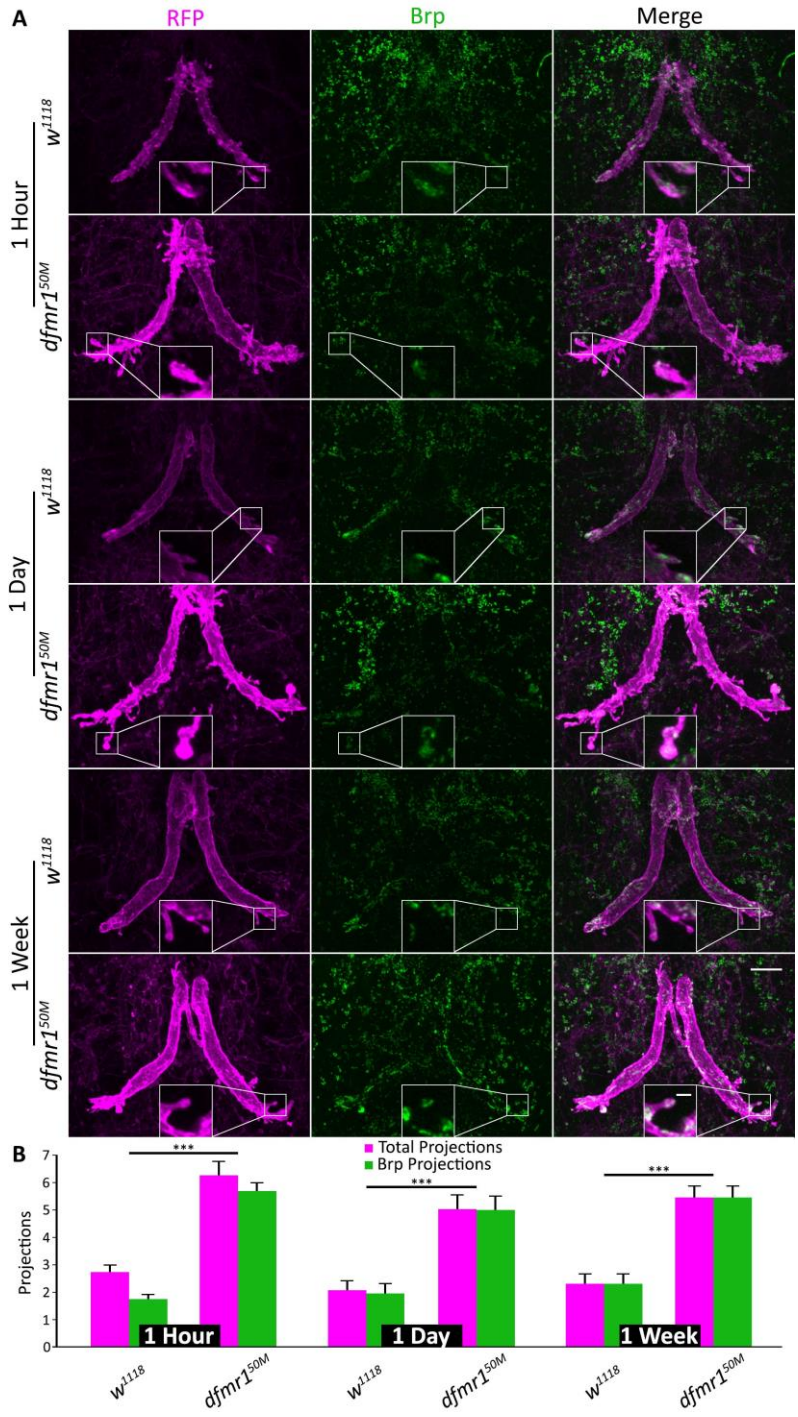

Figure 21. The GFI Axonal Projections Contain Chemical Synapse Markers

A, The Giant Fiber Interneuron (GFI) axonal bend labeled with 91H05-Gal4 driven mCD8::RFP (magenta, column 1) with STaR transgenic labeling of Bruchpilot (Brp) in presynaptic active zones (green, column 2). The merge reveals axonal projections with the chemical synapse marker (column 3). Genetic control (w^{1118}, top) and *dfmr1* null mutant ($dfmr1^{50M}$, bottom) are tested at 1 hour, 1 day, and 1 week after eclosion. Insets show magnified Brp-positive projections. Scale bars: 10µm (full image) and 2µm (inset). ***B,*** Quantification of total (magenta) and Brp-positive (green) axonal projections for the above 3 time points. Significance bars represent comparisons between each genotype for the two projection quantifications for each time point. Sample sizes: 1 hour: w^{1118}, *n*=17; $dfmr1^{50M}$, *n*=12; 1 day: w^{1118}, *n*=12; $dfmr1^{50M}$, *n*=13; 1 week: w^{1118}, *n*=8; $dfmr1^{50M}$, *n*=8.

been reported to use gap junctions during synaptogenesis, removing them when synapse formation is complete (Niculescu and Lohmann, 2014; Jabeen and Thirumalai, 2018).

GFI electrical synapses can be eliminated using the s*hakB*^{2} null mutant, which eliminates coupling (Blagburn et al., 1999). We tested this mutant alone and combined with *dfmr1*^{50M}*,* injecting the GFI with gap junction permeable NB (Fig. **22***C*). Dye injections were performed for 30 seconds, as longer injections cause these neurons to rupture (Kennedy and Broadie, 2017). In these experiments, no neurons aside from the GFI were labeled, indicating the successful removal of ShakB. Both single and double mutants still produce projections (Fig. **22***C,* left), though *shakB*^{2}*; dfmr1*^{50M} maintains overgrown projections relative to the control (Fig. **22**C*,* right). Quantification shows *dfmr1*^{50M} has a significant increase in projections (*shakB*^{2}: projections/bend 2.7±0.4; *shakB*^{2}*; dfmr1*^{50M}: projections/bend: 5.2±0.4, p=5.2×10^{-5}, two-tailed unpaired *t* test; Fig. **22***D*). These results suggest that some *dfmr1*^{50M} projections could be ShakB electrical synapse dependent, but not all of them. Taken together, the above findings show that the GFI axonal projections contain both chemical and electrical presynaptic markers (Brp and ShakB). The distance that these synaptic projections travel away from the GFI axonal bend suggests that they connect with postsynaptic partners other than the TTMn, which lays tightly along the main GFI axon (Blagburn et al., 1999). We therefore next pursued these partners to determine whether they were normal GF circuit neurons, or new, inappropriate targets.

GFI Synaptic Projections Target GFC Neurons to Cause Circuit Hyper-Connectivity

GF circuit connectivity can be mapped by injecting small tracers that pass through gap junctions to label partner neurons (Boerner and Godenschwege, 2011). We took advantage of this property by injecting the GFI with NB to test whether any unexpected neurons partner with the *dfmr1*^{50M} projections (Huang et al., 1992; Kennedy and Broadie, 2018). The *w*^{1118} control and *dfmr1*^{50M} null dye coupling patterns, though complex, appeared similar, with no new labeled neurons standing out in the mutant (Fig.

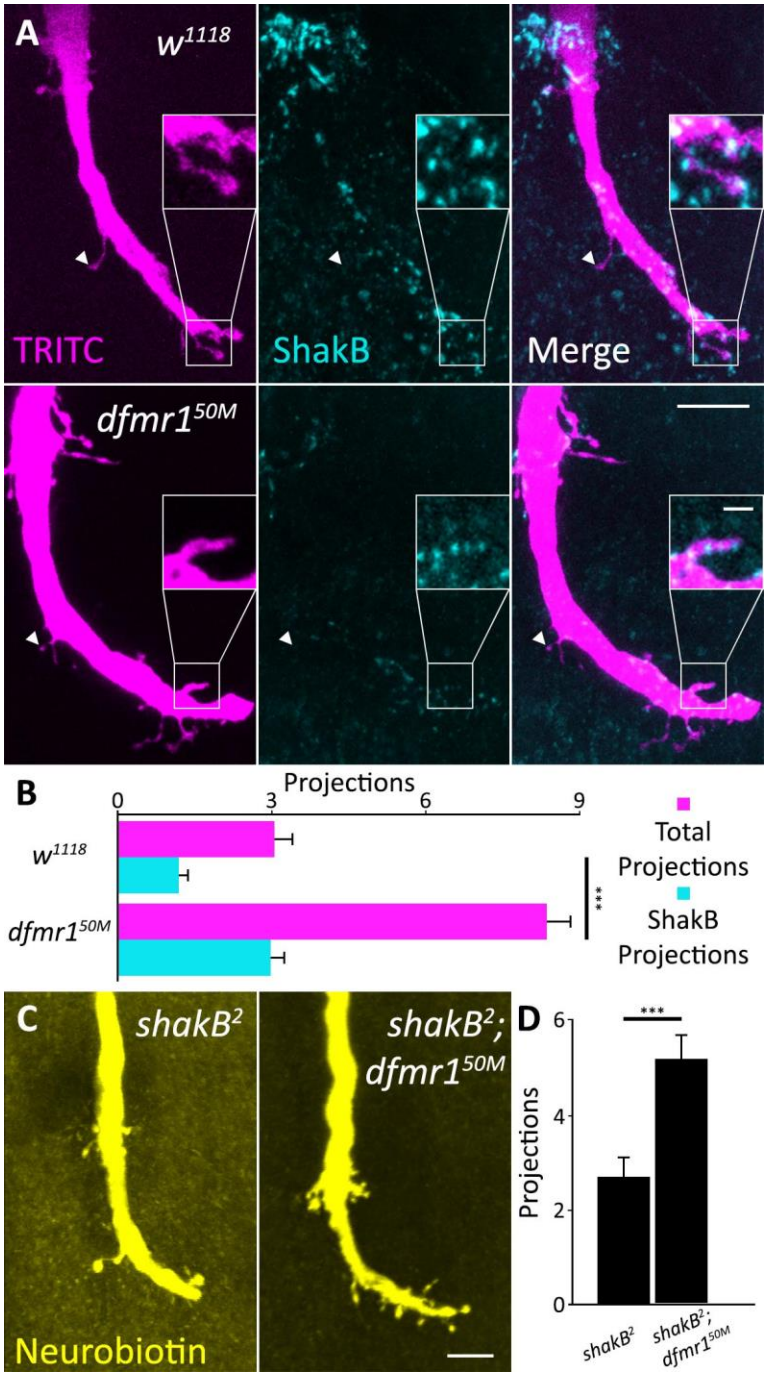

Figure 22. The GFI Axonal Projections Contain Electrical Synapse Markers

A, Giant Fiber Interneuron (GFI) dye injected with TRITC-dextran (magenta, left) and labeled for the ShakB innexin (cyan, center) reveals axonal bend projections containing electrical synapses (merge, right) in both w^{1118} (top) and $dfmr1^{50M}$ (bottom). Arrowheads indicate ShakB-negative projections, insets show magnified ShakB-positive projections. Scale bars: 10µm (full image) and 2µm (inset). ***B,*** Quantification of total (magenta) and ShakB-positive (cyan) projections for both genotypes. Significance bars represent comparisons between each genotype for the two projection quantifications. Sample sizes: w^{1118}, *n*=28; $dfmr1^{50M}$, *n*=26. ***C,*** GFI dye injected with Neurobiotin (yellow) in $shakB^{2}$ null mutant (left) and $shakB^{2}; dfmr1^{50M}$ double mutant (right). Scale bar: 10µm. ***D,*** Quantification of projections for both genotypes. Sample sizes: s$hakB^{2}$, *n*=27; $shakB^{2}; dfmr1^{50M}$, *n*=31.

23*A*). Moreover, upon close analyses of the *dfmr1*^{50M} projection locations, it appears that they contact recently identified neurons within the GF circuit, specifically GFC2 (Fig. **23***A*, arrow) and GFC3 (Fig. **23***A*, arrowhead; Kennedy and Broadie, 2018). Since transgenic tools are available to study these neurons, we tested whether the mutant projections are overgrowing these normal GFI targets. We combined the GFC2 (73C07-Gal4) and GFC3 (24H07-Gal4) drivers with UAS-*mcd8::gfp* and crossed these animals with the *dfmr1*^{50M} stock, since *dfmr1*^{50M}/+ increases projection number (see Fig. **24** below). We injected the GFI with TRITC and found that the GFI projections frequently oppose GFC2 and GFC3 (Fig. **23***B*, arrows), indicating putative connectivity. We next wished to test whether these direct contacts are incidental or indicate synaptic pairing.

To test synaptic connectivity, we repeated the above experiment with labeling for ShakB to identify electrical synapses. We find that ShakB is indeed present at the contact intersection of the GFI projections and GFC2 and 3 neurons (Fig. **23***C*, insets). As above, there were frequently cases where ShakB labeling is not present in projections contacting a GFC (Fig. **23***C*, arrowhead). Taken together these findings suggest that the synaptic projections characterizing the *dfmr1*^{50M} mutant make redundant connections onto known GF circuit neurons. It is unclear if GFC2 and 3 are the only targets of the excess projections, or whether other partners remain to be uncovered. It is interesting to note that GFC2 and 3 extensively contact the main axon shaft in both controls and *dfmr1* nulls and occasionally form synapses there, making the projections unnecessary (Kennedy and Broadie, 2018). This suggests either that the mutant condition drives the axon to seek out more synapses with its partners than it normally would require, or that developmental projections normally pruned away during GF circuit maturation are inappropriately stabilized (Fig. **20**). However, in the pursuit of this question we uncovered evidence that FMRP loss alone may not cause the synaptic projection phenotype, so we pursued a series of control experiments.

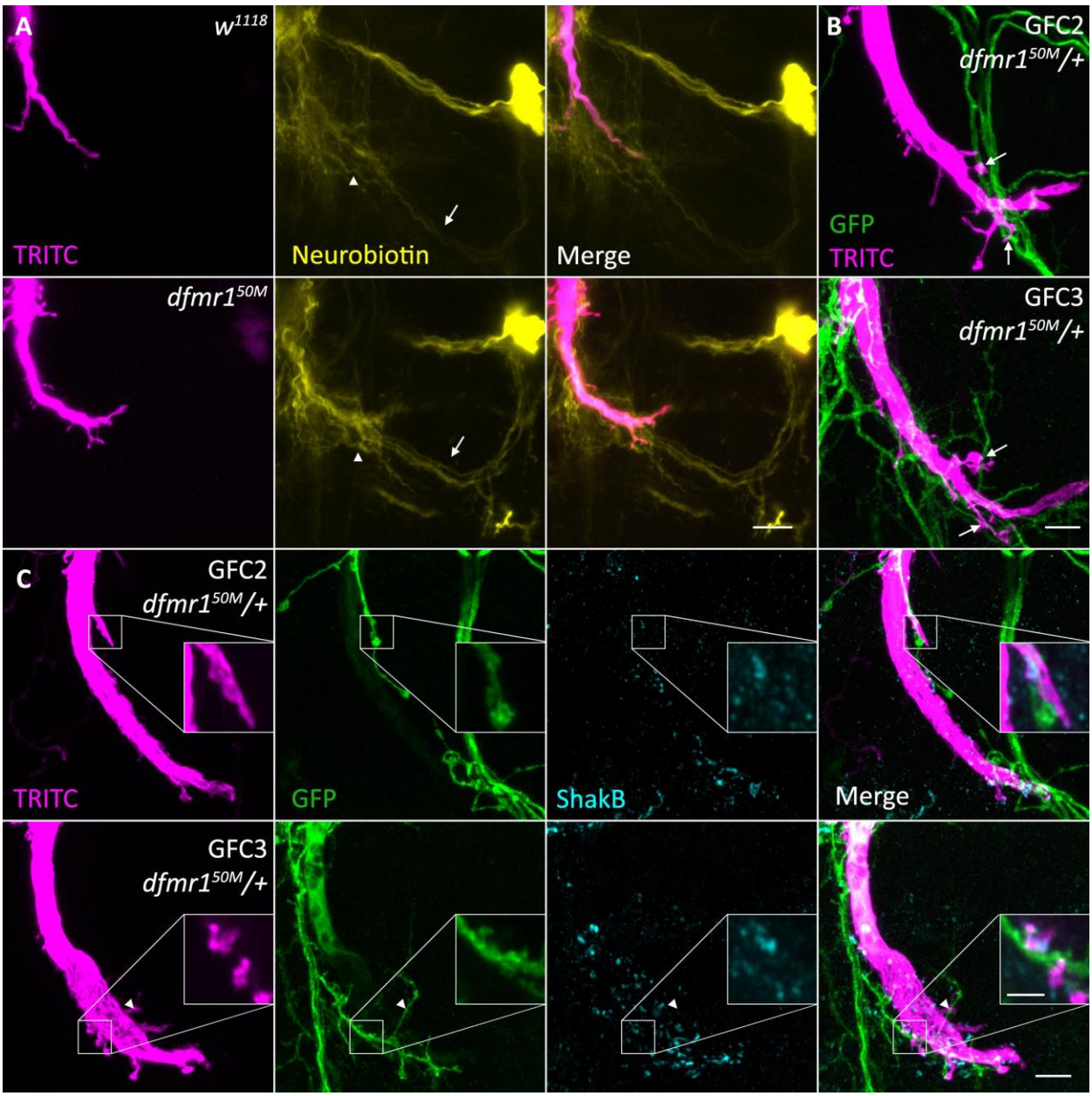

Figure 23. GFI Axonal Projections Synapse Within the GF Circuit on GFC Neurons

A, The Giant Fiber Interneuron (GFI) was co-injected with TRITC-dextran (magenta, left) and Neurobiotin (yellow, center) to examine downstream neurons (merge, right) in w^{1118} (top) and $dfmr1^{50M}$ (bottom). A presumptive GFC2 (arrow) and GFC3 (arrowhead) are contacted by GFI projections. Scale bar: 10µm. ***B,*** The GFI injected with TRITC-dextran (magenta) in 73C07-Gal4 driving mCD8::GFP (green) in GFC2 (top) and 24H07-Gal4 driving mCD8::GFP (green) in GFC3 (bottom) in the $dfmr1^{50M}$/+ background. Arrows point to overlaps between the GFI and the GFCs. Scale bar: 5µm. ***C,*** GFI injected with TRITC-dextran (magenta, column 1) with mCD8::GFP (green, column 2) labeling GFC2 (73C07-Gal4, top) and GFC3 (24H07-Gal4, bottom) in the $dfmr1^{50M}$/+ background were co-stained for ShakB (cyan, column 3) to reveal electrical synapses. All three channels are combined in the merge (column 4). Insets show magnified sub-stacks of ShakB-positive projections contacting GFC neurons. The arrowhead shows a ShakB-negative GFI-GFC contact. Scale bars: 5µm (full image) and 2µm (inset).

Background Mutation(s) in the FXS Disease Model Causes Synaptic Projections

To ensure that FMRP loss was responsible for the excess axonal synaptic projections, we performed transgenic rescue experiments and tested alternative *dfmr1* nulls for the phenotype. For the rescue experiment, we used a full length genomic *dfmr1* sequence, including its regulatory region, inserted on the second chromosome (*dfmr1.14*; Dockendorff et al., 2002). For alternative nulls, we examined the homozygous viable $dfmr1^{B55}$ allele and the $dfmr1^{2}$ allele over a deficiency (Df(3R)BSC621) that completely removes *dfmr1* and numerous adjacent genes (Dockendorff et al., 2002; Inoue et al., 2002; Cook et al., 2012). Both $dfmr1^{B55}$ and $dfmr1^{2}$ are reported to be complete protein nulls in the brain, although $dfmr1^{B55}$ has been found to express FMRP in the testes (Zhang et al., 2004). We also tested the heterozygous $dfmr1^{50M}$ condition ($dfmr1^{50M}$/+) to determine whether full protein loss is required for the phenotype or if the defect occurs in heterozygotes, as has been reported previously in the *Drosophila* FXS model (Kanellopoulos et al., 2012). Finally, to further test FMRP loss effects on synaptic projection overgrowth we took a transgenic RNAi approach using a highly-expressing ubiquitous Gal4 driver to express *dfmr1* RNAi (UH1-Gal4>*dfmr1* RNAi2; Callan et al., 2012). All these studies are summarized in Figure **24**.

We first tested rescue animals (*dfmr1.14*/+; $dfmr1^{50M/50M}$) by injecting the GFI with TRITC-dextran to assay projections. The rescue shows partial correction of the $dfmr1^{50M}$ null phenotype, with fewer projections present ($dfmr1^{50M}$ projections/bend 9.5±0.8, Rescue 5.6±0.4; unpaired ANOVA with Tukey *post-hoc* analysis, p=3.2x10^{-5}; Fig. **24***A,C*). The rescue does not appear complete as more projections are seen in the rescue condition than the w^{1118} background control (w^{1118} projections/bend 3.9±0.4; Fig. **24***A,C*), although this difference is not significant (unpaired ANOVA with Tukey *post-hoc* analysis, p=0.1). The $dfmr1^{50M}$/+ heterozygotes show an intermediate synaptic projection phenotype, similar to the rescue results (w^{1118} projections/bend 2.8±0.5, $dfmr1^{50M}$/+: 5.7±0.5, $dfmr1^{50M}/dfmr1^{50M}$: 8.3±0.7), with significant differences in all comparisons (unpaired ANOVA with Tukey *post-hoc* analysis: w^{1118} *v.* $dfmr1^{50M}$/+

p=0.001, *dfmr1*^{50M}/+ *vs. dfmr1*^{50M} *p*=0.006; *w*^{1118} *vs. dfmr1*^{50M} *p*=2.5x10^{-8}; Fig. **24***A,D*). Taken together, these results supported the conclusion that FMRP loss causes the excess synaptic projections.

Surprisingly, however, the alternate *dfmr1* mutants do not replicate the synaptic projection phenotype. The *dfmr1*^{B55} mutants appear nearly identical to control animals (*w*^{1118} projections/bend 2.8±0.5 vs. *dfmr1*^{B55} 3.3±0.6), with no significant difference seen (unpaired ANOVA with Tukey *post-hoc* analysis, *p*=0.9; Fig. **24***A,D*). We tested *dfmr1*^{B55} by Western blot and confirmed no FMRP is detectably expressed in the brain (Fig. **24***B*). The *dfmr1*^{2}/Df test, carried out separately, shows the same result, with no apparent projection increase (*w*^{1118} projections/bend 4.3±0.5, *dfmr1*^{50M} 7.9±0.8, *dfmr1*^{2}/Df 3.8±0.5) and no significant difference from the control seen (unpaired ANOVA with Tukey *post-hoc* analysis, *p*=0.8; Fig. **24***A,E*). Finally, ubiquitous RNAi FMRP knockdown also does not increase GFI synaptic projections (UH1-Gal4/+ control projections/bend 4.1±0.4 vs. UH1-Gal4>*dfmr1* RNAi2: 3.0±0.4) with no significant difference in projection number (two tailed unpaired *t* test, *p*=0.05; Fig. **24**A,*F*). Western blot analyses show that ubiquitous UH1-Gal4 driven *dfmr1* RNAi2 completely eliminates detectable FMRP from the brain, in contrast to an alternate knockdown approach of pan-neuronal *elav*-Gal4 driven *dfmr1* RNAi1, which shows a weak, residual FMRP signal (Fig. **24***B*).

Taking all of the above results together, we conclude that FMRP loss by itself does not cause the excess presynaptic projections on the GFI axonal bend and that a second site mutation(s) in the *dfmr1*^{50M} background is required for the circuit connectivity defect. Importantly, the rescue experiment was misleading in this case, causing us to draw the incorrect initial conclusion of an FMRP specific requirement. The simple interpretation would have been that the rescue reinserted a single wildtype *dfmr1* allele into a null background to provide partial phenotype restoration. However, considering the alternative *dfmr1* mutant and RNAi results, it may be that a background mutation was lost when *dfmr1.14* was combined with *dfmr1*^{50M}. We cannot rule out a role for FMRP loss, as it could be acting in concert with the background mutation(s) to enhance the synaptic projection phenotype. Interestingly, FXS in humans may

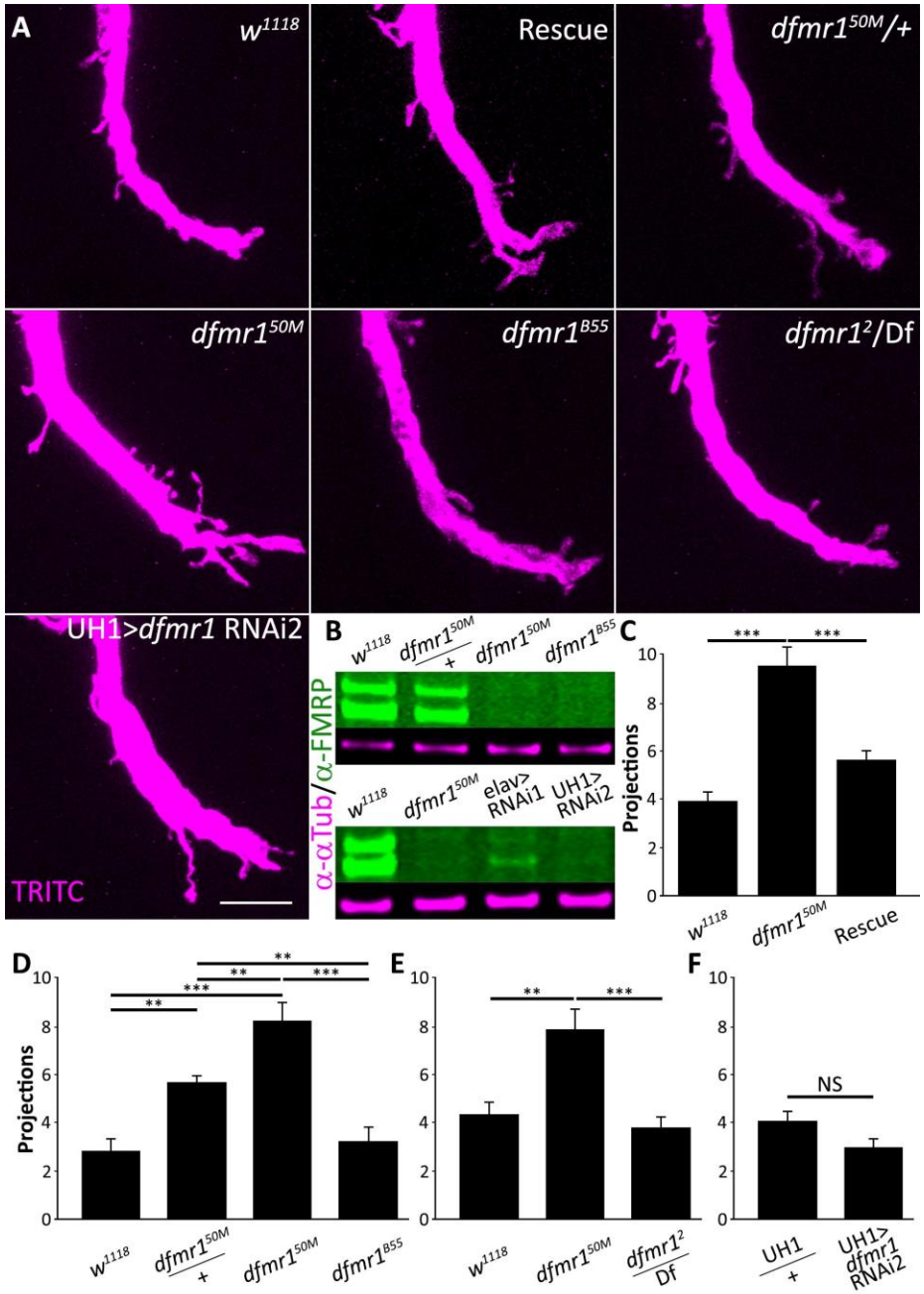

Figure 24. GFI Synaptic Projections Caused by *dfmr1^{50M}* Background Mutations

A, Giant Fiber Interneuron (GFI) dye injected with TRITC-dextran (magenta) in the indicated genotypes; genetic background control (*w^{1118}*), genomic rescue (*dfmr1.14/+; dfmr1^{50M}*), *dfmr1^{50M}* heterozygote (*dfmr1^{50M}*/+), homozygous null mutant *(dfmr1^{50M}*), independent *dfmr1* null (*dfmr1^{B55}*) and second independent *dfmr1* null over a deficiency (*dfmr1^{2}*/Df). FMRP was also removed using RNAi driven by the ubiquitous UH1-Gal4 driver (UH1>*dfmr1* RNAi2). Scale bar: 10µm. ***B,*** Western blot of FMRP levels in *w^{1118}*, *dfmr1^{50M}*/+, *dfmr1^{50M}* and *dfmr1^{B55}* (top); and *w^{1118}*, *dfmr1^{50M}*, elav> *dfmr1* RNAi1 and UH1> *dfmr1* RNAi2 (bottom). FMRP bands are labeled in green and α-Tubulin loading controls in magenta. ***C,*** Quantification of synaptic projections in *w^{1118}* (*n*=14), *dfmr1^{50M}* (*n*=13) and *dfmr1* rescue condition (*n*=14). ***D,*** Quantification of projections in *w^{1118}* (*n*=13), *dfmr1^{50M}*/+ (*n*=13), *dfmr1^{50M}* (*n*=10) and *dfmr1^{B55}* (*n*=12). ***E,*** Quantification of the synaptic projections in *w^{1118}* (*n*=9), *dfmr1^{50M}* (*n*=9) and *dfmr1^{2}*/deficiency (*n*=10). ***F,*** Quantification of projections in UH1/+ control (*n*=17) and UH1>*dfmr1* RNAi2 (*n*=16).

be related to such background effects, as severity of the disease symptoms present on a wide spectrum (Spencer et al., 2006; Chonchaiya et al., 2009; Cordeiro et al., 2011). We have chosen to identify the background mutation(s) as it may shed new light on the molecular players in synapse formation.

Identifying Background Mutation(s) Causing Excess GFI Synaptic Projections

As the w^{1118} background and $dfmr1^{50M}$ mutant lines diverged many generations ago and have since been subjected to an unknown number of crossing events, we suspected there would be a large number of genetic differences between these two lines. We therefore chose to employ Bulk Segregant Analysis (BSA) paired with whole genome sequencing (WGS) to identify the $dfmr1^{50M}$ background mutation(s). BSA has been successfully used to identify *de novo* mutations from divergent backgrounds in several organisms, including yeast, flies, lettuce and apple trees (Michelmore et al., 1991; Lai et al., 2007; Ehrenreich et al., 2010; Pool, 2016; Dougherty et al., 2018). We pursued this BSA strategy by inbreeding the heterozygous offspring of a cross between w^{1118} and $dfmr1^{50M}$ for 12 generations. We analyzed the number of synaptic projections by GFI dye injection in the later generation animals and sorted them into pools of low, medium and high phenotypes. A total of 239 animals were analyzed by single neuron dye injection, from which 85 were selected for the low pool, 70 for the medium pool and 34 for the high pool. The extracted DNA from these pools is currently undergoing WGS to identify enriched regions of the genome in the medium and high pools relative to the low pool. Once the mutation(s) has been identified, we intend to use lines from *Drosophila* stock centers to replicate and rescue the projection defects identified here.

Discussion

We began this study by searching for neurons that could be used to probe mechanisms underlying FXS excess synapse phenotypes (Comery et al., 1997; Zhang et al., 2001; Bilousova et al., 2009; Cruz-

Martín et al., 2010; Doll et al., 2017). The GF circuit appeared ideal for this work as it is known to be impacted by FMRP loss, is large and easy to visualize, can be imaged and manipulated at single-cell resolution, has a complex but well-established set of synaptic connections, and can be electrophysiologically and behaviorally assayed (Power, 1948; Tanouye and Wyman, 1980; Allen et al., 1998; Martinez et al., 2007; Augustin et al., 2011; Boerner and Godenschwege, 2011; von Reyn et al., 2014; Kennedy and Broadie, 2017, 2018). Unfortunately, while we found an FXS-like phenotype in the GF circuit, our work was complicated by a *dfmr1*^{50M} background mutation(s) (Zhang et al., 2001). This is the most commonly used allele, due to its complete null phenotype (in contrast to *dfmr1*^{B55}) and ability to produce viable homozygous offspring (in contrast to *dfmr1*^{2} and *dfmr1*^{3}, Dockendorff et al., 2002; Inoue et al., 2002). Interestingly, a second *dfmr1*^{50M} stock our lab maintains does not manifest the synaptic phenotype, suggesting the background mutation(s) spontaneously occurred or was brought in through a previous outcrossing event. As we had completed a detailed study of the synaptic projection phenotype we chose to pursue the mutation(s). Our identification strategy is ongoing, but we expect this work to expand our understanding of synapse formation.

The GFI synaptic projections assayed here likely arise from the extensive filopodial outgrowths observed during synaptogenesis, though disrupted pruning could also play a role (Fig. **20**; Gatto and Broadie, 2011; O'Connor et al., 2017; Lieberman et al., 2018). In many circuit contexts, excess synaptic processes are known to be pruned back to arrive at an optimized number of mature contacts (Schafer and Stevens, 2013; Riccomagno and Kolodkin, 2015; Kremer et al., 2017). The synaptic number at the end of this maturation phase is regulated by many factors, ranging from prosynaptic glia to Neurotrophins (Causing et al., 1997; Ullian et al., 2001; Sugiura and Lin, 2011; He et al., 2018a). Delayed synaptic pruning has been well demonstrated in FXS disease models; however, in contrast to the work here corrective pruning was shown to occur later in development (Connor et al., 2017). Since *Drosophila* axons employ both *en passant* synapses and extended terminal projections to contact their postsynaptic targets, an

alternative route to the overgrowth phenotype could be the mutation encouraging production of projections instead of *en passant* contacts (Egger et al., 1997; Menon et al., 2013; Doll et al., 2017; Takemura et al., 2017). Our synaptic labeling experiments show that the early projections stabilize into mature processes containing both the Brp active zone scaffold and the ShakB gap junction innexin (Zhang et al., 1999; Wagh et al., 2006). The projections also become thicker than the initial filopodia, and endure into adult maturity, showing that they are likely not transitory or immature contacts (Pielage et al., 2005; Holtmaat et al., 2009; He and Portera-Cailliau, 2013; Pacheco and Gallo, 2016; Armijo-Weingart and Gallo, 2017). Brp punctae occur in 90% of projections at 1 hour post-eclosion, and 100% of projections by 1 week, supporting the idea of maturing synaptic processes. It is worth noting however, that the STaR technique used to label Brp depends on a random recombination process that can occur at any time (Chen et al., 2014). The 10% of processes that do not contain labeled Brp at 1 hour may be due to a late recombination event that did not permit Brp-GFP to reach a high expression level.

We were not able to find any new neurons dye-coupled to the GFI caused by the mutant synaptic projection overgrowth, indicating no inappropriate synaptic partnerships were made by these overelaborated synaptic contacts. It is still possible that such inappropriate synapses exist in the dense synaptic region around the GFI axonal bends, but that the connections are too weak to give a robust dye signal, or are solely chemically synaptic (Namiki et al., 2018). Two targets of the excess synaptic projections were identified as the GFC2 and GFC3 neurons, recently uncovered GF circuit members (Kennedy and Broadie, 2018). GFC2 and 3 normally contact the GFI at both the IB and along the bends. It is therefore unclear why the mutant synaptic projections would be needed to increase connections to these partners, rather than increasing the density of the extant synaptic sites (Fig. **23***B*).

Our rescue studies to confirm the FMRP role in synaptic overgrowth provided equivocal results, showing this approach alone is not sufficient to correlate a mutation with a phenotype. Without further data the rescue would have been interpreted as proof of causation, with FMRP restored to heterozygosity

and giving an intermediate phenotype. However, knowing a background mutation is present, the result can now be interpreted as the *dfmr1*^{50M} line creating a heterozygous phenotype with a "clean" rescue line that lost the mutation. Even with homozygous rescue (i.e. *dfmr1.14*/*dfmr.14*; *dfmr1*$^{50M/50M}$), which unfortunately is not possible due to inviability, we would likely have an uninterpretable result, as an unintentionally "cleaned up" homozygous rescue would lack the background mutation and provide apparent complete rescue. We ruled out FMRP as the sole mutation causing synaptic overgrowth through three independent protein removal strategies: an alternative null, a null and deficiency transheterozygote and an RNAi knockdown (Fig. **24**). It is possible that FMRP loss interacts synergistically with the background mutation and is required for the synaptic projection phenotype. If this is the case, we expect our BSA results to show enriched *dfmr1*^{50M} mutation counts in medium and high projection pools (Michelmore et al., 1991). Unidentified background mutations have been shown to interact with FMRP loss in mice, creating learning defects and exacerbating autism-like behaviors (Paradee et al., 1999; Dobkin et al., 2000; Spencer et al., 2011). Similarly, FXS patients show a range of symptom severities, believed to depend on genetic modifiers (Hessl et al., 2001; Spencer et al., 2011). Thus, identifying interacting mutations here may help explain some of the human FXS variability and provide novel therapeutic targets (Maurin et al., 2014).

Based on the *dfmr1*^{50M}/+ results, we expect the background mutation operates via incomplete dominance, with heterozygous expression leading to an intermediate phenotype (Muller, 1935; Crawford, 1976). Our experiments with recombined *dfmr1*^{50M} support the conclusion that the background mutation is incompletely dominant. In each recombined case, synaptic projection number is lower than the pure *dfmr1*^{50M} line (Fig. **19***A*, **21***A*, **22***C* vs. Fig. **19***B*, **22***A,* **24***A*). We suspect recombination events either removed the mutation in one of the parental strains or diluted its frequency in the population, creating an intermediate phenotype. It is also important to note that multiple background mutations could be causing the phenotype, either additively or synergistically (Abrahams and Geschwind, 2008; Pérez-Pérez et al.,

2009; Grant, 2012). Potential mutation categories include single-nucleotide polymorphisms (SNPs), copy-number variants (CNVs) or rearrangements which could affect intergenic regulatory sites, untranslated regions (UTRs), splice acceptor/donor sites or coding sequences (Berger et al., 2001; Ng and Henikoff, 2003; McCarroll and Altshuler, 2007; Adzhubei et al., 2010; Cooper and Shendure, 2011; Ward and Kellis, 2012). Mutations could also affect non-coding RNAs regulating gene transcription and translation (Fire et al., 1998; Mehler and Mattick, 2007; Jeck et al., 2013). Regardless of the genomic change, the mutation will ultimately affect protein expression level, trafficking or functionality, which we will target using the extensive *Drosophila* genetic resources (Ng and Henikoff, 2003; Dietzl et al., 2007; East, 2010; McManus et al., 2010; Dawson et al., 2017; Li-Kroeger et al., 2018).

As the increased synaptic projections are apparent early in development, and are matured by eclosion, we suspect the mutation is related to synaptic outgrowth, stabilization or pruning, rather than activity-dependent refinement (Fields and Itoh, 1996; Wong and Ghosh, 2002). There are many proteins that could be responsible for increased synapse stabilization. The most likely categories include: 1) cytoskeletal elements responsible for filopodial outgrowth, along with their accessory and regulatory proteins (e.g. actin, profilin, Rho/Rac; Bishop and Hall, 2000), 2) cell adhesion molecules responsible for synaptic stabilization (e.g. Neuroglian, Neurexin, SynCAM; Biederer et al., 2002; Godenschwege et al., 2006; Südhof, 2018), 3) extracellular promoters of synaptic stability (e.g. Wnt, Neurotrophins; Rosso and Inestrosa, 2013), 4) synaptic pruning/degradation machinery (e.g. Draper, Ced-6; Awasaki et al., 2006), and 5) regulatory mechanisms controlling any of the above (e.g. transcription factors, epigenetic modifiers; Ayata et al., 2018; Hobert and Kratsios, 2019).

In conclusion, we report here on a *dfmr1* stock containing a background mutation that promotes GFI synaptic overgrowth. The excessive axonal presynaptic projections are present during synaptogenesis, incorporate both chemical and electrical synapse markers, are present 1 day post-eclosion, and endure to maturity (1 week post-eclosion). The projections electrically synapse on the recently identified GFC2/3

neurons, causing hyper-connectivity within the GF circuit. The background mutation(s) identity is currently being pursued and is expected to reveal a protein(s) involved in regulating synaptic connectivity during circuit formation.

Chapter V

Conclusions and Future Directions

The work in this dissertation explores a number of GF circuit properties, from ionic flow in mature neurons to synaptogenesis at the early stages of development. While these studies share a focus on the same set of neurons, they are quite distinct from each other in subject matter. As such, they each have their own set of conclusions and future directions, which will be laid out separately in this chapter. There were also several supporting experiments and two uncompleted projects that were not published due to time constraints or negative results. This data is included here either with the conclusions of the work it was performed for, or in its own section if it was not tied to any published work.

Dye Injection

The finding that a single genetic mutation can alter neuronal dye loading properties is surprising and appears to have no precedent in the literature. The only field that has considered electrically driven ionic movement through biological tissues is trans-dermal electromigration, in which medicine is delivered across the skin to the circulatory system (Marro et al., 2001; Pikal, 2001; Kalia et al., 2004). However, no molecular level work has been done to explore the cellular properties that enhance or inhibit this process. It still remains unclear how FMRP loss leads to increased dye loading, though the published research reported here has narrowed down the possibilities. I took two parallel approaches to identify the causative mechanisms underlying altered dye loading. First, I considered the known neuronal defects caused by FMRP loss. This led to experiments on potassium channels, neuron size, and interneuronal connectivity (Comery et al., 1997; Brown et al., 2010; Lee et al., 2011; Kong et al., 2014). Unfortunately, none of these properties appears to play a role in the phenotype. The second approach was to identify

the physical cause of increased dye signal in the mutant neurons, and thus narrow down the potential mechanisms involved in the phenotype. Three broad possibilities were considered: 1) dye leaked out of neurons slower in mutants, 2) dye was destroyed or sequestered in controls, or 3) more dye leaves the electrode to enter mutant neurons (Fig. **25***A-C*). My experiments effectively ruled out the first two options, as applying more current or rest time after injection, did not alter the signal levels and there did not appear to be any differential dye storage in the axons, dendrites or soma. The only remaining option was that more dye leaves the electrode to enter mutant neurons than control neurons (Fig. **25***C*).

There are a range of physical properties that could alter dye release from the electrode. One possibility is that there is simply more room for dye in the *dfmr1* null neural circuit than in the control, either because of larger neurons or a greater number of connected neurons. Similarly, there may be better gap junction conductance between the neurons in *dfmr1* mutants, allowing more dye to penetrate deeper through the neural circuit during the injection (Fig. **25***D*). These hypotheses were ruled out in several ways. First, no difference in neuron size was observed in *dfmr1* mutants compared to controls. Axonal shafts had no measurable size differences between the genotypes, nor did the primary dendritic branches. Second, removing all gap junctions, leaving only the GFI to be injected did not correct the *dfmr1* phenotype. Removal was accomplished with a mutant that lacks GFI specific isoforms of the ShakB gap junction protein. We found that even when NB could not leave the GFI, more still accumulated in the *dfmr1* mutant than the control. Third removing KAc from the dye solution caused a major increase in dye loading. This should not have been possible if the reduced dye loading in controls was caused by some intrinsic “dye capacity” that was reached. Since more dye was easily loaded into control neurons when KAc was removed we suspected that the rate of entry must be impacted rather than a threshold being reached. We chose to explore what factors could limit the dye transfer speed, focusing first on cytosolic ion movement as a potential mechanism.

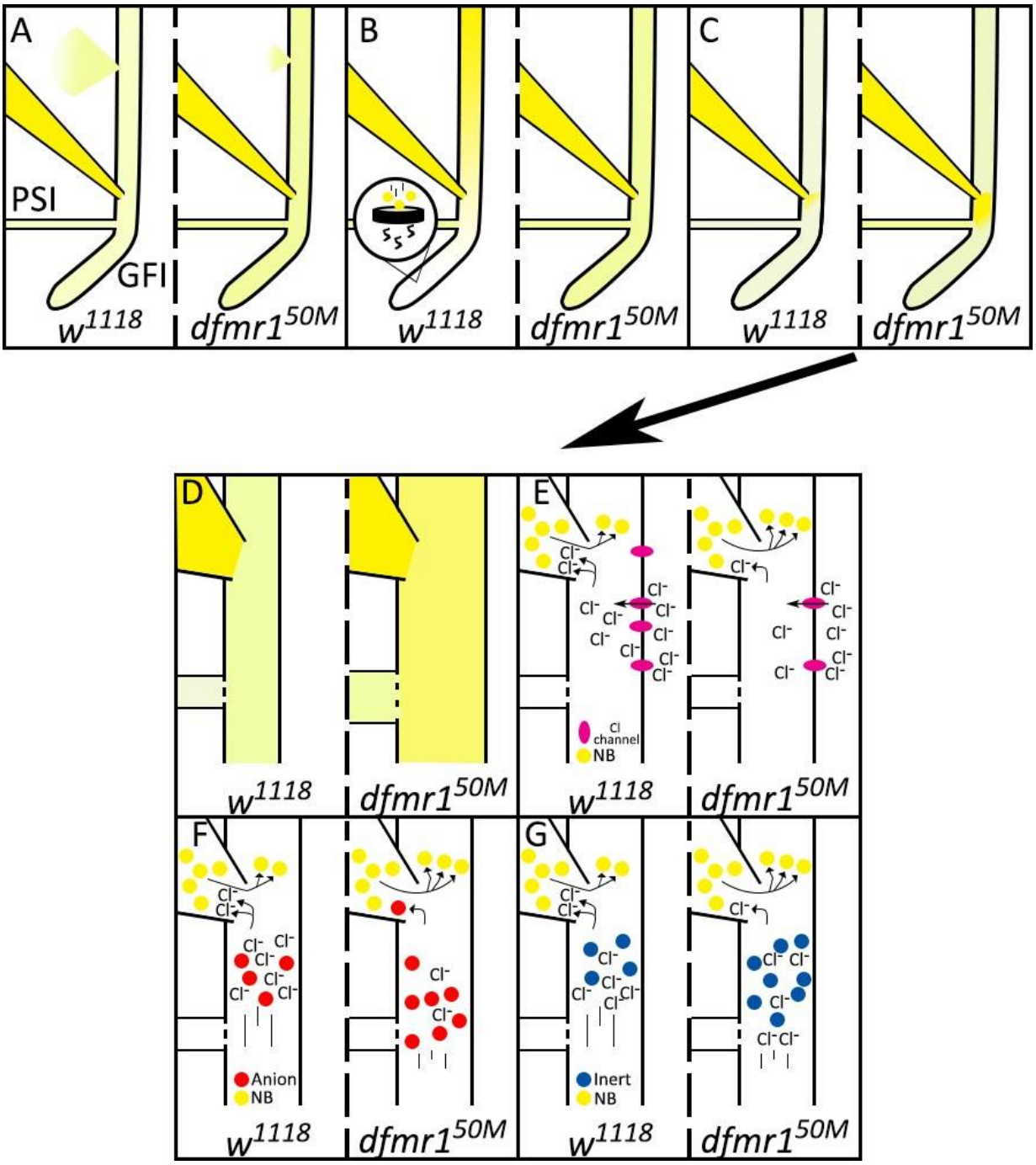

Figure 25. Potential Mechanisms of Differential Dye Loading

Many hypotheses for higher dye loading in mutants (*dfmr1*^{50M}) than controls (*w*^{1118}) were tested. ***A.*** Dye leaks faster from controls than mutants. ***B.*** The dye is destroyed or sequestered away from the axon in controls. ***C.*** More dye enters mutants than controls. After ***A*** and ***B*** were ruled out, a number of hypotheses were tested to explain possibility ***C.*** These included ***D.*** the mutant neurons are larger or better connected to downstream neurons. ***E.*** Ion channel conductivity is altered in the mutant, with fewer chloride channels as an example here. Lower anion flow would favor cation flow, increasing neurobiotin (NB) transfer. ***F.*** Average anion size is increased in mutants, favoring cation flow out of the electrode. ***G.*** Viscosity in mutant neurons is increased through a denser network of inert molecules. This would slow ion flow and favor ion exit from the electrode.

To discuss this hypothesis, it is necessary to describe the electrochemistry of dye injection. The work was conducted using two silver-chloride electrodes, one in the injection electrode and the other in the bath. When these electrodes are connected to an electrical source one becomes positively charged (cathode) and the other negatively charged (anode). This causes a reduction-oxidation reaction, with the silver oxidized at the cathode, allowing it bind negatively charged chloride ions (Cl^-), resulting in unpaired positively charged sodium (Na^+) ions ($Ag^0_{(S)} + Cl^{-1}_{(aq)} + Na^{+1}_{(aq)} \rightarrow AgCl_{(S)} + Na^{+1}_{(aq)} + e^-$). At the anode, this reaction happens in reverse ($e^- + Na^{+1}_{(aq)} + Cl^{-1}_{(aq)} + AgCl_{(S)} \rightarrow Ag^0_{(S)} + 2Cl^{-1}_{(aq)} + Na^{+1}_{(aq)}$), with the difference resolved as the ions migrate through the solution. For NB injection, the cathode was inserted in the GFI with the anode in the bath. For LY injection, the polarity of the electrodes was switched, making the GFI electrode an anode. Ions carry the charge between the electrodes and any impediment slows the ion flow, raising the resistance. Similarly, if ions are larger, and thus less mobile, resistance is also increased. When KAc was removed from the injection solution, the increased resistance of the circuit required a higher voltage to keep the current constant due to the loss of the small potassium ions. However, without potassium ions, NB carried more of the current, thus more moved into the neuron. The positive charge generated in the injection electrode is offset either by anions (such as Cl^{-1}) moving into the electrode or cations (including NB) moving out. Typically, a mix of the two occurs, but if, for example, anion movement toward the electrode were slowed, more cations would leave the electrode to compensate. Based on this logic, there were two possibilities for elevated dye loading in *dfmr1* null neurons: 1) a specific impediment to the ions is present, such as restricted flux across the neuronal membrane's channels (Fig. **25***E*), or 2) ion speed through the aqueous environment is restricted, because of increased friction (Fig. **25***F,G*). The bulk of my experiments tested the first option, as it was initially deemed more likely and had more ties to FMRP loss. However, the data, as described below, seems to better support the second option.

I first applied a potassium channel blocker (4-AP) to determine whether potassium flow affects dye loading. The drug reduced dye loading in both genotypes, albeit with maintained higher dye transfer

in *dfmr1* mutants. This suggested potassium flow plays a role in dye loading. However, follow-up experiments with 4-AP applied after the dye injection caused the same result of lowering dye transfer, suggesting 4-AP interferes with a separate process. 4-AP contains a primary amine group, the target of formaldehyde fixation, which could reduce the amount of NB covalently linked to the tissue (Thavarajah et al., 2012). However, attempts to test this hypothesis, such as washing out 4-AP extensively before fixing or using longer fix times, were unsuccessful in preventing this effect. The potassium channel blocker TEA also reduced dye transfer across genotypes; however, rinsing prior to fixing corrected this effect, and the drug showed no overall effect on either genotype. Importantly, TEA does not contain a primary amine and it is unclear how it interferes with the dye signal. Together, these studies suggest potassium channels are not related to the phenotype, despite extensive interactions with FMRP (Brown et al., 2010; Strumbos et al., 2010; Lee et al., 2011). Consistently, both endogenous potassium channels (Shaker cognate w (Shaw), and Inwardly rectifying potassium channel 2 (Irk2)) and exogenous cation-permeable ChR also had no impact on the *dfmr1* phenotype. However, it was not possible to test how effective any of these manipulations were on decreasing or increasing potassium flow, thus the channel hypothesis cannot be fully ruled out.

Restricted anion flow across the neuronal membrane could also increase *dfmr1* mutant dye loading, as it would increase the flow of cations out of the electrode through increased resistance. In unpublished experiments, I attempted to modify the flow of the primary neuronal cation, chloride, across the plasma membrane through various methods including replacing chloride with larger, less mobile anions such as acetate, propionate or iodine, or applying the chloride channel blocker 9-Anthracenecarboxylic acid (9-AC, Estévez et al., 2003; Ugarte et al., 2005). Replacing chloride with the larger acetate ion increased dye loading in both genotypes, suggesting a role for ion mobility. A mechanism similar to the removal of KAc may be at play here, where loss of the small chloride anion increases average anion size, making it harder for anions to flow and favoring cationic NB leaving the

electrode. However, contradicting this, replacing chloride with even larger anions, such as iodine or propionate, caused both genotypes to have significantly lower dye transfer. None of these experiments corrected the phenotype, with persistent increased dye loading of *dfmr1* nulls relative to controls. Attempts to block chloride channels using 9-AC, also failed to correct the defect, and were similar to 4-AP results with decreased loading. All of these experiments were preliminary and should be revisited to confirm the results. As with the potassium channel work, it was not possible to confirm these manipulations were having intended effects. There is very little literature suggesting 9-AC works well in fly neurons, and nothing to suggest how many chloride channel classes it blocks (Overall and Jaffe, 1985; Ugarte et al., 2005). For chloride replacement experiments, significant chloride likely remains in the system from the local tissue concentrations, which may be sufficient to maintain normal chloride flow across the plasma membrane.

The above experiments examined specific classes of ion channels, despite the fact that any combination of them could be involved in the *dfmr1* phenotype. In order to non-specifically test the entire membrane for a role in regulating ion flow, I designed two experiments. The first was application of Gramicidin, a bacterial pore-forming peptide mix often used as an antibiotic (Andersen et al., 2005). Gramicidin opens up pores in membranes allowing free flow of monovalent cationic ions. The intent was to create new pores in the GFI membrane and equalize cation flow through the membrane to revert the *dfmr1* phenotype, bypassing individual studies on sodium or potassium channels. This experiment is similar in concept to the ChR experiment, which was included in the published work. Unfortunately, Gramicidin was poorly soluble and it was unclear whether it had any effect on the GFI. Similar to 4-AP, total dye transfer was reduced by Gramicidin, but the relatively elevated dye iontophoresis phenotype in *dfmr1* mutants remained intact. The second manipulation was to insert the ground electrode into the GFI itself, near the dye injection electrode. This also did not correct the *dfmr1* phenotype, despite presumably bypassing the membrane completely. This experiment suggests the membrane does not play a role in the

dfmr1 defect, and that the source of the dye transfer phenotype is completely cytosolic. Aside from these experiments, another complication for the channel hypothesis is that the anionic dye LY, also displays the same *dfmr1* null phenotype. If anion flow were impaired in *dfmr1* nulls, then the LY dye should have trouble getting out of the electrode, as the local neuronal anions need to be displaced out of the cell. One could make the argument that both anion and cation flow into the cell is reduced in *dfmr1* null mutants, but this would require two separate channel defects, or one channel responsible for the movement of both types of ion, which is not supported by any of the above evidence.

The experiments listed above ruled out a wide range of physical properties that could be causing elevated dye loading in *dfmr1* mutants, including neuron size and connectivity. The process of elimination therefore suggests that altered ionic mobility is responsible (Fig. **25***F, G*). As noted, some of the above experiments are not wholly conclusive; however, based on the accumulated data, I believe the best route to pursue the differential dye loading mechanism would be to study whether ion mobility though the cytoplasm is responsible. Ion size could be tested by preloading large anions such as LY into the GFI, followed by a normal NB injection. If the presence of a large anion increases NB loading, this would suggest cytosolic ion size impacts dye loading (Fig. **25***F*). Similar experiments could be performed by modifying the amount of ionic proteins within the GFI using the Gal4/UAS system. If the hypothesis is correct, overexpression of negatively charged cytosolic proteins should lead to increases in NB loading. The next step would be to identify the large ions that have increased in concentration in the *dfmr1* nulls. Proteins are the obvious culprit, but it isn't clear that proteins are generally overexpressed in the *Drosophila* FXS model. It was suggested in my paper that the increased protein levels seen in *dfmr1*

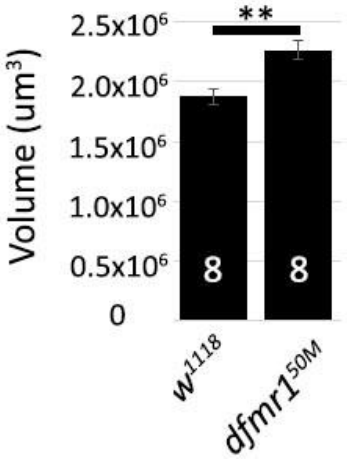

Figure 26. Brain Size is Increased in *dfmr1*^{50M} Animals
Quantification of brain size by whole-brain confocal imaging shows *dfmr1*^{50M} causes approximately a 20% increase in tissue volume.

nulls could be the cause of the dye loading phenotype; however, further experiments showed that while *dfmr1* nulls do indeed have increased protein over controls, their brains are also larger, at about the proportion seen for the protein increase: ~20% (Fig. **26**). This suggests that protein concentration in neurons between the genotypes may be equivalent, but the tissue size is different, indicating increased protein concentration is not at fault. Metabolites are another potential source of large ions. Metabolic screening has become an advanced field in recent years and these techniques could be used to identify differentiated product levels in the neuronal cytosol, which could then be traced back to an FMRP pathway (Zampieri et al., 2017).

Another means of slowing ion movement could be increasing cytosolic viscosity (Fig. **25***G*). This is an attractive solution to the differential dye transfer mechanism as it provides a simple answer to the observation that both NB and LY are impacted. Viscosity would be non-specific to ionic charge, and thus provides a parsimonious answer to how NB and LY are both impacted. To test for a viscosity role, I injected LY into droplets of saline containing increasing concentrations of sucrose, and thus higher viscosities. I live-imaged the process and quantified dye loading over one minute. The results show more viscous solutions take up more dye, supporting the hypothesis that ion mobility in the receiving solution impacts dye loading (Fig. **27**). This work could be expanded by performing Fluorescent Recovery After Photobleaching (FRAP) experiments, monitoring GFP diffusion in GFI neurons to determine if controls and *dfmr1* nulls alter protein mobility (Day et al., 2012). Longer recovery times would indicate slowed GFP diffusion. Were this the case, it would be necessary to identify the cause for the altered mobility. Cytoskeletal and macromolecular structures are known to play roles in cytosol viscosity, and would be good targets for the next step in this research (Luby-Phelps, 1999; Yu et al., 2017). Interestingly, links between FMRP and the microtubule stabilizing protein MAP1B/Futsch are well established, with FMRP loss causing increased MAP1B/Futsch expression (Zhang et al., 2001; Zalfa et al., 2003; Lu et al., 2004).

Increased cytosolic viscosity would have serious implications for any cell, as they are highly dependent on directed resource transport and diffusion of secondary messengers and metabolites (Periasamy et al.,

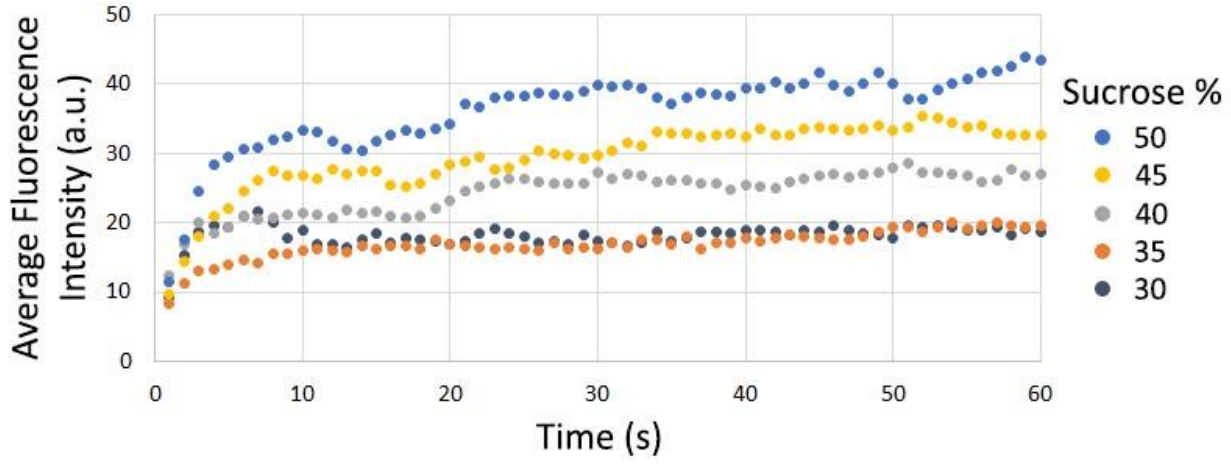

Figure 27. LY Dye Loading into Sucrose Droplets
Injected LY signal was measured over time in saline droplets with increasing concentrations of sucrose. The results suggest higher viscosity leads to higher dye transfer from the glass electrode into the saline. Each point represents the average of at least 9 experiments.

1992; Verkman, 2002). If these processes are slowed due to increased viscosity in *dfmr1* null neurons, there would be significant disruptions to their development and function, potentially explaining some FXS symptoms.

Before leaving this topic, it is worth acknowledging that the *dfmr1*^{50M} line used in this work contains background mutations not related to the target gene (*dfmr1*), as shown in Chapter 4. This raises the question of whether the dye injection phenotype was truly caused by FMRP loss in the first place. The published evidence, with trans-heterozygous null alleles for *dfmr1* and a *dfmr1* rescue experiment, strongly suggest FMRP is the culprit; however, no experiments were performed where the *dfmr1*^{50M} allele was not included. The recombination used to make the rescue line could theoretically have unintentionally removed a background mutation. If the dye transfer phenotype turned out to be caused by a background mutation, it would still be worthwhile to pursue, as it does seem that an important

neuronal property is being probed by the dye injection protocol. Should alternative alleles fail to replicate the results found here, a similar BSA-sequencing approach to that taken in Chapter 4 could be employed to identify the causative mutation behind the altered dye loading.

Circuit Mapping the Giant Fiber System

Studying the dye injection pattern of the GF circuit revealed an extensively dye-coupled neuron network. The GF circuit is likely reflective of most circuits in complex brains, where high degrees of interconnectivity permit communication with, and modification of, neighboring circuits (Arber, 2012; White et al., 2017; Kodama et al., 2018). The goal of my study was to identify single-neuron drivers for the newly identified members of the GF circuit, which could then be used for future research on electrical synapse formation and function. I was able to identify Gal4 drivers for four new neuron clusters within the GF circuit, creating a new toolkit (Kennedy and Broadie, 2018). In this section, I describe the remaining work in characterizing these neurons, and suggest questions they can be used to answer.

While the GFC neuron clusters are well defined in my work, the individual neuron structure is not yet resolved. GFC1 appears to have a simple morphology with defined axonal and dendritic regions, while GFC2 is more convoluted with apparently combined pre- and postsynaptic compartments. GFC3/4 seem more straightforward, though they both have a number of intertwining neurons that made it difficult to determine whether all neurons in the clusters share the same synaptic connections. GFC4 requires more defined drivers to better image and manipulate these neurons, which may be available already in the existing spGal4 driver collections. The best available strategy to image individual neurons within GFC clusters is MultiColor FlpOut (MCFO; Nern et al., 2015). MCFO is a gene cassette with a UAS sequence upstream of two Flippase (Flp) Recombination Targets (FRT) sites that flank a stop codon, and a downstream fluorophore sequence. Low Flp expression randomly causes the FRT sites and the stop codon to be removed, allowing fluorophore expression in subsets of Gal4 containing neurons. By combining the

GFC1-4 drivers with the MCFO cassette, single neurons within GFC clusters will be labeled, allowing their structure to be independently visualized.

Characterizing the individual neurons in the GFC clusters would give more information on the nervous system regions each neuron projects to, and thus suggest potential synaptic targets. However, in order to identify the actual targets of these neurons, other connectivity tracing tools are also required. The recently released *trans*-Tango transgenic system would be ideal for this purpose (Talay et al., 2017). *Trans*-Tango uses several genetic elements to trigger expression of a fluorophore in cells downstream of a neuron of interest. A presynaptic protein localizes a transgenic ligand to the membrane, which, when in contact with a postsynaptic receptor, initiates RFP production in the downstream neuron (Talay et al., 2017). Revealing the structure of the GFC neurons' downstream targets would permit their identification in the same manner as was used for the GFC neurons themselves (Kennedy and Broadie, 2018). While this tool has performed well in others' hands, my attempts to use *trans*-Tango in the GF circuit have not been successful. Expression of the presynaptic component in the GFI and the postsynaptic components pan-neuronally did not reveal any of the known GFI targets, instead labeling numerous uncharacterized neurons. It is unclear why the tool was ineffective. One possibility is the protein used to presynaptically localize the tool, Nrx, does not normally exist in the GFI, and cannot be properly trafficked. Another possibility is that the pan-neuronal driver used does not express well in the GFI targets. While this seems unlikely, it has been reported that the pan-neuronal nSyb-Gal4 driver does not express in the GFI, suggesting GF neurons may differ from other neurons in some ways (Namiki et al., 2018). Regardless, this tool may still be effective in some of the GFC neurons and could help complete the GF circuit map and identify the role of the GFCs in the circuit by finding their targets.

The GFC target neurons likely control some aspect of *Drosophila* behavior and the next step after identifying these neurons is the identification of the muscles they control. One approach is to activate GFC neurons and assay behavioral outputs. My preliminary efforts at GFC stimulation via multiple ChR forms

were unsuccessful in eliciting behavior, suggesting these neurons may not have strong control over muscle movement, or require specific stimulation paradigms or coincident activation. A first approach to exploring the function of these neurons could be to stimulate them before, during or after GFI stimulation to test for a modified escape response. For example, one could activate GFC neurons prior to the GFI to see if this alters the strength of the jump response. Another approach would be to image GFC neuron responses via GCaMP calcium reporters while triggering the GFI with electrical or ChR stimulation to determine how these neurons respond to GF circuit activity (Nagel et al., 2003; Akerboom et al., 2012). Taking the response pattern and replicating it with direct GFC ChR stimulation could trigger their behavioral output. Alternatively, GFC neurons could be killed using UAS-*hid* apoptosis, and the GFI could be triggered to test if any aspects of the behavior are diminished or enhanced (Kennedy and Broadie, 2018). Another approach to characterizing GFC roles would be to identify their neurotransmitters. The primary excitatory neurotransmitter in *Drosophila* CNS is acetylcholine (ACh), in contrast to glutamate in vertebrates (Yasuyama and Salvaterra, 1999; Liu and Wilson, 2013). If these neurons use ACh they may function as excitatory interneurons, while glutamate would suggest they act as motor neurons. GABA would suggest roles in silencing other neurons, and modulatory neurotransmitters such as dopamine, would imply functions that adjust responsiveness in their targets (Kim et al., 2017). Staining the brains for the enzymatic producers of these neurotransmitters and examining the GFC somas could quickly reveal which neurotransmitters are expressed.

These newly identified neurons could also be used to study GF circuit development. Circuit stabilization is believed to be mediated trans-synaptically, with synaptic activity maintaining neuronal connections (Luo and O'Leary, 2005; Pielage et al., 2008). Curiously, my work showed loss of only 1 out of the 6 GFI targets was sufficient for a GFI to retract and presumably die. Loss of the GFI often caused the GCI to be lost or disconnected as well, despite numerous known GCI partners (Mu et al., 2014). This is in contrast to NMJ retraction studies where the neuron only has one target and it is reasonable to expect

retraction when that target is lost (Valakh et al., 2012). It was not confirmed that GFI or GFC were killed, only that they lost dye coupling (Phelan et al., 2008). Future experiments using GFI/GCI GFP expression could test for neuronal survival. Regardless, this work suggests a single neuronal partner can control GFI fate, or that all members of a circuit must be present for a central neuron to maintain itself. Follow up experiments could test how the GFI responds to the loss of GFC2-4, the TTMn and the PSI. It would also be appropriate to determine when the GFI retracts. If this occurred during development it would suggest an anchoring mechanism was at play, while adulthood retraction could suggest an activity-based mechanism. An RNAi screen could come from this work, with candidate genes knocked down in GFC1 or the GFI to determine the proteins used in neuronal maintenance and identify new players in this process. I also found that the GFI can compensate for a lost partner by contralateral extension of an axonal bend but there is little research on the molecules involved in such compensation (Neuhaus-Follini and Bashaw, 2015). A complementary candidate screen could be designed to identify the molecular players in this compensation process.

Another interesting use of these neurons would be a proteomic screen for molecules used in target recognition during circuit formation. Now that six separate GFI targets are known, it may be possible to isolate the proteins used for partner recognition. One way to go about this would be to label the GFI and a specific partner with red and green fluorophore, respectively, and then track when these two neurons first contact. At this timepoint, synaptosomes could be isolated and FACs sorted for particles containing both fluorophores. The synaptosomes should contain both pre- and postsynaptic membranes as they generally adhere during the extraction (Luquet et al., 2017). The synaptosomes could then be analyzed via mass-spectrometry to identify the proteins contained in their membranes at this time point (Schreiner et al., 2017). By repeating this process with each of the six GFI partners, a comparative approach could be taken to identify the code used for each targeting event. If differences are seen, fluorescently tagged versions of the proteins could be introduced into the GFI to determine whether these

proteins indeed localize specifically to one partner's synaptic zone. For example, if the GFI used different target recognition proteins for the PSI and TTMn, one would expect those proteins to localize specifically to the IB or GFI bend during target recognition, respectively. Using these neurons for comparative research on neural circuit development and function should prove fruitful in determining the range of molecules different neurons use to accomplish different tasks.

Identification of Background Mutations in the *dfmr1*^{50M} Line

Genetic background is notoriously difficult to control, even in inbred lab strains, which can lead to a misinterpretation of research findings (Bailey, 1982; Gerlai, 1996). In *Drosophila*, lines are usually recombined and rebalanced many times throughout experimental work, bringing in new SNPs, deletions and rearrangements (Platts et al., 2009). While most background changes have no impact on the phenotype under study, it is critical to employ the proper controls and ensure this is the case. This means using multiple mutant alleles, verifying results with alternate knockdown methods (such as RNAi), and performing genetic rescue experiments (Chandler et al., 2013). Constant outcrossing with a control line can remove most background mutations but this is extremely time consuming and usually impractical, especially when working with many different genetic tools as is common in *Drosophila*. Another pernicious possibility is that the phenotype under study comes from the control line rather than the mutant. Using multiple alleles for the mutant will not be able to identify this problem, as they will incorrectly reinforce that a mutant phenotype exists. This problem requires using alternate control lines (such as Oregon-R or Canton-S as alternatives for w^{1118}) or wild-caught strains (Spencer et al., 2003; Yuan et al., 2006). These strategies should be implemented early to ensure a study is not following non-specific mutations and wasting valuable time and resources.

In my study on GF circuit synaptogenesis, late implementation of these controls caused a significant delay in work and many incorrect assumptions that changed the course of my research. It is

worth noting that the mutation I identified appeared to be present in only one of the *dfmr1*^{50M} lines our lab maintains. Unfortunately, I did not have a chance to test the *dfmr1*^{50M} line that is stored in the *Drosophila* Bloomington stock center, so I cannot be sure whether this mutation is being used by the greater FXS community or arose through an event in our lab. It is important to make this distinction so researchers can decide whether they should reevaluate some of the *dfmr1* phenotypes they have characterized (Pan et al., 2004; Tessier and Broadie, 2008; Yao et al., 2011; Liu et al., 2012; Coyne et al., 2015; Doll and Broadie, 2015; Novak et al., 2015). Regardless of whether this particular mutation is in other stocks, my work shows that it is possible for non-specific mutations to crop up unexpectedly in any *Drosophila* line and confound results. In this unfortunate circumstance, it may still be worth pursuing the unknown mutation causing the interesting phenotype. Sequencing has become cheap enough that most labs can afford to pursue the BSA-WGS approach taken in Chapter 4 (Shendure et al., 2017). Phenotypes that are correlated with novel genes and mutations can be cross referenced with large patient databases, such as BioVU, to help identify new links to genetic disorders (Roden et al., 2008). In some instances, there may even be benefits to the original field of study. As noted earlier, FXS may be exacerbated by background mutations that have not been identified yet. If some of the phenotypic variability in FXS models comes from background mutations that interact with FMRP, it should be possible to identify those genes, and potentially target them pharmacologically in FXS patients to correct aspects of the disorder.

Unfortunately, the identity and properties of the *dfmr1*^{50M} background mutation(s) was not determined in time to include in this dissertation. If the mutation can be successfully identified by BSA-WGS there are a number of follow-up experiments that will be informative. This research focused solely on synaptic outgrowths from the GFI axon bends; however, there did seem to be excessive growth at the IB as well. While this wasn't subjected to any formal analysis, due to the complexity of these outgrowths, the IB region would be worth examining if this project is continued. Synaptic overgrowth in a second GFI region would mean this phenotype is not specific to one set of synapses but affects multiple presynaptic

regions. From here, the extent of this phenotype throughout the nervous system should be evaluated. Is this a GFI-specific effect or is it universal that alterations to the protein cause hyper-connectivity? Interestingly, early in my graduate work I studied the GFI dendrites extensively for synaptic overgrowth and found evidence that *dfmr1*^{50M} caused overgrowth there as well (Fig. **28**). This suggests other synaptic partners are also subject to the mutation's effects. The dendritic arbor is much more complex and variable than the axonal bends however, and I pursued the axon phenotype due to simpler quantification.

Many other experiments remain for the characterization of these background mutations. The upcoming work involves confirming that this protein is the true cause of the synaptic overgrowth phenotype. This will involve studying the identified mutation in isolation to confirm the phenotype. Ideally such mutations already exist in the *Drosophila* stock centers, but new lines may have to be generated through CRISPR if not (Port et al., 2014). A rescue experiment is also required to attempt to correct the phenotype in *dfmr*^{50M} by expressing a functional version of the protein at appropriate levels. There also remains the possibility that the phenotype arises from multiple mutations working additively or synergistically (Pérez-Pérez et al., 2009). If this is the case, each of the mutations will have to be tested on their own and in combination to study how they interact. The mechanisms underlying these proteins' abilities to modify the localization of synaptic connections also requires a much deeper level of study. The localization of this protein throughout development should be tracked using CRISPR inserted fluorophore tags (Baena-Lopez et al., 2013).

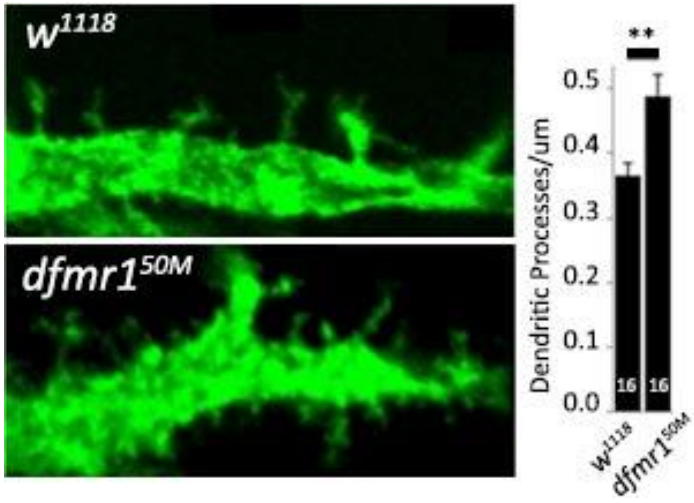

Figure 28. *dfmr1*^{50M} Causes Overgrowth in Dendrites
GFP was expressed in the GFI dendrites via the 91H05-Gal4 driver. Quantification of processes extending from the main branches showed a significant increase in the mutant over the control.

Further characterization could come from domain manipulation experiments, wherein versions of the protein with various regions removed are reintroduced into the mutant background to determine which segments are important for the protein's function (Kudumala et al., 2013). This approach could answer whether the mutation is causing inappropriate interactions through extracellular domains or altered signaling through intercellular domains.

Further Experiments Not Included in Publications

Two additional projects were undertaken during my dissertation work, which were not completed due to problems of feasibility, lack of time, or discouraging results. I will use this section to detail those experiments in the hopes that they may provide a starting point for others interested in similar work.

Western Blot Screen for FMRP Targets

One of my most ambitious projects was an attempt to use a Western blot (WB) screen to identify which proteins are misregulated in the FXS disease model. I began by cross-referencing a list of ~900 presumptive FMRP targets generated from a mouse high-throughput sequencing of RNA isolated by crosslinking immunoprecipitation (HITS-CLIP) experiment with lists of ASD and intellectual disability risk genes (Darnell et al., 2011; De Rubeis et al., 2014; Iossifov et al., 2014). I determined the *Drosophila* homologs for the overlapping genes and attempted to collect all available antibodies for these proteins that had been generated in laboratories around the world. There were 205 genes of interest, of which 170 had *Drosophila* homologs. Of these, I was able to obtain 46 antibodies (Table **4**). In addition, I included another 36 neuronal antibodies already available in our lab (Table **5**). The proteins on this second list were either FMRP targets, but not on the ASD/intellectual disability lists, or were tested to try and identify developmental pathways that are disrupted by FMRP loss. I worked with a laboratory technician, Ryan Moore, to compare the protein levels in controls and *dfmr1*^{50M} animals to identify highly misregulated

targets. Protein changes were tested in the head at three different time points: the early (tan) pupae stage (25-60 hours pupation), the late (dark) pupae stage (60-90 hours pupation) and adult. The goal was to identify proteins transiently misregulated in development as well as adult stages (Tessier and Broadie, 2012).

A	CaMKII	Dcr-2	Her	Kug	Nej	Nlg3	Nrv2	Pink1	RhoGEF2	Spg	Trio
Als2	Csw	Galphao	Ih	Lap	Nf1	Nlg4	Nrv3	PlexA	RyR	Sti	X11L
Ank2	Cv-c	Gek	Itp-r83a	Lar	Nlg1	Nmdar2	Nrx-1	PlexB	Sbf	Syt7	
Calx	Dcr-1	Gig	Kis	Ndae1	Nlg2	Nrv1	Pat	Pten	Sick	Tor	

Table 4. Known FMRP Targets for Western Blot Screen
These targets were selected from a cross-referenced list between human FMRP targets and known autism/ intellectual disability associated genes. This final list of *Drosophila* homologs contains those targets for which an antibody was available.

a-Spec	Ato	Cher	Dlg	Foxo	Jim	MMP1	Nr2	Rhea	Scar	Stau	Timp
Arm	Bap	Cora	Fas	Gro	Ken	MMP2	Nrg	Rho1	Shot	Syn	Toy
Atf-2	Cf2	Cut	Fas2	Hts	Lilli	Nr1	Pum	Scar	Stan	Tgo	Zif

Table 5. Alternative Neuronal Targets Tested in FMRP Western Blot Screen
These targets were selected due to their importance in neuronal development and function as well as the accessibility of the antibodies. Some of these proteins are FMRP targets but were not identified in ASD/intellectual disability gene lists. The remaining targets were expected to help identify the pathways disrupted by FMRP loss.

This project unfortunately suffered several setbacks and did not result in high quality targets. One major shortcoming of this work was difficulties with protein extraction. Many WB protein extraction protocols exist, but they are typically specific to the species, tissue and protein of interest, requiring optimization for each new experiment. For example, membrane proteins are notoriously difficult to extract and maintain in solution and typically require different extraction protocols from cytosolic proteins (MacPhee, 2010). Unfortunately, during a screen, fully accommodating such specific requirements is not possible, and a generic protocol must be applied due to time limitations. The extraction method used for this screen, an LDS buffer combined with mechanical grinding, was chosen because it provided a relatively

swift protocol with some ability to extract and stabilize membrane proteins. While this method showed strong yield during preparation for this project, I did not explore how reliable the extraction process was before beginning the screen. During follow up work on favorable targets, I used more rigorous controls and found that the technique had been giving highly variable extraction efficiencies, even for cytosolic proteins. This unexpected source of variability made it impossible to trust the data from the screen as differences in protein levels could either be due to differences in FMRP regulation or inefficient extractions. I designed a more effective extraction protocol for later work, testing multiple extraction buffers and cell disruption methods to maximize reproducibility. Interestingly, even using the best protocol I could design based on the literature and available equipment (RIPA buffer and ultrasonic sonicator), I still found replicates could be twice the value of other samples in the set. Such results suggest that WB variability is too large to detect moderate protein changes and may only be appropriate for quantifying much larger shifts.

There were other protocol issues in this work that should have been worked out prior to implementation. Protein quantification was performed by radiometric quantitation of fluorescent signal (measuring the net fluorescent signal coming from each band). This signal is linear over certain ranges but becomes non-linear at low or high levels of protein. It is important to ensure that signal is within the linear range when performing quantification experiments to ensure measurements are correct (e.g. a doubling of loaded protein should cause a doubling of signal). This requires performing a calibration curve with each antibody to determine the appropriate analysis range. Again, this would have been too much work for all of the antibodies in this screen, but a rough approximation of proper loading levels could have been performed for high and low level targets in order to avoid the extreme regions of signal loss. An issue at the intersection of extraction efficiency and linear range is loading controls. The loading control is a protein in the sample which is not expected to be affected by the treatment, typically a housekeeping gene. Measuring the level of this protein can indicate whether the extraction efficiency and total protein

loaded onto a gel is equivalent between conditions. If not, the samples can be corrected against the loading control to make them comparable. Alpha-tubulin is a commonly chosen loading control, especially in FXS models as it is believed not to be regulated by FMRP (Zhang et al., 2001). However, alpha-tubulin is a highly abundant protein and is typically saturated at the loading levels required for most other proteins. Using a protein with saturated signal to correct the loading of other proteins is ineffective, as altered levels of extraction or loading will not be faithfully reported by the control. I believe use of tubulin here to normalize signal masked the variable protein extraction efficiencies and was not appropriate for this work. Tests should have been done to determine if tubulin was in the linear range, and if not, a separate, less abundant loading control should have been chosen. The difficulty with this is the long reach of FMRP's regulation. Few proteins have been proven not to be affected by FMRP loss, so finding an appropriate loading control requires a significant investment of work. For later WBs, I switched to total protein quantification assays, namely the Bicinchoninic Acid (BCA) assay, to confirm the same amount of protein was extracted between experiments (Walker, 1996). I also began using reversible general protein staining assays, such as MemCode, to measure total protein loaded onto the gel, avoiding the complications of a single loading control (Antharavally et al., 2004). However, neither of these techniques can correct for incomplete liberation, solubilization or depolymerization that can lead to individual proteins not fully extracting into the buffer.

Another issue I routinely encountered was the non-specificity of published antibodies. Many of the antibodies I received had not been rigorously tested to confirm the labeled bands were indeed due to the protein of interest rather than an off-target protein. Often, they had been designed for tissues other than the brain meaning neural isoforms and non-specific targets had not been studied or reported. It was frequently unclear whether bands outside of predicted sizes were alternate isoforms, functionally modified proteins or non-specific targets (Brion et al., 1991). There were often very dim bands at the

expected size and very bright bands at unexpected sizes, making it unclear whether we had successfully extracted the target or were even quantifying the correct protein.

Finally, after this work was complete, I discovered the *dfmr1*^{50M} brain is larger than the *w*^{1118} control, a complicating factor for the WB screen results (Fig. **26**). Since I was looking for major shifts in target abundance, I had instituted a 25% cutoff for follow-up experiments, making the brain size less of an issue. This effect could still act additively to make a change in protein level look higher than it truly is and bring it above the threshold, or mask a drop in protein. The change in brain size deserves a deeper investigation as it is unclear where the extra volume comes from. Increases in overall cell number or size should be easy to correct for; however, if the increase is due to subpopulations of cells, such as glia or dopaminergic neurons or retention of metabolites or water, this could make the data more difficult to appropriately normalize.

Despite all of these limitations, several highly altered proteins were identified by this WB screen, although most came from off-target bands. The strongest changes were all off-target proteins seen in antibodies against Corkscrew (Csw), Gigas (Gig), Phosphatase and Tensin Homolog (Pten) and Bagpipe (Bap). Csw showed two off-target bands at 250kDa and 160kDa, which were, respectively, 125% and 309% of control on average. Csw also had two bands at predicted sizes that showed significant elevation of protein levels (Flybase). The 100kDa band was approximately 183% of control, while the 75kDa band was 157% of control (Fig. **29**). The on-target Csw result was an exciting finding since gain of function (GOF) mutations in the human Csw homolog (PTPN11) result in

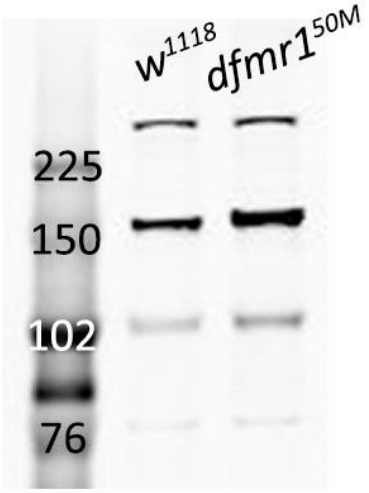

Figure 29. Csw Western Blot
The blot demonstrates two off target bands at 250 and 160 kDa, as well as two bands that match predicted protein sizes of ~100 and ~75kDa. Signal is increased for all four proteins in the *dfmr1*^{50M} line. Each lane contains two brains.

Noonan syndrome, a heritable condition with some similarities to the FXS disease state, including reports of ASD and mild to occasionally severe intellectual and learning deficits (Ghaziuddin et al., 1994; Lee et al., 2005; Sinkey and Odibo, 2017). Unfortunately, rigorous testing of the FMRP-Csw association using improved extraction and quantification methods at multiple timepoints eventually showed the increase in Csw protein was due to extraction variability and the enlarged *dfmr1*^{50M} brain (this was not the case for the off-target bands which still showed significant increases). While there may be overlapping and interacting pathways between Csw and FMRP that are responsible for the similar natures of Noonan syndrome and FXS, I felt the evidence for a direct FMRP-Csw interaction was too slim to pursue. I initially hoped to follow up on the off-target bands of Csw, Gig, Pten and Bap, but the only way to do so was through proteomic mass-spectroscopy methods. This would have required a significant resource investment and large amounts of the antibodies to immunoprecipitate the unknown targets, which we lacked. While these targets remain of great interest, some hesitation in pursuing them exists due to the finding that the *dfmr1*^{50M} allele, with which this work was performed, has background mutations. Alternate null alleles must be tested before these targets are pursued further.

Though there were a number of qualms about these data, the overall results suggested most presumptive FMRP targets are not significantly disrupted in the FXS disease model, consistent with published FMRP proteomic work (Table **6;** Zhang et al., 2004, 2005; Monzo et al., 2010). This indicates that protein misregulation is on a small scale (50% or less), which is perhaps not a surprising result from the loss of one translational regulator. However, this interpretation must be viewed with some skepticism based on the issues with sample preparation and analysis noted above. There were several cases where proteins showed large changes in expression and low variability (Table **6**). These were reanalyzed, but only the targets mentioned above were consistent in altered expression. Unfortunately, the overall results of these experiment were too variable to pursue or publish, and this large body of work was therefore abandoned.

Protein	Size (Kda)	Tan Pupae	Rel Std Dev	Dark Pupae	Rel Std Dev	Adult	Rel Std Dev
A	150	105%	9%	104%	27%	104%	3%
a-Spec	278	95%	7%	104%	25%	89%	12%
Als2	166	120%	88%	104%	18%	103%	18%
Ank2	450	117%	69%	93%	22%	116%	25%
Arm	110	138%	4%	94%	15%	77%	19%
Atf-2	50	83%	12%	146%	14%	121%	3%
Ato	34	99%	21%	127%	13%	125%	23%
Bap	42	102%	13%	113%	21%	119%	16%
Calx	110	152%	34%	165%	69%	108%	87%
Cf2	70	89%	12%	103%	35%	152%	7%
	60	107%	8%	93%	78%	111%	6%
Cher	240	114%	26%	138%	30%	107%	37%
Cora	200	111%	12%	124%	13%	121%	19%
Csw	100	126%	11%	102%	23%	183%	3%
	74	33%	11%	126%	13%	157%	12%
Cut	250	176%	13%	97%	18%	104%	14%
Cv-c	150	155%	2%	134%	5%	117%	2%
Dcr-1	250	97%	5%	76%	26%	92%	14%
Dcr-2	198	183%	58%	91%	27%	165%	47%
Dlg	140	71%	6%	97%	20%	101%	54%
	130	92%	6%	108%	12%	109%	2%
	120	x	x	152%	1%	131%	14%
	110	91%	0%	114%	9%	82%	30%
Fas	57	105%	3%	111%	2%	125%	0%
Fas2	90	112%	32%	102%	27%	97%	24%
Galphao	38	84%	34%	131%	35%	118%	17%
Gek	188	86%	31%	101%	17%	100%	18%
Gro	80	119%	31%	126%	16%	66%	10%
Her	34	x	x	83%	44%	102%	37%
	57	97%	131%	120%	11%	111%	125%
	57	123%	11%	144%	6%	113%	1%
	57	86%	12%	118%	39%	127%	2%
	60	x	x	30%	60%	68%	36%
	57	120%	4%	265%	37%	145%	2%
	60	x	x	131%	17%	101%	0%
Itp-r38a	318	100%	13%	165%	42%	98%	31%
	85	116%	25%	78%	20%	143%	10%
Kug	500	23%	141%	106%	11%	123%	24%
Lilli	250	73%	2%	114%	7%	77%	20%
MMP1	250	179%	15%	125%	12%	98%	9%
	50	152%	26%	129%	18%	172%	44%
Ndae1	105	94%	3%	112%	14%	134%	3%

Nej	341	113%	25%	66%	28%	69%	2%
Nf1	350	120%	27%	140%	45%	77%	76%
Nlg1	50-125	283%	45%	440%	70%	176%	7%
	150	125%	7%	103%	12%	141%	7%
Nlg2	136	67%	8%	111%	89%	216%	47%
Nmdar1	112	120%	29%	149%	1%	183%	28%
Nmdar1	130	x	x	113%	20%	149%	9%
	130	135%	42%	100%	25%	151%	34%
	130	x	x	105%	5%	96%	10%
Nrg	190	105%	10%	71%	44%	97%	63%
Nrx-1	150	85%	30%	78%	3%	124%	18%
Pat	225	101%	15%	117%	24%	101%	34%
PlexA	225	102%	30%	111%	1%	88%	51%
PlexB	150	103%	28%	114%	36%	135%	27%
Pum	200	94%	10%	141%	19%	55%	39%
Rho1	21	182%	36%	119%	8%	111%	19%
Scar	85	101%	5%	113%	12%	157%	14%
Shot	600	148%	3%	113%	24%	101%	12%
Spg	200	118%	3%	100%	4%	129%	11%
Stan	200	130%	31%	86%	17%	72%	8%
Sti	230	105%	27%	132%	21%	117%	13%
Syn	150	125%	55%	79%	16%	104%	31%
	70	218%	67%	118%	7%	116%	58%
Syt7	75	114%	16%	155%	14%	101%	6%
Tgo	72	152%	31%	124%	25%	115%	26%
Timp	28	76%	0%	135%	17%	121%	2%
Tor	281	104%	13%	105%	18%	106%	12%
Trio	257	68%	54%	63%	24%	95%	55%
	110	89%	103%	80%	13%	107%	29%
	70	70%	1%	89%	6%	115%	23%
X11L	120	106%	10%	113%	4%	102%	2%

Heat map for degree of change

> 200%	150% - 200%	125% - 150%	100% - 125%	100% - 80%	80% - 66%	66% - 50%	< 50%

Heat map for degree of RSD

0% - 15%	15% - 25%	> 25%

Table 6. Initial Results of FMRP Target Western Blot Screen.
This table represents the percent increase seen *dfmr1*^{50M} animals relative to *w*^{1118} controls for each protein listed. The first column gives the protein's name and the second gives the predicted size(s) of that protein, according to Flybase.org. Sizes or proteins not shown here did not produce a band on the blots. Sizes listed more than once are due to a second antibody being tested. Three timepoints were analyzed: light pupae, dark pupae and adult. An "x" indicates no band was seen at that timepoint. The percent increase or decrease is color coded based on the heat map at the bottom of the table to indicate the degree of change in the mutant relative to the control. Next

to the percent change is the relative standard deviation (RSD), which represents the standard deviation normalized to the degree of expression change. Higher RSDs indicate more variable data. These values are also color coded based on a heatmap at the bottom of the table. This table was generated by Ryan Moore and modified by Tyler Kennedy.

Neuron-Specific Protein Labeling

Another project I undertook during my research was the generation of tools to label proteins of interest at endogenous expression levels in subsets of neurons. Such tools are necessary for examining how neural proteins change expression over time or are altered in mutants. The current approaches for studying such questions have shortcomings that limit their applicability in some circumstances. Immunohistochemistry (IHC) staining with synaptic antibodies can be ineffective in the CNS due to the density of neurons or synaptic connections. The extensive signal often makes it impossible to tell if a protein is localized to a target neuron or its neighbor. Similarly, fluorophore tagged versions of endogenous proteins made by homologous recombination techniques such as CRISPR, often lead to a signal that is too dense to interpret. Examples such as ShakB labeling in the GFI are rare exceptions (Fig. **7**; Phelan et al., 1996). One common solution to this problem is expression of a tagged version of a protein of interest expressed via the Gal4/UAS system (Zhang et al., 2002; Christiansen et al., 2011). While this avoids competing signal from nearby neurons, protein properties can be misrepresented if the Gal4 driver causes higher than endogenous levels of protein expression. Common issues are mis-localization, aggregation and inappropriate protein-protein interactions (Christiansen et al., 2011; Chen et al., 2014). A recent solution to this limitation was provided with the STaR technique, wherein the genetic sequence for a protein of interest is followed by a stop codon which is followed by a fluorophore sequence (Fig. **21;** Chen et al., 2014). The stop codon is flanked by FRT sites, which can be removed by Flp through recombination (Chen et al., 2014). Thus, in neurons where Flp is expressed via Gal4/UAS, there is read-through to the GFP and a tagged version of the protein is produced from its endogenous promoter. This technique was used in Chapter 4. While this system is an extremely effective solution to the labeling

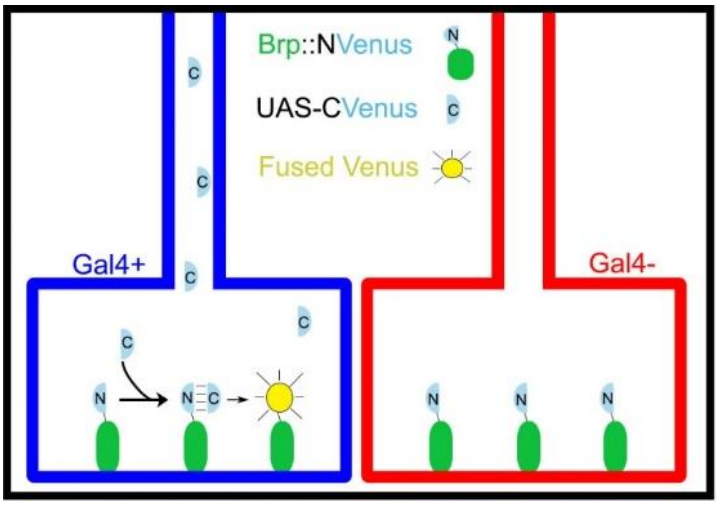

Figure 30. The GLEAM Technique for Cell-Specific Labeling of Endogenously Expressed Proteins
The GLEAM technique uses a split Venus protein, fusing the smaller, N-terminal half (NVenus) to the protein of interest, and expressing the larger C-terminal half (CVenus) cell-specifically with the Gal4/UAS system. The protein is only able to recombine and fluoresce when both halves are present, leading to fully functional Venus proteins only in Gal4 containing cells.

problem, two problems arose during my use of this approach. First, the recombination is a random process, and it is impossible to know when it happens. If one is trying to quantify the number of synapses in a neuron with STaR, there may be more variability than is tolerable due to the marker turning on at different times during development in animals from the same experiment. Second, once recombination has happened it is irreversible. If the Gal4 line used in an experiment turns on briefly in development and alters a progenitor cell, all of the offspring of that cell will have a labeled version of the protein, even if the Gal4 line is no longer active. This can cause excessive labeling in promiscuous Gal4 lines. This can be corrected for by using spGal4 lines to reduce the unintentional signal, but this solution has not been perfect in my hands either (Pfeiffer et al., 2010).

I therefore attempted to create two tools to solve these problems: Gal4 Limited Enchainment Activated Marker (GLEAM) and an RNA-editing technique based on the ER unfolded protein response (UPR). GLEAM takes advantage of a split fluorophore, Venus (a GFP variant) in this case, which can form a complete, functional protein if the two pieces encounter each other. The goal of this project was to tag an endogenous protein with the small half of Venus, using the lines from the Minos Mediated Integration Cassette (MiMIC) transgenic library, and express the large half of Venus cell-specifically using the Gal4/UAS system (Hudry et al., 2011; Venken et al., 2011; Li-Kroeger et al., 2018). The MiMIC library contains thousands of *Drosophila* lines, which have had a cassette randomly inserted into the genome,

often in introns. The cassette can easily be swapped out for any other cassette via plasmid injection and directed recombination (Rong and Golic, 2000). If the insertion is intronic, splice acceptors and donors can flank the cassette to ensure it is transcribed with the protein of interest. Thus, any gene that has an available MiMIC line can be quickly made to include the small Venus fragment (Venken et al., 2011). In the converted animals, all cells that normally express the protein of interest will produce the tagged form, while only those with Gal4 expression will contain the large half of Venus, and create a fluorescently labeled protein (Fig. **30**).

I attempted create this system using the presynaptic markers Synaptotagmin (Syt) and Bruchpilot (Brp; Perin et al., 1991; Wagh et al., 2006). The construct was not successfully inserted into Brp, but did lead to a tagged version of Syt, which I verified via PCR. However, after extensive testing of this line, I was unable to show a successful example of a fluorescent Syt::Venus protein. I believe this is likely due to the endogenous expression of Syt::Venus not creating very much overall fluorescent signal. Alongside the poor signal, the GFI bend, where I imaged these proteins, is very deep in the VNC tissue, likely obstructing much of the fluorescence. Unfortunately, I was not able to identify an antibody that could specifically recognize the recombined Venus to compensate for the issue of low expression. A published example of such an antibody did not work in my hands (Macpherson et al., 2015). Another issue is that the small Venus fragment was inserted into an intron, rather than the terminal end of the protein. This location may have buried the fragment within the protein, preventing it from encountering the cytosolic Venus half. In the meantime, another laboratory has been able to demonstrate that this technique works. Their tool, termed Native And Tissue specific Fluorescence (NATF), is reported to be an excellent marker for endogenous, cell-specific protein labeling (He et al., 2018b). This method used seven repeats of a short GFP fragment attached to the terminal end of the protein of interest, thus bolstering the signal and accessibility of the fragment.

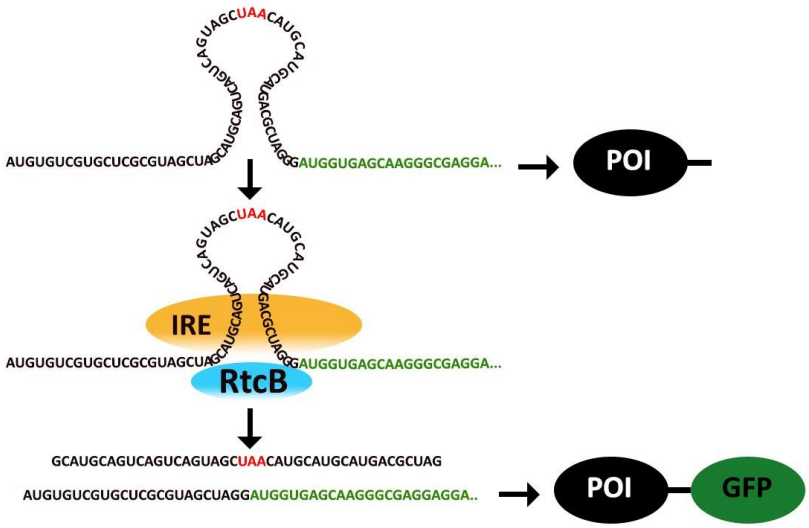

Figure 31. RNA Editing Mechanism to Cell-Specifically Label Proteins
In order to cell-specifically label a protein of interest (POI), the end of that protein's sequence would be modified to include a stop codon (red) in the middle of the XBP stem-loop target region, followed by the sequence for a tag, such as GFP (Green). Without any editing, the cell will produce the POI with a small extra domain on the end. When IRE and RtcB are cell-specifically expressed, the stem-loop is edited out, removing the stop codon and allowing readthrough to the GFP sequence.

My second cell-specific protein labeling technique was designed to manipulate the RNA of proteins of interest and avoid the difficulties of split GFP, such as lack of antibodies and dim signal. This approach took advantage of a set of proteins and RNAs involved in the metazoan UPR pathway, namely IRE, RtcB and XBP1. Normally in the ER, the IRE protein is kept in a monomeric state through attachment to HSPA5/BiP. When HSPA5/BiP detects a high accumulation of misfolded proteins, it releases from IRE, which then dimerizes. The dimerized form of IRE auto-phosphorylates and becomes catalytically active. IRE then excises 26 nucleotides from XBP1 mRNA. RtcB is required during this process to ligate the RNA back together (Kosmaczewski et al., 2014). This modified XBP1 mRNA can then be translated into a transcription factor that upregulates UPR genes to correct folding errors in the ER (Calfon et al., 2002). An approach coopting this pathway to monitor ER stress via GFP in the mouse has been published, and I built upon these findings for my project (Iwawaki et al., 2004). Due to the novelty of this approach in *Drosophila*, I attempted to optimize this technique in *Drosophila* S2 cell culture (Fig. **31**, Moraes et al., 2012). I used human versions of the proteins to avoid interfering with the endogenous *Drosophila* UPR, and only expressed the catalytic domain of IRE which should be able to dimerize and auto-phosphorylate without any outside signals

(Welihinda and Kaufmant, 1996). I was able to generate plasmids that expressed each component of interest in the S2 cells as well as a membrane protein, mCD8, with a stop codon flanked by the XBP1 edit sequences and a GFP transcript at the C terminus. Despite repeated attempts and optimizations of the XBP1 editing sequence, the expression of all of these pieces together in a S2 cell never led to the production of a GFP tagged version of mCD8. Expression of each protein was confirmed by antibody labeling, so It was not clear why the editing process did not proceed. Future work might require RT-PCR amplification of the target sequences to see how far along the enzymes were proceeding, so that the problematic step can be identified. While this tool has promise, the reactions involved are complicated and may not be robust enough to function in all circumstances. As an alternative to this approach, a recent report showed CRISPR machinery can be harnessed to an ADAR2 protein capable of swapping adenosine for inosine on RNA molecules (Cox et al., 2017). This CRISPR RNA editing system could provide a more straightforward method to edit transcripts. For example, a gene of interest could be modified to have a GFP sequence after a UAG stop codon. The CRISPR system could be expressed in the cells of interest with a targeting RNA aimed at the stop codon. This would result in A-to-I conversion, which is read by the ribosome as a G. Thus, the UAG stop codon becomes UGG (tryptophan), allowing the ribosome to read through to the GFP sequence. This would be a very powerful method, as the process would not affect the genome, thus circumventing several of the STaR drawbacks. This approach also opens up a greater range of labeling options than the GLEAM/NATF technique as any fluorophore or epitope tag, such as FLAG or V5 could be used, making multicolor and pulldown experiments feasible (Fan et al., 2008).

Conclusion

Overall, the GF circuit has proved a reliable model for studying neuron development and function. This is perhaps the only currently studied circuit in *Drosophila* where multiple connected neurons can be imaged in series and parallel at single-neuron resolution. Analysis at the cellular and molecular level is

made easy by the large size of these neurons (Power, 1948; Bacon and Strausfeld, 1986). Gal4 drivers and the similarly designed LexA drivers are available for multiple members of the circuit allowing different UAS/LexAop transgenics to be expressed in connected neurons (Pfeiffer et al., 2010; Tirian and Dickson, 2017). While not reported here, I performed electrophysiology recordings from the two muscles the GF circuit terminates on, the TTM and the DLM. The process is fairly simple, making activity recordings an accessible parameter of study (Gu and O'Dowd, 2007). Interestingly, the synapses leading to the TTM are all mixed electrical and ACh chemical synapses, with the exception of the NMJ, which is glutamatergic. In contrast, the DLM pathway has one synapse (PSI-DLMn) which is solely cholinergic. By measuring these two outputs separately, the impact of mutations on electrical or cholinergic synapses can be functionally evaluated (Mejia et al., 2013). Jump reflex assays were not pursued in this work, but they can be rapidly assayed with simple equipment, meaning these neurons can be studied from the molecular to the behavioral level (Martinez et al., 2007; de Vries and Clandinin, 2013; von Reyn et al., 2014). While it is unclear what the motor outputs of the GFCs are, once they have been identified, another behavioral assay may become linked to this circuit. There has even been some work suggesting activity dependent modulation of the GF circuit occurs, indicating habituation and potentiation can be studied in this collection of neurons (Engel and Wu, 1996; Engel et al., 2000). The expansive protocols and tools available for the GF circuit, make this an ideal model for studying how the brain assembles and operates in *Drosophila*.

References

Abrahams BS, Geschwind DH (2008) Advances in autism genetics: On the threshold of a new neurobiology. Nat Rev Genet.

Adinolfi S, Ramos A, Martin SR, Dal Piaz F, Pucci P, Bardoni B, Mandel JL, Pastore A (2003) The N-terminus of the fragile X mental retardation protein contains a novel domain involved in dimerization and RNA binding. Biochemistry.

Adzhubei IA, Schmidt S, Peshkin L, Ramensky VE, Gerasimova A, Bork P, Kondrashov AS, Sunyaev SR (2010) A method and server for predicting damaging missense mutations. Nat Methods.

Ahmad-Annuar A, Ciani L, Simeonidis I, Herreros J, Fredj N Ben, Rosso SB, Hall A, Brickley S, Salinas PC (2006) Signaling across the synapse: A role for Wnt and Dishevelled in presynaptic assembly and neurotransmitter release. J Cell Biol.

Akerboom J et al. (2012) Optimization of a GCaMP Calcium Indicator for Neural Activity Imaging. J Neurosci 32:13819–13840.

Akins MR, Berk-Rauch HE, Kwan KY, Mitchell ME, Shepard KA, Korsak LIT, Stackpole EE, Warner-Schmidt JL, Sestan N, Cameron HA, Fallon JR (2017) Axonal ribosomes and mRNAs associate with fragile X granules in adult rodent and human brains. Hum Mol Genet 0:1–18.

Akram MA, Nanda S, Maraver P, Armañanzas R, Ascoli GA (2018) An open repository for single-cell reconstructions of the brain forest. Sci Data 5:180006.

Aleksic J, Lazic R, Müller I, Russell SR, Adryan B (2009) Biases in Drosophila melanogaster protein trap screens. BMC Genomics.

Allen M, Shan X, Caruccio P, Froggett S, Moffat K, Murphey R (1999) Targeted Expression of Truncated Glued Disrupts Giant Fiber Synapse Formation in Drosophila. J Neurosci.

Allen MJ, Drummond JA, Moffat KG (1998) Development of the giant fiber neuron of Drosophila melanogaster. J Comp Neurol 397:519–531.

Allen MJ, Godenschwege TA, Tanouye MA, Phelan P (2006) Making an escape: development and function of the Drosophila giant fibre system. Semin Cell Dev Biol 17:31–41.

Alpatov R et al. (2014) A chromatin-dependent role of the fragile X mental retardation protein FMRP in the DNA damage response. Cell 157:869–881.

Ambrosi C, Gassmann O, Pranskevich JN, Boassa D, Smock A, Wang J, Dahl G, Steinem C, Sosinsky GE (2010) Pannexin1 and pannexin2 channels show quaternary similarities to connexons and different oligomerization numbers from each other. J Biol Chem.

Andersen OS, Koeppe RE, Roux B (2005) Gramicidin channels. IEEE Trans Nanobioscience.

Anderson BR, Chopra P, Suhl JA, Warren ST, Bassell GJ (2016) Identification of consensus binding sites clarifies FMRP binding determinants. Nucleic Acids Res.

Anderson P, Kedersha N (2006) RNA granules. J Cell Biol.

Ango F, di Cristo G, Higashiyama H, Bennett V, Wu P, Huang ZJ (2004) Ankyrin-based subcellular gradient of neurofascin, an immunoglobulin family protein, directs GABAergic innervation at purkinje axon initial segment. Cell 119:257–272.

Antar LN, Dictenberg JB, Plociniak M, Afroz R, Bassell GJ (2005) Localization of FMRP-associated mRNA granules and requirement of microtubules for activity-dependent trafficking in hippocampal neurons. Genes, Brain Behav.

Antar LN, Li C, Zhang H, Carroll RC, Bassell GJ (2006) Local functions for FMRP in axon growth cone motility and activity-dependent regulation of filopodia and spine synapses. Mol Cell Neurosci 32:37–48.

Antharavally BS, Carter B, Bell PA, Mallia AK (2004) A high-affinity reversible protein stain for Western blots. Anal Biochem.

Antonini A, Stryker MP (1993) Rapid remodeling of axonal arbors in the visual cortex. Science 260:1819–1821.

Arber S (2012) Motor Circuits in Action: Specification, Connectivity, and Function. Neuron.

Armijo-Weingart L, Gallo G (2017) It takes a village to raise a branch: Cellular mechanisms of the initiation of axon collateral branches. Mol Cell Neurosci.

Arnth-Jensen N, Jabaudon D, Scanziani M (2002) Cooperation between independent hippocampal synapses is controlled by glutamate uptake. Nat Neurosci.

Ascano M, Mukherjee N, Bandaru P, Miller JB, Nusbaum J, Corcoran DL, Langlois C, Munschauer M, Dewell S, Hafner M, Williams Z, Ohler U, Tuschl T (2013) FMR1 targets distinct mRNA sequence elements to regulate protein expression. Nature 492:382–386.

Ashley CT, Wilkinson KD, Reines D, Warren ST (1993) FMR1 protein: Conserved RNP family domains and selective RNA binding. Science.

Ataman B, Ashley J, Gorczyca M, Ramachandran P, Fouquet W, Sigrist SJ, Budnik V (2008) Rapid activity-dependent modifications in synaptic structure and function require bidirectional wnt signaling. Neuron 57:705–718.

Augustin H, Allen MJ, Partridge L (2011) Electrophysiological Recordings from the Giant Fiber Pathway of D. melanogaster. J Vis Exp.

Awasaki T, Tatsumi R, Takahashi K, Arai K, Nakanishi Y, Ueda R, Ito K (2006) Essential Role of the Apoptotic Cell Engulfment Genes draper and ced-6 in Programmed Axon Pruning during Drosophila Metamorphosis. Neuron.

Ayata P, Badimon A, Strasburger HJ, Duff MK, Montgomery SE, Loh YHE, Ebert A, Pimenova AA, Ramirez BR, Chan AT, Sullivan JM, Purushothaman I, Scarpa JR, Goate AM, Busslinger M, Shen L, Losic B, Schaefer A (2018) Epigenetic regulation of brain region-specific microglia clearance activity. Nat

Neurosci.

Bacon JP, Strausfeld NJ (1986) The dipteran “Giant fibre” pathway: neurons and signals. J Comp Physiol A 158:529–548.

Baena-Lopez LA, Alexandre C, Mitchell A, Pasakarnis L, Vincent J-P (2013) Accelerated homologous recombination and subsequent genome modification in Drosophila. Development.

Bailey DB, Raspa M, Olmsted M, Holiday DB (2008) Co-occurring conditions associated with FMR1 gene variations: Findings from a national parent survey. Am J Med Genet Part A.

Bailey DW (1982) How pure are inbred strains of mice? Immunol Today.

Baker MW, Macagno ER (2017) Gap junction proteins and the wiring (Rewiring) of neuronal circuits. Dev Neurobiol 77:575–586.

Baranova A, Ivanov D, Petrash N, Pestova A, Skoblov M, Kelmanson I, Shagin D, Nazarenko S, Geraymovych E, Litvin O, Tiunova A, Born TL, Usman N, Staroverov D, Lukyanov S, Panchin Y (2004) The mammalian pannexin family is homologous to the invertebrate innexin gap junction proteins. Genomics.

Barbee SA, Estes PS, Cziko A, Hillebrand J, Luedeman RA, Coller JM, Johnson N, Howlett IC, Geng C, Ueda R, Brand AH, Newbury SF, Wilhelm JE, Levine RB, Nakamura A, Parker R, Ramaswami M (2006) Staufen-and FMRP-containing neuronal RNPs are structurally and functionally related to somatic P bodies. Neuron 52:997–1009.

Bartley CM, OKeefe RA, Blice-Baum A, Mihailescu M-R, Gong X, Miyares L, Karaca E, Bordey A (2016) Mammalian FMRP S499 Is Phosphorylated by CK2 and Promotes Secondary Phosphorylation of FMRP. eNeuro.

Bassett AR, Kong L, Liu JL (2015) A Genome-Wide CRISPR Library for High-Throughput Genetic Screening in Drosophila Cells. J Genet Genomics 42:301–309.

Bear MF, Huber KM, Warren ST (2004) The mGluR theory of fragile X mental retardation. Trends Neurosci 27:370–377.

Bechara EG, Didiot MC, Melko M, Davidovic L, Bensaid M, Martin P, Castets M, Pognonec P, Khandjian EW, Moine H, Bardoni B (2009) A novel function for fragile X mental retardation protein in translational activation. PLoS Biol 7:e16.

Bellen HJ, Levis RW, Liao G, He Y, Carlson JW, Tsang G, Evans-Holm M, Hiesinger PR, Schulze KL, Rubin GM, Hoskins RA, Spradling AC (2004) The BDGP gene disruption project: Single transposon insertions associated with 40% of Drosophila genes. Genetics.

Belousov AB, Fontes JD (2013) Neuronal gap junctions: Making and breaking connections during development and injury. Trends Neurosci 36:227–236.

Bennett MVL, Contreras JE, Bukauskas FF, Sáez JC (2003) New roles for astrocytes: Gap junction hemichannels have something to communicate. Trends Neurosci 26:610–617.

Berger J, Suzuki T, Senti KA, Stubbs J, Schaffner G, Dickson BJ (2001) Genetic mapping with SNP markers in Drosophila. Nat Genet.

Berry-Kravis E, Hessl D, Abbeduto L, Reiss AL, Beckel-Mitchener A, Urv TK (2013) Outcome measures for clinical trials in fragile X syndrome. J Dev Behav Pediatr.

Beyer EC, Berthoud VM (2018) Gap junction gene and protein families: Connexins, innexins, and pannexins. Biochim Biophys Acta - Biomembr.

Bhattacharya A, Kaphzan H, Alvarez-Dieppa AC, Murphy JP, Pierre P, Klann E (2012) Genetic Removal of p70 S6 Kinase 1 Corrects Molecular, Synaptic, and Behavioral Phenotypes in Fragile X Syndrome Mice. Neuron.

Bidaye SS, Machacek C, Wu Y, Dickson BJ (2014) Neuronal control of Drosophila walking direction. Science 344:97–101.

Biederer T, Sara Y, Mozhayeva M, Atasoy D, Liu X, Kavalali ET, Südhof TC (2002) SynCAM, a synaptic adhesion molecule that drives synapse assembly. Science.

Bilousova T V., Dansie L, Ngo M, Aye J, Charles JR, Ethell DW, Ethell IM (2009) Minocycline promotes dendritic spine maturation and improves behavioural performance in the fragile X mouse model. J Med Genet.

Bishop AL, Hall A (2000) Rho GTPases and their effector proteins. Biochem J.

Blagburn JM, Alexopoulos H, Davies JA, Bacon JP (1999) Null mutation in shaking-B eliminates electrical, but not chemical, synapses in the Drosophila giant fiber system: a structural study. J Comp Neurol 404:449–458.

Bock T, Stuart GJ (2016) The Impact of BK Channels on Cellular Excitability Depends on their Subcellular Location. Front Cell Neurosci.

Boerner J, Godenschwege TA (2010) Application for the Drosophila ventral nerve cord standard in neuronal circuit reconstruction and in-depth analysis of mutant morphology. J Neurogenet 24:158–167.

Boerner J, Godenschwege TA (2011) Whole mount preparation of the adult Drosophila ventral nerve cord for giant fiber dye injection. J Vis Exp 52:3080.

Boivin JR, Nedivi E (2018) Functional implications of inhibitory synapse placement on signal processing in pyramidal neuron dendrites. Curr Opin Neurobiol.

Bolduc F, Bell K, Cox H, Broadie K, Tully T (2008) Excess protein synthesis in Drosophila fragile X mutants impairs long-term memory. Nat Neurosci 11:1143–1145.

Borgen M, Rowland K, Boerner J, Lloyd B, Khan A, Murphey R (2017) Axon termination, pruning, and synaptogenesis in the giant fiber system of Drosophila melanogaster is promoted by highwire. Genetics 205:1229–1245.

Braat S, D'Hulst C, Heulens I, De Rubeis S, Mientjes E, Nelson DL, Willemsen R, Bagni C, Van Dam D, De Deyn PP, Kooy RF (2015) The GABA $_A$ receptor is an FMRP target with therapeutic potential in fragile X syndrome. Cell Cycle 14:2985–2995.

Brager DH, Johnston D (2014) Channelopathies and dendritic dysfunction in fragile X syndrome. Brain Res Bull 103:11–17.

Brand AH, Perrimon N (1993) Targeted gene expression as a means of altering cell fates and generating dominant phenotypes. Development 118:401–415.

Braz JM, Rico B, Basbaum AI (2002) Transneuronal tracing of diverse CNS circuits by Cre-mediated induction of wheat germ agglutinin in transgenic mice. Proc Natl Acad Sci.

Brion J-P, Hanger DP, Couck A-M, Anderton BH (1991) A68 proteins in Alzheimer's disease are composed of several tau isoforms in a phosphorylated state which affects their electrophoretic mobilities. Biochem J.

Broadie K, Bate M (1993) Innervation directs receptor synthesis and localization in Drosophila embryo synaptogenesis. Nature.

Brown MR, Kronengold J, Gazula V-RR, Chen Y, Strumbos JG, Sigworth FJ, Navaratnam D, Kaczmarek LK (2010) Fragile X mental retardation protein controls gating of the sodium-activated potassium channel Slack. Nat Neurosci 13:819–821.

Brown V, Jin P, Ceman S, Darnell JC, O'Donnell WT, Tenenbaum S, Jin X, Feng Y, Wilkinson KD, Keene JD, Darnell RB, Warren ST (2001) Microarray identification of FMRP-associated brain mRNAs and altered mRNA translational profiles in fragile X syndrome. Cell 107:477–487.

Brown V, Small K, Lakkis L, Feng Y, Gunter C, Wilkinson KD, Warren ST (1998) Purified recombinant Fmrp exhibits selective RNA binding as an intrinsic property of the fragile X mental retardation protein. J Biol Chem.

Budnik V, Salinas P (2011) Wnt signaling during synaptic development and plasticity. Curr Opin Neurobiol 21:151–159.

Burgess DJ (2011) Model organisms: The dangers lurking in the genetic background. Nat Rev Genet.

Büschges A, Djokaj S, Bässler D, Bässler U, Rathmayer W (2000) Neuromuscular plasticity in the locust after permanent removal of an excitatory motoneuron of the extensor tibiae muscle. J Neurobiol 42:148–159.

Caldwell PH, Murphy SB, Butow PN, Craig JC (2004) Clinical trials in children. Lancet 364:803–811.

Calfon M, Zeng H, Urano F, Till JH, Hubbard SR, Harding HP, Clark SG, Ron D (2002) IRE1 couples endoplasmic reticulum load to secretory capacity by processing the XBP-1 mRNA. Nature.

Callan MA, Clements N, Ahrendt N, Zarnescu DC (2012) Fragile X Protein is required for inhibition of insulin signaling and regulates glial-dependent neuroblast reactivation in the developing brain. Brain Res.

Cande J, Berman GJ, Namiki S, Qiu J, Korff W, Card G, Shaevitz JW, Stern DL (2018) Optogenetic dissection of descending behavioral control in Drosophila. Elife 7.

Cardona A, Larsen C, Hartenstein V (2009) Neuronal fiber tracts connecting the brain and ventral nerve cord of the early Drosophila larva. J Comp Neurol 515:427–440.

Casso D, Ramírez-Weber FA, Kornberg TB (1999) GFP-tagged balancer chromosomes for Drosophila melanogaster. Mech Dev.

Causing CG, Gloster A, Aloyz R, Bamji SX, Chang E, Fawcett J, Kuchel G, Miller FD (1997) Synaptic innervation density is regulated by neuron-derived BDNF. Neuron.

Ceman S, O'Donnell WT, Reed M, Patton S, Pohl J, Warren ST (2003) Phosphorylation influences the translation state of FMRP-associated polyribosomes. Hum Mol Genet.

Chandler CH, Chari S, Dworkin I (2013) Does your gene need a background check? How genetic background impacts the analysis of mutations, genes, and evolution. Trends Genet.

Chen L, Yun SW, Seto J, Liu W, Toth M (2003) The fragile X mental retardation protein binds and regulates a novel class of mRNAs containing u rich target sequences. Neuroscience.

Chen Q, Cichon J, Wang W, Qiu L, Lee SJR, Campbell NR, DeStefino N, Goard MJ, Fu Z, Yasuda R, Looger LL, Arenkiel BR, Gan WB, Feng G (2012) Imaging Neural Activity Using Thy1-GCaMP Transgenic Mice. Neuron.

Chen Y, Akin O, Nern A, Tsui CYK, Pecot MY, Zipursky SL (2014) Cell-type-specific labeling of synapses in vivo through synaptic tagging with recombination. Neuron 81:280–293.

Chiang AS et al. (2011) Three-dimensional reconstruction of brain-wide wiring networks in drosophila at single-cell resolution. Curr Biol 21:1–11.

Chonchaiya W, Schneider A, Hagerman RJ (2009) Fragile X: A Family of Disorders. Adv Pediatr.

Christiansen F, Zube C, Andlauer TFM, Wichmann C, Fouquet W, Owald D, Mertel S, Leiss F, Tavosanis G, Farca Luna AJ, Fiala A, Sigrist SJ (2011) Presynapses in Kenyon Cell Dendrites in the Mushroom Body Calyx of Drosophila. J Neurosci 31:9696–9707.

Ciani L, Krylova O, Smalley MJ, Dale TC, Salinas PC (2004) A divergent canonical WNT-signaling pathway regulates microtubule dynamics: Dishevelled signals locally to stabilize microtubules. J Cell Biol.

Cline HT (2001) Dendritic arbor development and synaptogenesis. Curr Opin Neurobiol.

Coffee LR, Williamson AJ, Adkins CM, Gray MC, Page TL, Broadie K (2012) In vivo neuronal function of the fragile X mental retardation protein is regulated by phosphorylation. Hum Mol Genet.

Cohen-Cory S (2002) The developing synapse: Construction and modulation of synaptic structures and circuits. Science 298:770–776.

Collignon O, Voss P, Lassonde M, Lepore F (2009) Cross-modal plasticity for the spatial processing of

sounds in visually deprived subjects. Exp Brain Res 192:343–358.

Comery T, Harris J, Willems P, Oostra B, Irwin S, Weiler I, Greenough W (1997) Abnormal dendritic spines in fragile X knockout mice: maturation and pruning deficits. Proc Natl Acad Sci U S A 94:5401–5404.

Connor RMO, Stone EF, Wayne CR, Marcinkevicius E V, Ulgherait M, Delventhal R, Pantalia MM, Hill VM, Zhou CG, Mcallister S, Chen A, Ziegenfuss JS, Grueber WB, Canman JC, Hiza MMS (2017) A Drosophila model of Fragile X syndrome exhibits defects in phagocytosis by innate immune cells. 216:1–11.

Contet C, Goulding SP, Kuljis DA, Barth AL (2016) BK Channels in the Central Nervous System. In: International Review of Neurobiology.

Contractor A, Klyachko VA, Portera-Cailliau C (2015) Altered neuronal and circuit excitability in fragile X syndrome. Neuron 87:699–715.

Cook RK, Christensen SJ, Deal JA, Coburn RA, Deal ME, Gresens JM, Kaufman TC, Cook KR (2012) The generation of chromosomal deletions to provide extensive coverage and subdivision of the Drosophila melanogaster genome. Genome Biol 13:R21.

Cooper GM, Shendure J (2011) Needles in stacks of needles: Finding disease-causal variants in a wealth of genomic data. Nat Rev Genet.

Cordeiro L, Ballinger E, Hagerman R, Hessl D (2011) Clinical assessment of DSM-IV anxiety disorders in fragile X syndrome: prevalence and characterization. J Neurodev Disord.

Corty MM, Freeman MR (2013) Architects in neural circuit design: Glia control neuron numbers and connectivity. J Cell Biol.

Cowley B, Kirjanen S, Partanen J, Castren M (2016) Epileptic electroencephalography profile associates with attention problems in children with fragile X syndrome: Review and case series. Front Hum Neurosci 10:353.

Cox DBT, Gootenberg JS, Abudayyeh OO, Franklin B, Kellner MJ, Joung J, Zhang F (2017) RNA editing with CRISPR-Cas13. Science.

Coyne AN, Yamada SB, Siddegowda BB, Estes PS, Zaepfel BL, Johannesmeyer JS, Lockwood DB, Pham LT, Hart MP, Cassel JA, Freibaum B, Boehringer A V., Paul Taylor J, Reitz AB, Gitler AD, Zarnescu DC (2015) Fragile X protein mitigates TDP-43 toxicity by remodeling RNA granules and restoring translation. Hum Mol Genet.

Crawford RD (1976) Incomplete dominance of the gene for naked neck in domestic fowl. Poult Sci.

Crittenden JR, Skoulakis EMC, Han K-A, Kalderon D, Davis RL (1998) Tripartite Mushroom Body Architecture Revealed by Antigenic Markers. Learn Mem 5:38–51.

Crowley C, Spencer SD, Nishimura MC, Chen KS, Pitts-Meek S, Armaninl MP, Ling LH, McMahon SB, Shelton DL, Levinson AD, Phillips HS (1994) Mice lacking nerve growth factor display perinatal loss

of sensory and sympathetic neurons yet develop basal forebrain cholinergic neurons. Cell 76:1001–1011.

Cruz-Martín A, Crespo M, Portera-Cailliau C (2010) Delayed stabilization of dendritic spines in fragile X mice. J Neurosci 30:7793–7803.

Cvetkovska V, Hibbert AD, Emran F, Chen BE (2013) Overexpression of down syndrome cell adhesion molecule impairs precise synaptic targeting. Nat Neurosci 16:677–682.

Dahal GR, Rawson J, Gassaway B, Kwok B, Tong Y, Ptacek LJ, Bates E (2012) An inwardly rectifying K+ channel is required for patterning. Development 139:3653–3664.

Darabid H, Perez-Gonzalez AP, Robitaille R (2014) Neuromuscular synaptogenesis: Coordinating partners with multiple functions. Nat Rev Neurosci.

Darnell J, Van Driesche S, Zhang C, Hung K, Mele A, Fraser C, Stone E, Chen C, Fak J, Chi S, Licatalosi D, Richter J, Darnell R (2011) FMRP stalls ribosomal translocation on mRNAs linked to synaptic function and autism. Cell 146:247–261.

Darnell JC, Fraser CE, Mostovetsky O, Darnell RB (2009) Discrimination of common and unique RNA-binding activities among Fragile X mental retardation protein paralogs. Hum Mol Genet.

Darnell JC, Fraser CE, Mostovetsky O, Stefani G, Jones TA, Eddy SR, Darnell RB (2005a) Kissing complex RNAs mediate interaction between the Fragile-X mental retardation protein KH2 domain and brain polyribosomes. Genes Dev.

Darnell JC, Jensen KB, Jin P, Brown V, Warren ST, Darnell RB (2001) Fragile X mental retardation protein targets G quartet mRNAs important for neuronal function. Cell 107:489–499.

Darnell JC, Klann E (2013) The translation of translational control by FMRP: Therapeutic targets for FXS. Nat Neurosci.

Darnell JC, Mostovetsky O, Darnell RB (2005b) FMRP RNA targets: Identification and validation. Genes, Brain Behav.

Davenport MH, Schaefer TL, Friedmann KJ, Fitzpatrick SE, Erickson CA (2016) Pharmacotherapy for Fragile X Syndrome: Progress to Date. Drugs.

Dawson N, Sillitoe I, Marsden RL, Orengo CA (2017) The Classification of Protein Domains. In: Methods in molecular biology (Clifton, N.J.), pp 137–164.

Dawydow A, Gueta R, Ljaschenko D, Ullrich S, Hermann M, Ehmann N, Gao S, Fiala A, Langenhan T, Nagel G, Kittel RJ (2014) Channelrhodopsin-2-XXL, a powerful optogenetic tool for low-light applications. Proc Natl Acad Sci U S A 111:13972–13977.

Day CA, Kraft LJ, Kang M, Kenworthy AK (2012) Analysis of protein and lipid dynamics using confocal fluorescence recovery after photobleaching (FRAP). Curr Protoc Cytom Chapter 2:Unit2.19.

De Boulle K, Verkerk AJMH, Reyniers E, Vits L, Hendrickx J, Van Roy B, Van Den Bos F, de Graaff E, Oostra

BA, Willems PJ (1993) n in the FMR-1 gA point mutatioene associated with fragile X mental retardation. Nat Genet.

De Rubeis S et al. (2014) Synaptic, transcriptional and chromatin genes disrupted in autism. Nature.

de Vries SEJ, Clandinin T (2013) Optogenetic Stimulation of Escape Behavior in Drosophila melanogaster. J Vis Exp.

Dear ML, Shilts J, Broadie K (2017) Neuronal activity drives FMRP- and HSPG-dependent matrix metalloproteinase function required for rapid synaptogenesis. Sci Signal.

Deng PY, Rotman Z, Blundon JA, Cho Y, Cui J, Cavalli V, Zakharenko SS, Klyachko VA (2013) FMRP regulates neurotransmitter release and synaptic information transmission by modulating action potential duration via BK channels. Neuron 77:696–711.

Desbois M, Cook SJ, Emmons SW, Bülow HE (2015) Directional Trans-synaptic labeling of specific neuronal connections in live animals. Genetics.

Dietrich A, Kioschis P, Monaco AP, Gross B, Korn B, Williams S V., Sheer D, Heitz D, Oberie I, Toniolo D, Warren ST, Lehrach H, Poustka A (1991) Molecular cloning and analysis of the fragile X region in man. Nucleic Acids Res 19:2567–2572.

Dietzl G, Chen D, Schnorrer F, Su KC, Barinova Y, Fellner M, Gasser B, Kinsey K, Oppel S, Scheiblauer S, Couto A, Marra V, Keleman K, Dickson BJ (2007) A genome-wide transgenic RNAi library for conditional gene inactivation in Drosophila. Nature.

Dionne H, Hibbard KL, Cavallaro A, Kao JC, Rubin GM (2018) Genetic reagents for making split-GAL4 lines in Drosophila. Genetics 209:31–35.

Dobkin C, Rabe A, Dumas R, El Idrissi A, Haubenstock H, Ted Brown W (2000) Fmr1 knockout mouse has a distinctive strain-specific learning impairment. Neuroscience.

Dockendorff TC, Su HS, McBride SMJ, Yang Z, Choi CH, Siwicki KK, Sehgal A, Jongens TA (2002) Drosophila lacking dfmr1 activity show defects in circadian output and fail to maintain courtship interest. Neuron 34:973–984.

Dolan BM, Duron SG, Campbell DA, Vollrath B, Rao BSS, Ko H-Y, Lin GG, Govindarajan A, Choi S-Y, Tonegawa S (2013) Rescue of fragile X syndrome phenotypes in Fmr1 KO mice by the small-molecule PAK inhibitor FRAX486. Proc Natl Acad Sci.

Doll C, Broadie K (2014) Impaired activity-dependent neural circuit assembly and refinement in autism spectrum disorder genetic models. Front Cell Neurosci 8:1–26.

Doll C, Broadie K (2015) Activity-dependent FMRP requirements in development of the neural circuitry of learning and memory. Development 142:1346–1356.

Doll C, Broadie K (2016) Neuron class-specific requirements for fragile X mental retardation protein in critical period development of calcium signaling in learning and memory circuitry. Neurobiol Dis 89:76–87.

Doll CA, Vita DJ, Broadie K (2017) Fragile X Mental Retardation Protein Requirements in Activity-Dependent Critical Period Neural Circuit Refinement. Curr Biol.

Dolzhanskaya N, Sung YJ, Conti J, Currie JR, Denman RB (2003) The fragile X mental retardation protein interacts with U-rich RNAs in a yeast three-hybrid system. Biochem Biophys Res Commun.

Dougherty L, Singh R, Brown S, Dardick C, Xu K (2018) Exploring DNA variant segregation types in pooled genome sequencing enables effective mapping of weeping trait in Malus. J Exp Bot.

Dubnau J, Chiang A-S, Grady L, Barditch J, Gossweiler S, McNeil J, Smith P, Buldoc F, Scott R, Certa U, Broger C, Tully T (2003) The staufen/pumilio pathway is involved in Drosophila long-term memory. Curr Biol 13:286–296.

Duffy JB, Harrison DA, Perrimon N (1998) Identifying loci required for follicular patterning using directed mosaics. Development.

East JM (2010) Membrane trafficking. Mol Membr Biol.

Egger MD, Nowakowski RS, Peng B, Wyman RJ (1997) Patterns of connectivity in a Drosophila nerve. J Comp Neurol 387:63–72.

Ehrenreich IM, Torabi N, Jia Y, Kent J, Martis S, Shapiro JA, Gresham D, Caudy AA, Kruglyak L (2010) Dissection of genetically complex traits with extremely large pools of yeast segregants. Nature.

Ehyai S, Miyake T, Williams D, Vinayak J, Bayfield MA, McDermott JC (2018) FMRP recruitment of β-catenin to the translation pre-initiation complex represses translation. EMBO Rep.

Eichler K, Li F, Litwin-Kumar A, Park Y, Andrade I, Schneider-Mizell CM, Saumweber T, Huser A, Eschbach C, Gerber B, Fetter RD, Truman JW, Priebe CE, Abbott LF, Thum AS, Zlatic M, Cardona A (2017) The complete connectome of a learning and memory centre in an insect brain. Nature 548:175–182.

Elias LAB, Kriegstein AR (2008) Gap junctions: multifaceted regulators of embryonic cortical development. Trends Neurosci 31:243–250.

Elvira G, Wasiak S, Blandford V, Tong X-K, Serrano A, Fan X, del Rayo Sánchez-Carbente M, Servant F, Bell AW, Boismenu D, Lacaille J-C, McPherson PS, DesGroseillers L, Sossin WS (2006) Characterization of an RNA Granule from Developing Brain. Mol Cell Proteomics.

Engel J, Wu C (1996) Altered habituation of an identified escape circuit in Drosophila memory mutants. J Neurosci 76:3486–3499.

Engel JE, Xie XJ, Sokolowski MB, Wu CF (2000) A cGMP-dependent protein kinase gene, foraging, modifies habituation-like response decrement of the giant fiber escape circuit in Drosophila. Learn Mem.

Enneking E-M, Kudumala SR, Moreno E, Stephan R, Boerner J, Godenschwege TA, Pielage J (2013) Transsynaptic coordination of synaptic growth, function, and stability by the L1-type CAM Neuroglian. PLoS Biol 11:e1001537.

Erickson CA, Davenport MH, Schaefer TL, Wink LK, Pedapati E V., Sweeney JA, Fitzpatrick SE, Brown WT, Budimirovic D, Hagerman RJ, Hessl D, Kaufmann WE, Berry-Kravis E (2017) Fragile X targeted pharmacotherapy: Lessons learned and future directions. J Neurodev Disord.

Erickson CA, Weng N, Weiler IJ, Greenough WT, Stigler KA, Wink LK, McDougle CJ (2011) Open-label riluzole in fragile X syndrome. Brain Res.

Estévez R, Schroeder BC, Accardi A, Jentsch TJ, Pusch M (2003) Conservation of chloride channel structure revealed by an inhibitor binding site in ClC-1. Neuron.

Fan JY, Cui ZQ, Wei HP, Zhang ZP, Zhou YF, Wang YP, Zhang XE (2008) Split mCherry as a new red bimolecular fluorescence complementation system for visualizing protein-protein interactions in living cells. Biochem Biophys Res Commun.

Farhy-Tselnicker I, van Casteren ACM, Lee A, Chang VT, Aricescu AR, Allen NJ (2017) Astrocyte-Secreted Glypican 4 Regulates Release of Neuronal Pentraxin 1 from Axons to Induce Functional Synapse Formation. Neuron.

Farías GG, Alfaro IE, Cerpa W, Grabowski CP, Godoy JA, Bonansco C, Inestrosa NC (2009) Wnt-5a/JNK signaling promotes the clustering of PSD-95 in hippocampal neurons. J Biol Chem.

Favuzzi E, Rico B (2018) Molecular diversity underlying cortical excitatory and inhibitory synapse development. Curr Opin Neurobiol.

Fayyazuddin A, Zaheer MA, Hiesinger PR, Bellen HJ (2006) The nicotinic acetylcholine receptor Dalpha7 is required for an escape behavior in Drosophila. PLoS Biol 4.

Feinberg EH, VanHoven MK, Bendesky A, Wang G, Fetter RD, Shen K, Bargmann CI (2008) GFP Reconstitution Across Synaptic Partners (GRASP) Defines Cell Contacts and Synapses in Living Nervous Systems. Neuron.

Feng Y, Absher D, Eberhart DE, Brown V, Malter HE, Warren ST (1997a) FMRP associates with polyribosomes as an mRNP, and the I304N mutation of severe fragile X syndrome abolishes this association. Mol Cell.

Feng Y, Gutekunst C a, Eberhart DE, Yi H, Warren ST, Hersch SM (1997b) Fragile X mental retardation protein: Nucleocytoplasmic shuttling and association with somatodendritic ribosomes. J Neurosci.

Ferron L (2016) Fragile X mental retardation protein controls ion channel expression and activity. J Physiol 0:1–7.

Ferron L, Nieto-Rostro M, Cassidy JS, Dolphin AC (2014) Fragile X mental retardation protein controls synaptic vesicle exocytosis by modulating N-type calcium channel density. Nat Commun.

Fields RD, Itoh K (1996) Neural cell adhesion molecules in activity-dependent development and synaptic plasticity. Trends Neurosci.

Filippini A, Bonini D, Lacoux C, Pacini L, Zingariello M, Sancillo L, Bosisio D, Salvi V, Mingardi J, La Via L, Zalfa F, Bagni C, Barbon A (2017) Absence of the Fragile X Mental Retardation Protein results in

defects of RNA editing of neuronal mRNAs in mouse. RNA Biol.

Fire A, Xu S, Montgomery MK, Kostas SA, Driver SE, Mello CC (1998) Potent and specific genetic interference by double-stranded RNA in caenorhabditis elegans. Nature.

Flybase (n.d.) Flybase. Available at: http://flybase.org/ [Accessed March 12, 2018].

Fotowat H, Fayyazuddin A, Bellen HJ, Gabbiani F (2009) A Novel Neuronal Pathway for Visually Guided Escape in Drosophila melanogaster. J Neurophysiol 102:875–885.

Frank DD, Jouandet GC, Kearney PJ, MacPherson LJ, Gallio M (2015) Temperature representation in the Drosophila brain. Nature 519:358–361.

Fu YH, Kuhl DPA, Pizzuti A, Pieretti M, Sutcliffe JS, Richards S, Verkert AJMH, Holden JJA, Fenwick RG, Warren ST, Oostra BA, Nelson DL, Caskey CT (1991) Variation of the CGG repeat at the fragile X site results in genetic instability: Resolution of the Sherman paradox. Cell.

Gantois I et al. (2017) Metformin ameliorates core deficits in a mouse model of fragile X syndrome. Nat Med.

Gatto CL, Broadie K (2008) Temporal requirements of the fragile X mental retardation protein in the regulation of synaptic structure. Development.

Gatto CL, Broadie K (2011) Fragile X mental retardation protein is required for programmed cell death and clearance of developmentally-transient peptidergic neurons. Dev Biol.

Gaudry Q, Kristan WB (2009) Behavioral choice by presynaptic inhibition of tactile sensory terminals. Nat Neurosci 12:1450–1457.

Gerlai R (1996) Gene-targeting studies of mammalian behavior: Is it the mutation or the background genotype? Trends Neurosci.

Ghaziuddin M, Bolyard B, Alessi N (1994) Autistic disorder in Noonan syndrome. J Intellect Disabil Res.

Gholizadeh S, Arsenault J, Xuan IC on. Y, Pacey LK, Hampson DR (2014) Reduced phenotypic severity following adeno-associated virus-mediated Fmr1 gene delivery in fragile X mice. Neuropsychopharmacology.

Ghosh AS, Wang B, Pozniak CD, Chen M, Watts RJ, Lewcock JW (2011) DLK induces developmental neuronal degeneration via selective regulation of proapoptotic JNK activity. J Cell Biol 194:751–764.

Gibson DA, Ma L (2011) Developmental regulation of axon branching in the vertebrate nervous system. Development 138:183–195.

Gkogkas CG, Khoutorsky A, Cao R, Jafarnejad SM, Prager-Khoutorsky M, Giannakas N, Kaminari A, Fragkouli A, Nader K, Price TJ, Konicek BW, Graff JR, Tzinia AK, Lacaille J-C, Sonenberg N (2014) Pharmacogenetic Inhibition of eIF4E-Dependent Mmp9 mRNA Translation Reverses Fragile X Syndrome-like Phenotypes. Cell Rep:1–14.

Godenschwege T, Murphey R (2008) Genetic interaction of Neuroglian and Semaphorin1a during guidance and synapse formation. J Neurogenet 23:147–155.

Godenschwege TA, Hu H, Shan-Crofts X, Goodman CS, Murphey RK (2002) Bi-directional signaling by Semaphorin 1a during central synapse formation in Drosophila. Nat Neurosci 5:1294–1301.

Godenschwege TA, Kristiansen L V, Uthaman SB, Hortsch M, Murphey RK (2006) A conserved role for Drosophila Neuroglian and human L1-CAM in central-synapse formation. Curr Biol 16:12–23.

Golovin RM, Broadie K (2016) Developmental experience-dependent plasticity in the first synapse of the Drosophila olfactory circuit. J Neurophysiol 116:2730–2738.

Gorin PD, Johnson EM (1979) Experimental autoimmune model of nerve growth factor deprivation: effects on developing peripheral sympathetic and sensory neurons. Proc Natl Acad Sci U S A 76:5382–5386.

Goritz C, Mauch DH, Pfrieger FW (2005) Multiple mechanisms mediate cholesterol-induced synaptogenesis in a CNS neuron. Mol Cell Neurosci.

Grant SGN (2012) Synaptopathies: Diseases of the synaptome. Curr Opin Neurobiol.

Gratz SJ, Cummings AM, Nguyen JN, Hamm DC, Donohue LK, Harrison MM, Wildonger J, O'connor-Giles KM (2013) Genome engineering of Drosophila with the CRISPR RNA-guided Cas9 nuclease. Genetics.

Greenblatt EJ, Spradling AC (2018) Fragile X mental retardation 1 gene enhances the translation of large autism-related proteins. Science 361:709–712.

Greenough WT, Klintsova AY, Irwin SA, Galvez R, Bates KE, Weiler IJ (2001) Synaptic regulation of protein synthesis and the fragile X protein. Proc Natl Acad Sci.

Gross C, Yao X, Pong DL, Jeromin A, Bassell GJ (2011) Fragile X mental retardation protein regulates protein expression and mRNA translation of the potassium channel Kv4.2. J Neurosci 31:5693–5698.

Gu H, O'Dowd DK (2007) Whole cell recordings from brain of adult Drosophila. J Vis Exp:248.

Guo Y, Chen X, Xing R, Wang M, Zhu X, Guo W (2017) Interplay between FMRP and lncRNA TUG1 regulates axonal development through mediating SnoN-Ccd1 pathway. Hum Mol Genet.

Hammarlund M, Hobert O, Miller DM, Sestan N (2018) The CeNGEN Project: The Complete Gene Expression Map of an Entire Nervous System. Neuron.

Hanani M (2012) Lucifer yellow - an angel rather than the devil. J Cell Mol Med 16:22–31.

Hanganu IL, Okabe A, Lessmann V, Luhmann HJ (2009) Cellular mechanisms of subplate-driven and cholinergic input-dependent network activity in the neonatal rat somatosensory cortex. Cereb Cortex 19:89–105.

Harris SW, Hessl D, Goodlin-Jones B, Ferranti J, Bacalman S, Barbato I, Tassone F, Hagerman PJ, Herman K, Hagerman RJ, Herman H, Hagerman RJ (2008) Autism profiles of males with fragile X syndrome. Am J Ment Retard 113:427–438.

Harwell CC, Parker PRL, Gee SM, Okada A, McConnell SK, Kreitzer AC, Kriegstein AR (2012) Sonic Hedgehog Expression in Corticofugal Projection Neurons Directs Cortical Microcircuit Formation. Neuron.

He C-W, Liao C-P, Pan C-L (2018a) Wnt signalling in the development of axon, dendrites and synapses. Open Biol 8:180116.

He CX, Portera-Cailliau C (2013) The trouble with spines in fragile X syndrome: density, maturity and plasticity. Neuroscience 251:120–128.

He Q, Ge W (2017) The tandem Agenet domain of fragile X mental retardation protein interacts with FUS. Sci Rep.

He S, Cuentas-Condori A, Miller DM (2018b) NATF (Native And Tissue-specific Fluorescence): A strategy for bright, tissue-specific GFP labeling of native proteins. bioRxiv:1–29.

Heigwer F, Port F, Boutros M (2018) Rna interference (RNAi) screening in Drosophila. Genetics 208:853–874.

Herculano-Houzel S, Mota B, Lent R (2006) Cellular scaling rules for rodent brains. Proc Natl Acad Sci.

Hessl D, Dyer-Friedman J, Glaser B, Wisbeck J, Barajas RG, Taylor A, Reiss AL (2001) The Influence of Environmental and Genetic Factors on Behavior Problems and Autistic Symptoms in Boys and Girls With Fragile X Syndrome. Pediatrics.

Hiesinger PR, Scholz M, Meinertzhagen IA, Fischbach KF, Obermayer K (2001) Visualization of synaptic markers in the optic neuropils of Drosophila using a new constrained deconvolution method. J Comp Neurol.

Higashimori H, Morel L, Huth J, Lindemann L, Dulla C, Taylor A, Freeman M, Yang Y (2013) Astroglial FMRP-dependent translational down-regulation of mglur5 underlies glutamate transporter GLT1 dysregulation in the fragile X mouse. Hum Mol Genet 22:2041–2054.

Higashimori H, Schin CS, Chiang MSR, Morel L, Shoneye TA, Nelson DL, Yang Y (2016) Selective Deletion of Astroglial FMRP Dysregulates Glutamate Transporter GLT1 and Contributes to Fragile X Syndrome Phenotypes In Vivo. J Neurosci 36:7079–7094.

Hige T (2018) What can tiny mushrooms in fruit flies tell us about learning and memory? Neurosci Res 129:8–16.

Hinton VJ, Brown WT, Wisniewski K, Rudelli RD (1991) Analysis of neocortex in three males with the fragile X syndrome. Am J Med Genet 41:289–294.

Hobert O, Kratsios P (2019) Neuronal identity control by terminal selectors in worms, flies, and chordates. Curr Opin Neurobiol 56:97–105.

Hodge JJL, Choi JC, O'Kane CJ, Griffith LC (2005) Shaw potassium channel genes in Drosophila. J Neurobiol 63:235–254.

Hodgkin AL, Huxley AF (1939) Action potentials recorded from inside a nerve fibre. Nature.

Holtmaat A, Bonhoeffer T, Chow DK, Chuckowree J, De Paola V, Hofer SB, Hübener M, Keck T, Knott G, Lee W-CA, Mostany R, Mrsic-Flogel TD, Nedivi E, Portera-Cailliau C, Svoboda K, Trachtenberg JT, Wilbrecht L (2009) Long-term, high-resolution imaging in the mouse neocortex through a chronic cranial window. Nat Protoc 4:1128–1144.

Hsu CT, Bhandawat V (2016) Organization of descending neurons in Drosophila melanogaster. Sci Rep.

Huang Q, Zhou D, DiFiglia M (1992) Neurobiotin(TM), a useful neuroanatomical tracer for in vivo anterograde, retrograde and transneuronal tract-tracing and for in vitro labeling of neurons. J Neurosci Methods 41:31–43.

Hubel DH, Wiesel TN (1970) The period of susceptibility to the physiological effects of unilateral eye closure in kittens. J Physiol 206:419–436.

Hubel DH, Wiesel TN, LeVay S (1977) Plasticity of ocular dominance columns in monkey striate cortex. Philos Trans R Soc Lond B Biol Sci 278:377–409.

Hudry B, Viala S, Graba Y, Merabet S (2011) Visualization of protein interactions in living Drosophila embryos by the bimolecular fluorescence complementation assay. BMC Biol.

Hunter J, Rivero-Arias O, Angelov A, Kim E, Fotheringham I, Leal J (2014) Epidemiology of fragile X syndrome: A systematic review and meta-analysis. Am J Med Genet Part A.

Hunter JE, Epstein MP, Tinker SW, Charen KH, Sherman SL (2008) Fragile X-associated primary ovarian insufficiency: Evidence for additional genetic contributions to severity. Genet Epidemiol.

Ifrim MF, Williams KR, Bassell GJ (2015) Single-molecule imaging of PSD-95 mRNA translation in dendrites and its dysregulation in a mouse model of fragile X syndrome. J Neurosci 35:7116–7130.

Inoue SB, Shimoda M, Nishinokubi I, Siomi MC, Okamura M, Nakamura A, Kobayashi S, Ishida N, Siomi H (2002) A role for the Drosophila fragile X-related gene in circadian output. Curr Biol.

Iossifov I et al. (2014) The contribution of de novo coding mutations to autism spectrum disorder. Nature.

Irwin S, Galvez R, Greenough WT (2000) Dendritic spine structural anomalies in fragile-X mental retardation syndrome. Cereb Cortex 10:1038–1044.

Irwin S, Patel B, Idupulapati M, Harris JB, Crisostomo R, Larsen BP, Kooy F, Willems PJ, Cras P, Kozlowski PB, Swain R, Weiler IJ, Greenough WT (2001) Abnormal dendritic spine characteristics in the temporal and visual cortices of patients with fragile-X syndrome: a quantitative examination. Am J Med Genet 98:161–167.

Iwawaki T, Akai R, Kohno K, Miura M (2004) A transgenic mouse model for monitoring endoplasmic

reticulum stress. Nat Med.

Jabeen S, Thirumalai V (2018) The interplay between electrical and chemical synaptogenesis. J Neurophysiol.

Jacobs K, Todman MG, Allen MJ, Davies JA, Bacon JP (2000) Synaptogenesis in the giant-fibre system of Drosophila: interaction of the giant fibre and its major motorneuronal target. Development 127:5203–5212.

Jacquemont S, Berry-Kravis E, Hagerman R, Von Raison F, Gasparini F, Apostol G, Ufer M, Des Portes V, Gomez-Mancilla B (2014) The challenges of clinical trials in fragile X syndrome. Psychopharmacology (Berl).

Jacquemont S, Hagerman RJ, Hagerman PJ, Leehey MA (2007) Fragile-X syndrome and fragile X-associated tremor/ataxia syndrome: two faces of FMR1. Lancet Neurol.

Jan LY, Jan YN (1976) L-glutamate as an excitatory transmitter at the Drosophila larval neuromuscular junction. J Physiol 262:215–236.

Jarrell TA, Wang Y, Bloniarz AE, Brittin CA, Xu M, Thomson JN, Albertson DG, Hall DH, Emmons SW (2012) The connectome of a decision-making neural network. Science.

Jeck WR, Sorrentino JA, Wang K, Slevin MK, Burd CE, Liu J, Marzluff WF, Sharpless NE (2013) Circular RNAs are abundant, conserved, and associated with ALU repeats. RNA.

Jenett A et al. (2012) A gal4-driver line resource for Drosophila neurobiology. Cell Rep 2:991–1001.

Jeste SS, Geschwind DH (2016) Clinical trials for neurodevelopmental disorders: At a therapeutic frontier. Sci Transl Med.

Jin P, Zarnescu DC, Ceman S, Nakamoto M, Mowrey J, Jongens TA, Nelson DL, Moses K, Warren ST (2004) Biochemical and genetic interaction between the fragile X mental retardation protein and the microRNA pathway. Nat Neurosci 7:113–117.

Jinek M, Chylinski K, Fonfara I, Hauer M, Doudna JA, Charpentier E (2012) A programmable dual-RNA-guided DNA endonuclease in adaptive bacterial immunity. Science.

Jing L, Lefebvre JL, Gordon LR, Granato M (2009) Wnt Signals Organize Synaptic Prepattern and Axon Guidance through the Zebrafish unplugged/MuSK Receptor. Neuron.

Jontes JD, Buchanan JA, Smith SJ (2000) Growth cone and dendrite dynamics in zebrafish embryos: Early events in synaptogenesis imaged in vivo. Nat Neurosci.

Joseph RM, Sun JS, Tam E, Carlson JR (2017) A receptor and neuron that activate a circuit limiting sucrose consumption. Elife.

Kadas D, Papanikolopoulou K, Xirou S, Consoulas C, Skoulakis EMC (2019) Human Tau isoform-specific presynaptic deficits in a Drosophila Central Nervous System circuit. Neurobiol Dis 124:311–321.

Kalia YN, Naik A, Garrison J, Guy RH (2004) Iontophoretic drug delivery. Adv Drug Deliv Rev 56:619–658.

Kanai Y, Dohmae N, Hirokawa N (2004) Kinesin transports RNA: isolation and characterization of an RNA-transporting granule. Neuron 43:513–525.

Kanca O, Bellen HJ, Schnorrer F (2017) Gene tagging strategies to assess protein expression, localization, and function in Drosophila. Genetics 207:389–412.

Kandler K, Katz LC (1995) Neuronal coupling and uncoupling in the developing nervous system. Curr Opin Neurobiol 5:98–105.

Kanellopoulos AK, Semelidou O, Kotini AG, Anezaki M, Skoulakis EMC (2012) Learning and Memory Deficits Consequent to Reduction of the Fragile X Mental Retardation Protein Result from Metabotropic Glutamate Receptor-Mediated Inhibition of cAMP Signaling in Drosophila. J Neurosci.

Kasthuri N et al. (2015) Saturated Reconstruction of a Volume of Neocortex. Cell.

Katz B, Miledi R (1965) Release of acetylcholine from a nerve terminal by electric pulses of variable strength and duration. Nature.

Katz B, Miledi R (1967) The Release of Acetylcholine from Nerve Endings by Graded Electric Pulses. Proc R Soc B Biol Sci.

Kebschull JM, Garcia da Silva P, Reid AP, Peikon ID, Albeanu DF, Zador AM (2016) High-Throughput Mapping of Single-Neuron Projections by Sequencing of Barcoded RNA. Neuron.

Keegan AP, Comer CM (1993) The wind-elicited escape response of cockroaches (Periplaneta americana) is influenced by lesions rostral to the escape circuit. Brain Res.

Kennedy T, Broadie K (2017) Fragile X Mental Retardation Protein Restricts Small Dye Iontophoresis Entry into Central Neurons. J Neurosci:0723-17.

Kennedy T, Broadie K (2018) Newly Identified Electrically Coupled Neurons Support Development of the *Drosophila* Giant Fiber Model Circuit. eneuro 5:ENEURO.0346-18.2018.

Khayachi A et al. (2018) Sumoylation regulates FMRP-mediated dendritic spine elimination and maturation. Nat Commun.

Kim JH, Wang X, Coolon R, Ye B (2013) Dscam expression levels determine presynaptic arbor sizes in Drosophila sensory neurons. Neuron 78:827–838.

Kim M, Bellini M, Ceman S (2009) Fragile X Mental Retardation Protein FMRP Binds mRNAs in the Nucleus. Mol Cell Biol 29:214–228.

Kim SM, Su C-Y, Wang JW (2017) Neuromodulation of Innate Behaviors in *Drosophila*. Annu Rev Neurosci.

King DG, Wyman RJ (1980) Anatomy of the giant fibre pathway in Drosophila. I. Three thoracic

components of the pathway. J Neurocytol 9:753–770.

Klassen MP, Shen K (2007) Wnt Signaling Positions Neuromuscular Connectivity by Inhibiting Synapse Formation in C. elegans. Cell.

Koch C, Poggio T, Torre V (1983) Nonlinear interactions in a dendritic tree: localization, timing, and role in information processing. Proc Natl Acad Sci U S A.

Kodama NX, Feng T, Ullett JJ, Chiel HJ, Sivakumar SS, Galán RF (2018) Anti-correlated cortical networks arise from spontaneous neuronal dynamics at slow timescales. Sci Rep.

Koga K, Liu M-G, Qiu S, Song Q, O'Den G, Chen T, Zhuo M (2015) Impaired Presynaptic Long-Term Potentiation in the Anterior Cingulate Cortex of Fmr1 Knock-out Mice. J Neurosci.

Koles K, Yeh AR, Rodal AA (2016) Tissue-specific tagging of endogenous loci in Drosophila melanogaster. Biol Open.

Kong S, Sahin M, Collins CD, Wertz MH, Campbell MG, Leech JD, Krueger D, Bear MF, Kunkel LM, Kohane IS (2014) Divergent dysregulation of gene expression in murine models of fragile X syndrome and tuberous sclerosis. Mol Autism 5:1–11.

Kosmaczewski SG, Edwards TJ, Han SM, Eckwahl MJ, Meyer BI, Peach S, Hesselberth JR, Wolin SL, Hammarlund M (2014) The RtcB RNA ligase is an essential component of the metazoan unfolded protein response. EMBO Rep.

Koto M, Tanouye M, Ferrus A, Thomas J, Wyman R (1981) The morphology of the cervical giant fiber neuron of Drosophila. Brain Res 221:213–217.

Kremer MC, Jung C, Batelli S, Rubin GM, Gaul U (2017) The glia of the adult *Drosophila* nervous system. Glia.

Kudumala S, Freund J, Hortsch M, Godenschwege TA (2013) Differential effects of human L1CAM mutations on complementing guidance and synaptic defects in Drosophila melanogaster. PLoS One 8:e76974.

Kühn T, Ihalainen TO, Hyväluoma J, Dross N, Willman SF, Langowski J, Vihinen-Ranta M, Timonen J (2011) Protein diffusion in mammalian cell cytoplasm. PLoS One 6:e22962.

Kummer TT, Misgeld T, Sanes JR (2006) Assembly of the postsynaptic membrane at the neuromuscular junction: Paradigm lost. Curr Opin Neurobiol.

Kurshan PT, Merrill SA, Dong Y, Ding C, Hammarlund M, Bai J, Jorgensen EM, Shen K (2018) γ-Neurexin and Frizzled mediate parallel synapse assembly pathways antagonized by receptor endocytosis. Neuron.

Lai CQ, Leips J, Zou W, Roberts JF, Wollenberg KR, Parnell LD, Zeng ZB, Ordovas JM, Mackay TFC (2007) Speed-mapping quantitative trait loci using microarrays. Nat Methods.

Lanciego JL, Wouterlood FG (2011) A half century of experimental neuroanatomical tracing. J Chem

Neuroanat 42:157–183.

Lapper SR, Bolam JP (1991) The anterograde and retrograde transport of neurobiotin in the central nervous system of the rat: comparison with biocytin. J Neurosci Methods 39:163–174.

Lee A, Li W, Xu K, Bogert B, Su K, Gao F (2003a) Control of dendritic development by the Drosophila fragile X-related gene involves the small GTPase Rac1. Development.

Lee DA, Portnoy S, Hill P, Gillberg C, Patton MA (2005) Psychological profile of children with Noonan syndrome. Dev Med Child Neurol.

Lee HY, Ge W-P, Huang W, He Y, Wang GX, Rowson-Baldwin A, Smith SJ, Jan YN, Jan LY (2011) Bidirectional regulation of dendritic voltage-gated potassium channels by the fragile X mental retardation protein. Neuron 72:630–642.

Lee LH, Godenschwege TA (2014) Structure-function analyses of tyrosine phosphatase PTP69D in giant fiber synapse formation of Drosophila. Mol Cell Neurosci 64:24–31.

Lee RC, Clandinin TR, Lee CH, Chen PL, Meinertzhagen IA, Zipursky SL (2003b) The protocadherin Flamingo is required for axon target selection in the Drosophila visual system. Nat Neurosci.

Levine J, Tracey D (1973) Structure and function of the giant motorneuron ofDrosophila melanogaster. J Comp Physiol 87:213–235.

Li-Kroeger D, Kanca O, Lee P-T, Cowan S, Lee M, Jaiswal M, Salazar JL, He Y, Bellen H (2018) An expanded toolkit for gene tagging based on MiMIC and scarless CRISPR tagging in Drosophila. bioRxiv:337337.

Lichtman JW, Livet J, Sanes JR (2008) A technicolour approach to the connectome. Nat Rev Neurosci.

Lieberman OJ, McGuirt AF, Tang G, Sulzer D (2018) Roles for neuronal and glial autophagy in synaptic pruning during development. Neurobiol Dis.

Ligsay A, Hagerman RJ (2016) Review of targeted treatments in fragile X syndrome. Intractable Rare Dis Res.

Lima-Cabello E, Garcia-Guirado F, Calvo-Medina R, El Bekay R, Perez-Costillas L, Quintero-Navarro C, Sanchez-Salido L, De Diego-Otero Y (2016) An abnormal nitric oxide metabolism contributes to brain oxidative stress in the mouse model for the fragile X Syndrome, a possible role in intellectual disability. Oxid Med Cell Longev 2016.

Lin TY, Luo J, Shinomiya K, Ting CY, Lu Z, Meinertzhagen IA, Lee CH (2016) Mapping chromatic pathways in the Drosophila visual system. J Comp Neurol 524:213–227.

Lin W, Burgess RW, Dominguez B, Pfaff SL, Sanes JR, Lee KF (2001) Distinct roles of nerve and muscle in postsynaptic differentiation of the neuromuscular synapse. Nature.

Liu W, Jiang F, Bi X, Zhang YQ (2012) Drosophila FMRP participates in the DNA damage response by regulating G2/M cell cycle checkpoint and apoptosis. Hum Mol Genet.

Liu WW, Wilson RI (2013) Glutamate is an inhibitory neurotransmitter in the Drosophila olfactory system. Proc Natl Acad Sci.

Longair MH, Baker DA, Armstrong JD (2011) Simple neurite tracer: Open source software for reconstruction, visualization and analysis of neuronal processes. Bioinformatics 27:2453–2454.

Lu R, Wang H, Liang Z, Ku L, O'Donnell WT, Li W, Warren ST, Feng Y (2004) The fragile X protein controls microtubule-associated protein 1B translation and microtubule stability in brain neuron development. Proc Natl Acad Sci.

Luan H, Peabody NC, Vinson CR, White BH (2006) Refined Spatial Manipulation of Neuronal Function by Combinatorial Restriction of Transgene Expression. Neuron 52:425–436.

Luby-Phelps K (1999) Cytoarchitecture and Physical Properties of Cytoplasm: Volume, Viscosity, Diffusion, Intracellular Surface Area. Int Rev Cytol 192:189–221.

Luo L, Joyce Liao Y, Jan LY, Jan YN (1994) Distinct morphogenetic functions of similar small GTPases: Drosophila Drac1 is involved in axonal outgrowth and myoblast fusion. Genes Dev.

Luo L, O'Leary DDM (2005) Axon Retraction and Degeneration in Development and Disease. Annu Rev Neurosci.

Luquet E, Biesemann C, Munier A, Herzog E (2017) Purification of synaptosome populations using fluorescence-activated synaptosome sorting. In: Methods in Molecular Biology, pp 121–134.

MacPhee DJ (2010) Methodological considerations for improving Western blot analysis. J Pharmacol Toxicol Methods.

Macpherson LJ, Zaharieva EE, Kearney PJ, Alpert MH, Lin TY, Turan Z, Lee CH, Gallio M (2015) Dynamic labelling of neural connections in multiple colours by trans-synaptic fluorescence complementation. Nat Commun.

Maher BJ, McGinley MJ, Westbrook GL (2009) Experience-dependent maturation of the glomerular microcircuit. Proc Natl Acad Sci 106:16865–16870.

Marro D, Kalia YN, Delgado-Charro MB, Guy RH (2001) Optimizing iontophoretic drug delivery: Identification and distribution of the charge-carrying species. Pharm Res 18:1709–1713.

Martinez VG, Javadi CS, Ngo E, Ngo L, Lagow RD, Zhang B (2007) Age-related changes in climbing behavior and neural circuit physiology in drosophila. Dev Neurobiol 67:778–791.

Maurin T, Zongaro S, Bardoni B (2014) Fragile X Syndrome: From molecular pathology to therapy. Neurosci Biobehav Rev:1–14.

McBride SMJ, Choi CH, Wang Y, Liebelt D, Braunstein E, Ferreiro D, Sehgal A, Siwicki KK, Dockendorff TC, Nguyen HT, McDonald T V., Jongens TA (2005) Pharmacological rescue of synaptic plasticity, courtship behavior, and mushroom body defects in a Drosophila model of Fragile X syndrome. Neuron.

McCarroll SA, Altshuler DM (2007) Copy-number variation and association studies of human disease. Nat Genet.

McMahon AC, Rosbash M (2016) Promiscuous or discriminating: Has the favored mRNA target of Fragile X Mental Retardation Protein been overlooked? Proc Natl Acad Sci.

McManus CJ, Coolon JD, Duff MO, Eipper-Mains J, Graveley BR, Wittkopp PJ (2010) Regulatory divergence in Drosophila revealed by mRNA-seq. Genome Res.

Mehler MF, Mattick JS (2007) Noncoding RNAs and RNA Editing in Brain Development, Functional Diversification, and Neurological Disease. Physiol Rev.

Mejia M, Heghinian MD, Busch A, Armishaw CJ, Marí F, Godenschwege T a (2010) A novel approach for in vivo screening of toxins using the Drosophila Giant Fiber circuit. Toxicon 56:1398–1407.

Mejia M, Heghinian MD, Marí F, Godenschwege T a (2013) New tools for targeted disruption of cholinergic synaptic transmission in Drosophila melanogaster. PLoS One 8:e64685.

Melom JE, Littleton JT (2011) Synapse development in health and disease. Curr Opin Genet Dev.

Menon KP, Carrillo RA, Zinn K (2013) Development and plasticity of the *Drosophila* larval neuromuscular junction. Wiley Interdiscip Rev Dev Biol.

Meyers JR, MacDonald RB, Duggan A, Lenzi D, Standaert DG, Corwin JT, Corey DP (2003) Lighting up the senses: FM1-43 loading of sensory cells through nonselective ion channels. J Neurosci 23:4054–4065.

Michalon A, Sidorov M, Ballard TM, Ozmen L, Spooren W, Wettstein JG, Jaeschke G, Bear MF, Lindemann L (2012) Chronic Pharmacological mGlu5 Inhibition Corrects Fragile X in Adult Mice. Neuron.

Michel CI (2004) Defective Neuronal Development in the Mushroom Bodies of Drosophila Fragile X Mental Retardation 1 Mutants. J Neurosci.

Michelmore RW, Paran I, Kesseli R V. (1991) Identification of markers linked to disease-resistance genes by bulked segregant analysis: a rapid method to detect markers in specific genomic regions by using segregating populations. Proc Natl Acad Sci.

Mishra A, Dhingra K, Schüz A, Logothetis NK, Canals S (2010) Improved neuronal tract tracing with stable biocytin-derived neuroimaging agents. ACS Chem Neurosci 1:129–138.

Mlodzik M, Hiromi Y (1992) Enhancer Trap Method in Drosophila: Its Application to Neurobiology. Methods Neurosci.

Modney B, Muller KJ (1994) Novel synapses compensate for a neuron ablated in embryos. Proc R Soc B Biol Sci 257:263–269.

Mohr SE (2014) RNAi screening in Drosophila cells and in vivo. Methods 68:82–88.

Monzo K, Dowd SR, Minden JS, Sisson JC (2010) Proteomic analysis reveals CCT is a target of Fragile X mental retardation protein regulation in Drosophila. Dev Biol.

Moraes ÂM, Jorge SAC, Astray RM, Suazo CAT, Calderón Riquelme CE, Augusto EFP, Tonso A, Pamboukian MM, Piccoli RAM, Barral MF, Pereira CA (2012) Drosophila melanogaster S2 cells for expression of heterologous genes: From gene cloning to bioprocess development. Biotechnol Adv.

Mu L, Bacon JP, Ito K, Strausfeld NJ (2014) Responses of Drosophila giant descending neurons to visual and mechanical stimuli. J Exp Biol 217:2121–2129.

Muller HJ (1935) On the incomplete dominance of the normal allelomorphs of white in Drosophila. J Genet.

Muralidhar MG, Thomas JB (1993) The Drosophila bendless gene encodes a neural protein related to ubiquitin-conjugating enzymes. Neuron.

Murphey RK (2003) Targeted expression of shibirets and semaphorin 1a reveals critical periods for synapse formation in the giant fiber of Drosophila. Development 130:3671–3682.

Muthukumar AK, Stork T, Freeman MR (2014) Activity-dependent regulation of astrocyte GAT levels during synaptogenesis. Nat Neurosci 17:1340–1350.

Myrick LK, Deng P-Y, Hashimoto H, Oh YM, Cho Y, Poidevin MJ, Suhl J a., Visootsak J, Cavalli V, Jin P, Cheng X, Warren ST, Klyachko V a. (2015) Independent role for presynaptic FMRP revealed by an FMR1 missense mutation associated with intellectual disability and seizures. Proc Natl Acad Sci 112:949–956.

Nadim F, Bucher D (2014) Neuromodulation of neurons and synapses. Curr Opin Neurobiol.

Nagel G, Brauner M, Liewald JF, Adeishvili N, Bamberg E, Gottschalk A (2005) Light activation of Channelrhodopsin-2 in excitable cells of caenorhabditis elegans triggers rapid behavioral responses. Curr Biol.

Nagel G, Szellas T, Huhn W, Kateriya S, Adeishvili N, Berthold P, Ollig D, Hegemann P, Bamberg E (2003) Channelrhodopsin-2, a directly light-gated cation-selective membrane channel. Proc Natl Acad Sci U S A 100:13940–13945.

Namiki S, Dickinson MH, Wong AM, Korff W, Card GM (2018) The functional organization of descending sensory-motor pathways in Drosophila. Elife 7:50.

Narayanan U, Nalavadi V, Nakamoto M, Pallas DC, Ceman S, Bassell GJ, Warren ST (2007) FMRP Phosphorylation Reveals an Immediate-Early Signaling Pathway Triggered by Group I mGluR and Mediated by PP2A. J Neurosci.

Narayanan U, Nalavadi V, Nakamoto M, Thomas G, Ceman S, Bassell GJ, Warren ST (2008) S6K1 phosphorylates and regulates fragile X mental retardation protein (FMRP) with the neuronal protein synthesis-dependent mammalian target of rapamycin (mTOR) signaling cascade. J Biol Chem.

Naviaux RK, Zolkipli Z, Wang L, Nakayama T, Naviaux JC, Le TP, Schuchbauer MA, Rogac M, Tang Q, Dugan LL, Powell SB (2013) Antipurinergic therapy corrects the autism-like features in the poly(IC) mouse model. PLoS One 8:e57380.

Nern A, Pfeiffer BD, Rubin GM (2015) Optimized tools for multicolor stochastic labeling reveal diverse stereotyped cell arrangements in the fly visual system. Proc Natl Acad Sci 112:E2967–E2976.

Neuhaus-Follini A, Bashaw GJ (2015) Crossing the embryonic midline: Molecular mechanisms regulating axon responsiveness at an intermediate target. Wiley Interdiscip Rev Dev Biol.

Ng PC, Henikoff S (2003) SIFT: Predicting amino acid changes that affect protein function. Nucleic Acids Res.

Ni JQ, Liu LP, Binari R, Hardy R, Shim HS, Cavallaro A, Booker M, Pfeiffer BD, Markstein M, Wang H, Villalta C, Laverty TR, Perkins LA, Perrimon N (2009) A drosophila resource of transgenic RNAi lines for neurogenetics. Genetics.

Nicolai LJJ, Ramaekers A, Raemaekers T, Drozdzecki A, Mauss AS, Yan J, Landgraf M, Annaert W, Hassan BA (2010) Genetically encoded dendritic marker sheds light on neuronal connectivity in Drosophila. Proc Natl Acad Sci 107:20553–20558.

Niculescu D, Lohmann C (2014) Gap junctions in developing thalamic and neocortical neuronal networks. Cereb Cortex 24:3097–3106.

Nielsen MS, Axelsen LN, Sorgen PL, Verma V, Delmar M, Holstein-Rathlou NH (2012) Gap junctions. Compr Physiol.

Niere F, Wilkerson JR, Huber KM (2012) Evidence for a Fragile X Mental Retardation Protein-Mediated Translational Switch in Metabotropic Glutamate Receptor-Triggered Arc Translation and Long-Term Depression. J Neurosci.

Nimchinsky EA, Oberlander AM, Svoboda K (2001) Abnormal Development of Dendritic Spines in FMR1 Knock-Out Mice. J Neurosci.

Novak SM, Joardar A, Gregorio CC, Zarnescu DC (2015) Regulation of Heart Rate in Drosophila via Fragile X Mental Retardation Protein Bardoni B, ed. PLoS One 10:e0142836.

Nusser Z, Lujan R, Laube G, Roberts JDB, Molnar E, Somogyi P (1998) Cell type and pathway dependence of synaptic AMPA receptor number and variability in the hippocampus. Neuron.

O'Connor RM, Stone EF, Wayne CR, Marcinkevicius E V., Ulgherait M, Delventhal R, Pantalia MM, Hill VM, Zhou CG, McAllister S, Chen A, Ziegenfuss JS, Grueber WB, Canman JC, Shirasu-Hiza MM (2017) A Drosophila model of Fragile X syndrome exhibits defects in phagocytosis by innate immune cells. J Cell Biol.

O'Kane CJ (2011) Drosophila as a model organism for the study of neuropsychiatric disorders. Curr Top Behav Neurosci.

Oberlé I, Rousseau F, Heitz D, Kretz C, Devys D, Hanauer A, Boué J, Bertheas MF, Mandel JL (1991)

Instability of a 550-base pair DNA segment and abnormal methylation in fragile X syndrome. Science.

Olesnicky E, Bhogal B, Gavis E (2012) Combinatorial use of translational co-factors for cell type-specific regulation during neuronal morphogenesis in Drosophila. Dev Biol 365:208–218.

Orr BO, Borgen MA, Caruccio PM, Murphey RK (2014) Netrin and frazzled regulate presynaptic gap junctions at a Drosophila giant synapse. J Neurosci 34:5416–5430.

Osterweil EK, Chuang SC, Chubykin AA, Sidorov M, Bianchi R, Wong RKS, Bear MF (2013) Lovastatin corrects excess protein synthesis and prevents epileptogenesis in a mouse model of fragile X syndrome. Neuron 77:243–250.

Otsuna H, Ito M, Kawase T (2018) Color depth MIP mask search: a new tool to expedite Split-GAL4 creation. bioRxiv:318006.

Overall R, Jaffe LF (1985) Patterns of ionic current through Drosophila follicles and eggs. Dev Biol.

Pacey LKK, Xuan ICY, Guan S, Sussman D, Henkelman RM, Chen Y, Thomsen C, Hampson DR (2013) Delayed myelination in a mouse model of fragile X syndrome. Hum Mol Genet.

Pacheco A, Gallo G (2016) Actin filament-microtubule interactions in axon initiation and branching. Brain Res Bull.

Page-McCaw A, Ewald AJ, Werb Z (2007) Matrix metalloproteinases and the regulation of tissue remodelling. Nat Rev Mol Cell Biol.

Pai T, Chen C, Lin H, Chin A, Lai JS, Lee P, Tully T, Chiang A (2013) Drosophila ORB protein in two mushroom body output neurons is necessary for long-term memory formation. Proc Natl Acad Sci U S A 110:7898–7903.

Pan L, Broadie KS (2007) Drosophila Fragile X Mental Retardation Protein and Metabotropic Glutamate Receptor A Convergently Regulate the Synaptic Ratio of Ionotropic Glutamate Receptor Subclasses. J Neurosci.

Pan L, Woodruff E, Liang P, Broadie K (2008) Mechanistic relationships between Drosophila fragile X mental retardation protein and metabotropic glutamate receptor A signaling. Mol Cell Neurosci.

Pan L, Zhang YQ, Woodruff E, Broadie K (2004) The Drosophila fragile X gene negatively regulates neuronal elaboration and synaptic differentiation. Curr Biol.

Paradee W, Melikian HE, Rasmussen DL, Kenneson A, Conn PJ, Warren ST (1999) Fragile X mouse: Strain effects of knockout phenotype and evidence suggesting deficient amygdala function. Neuroscience.

Park CY, Halevy T, Lee DR, Sung JJ, Lee JS, Yanuka O, Benvenisty N, Kim DW (2015) Reversion of FMR1 Methylation and Silencing by Editing the Triplet Repeats in Fragile X iPSC-Derived Neurons. Cell Rep 13:234–241.

Park M, Shen K (2012) WNTs in synapse formation and neuronal circuitry. EMBO J.

Patel a B, Loerwald KW, Huber KM, Gibson JR (2014) Postsynaptic FMRP promotes the pruning of cell-to-cell connections among pyramidal neurons in the L5A neocortical network. J Neurosci 34:3413–3418.

Patel MR, Lehrman EK, Poon VY, Crump JG, Zhen M, Bargmann CI, Shen K (2006) Hierarchical assembly of presynaptic components in defined C. elegans synapses. Nat Neurosci.

Paul S, Bownes M (1981) Staging the metamorphosis of Drosophila melanogaster. Embryol exp Morph.

Pearson HE, Stoffler DJ (1992) Retinal ganglion cell degeneration following loss of postsynaptic target neurons in the dorsal lateral geniculate nucleus of the adult cat. Exp Neurol 116:163–171.

Penn AA (2001) Early brain wiring: Activity-dependent processes. Schizophr Bull.

Pérez-Pérez JM, Candela H, Micol JL (2009) Understanding synergy in genetic interactions. Trends Genet.

Periasamy N, Kao HP, Fushimi K, Verkman a S (1992) Organic osmolytes increase cytoplasmic viscosity in kidney cells. Am J Physiol.

Perin MS, Johnston PA, Ozcelik T, Jahn R, Francke U, Sudhof TC (1991) Structural and functional conservation of synaptotagmin (p65) in Drosophila and humans. J Biol Chem.

Perkins LA et al. (2015) The transgenic RNAi project at Harvard medical school: Resources and validation. Genetics.

Pézier A, Jezzini SH, Marie B, Blagburn JM (2014) Engrailed alters the specificity of synaptic connections of Drosophila auditory neurons with the giant fiber. J Neurosci 34:11691–11704.

Pfeiffer B, Huber K (2009) The state of synapses in fragile X syndrome. Neurosci 15:549–567.

Pfeiffer BD, Ngo TTB, Hibbard KL, Murphy C, Jenett A, Truman JW, Rubin GM (2010) Refinement of tools for targeted gene expression in Drosophila. Genetics 186:735–755.

Phan AT, Kuryavyi V, Darnell JC, Serganov A, Majumdar A, Ilin S, Raslin T, Polonskaia A, Chen C, Clain D, Darnell RB, Patel DJ (2011) Structure-function studies of FMRP RGG peptide recognition of an RNA duplex-quadruplex junction. Nat Struct Mol Biol.

Phelan P (2005) Innexins: members of an evolutionarily conserved family of gap-junction proteins. Biochim Biophys Acta 1711:225–245.

Phelan P, Bacon P, Moffat KG, Kane CJO, Davies JA (1996) Mutations in shaking-B prevent electrical synapse formation in the Drosophila giant fiber system. J Neurosci 6:1101–1113.

Phelan P, Goulding LA, Tam JLY, Allen MJ, Dawber RJ, Davies JA, Bacon JP (2008) Molecular mechanism of rectification at identified electrical synapses in the Drosophila giant fiber system. Curr Biol 18:1955–1960.

Philbrook A, Ramachandran S, Lambert CM, Oliver D, Florman J, Alkema MJ, Lemons M, Francis MM

(2018) Neurexin directs partner-specific synaptic connectivity in C. elegans. Elife.

Pielage J, Cheng L, Fetter RD, Carlton PM, Sedat JW, Davis GW (2008) A Presynaptic Giant Ankyrin Stabilizes the NMJ through Regulation of Presynaptic Microtubules and Transsynaptic Cell Adhesion. Neuron.

Pielage J, Fetter RD, Davis GW (2005) Presynaptic spectrin is essential for synapse stabilization. Curr Biol.

Pikal MJ (2001) The role of electroosmotic flow in transdermal iontophoresis. Adv Drug Deliv Rev 46:281–305.

Platts AE, Land SJ, Chen L, Page GP, Rasouli P, Wang L, Lu X, Ruden DM (2009) Massively parallel resequencing of the isogenic Drosophila melanogaster strain w1118; Iso-2; iso-3 identifies hotspots for mutations in sensory perception genes. Fly (Austin).

Poirier C, Collignon O, Scheiber C, Renier L, Vanlierde A, Tranduy D, Veraart C, De Volder AG (2006) Auditory motion perception activates visual motion areas in early blind subjects. Neuroimage 31:279–285.

Pool JE (2016) Genetic mapping by bulk segregant analysis in Drosophila: Experimental design and simulation-based inference. Genetics.

Port F, Chen H-M, Lee T, Bullock SL (2014) Optimized CRISPR/Cas tools for efficient germline and somatic genome engineering in Drosophila. Proc Natl Acad Sci U S A.

Portera-Cailliau C (2011) Which Comes First in Fragile X Syndrome, Dendritic Spine Dysgenesis or Defects in Circuit Plasticity? Neurosci 18:28–44.

Power ME (1948) The thoracico-abdominal nervous system of an adult insect, Drosophila melanogaster. J Comp Neurol 88:347–409.

Prevedel R, Yoon Y-G, Hoffmann M, Pak N, Wetzstein G, Kato S, Schrödel T, Raskar R, Zimmer M, Boyden ES, Vaziri A (2014) Simultaneous whole-animal 3D imaging of neuronal activity using light-field microscopy. Nat Methods 11:727–730.

Price JL (2005) Genetic screens for clock mutants in Drosophila. Methods Enzymol.

Price TJ, Flores CM, Cervero F, Hargreaves KM (2006) The RNA binding and transport proteins staufen and fragile X mental retardation protein are expressed by rat primary afferent neurons and localize to peripheral and central axons. Neuroscience.

Qin M, Kang J, Burlin T V, Jiang C, Smith CB (2005) Postadolescent changes in regional cerebral protein synthesis: an in vivo study in the FMR1 null mouse. J Neurosci 25:5087–5095.

Rabinowitch I, Laurent P, Zhao B, Walker D, Beets I, Schoofs L, Bai J, Schafer WR, Treinin M (2016) Neuropeptide-Driven Cross-Modal Plasticity following Sensory Loss in Caenorhabditis elegans. PLoS Biol 14.

Ramos A, Hollingworth D, Pastore A (2003) G-quartet-dependent recognition between the FMRP RGG

box and RNA. RNA.

Ray D et al. (2013) A compendium of RNA-binding motifs for decoding gene regulation. Nature.

Reiter LT, Potocki L, Chien S, Gribskov M, Bier E (2001) A systematic analysis of human disease-associated gene sequences in Drosophila melanogaster. Genome Res.

Ribeiro LF, Verpoort B, de Wit J (2018) Trafficking mechanisms of synaptogenic cell adhesion molecules. Mol Cell Neurosci.

Riccomagno MM, Kolodkin AL (2015) Sculpting Neural Circuits by Axon and Dendrite Pruning. Annu Rev Cell Dev Biol.

Richter JD, Bassell GJ, Klann E (2015) Dysregulation and restoration of translational homeostasis in fragile X syndrome. Nat Rev Neurosci.

Rizzi G, Tan KR (2017) Dopamine and Acetylcholine, a Circuit Point of View in Parkinson's Disease. Front Neural Circuits.

Roden DM, Pulley JM, Basford MA, Bernard GR, Clayton EW, Balser JR, Masys DR (2008) Development of a large-scale de-identified DNA biobank to enable personalized medicine. Clin Pharmacol Ther.

Rong YS, Golic KG (2000) Gene targeting by homologous recombination in Drosophila. Science.

Rorth P, Szabo K, Bailey A, Laverty T, Tehm J, Rubin GM, Weigmann K, Milan M, Benes V, Ansorge W, Cohen SM, Rørth P, Rehm J, Milán M (1998) Systematic gain-of-function genetics in Drosophila. Development.

Rosso SB, Inestrosa NC (2013) WNT signaling in neuronal maturation and synaptogenesis. Front Cell Neurosci.

Ruby K, Falvey K, Kulesza RJ (2015) Abnormal neuronal morphology and neurochemistry in the auditory brainstem of Fmr1 knockout rats. Neuroscience.

Sackin H, Boulpaep EL (1981) Isolated perfused salamander proximal tubule: methods, electrophysiology, and transport. Am J Physiol 241:F39-52.

Salinas PC (2003) Synaptogenesis: Wnt and TGF-β take centre stage. Curr Biol.

Sanes JR, Masland RH (2015) The Types of Retinal Ganglion Cells: Current Status and Implications for Neuronal Classification. Annu Rev Neurosci.

Sanes JR, Zipursky SL (2010) Design Principles of Insect and Vertebrate Visual Systems. Neuron.

Sawicka K, Pyronneau A, Chao M, Bennett MVL, Zukin RS (2016) Elevated ERK/p90 ribosomal S6 kinase activity underlies audiogenic seizure susceptibility in fragile X mice. Proc Natl Acad Sci.

Schafer DP, Stevens B (2013) Phagocytic glial cells: Sculpting synaptic circuits in the developing nervous system. Curr Opin Neurobiol.

Scheiffele P, Fan J, Choih J, Fetter R, Serafini T (2000) Neuroligin expressed in nonneuronal cells triggers presynaptic development in contacting axons. Cell.

Schikorski T, Stevens CF (1997) Quantitative Ultrastructural Analysis of Hippocampal Excitatory Synapses. J Neurosci.

Schindelin J, Arganda-Carreras I, Frise E, Kaynig V, Longair M, Pietzsch T, Preibisch S, Rueden C, Saalfeld S, Schmid B, Tinevez J-Y, White DJ, Hartenstein V, Eliceiri K, Tomancak P, Cardona A (2012) Fiji: an open-source platform for biological-image analysis. Nat Methods 9:676–682.

Schneider CA, Rasband WS, Eliceiri KW (2012) NIH Image to ImageJ: 25 years of image analysis. Nat Methods 9:671–675.

Schofield BR (2008) Retrograde axonal tracing with fluorescent markers. Curr Protoc Neurosci 1.17:1–24.

Schreiner D, Savas JN, Herzog E, Brose N, de Wit J (2017) Synapse biology in the 'circuit-age'—paths toward molecular connectomics. Curr Opin Neurobiol.

Sestan N, State MW (2018) Lost in Translation: Traversing the Complex Path from Genomics to Therapeutics in Autism Spectrum Disorder. Neuron.

Sethna F, Feng W, Ding Q, Robison AJ, Feng Y, Wang H (2017) Enhanced expression of ADCY1 underlies aberrant neuronal signalling and behaviour in a syndromic autism model. Nat Commun 8:14359.

Shamay-Ramot A, Khermesh K, Porath HT, Barak M, Pinto Y, Wachtel C, Zilberberg A, Lerer-Goldshtein T, Efroni S, Levanon EY, Appelbaum L (2015) Fmrp Interacts with Adar and Regulates RNA Editing, Synaptic Density and Locomotor Activity in Zebrafish. PLOS Genet 11:e1005702.

Sharma A, Hoeffer CA, Takayasu Y, Miyawaki T, McBride SM, Klann E, Zukin RS (2010) Dysregulation of mTOR Signaling in Fragile X Syndrome. J Neurosci.

Shen K, Bargmann CI (2003) The immunoglobulin superfamily protein SYG-1 determines the location of specific synapses in C. elegans. Cell.

Shendure J, Balasubramanian S, Church GM, Gilbert W, Rogers J, Schloss JA, Waterston RH (2017) DNA sequencing at 40: Past, present and future. Nature.

Shtang S, Perry MD, Percy ME (1999) Search for a Caenorhabditis elegans FMR1 homologue: Identification of a new putative RNA-binding protein (PRP-1) that hybridizes to the mouse FMR1 double K homology domain. Am J Med Genet.

Sialana FJ, Gulyassy P, Májek P, Sjöstedt E, Kis V, Müller AC, Rudashevskaya EL, Mulder J, Bennett KL, Lubec G (2016) Mass spectrometric analysis of synaptosomal membrane preparations for the determination of brain receptors, transporters and channels. Proteomics 16:2911–2920.

Siller SS, Broadie K (2011) Neural circuit architecture defects in a Drosophila model of Fragile X syndrome are alleviated by minocycline treatment and genetic removal of matrix metalloproteinase. Dis Model Mech 4:673–685.

Singh A, Singh S (1999) Unmasking of a novel potassium current in Drosophila by a mutation and drugs. J Neurosci 19:6838–6843.

Singh SK, Stogsdill JA, Pulimood NS, Dingsdale H, Kim YH, Pilaz LJ, Kim IH, Manhaes AC, Rodrigues WS, Pamukcu A, Enustun E, Ertuz Z, Scheiffele P, Soderling SH, Silver DL, Ji RR, Medina AE, Eroglu C (2016) Astrocytes Assemble Thalamocortical Synapses by Bridging NRX1α and NL1 via Hevin. Cell.

Sinkey RG, Odibo AO (2017) Noonan Syndrome. In: Obstetric Imaging: Fetal Diagnosis and Care: Second Edition.

Siomi H, Choi M, Siomi MC, Nussbaum RL, Dreyfuss G (1994) Essential role for KH domains in RNA binding: Impaired RNA binding by a mutation in the KH domain of FMR1 that causes fragile X syndrome. Cell.

Siomi H, Siomi MC, Nussbaum RL, Dreyfuss G (1993) The protein product of the fragile X gene, FMR1, has characteristics of an RNA-binding protein. Cell.

Siomi MC, Siomi H, Sauer WH, Srinivasan S, Nussbaum RL, Dreyfuss G (1995) FXR1, an autosomal homolog of the fragile X mental retardation gene. Eur Mol Biol Organ J.

Sivaguru M, Urban MA, Fried G, Wesseln CJ, Mander L, Punyasena SW (2016) Comparative performance of airyscan and structured illumination superresolution microscopy in the study of the surface texture and 3D shape of pollen. Microsc Res Tech.

Smith HK, Roberts IJH, Allen MJ, Connolly JB, Moffat KG, O'Kane CJ (1996) Inducible ternary control of transgene expression and cell ablation in Drosophila. Dev Genes Evol 206:14–24.

Snyder EM, Philpot BD, Huber KM, Dong X, Fallon JR, Bear MF (2001) Internalization of ionotropic glutamate receptors in response to mGluR activation. Nat Neurosci.

Söhl G, Willecke K (2003) An Update on Connexin Genes and their Nomenclature in Mouse and Man. Cell Commun Adhes.

Spencer CC, Howell CE, Wright AR, Promislow DEL (2003) Testing an "aging gene" in long-lived drosophila strains: increased longevity depends on sex and genetic background. Aging Cell.

Spencer CM, Alekseyenko O, Hamilton SM, Thomas AM, Serysheva E, Yuva-Paylor LA, Paylor R (2011) Modifying behavioral phenotypes in Fmr1KO mice: Genetic background differences reveal autistic-like responses. Autism Res.

Spencer CM, Serysheva E, Yuva-Paylor LA, Oostra BA, Nelson DL, Paylor R (2006) Exaggerated behavioral phenotypes in Fmr1/Fxr2 double knockout mice reveal a functional genetic interaction between Fragile X-related proteins. Hum Mol Genet.

Spradling AC, Rubin GM (1982) Transposition of cloned P elements into Drosophila germ line chromosomes. Science.

Staudt T, Lang MC, Medda R, Engelhardt J, Hell SW (2007) 2,2 '-thiodiethanol: A new water soluble mounting medium for high resolution optical microscopy. Microsc Res Tech 70:1–9.

Stebbings LA, Todman MG, Phillips R, Greer CE, Tam J, Phelan P, Jacobs K, Bacon JP, Davies JA (2002) Gap junctions in Drosophila: Developmental expression of the entire innexin gene family. Mech Dev 113:197–205.

Stensmyr MC, Dweck HKM, Farhan A, Ibba I, Strutz A, Mukunda L, Linz J, Grabe V, Steck K, Lavista-Llanos S, Wicher D, Sachse S, Knaden M, Becher PG, Seki Y, Hansson BS (2012) A conserved dedicated olfactory circuit for detecting harmful microbes in drosophila. Cell 151:1345–1357.

Stepan J, Dine J, Eder M (2015) Functional optical probing of the hippocampal trisynaptic circuit in vitro: Network dynamics, filter properties, and polysynaptic induction of CA1 LTP. Front Neurosci.

Streit AK, Fan YN, Masullo L, Baines RA (2016) Calcium imaging of neuronal activity in Drosophila can identify anticonvulsive compounds. PLoS One.

Strumbos JG, Brown MR, Kronengold J, Polley DB, Kaczmarek LK (2010) Fragile X mental retardation protein is required for rapid experience-dependent regulation of the potassium channel Kv3.1b. J Neurosci 30:10263–10271.

Südhof TC (2018) Towards an Understanding of Synapse Formation. Neuron.

Sugiura Y, Lin W (2011) Neuron–glia interactions: the roles of Schwann cells in neuromuscular synapse formation and function. Biosci Rep.

Suhl JA, Chopra P, Anderson BR, Bassell GJ, Warren ST (2014) Analysis of FMRP mRNA target datasets reveals highly associated mRNAs mediated by G-quadruplex structures formed via clustered WGGA sequences. Hum Mol Genet.

Sun M-K, Hongpaisan J, Alkon DL (2016) Rescue of Synaptic Phenotypes and Spatial Memory in Young Fragile X Mice. J Pharmacol Exp Ther.

Sun Y, Wyman RJ (1997) Neurons of the Drosophila giant fiber system: I. Dorsal longitudinal motor neurons. J Comp Neurol 387:157–166.

Sun YA, Wyman RJ (1996) Passover eliminates gap junctional communication between neurons of the giant fiber system in Drosophila. J Neurobiol 30:340–348.

Sung YJ, Dolzhanskaya N, Nolin SL, Brown T, Currie JR, Denman RB (2003) The fragile X mental retardation protein FMRP binds elongation factor 1A mRNA and negatively regulates its translation in vivo. J Biol Chem.

Tabet R, Moutin E, Becker JAJ, Heintz D, Fouillen L, Flatter E, Krężel W, Alunni V, Koebel P, Dembélé D, Tassone F, Bardoni B, Mandel J-L, Vitale N, Muller D, Le Merrer J, Moine H (2016) Fragile X Mental Retardation Protein (FMRP) controls diacylglycerol kinase activity in neurons. Proc Natl Acad Sci:201522631.

Takemura S ya et al. (2017) A connectome of a learning and memory center in the adult Drosophila brain. Elife.

Talay M, Richman EB, Snell NJ, Hartmann GG, Fisher JD, Sorkaç A, Santoyo JF, Chou-Freed C, Nair N,

Johnson M, Szymanski JR, Barnea G (2017) Transsynaptic Mapping of Second-Order Taste Neurons in Flies by trans-Tango. Neuron:1–13.

Tamanini F, Willemsen R, Van Unen L, Bontekoe C, Galjaard H, Oostra BA, Hoogeveen AT (1997) Differential expression of FMR1, FXR1 and FXR2 proteins in human brain and testis. Hum Mol Genet.

Tang SJ, Meulemans D, Vazquez L, Colaco N, Schuman E (2001) A role for a rat homolog of staufen in the transport of RNA to neuronal dendrites. Neuron 32:463–475.

Tanouye M a, Ferrus A, Fujita SC (1981) Abnormal action potentials associated with the Shaker complex locus of Drosophila. Proc Natl Acad Sci U S A 78:6548–6552.

Tanouye MA, Wyman RJ (1980) Motor outputs of giant nerve fiber in Drosophila. J Neurophysiol 44:405–421.

Tashiro A, Dunaevsky A, Blazeski R, Mason CA, Yuste R (2003) Bidirectional regulation of hippocampal mossy fiber filopodial motility by kainate receptors: A two-step model of synaptogenesis. Neuron.

Tessier C, Broadie K (2008) Drosophila fragile X mental retardation protein developmentally regulates activity-dependent axon pruning. Development 135:1547–1557.

Tessier CR (2009) Activity-dependent modulation of neural circuit synaptic connectivity. Front Mol Neurosci.

Tessier CR, Broadie K (2012) Molecular and genetic analysis of the Drosophila model of fragile X syndrome. Results Probl Cell Differ 54:119–156.

Thavarajah R, Mudimbaimannar V, Rao U, Ranganathan K, Elizabeth J (2012) Chemical and physical basics of routine formaldehyde fixation. J Oral Maxillofac Pathol.

The Dutch-Belgian Fragile X Consorthium et al. (1994) Fmr1 knockout mice: A model to study fragile X mental retardation. Cell.

Thomas JB, Wyman RJ (1984) Mutations altering synaptic connectivity between identified neurons in Drosophila. J Neurosci 4:530–538.

Thomas MG, Loschi M, Desbats MA, Boccaccio GL (2011) RNA granules: The good, the bad and the ugly. Cell Signal.

Tian Y, Yang C, Shang S, Cai Y, Deng X, Zhang J, Shao F, Zhu D, Liu Y, Chen G, Liang J, Sun Q, Qiu Z, Zhang C (2017) Loss of FMRP Impaired Hippocampal Long-Term Plasticity and Spatial Learning in Rats. Front Mol Neurosci 10:1–14.

Tierney AJ (1986) The evolution of learned and innate behavior: Contributions from genetics and neurobiology to a theory of behavioral evolution. Anim Learn Behav.

Tirian L, Dickson B (2017) The VT GAL4, LexA, and split-GAL4 driver line collections for targeted expression in the Drosophila nervous system. bioRxiv:198648.

Tosches MA (2017) Developmental and genetic mechanisms of neural circuit evolution. Dev Biol.

Trimarchi JR, Jin P, Murphey RK (1999) Controlling the motor neuron. Int Rev Neurobiol 43:241–264.

Trimarchi JR, Schneiderman a M (1995) Different neural pathways coordinate Drosophila flight initiations evoked by visual and olfactory stimuli. J Exp Biol 198:1099–1104.

Trimarchi JR, Schneiderman AM (1993) Giant fiber activation of an intrinsic muscle in the mesothoracic leg of Drosophila melanogaster. J Exp Biol 177:149–167.

Turner T, Adams M, Dunlap K (1993) Multiple Ca2+ channel types coexist to regulate synaptosomal neurotransmitter release. Proc Natl Acad Sci U S A.

Uesaka N (2005) Activity Dependence of Cortical Axon Branch Formation: A Morphological and Electrophysiological Study Using Organotypic Slice Cultures. J Neurosci 25:1–9.

Ugarte G, Delgado R, O'Day PM, Farjah F, Cid LP, Vergara C, Bacigalupo J (2005) Putative ClC-2 chloride channel mediates inward rectification in Drosophila retinal photoreceptors. J Membr Biol.

Ullian EM, Sapperstein SK, Christopherson KS, Barres BA (2001) Control of synapse number by glia. Science.

Unsain N, Barker PA (2015) New Views on the Misconstrued: Executioner Caspases and Their Diverse Non-apoptotic Roles. Neuron.

Urwyler O, Izadifar A, Dascenco D, Petrovic M, He H, Ayaz D, Kremer A, Lippens S, Baatsen P, Guerin CJ, Schmucker D (2015) Investigating CNS synaptogenesis at single-synapse resolution by combining reverse genetics with correlative light and electron microscopy. Development.

Uthaman SB, Godenschwege T a, Murphey RK (2008) A mechanism distinct from highwire for the Drosophila ubiquitin conjugase bendless in synaptic growth and maturation. J Neurosci 28:8615–8623.

Valakh V, Naylor SA, Berns DS, DiAntonio A (2012) A large-scale RNAi screen identifies functional classes of genes shaping synaptic development and maintenance. Dev Biol.

Veneri M, Zalfa F, Bagni C (2004) FMRP and its target RNAs: Fishing for the specificity. Neuroreport.

Venken KJT, Schulze KL, Haelterman NA, Pan H, He Y, Evans-Holm M, Carlson JW, Levis RW, Spradling AC, Hoskins RA, Bellen HJ (2011) MiMIC: a highly versatile transposon insertion resource for engineering Drosophila melanogaster genes. Nat Methods 8:737–743.

Verkman AS (2002) Solute and macromolecule diffusion in cellular aqueous compartments. Trends Biochem Sci.

Vessey JP, Vaccani A, Xie Y, Dahm R, Karra D, Kiebler MA, Macchi P (2006) Dendritic localization of the translational repressor Pumilio 2 and its contribution to dendritic stress granules. J Neurosci 26:6496–6508.

Vicario-Abejón C, Owens D, McKay R, Segal M (2002) Role of neurotrophins in central synapse formation and stabilization. Nat Rev Neurosci.

Vita DJ, Broadie K (2017) ESCRT-III Membrane Trafficking Misregulation Contributes to Fragile X Syndrome Synaptic Defects. Sci Rep.

von Reyn CR, Breads P, Peek MY, Zheng GZ, Williamson WR, Yee AL, Leonardo A, Card GM (2014) A spike-timing mechanism for action selection. Nat Neurosci 17:962–970.

Wagh DA, Rasse TM, Asan E, Hofbauer A, Schwenkert I, Dürrbeck H, Buchner S, Dabauvalle MC, Schmidt M, Qin G, Wichmann C, Kittel R, Sigrist SJ, Buchner E (2006) Bruchpilot, a protein with homology to ELKS/CAST, is required for structural integrity and function of synaptic active zones in Drosophila. Neuron.

Waites CL, Craig AM, Garner CC (2005) Mechanisms of Vertebrate Synaptogenesis. Annu Rev Neurosci.

Walker JM (1996) The Bicinchoninic Acid (BCA) Assay for Protein Quantitation. In: The Protein Protocols Handbook.

Wan L, Dockendorff TC, Jongens TA, Dreyfuss G (2000) Characterization of dFMR1, a Drosophila melanogaster homolog of the fragile X mental retardation protein. Mol Cell Biol 20:8536–8547.

Wang X, Snape M, Klann E, Stone JG, Singh A, Petersen RB, Castellani RJ, Casadesus G, Smith MA, Zhu X (2012) Activation of the extracellular signal-regulated kinase pathway contributes to the behavioral deficit of fragile x-syndrome. J Neurochem.

Ward A, Hong W, Favaloro V, Luo L (2015) Toll Receptors Instruct Axon and Dendrite Targeting and Participate in Synaptic Partner Matching in a Drosophila Olfactory Circuit. Neuron 85:1013–1028.

Ward LD, Kellis M (2012) Interpreting noncoding genetic variation in complex traits and human disease. Nat Biotechnol.

Watson KK, Platt ML (2012) Of mice and monkeys: Using non-human primate models to bridge mouse- and human-based investigations of autism spectrum disorders. J Neurodev Disord.

Weber PA, Chang HC, Spaeth KE, Nitsche JM, Nicholson BJ (2004) The permeability of gap junction channels to probes of different size is dependent on connexin composition and permeant-pore affinities. Biophys J 87:958–973.

Weiler IJ, Spangler CC, Klintsova AY, Grossman AW, Kim SH, Bertaina-Anglade V, Khaliq H, de Vries FE, Lambers F a E, Hatia F, Base CK, Greenough WT (2004) Fragile X mental retardation protein is necessary for neurotransmitter-activated protein translation at synapses. Proc Natl Acad Sci USA.

Welihinda AA, Kaufmant RJ (1996) The unfolded protein response pathway in Saccharomyces cerevisiae. Oligomerization and trans-phosphorylation of Ire1p (Ern1p) are required for kinase activation. J Biol Chem.

Wells DG (2006) RNA-Binding Proteins: A Lesson in Repression. J Neurosci.

Wheatley D. (1998) Diffusion theory, the cell and the synapse. Biosystems 45:151–163.

White JG, Southgate E, Thomson JN, Brenner S (1986) The Structure of the Nervous System of the Nematode Caenorhabditis elegans. Philos Trans R Soc B Biol Sci.

White MG, Cody PA, Bubser M, Wang HD, Deutch AY, Mathur BN (2017) Cortical hierarchy governs rat claustrocortical circuit organization. J Comp Neurol.

Wickersham IR, Finke S, Conzelmann KK, Callaway EM (2007) Retrograde neuronal tracing with a deletion-mutant rabies virus. Nat Methods.

Willemsen R, Kooy F (2017) Fragile X syndrome: from genetics to targeted treatment. Academic Press.

Williams SR, Stuart GJ (2003) Role of dendritic synapse location in the control of action potential output. Trends Neurosci.

Wodarz A, Hinz U, Engelbert M, Knust E (1995) Expression of crumbs confers apical character on plasma membrane domains of ectodermal epithelia of drosophila. Cell.

Wong ROL, Ghosh A (2002) Activity-dependent regulation of dendritic growth and patterning. Nat Rev Neurosci.

Xiao MY, Zhou Q, Nicoll RA (2001) Metabotropic glutamate receptor activation causes a rapid redistribution of AMPA receptors. Neuropharmacology.

Xu CS, Hayworth KJ, Lu Z, Grob P, Hassan AM, García-Cerdán JG, Niyogi KK, Nogales E, Weinberg RJ, Hess HF (2017) Enhanced FIB-SEM systems for large-volume 3D imaging. Elife.

Yan QJ, Rammal M, Tranfaglia M, Bauchwitz RP (2005) Suppression of two major Fragile X Syndrome mouse model phenotypes by the mGluR5 antagonist MPEP. Neuropharmacology.

Yan X, Denman RB (2011) Conformational-dependent and independent RNA binding to the fragile x mental retardation protein. J Nucleic Acids 2011:246127.

Yao A, Jin S, Li X, Liu Z, Ma X, Tang J, Zhang YQ (2011) Drosophila FMRP regulates microtubule network formation and axonal transport of mitochondria. Hum Mol Genet.

Yasuyama K, Salvaterra PM (1999) Localization of choline acetyltransferase-expressing neurons in Drosophila nervous system. Microsc Res Tech.

Yrigollen C, Davidson B (2019) CRISPR to the Rescue: Advances in Gene Editing for the FMR1 Gene. Brain Sci 9:17.

Yu CC, Reddy BJN, Wortman JC, Gross SP (2017) Axonal Transport: A Constrained System. J Neurol neuromedicine 2:20–24.

Yu H-H, Yang JS, Wang J, Huang Y, Lee T (2009) Endodomain diversity in the Drosophila Dscam and its roles in neuronal morphogenesis. J Neurosci 29:1904–1914.

Yuan Q, Joiner WJ, Sehgal A (2006) A Sleep-Promoting Role for the Drosophila Serotonin Receptor 1A.

Curr Biol.

Zalfa F, Adinolfi S, Napoli I, Kühn-Hölsken E, Urlaub H, Achsel T, Pastore A, Bagni C (2005) Fragile X mental retardation protein (FMRP) binds specifically to the brain cytoplasmic RNAs BC1/BC200 via a novel RNA-binding motif. J Biol Chem.

Zalfa F, Eleuteri B, Dickson KS, Mercaldo V, De Rubeis S, Di Penta A, Tabolacci E, Chiurazzi P, Neri G, Grant SGN, Bagni C (2007) A new function for the fragile X mental retardation protein in regulation of PSD-95 mRNA stability. Nat Neurosci.

Zalfa F, Giorgi M, Primerano B, Moro A, Di Penta A, Reis S, Oostra B, Bagni C (2003) The Fragile X syndrome protein FMRP associates with BC1 RNA and regulates the translation of specific mRNAs at synapses. Cell.

Zampieri M, Sekar K, Zamboni N, Sauer U (2017) Frontiers of high-throughput metabolomics. Curr Opin Chem Biol.

Zhang M, Chen D, Xia J, Han W, Cui X, Neuenkirchen N, Hermes G, Sestan N, Lin H (2017) Post-transcriptional regulation of mouse neurogenesis by Pumilio proteins. Genes Dev.

Zhang Y, Bonnan A, Bony G, Ferezou I, Pietropaolo S, Ginger M, Sans N, Rossier J, Oostra B, LeMasson G, Frick A (2014a) Dendritic channelopathies contribute to neocortical and sensory hyperexcitability in Fmr1−/y mice. Nat Neurosci 17:1701–1709.

Zhang Y, Brown MR, Hyland C, Chen Y, Kronengold J, Fleming MR, Kohn AB, Moroz LL, Kaczmarek LK (2012) Regulation of neuronal excitability by interaction of fragile X mental retardation protein with slack potassium channels. J Neurosci 32:15318–15327.

Zhang Y, Connor JPO, Siomi MCMC, Srinivasan S, Dutra A, Nussbaum RL, Dreyfuss G, O'Connor JP (1995) The fragile X mental retardation syndrome protein interacts with novel homologs FXR1 and FXR2. EMBO J.

Zhang Y, Gaetano CM, Williams KR, Bassell GJ, Mihailescu MR (2014b) FMRP interacts with G-quadruplex structures in the 3 '-UTR of its dendritic target shank1 mRNA. RNA Biol.

Zhang YQ, Bailey AM, Matthies HJ, Renden RB, Smith MA, Speese SD, Rubin GM, Broadie K (2001) Drosophila fragile X-related gene regulates the MAP1B homolog Futsch to control synaptic structure and function. Cell 107:591–603.

Zhang YQ, Friedman DB, Wang Z, Woodruff E, Pan L, O'Donnell J, Broadie K (2005) Protein Expression Profiling of the Drosophila fragile X Mutant Brain Reveals Up-regulation of Monoamine Synthesis. Mol Cell Proteomics.

Zhang YQ, Matthies HJG, Mancuso J, Andrews HK, Woodruff E, Friedman D, Broadie K (2004) The Drosophila fragile X-related gene regulates axoneme differentiation during spermatogenesis. Dev Biol.

Zhang YQ, Rodesch CK, Broadie K (2002) Living synaptic vesicle marker: Synaptotagmin-GFP. Genesis 34:142–145.

Zhang Z, Curtin KD, Sun Y a, Wyman RJ (1999) Nested transcripts of gap junction gene have distinct expression patterns. J Neurobiol 40:288–301.

Zhao T, Olbris DJ, Yu Y, Plaza SM (2018) NeuTu: Software for Collaborative, Large-Scale, Segmentation-Based Connectome Reconstruction. Front Neural Circuits 12:101.

Zheng Z et al. (2017) A Complete Electron Microscopy Volume Of The Brain Of Adult Drosophila melanogaster. bioRxiv:140905.

Zheng Z, Lauritzen JS, Perlman E, Saalfeld S, Fetter RD, Bock Correspondence DD (2018) A Complete Electron Microscopy Volume of the Brain of Adult Drosophila melanogaster. Cell 174:1–14.

Zhou L-T, Ye S-H, Yang H-X, Zhou Y-T, Zhao Q-H, Sun W-W, Gao M-M, Yi Y-H, Long Y-S (2017) A novel role of fragile X mental retardation protein in pre-mRNA alternative splicing through RNA-binding protein 14. Neuroscience 349:64–75.

Zhou L, Schnitzler A, Agapite J, Schwartz LM, Steller H, Nambu JR (1997) Cooperative functions of the reaper and head involution defective genes in the programmed cell death of Drosophila central nervous system midline cells. Proc Natl Acad Sci U S A 94:5131–5136.